



THE UNIVERSITY OF QUEENSLAND
AUSTRALIA

**Physical and chemical interactions between bile pigments
and polyaromatic mutagens**

Hung Trieu Hong

BSc. and Master in Organic Chemistry

A thesis submitted for the degree of Doctor of Philosophy at

The University of Queensland in 2016

School of Chemistry and Molecular Biosciences

Abstract

A major cause of cancer in humans is exposure to mutagenic compounds. This raises the question of how humans can be protected from these environmental mutagens. Bile pigments (BPs) such as biliverdin, unconjugated bilirubin and protoporphyrin and their derivatives have recently been found to act as antioxidants and inhibit the mutagenic effects of several known environmental mutagens including 2-aminofluorene, benzo[α]pyrene, and 2-amino-1-methyl-6-phenylimido[4,5-*b*]pyridine. Despite these promising results, very little is known about the mechanisms by which this inhibition is achieved. Understanding these mechanisms would be useful for future drug development. Therefore, this PhD thesis aims to explore physical and chemical interactions between BPs and mutagens. Effects of BPs on the bioavailability and metabolism of mutagens were also examined *in vitro* using the colorectal adenocarcinoma (Caco-2 cell) monolayer model and the human liver S9 fraction.

The physical interactions between mutagens and BPs were examined using three different methods: NMR, UV and effects of bioavailability. The results of the comparison of the NMR spectra of mutagens in the absence and presence of BPs showed very little changes in the chemical shifts of the protons and the changes that did occur were the result of acid/base interactions between the BPs and mutagens. The UV spectrum of each mutagen was measured in the presence and absence of varying concentrations of BPs, and there were no changes to the UV spectra of any of the compounds. Strong physical interactions or aggregation of compounds can also affect their absorption across cell monolayers and so the apparent permeability of mutagens across Caco-2 cell monolayers in the presence and absence of BPs were measured. The results indicated that BPs increased the permeability of the mutagens slightly and effected how much of the compounds remained in tight association with the monolayer but the effects were small. These experiments provided evidence to suggest that physical interactions and aggregations are unlikely to be a major contributing mechanism of the inhibitory effects of BPs on environmental mutagens.

Chemical reactions between BPs and the DNA modifying metabolites of mutagens (epoxides) were studied using styrene epoxide as a model for the reactive metabolites. Styrene epoxide is commercially available, stable and less toxic than the reactive metabolites of the mutagens. Competitive reactions were performed in which BPs and their derivatives were placed in solution with guanine and allowed to react with styrene epoxide. These reactions showed that BPs and their dimethyl esters are more reactive to the epoxide than guanine. Bile pigments primarily react through their carboxylic acid groups with the mono- and di-styrene epoxide esters being the major products isolated from the reactions. The pyrrole rings in bilirubin also showed some evidence of

reaction with styrene epoxide though the products were too unstable to isolate. Thus, it was clear that BPs can effectively scavenge reactive metabolites, but the free carboxylic acids were significantly more effective at this than the dimethyl ester derivatives. This is not reflected in the anti-mutagenic activities of the compounds. Also, the ubiquitous nature of carboxylic acid groups in the cellular environment makes it unlikely that this reaction with activated epoxides would be unique to BPs. For these reasons we concluded that it is unlikely that chemical scavenging of reactive metabolites is the sole or even major mechanism of the inhibition of BPs.

Another possible mechanism of action of the BPs is that they inhibit the formation of the DNA modifying metabolites of the mutagens. We investigated this by performing in vitro experiments in which mutagens were co-incubated in the human liver S9 fraction in the presence and absence of BPs. The results indicated BPs were inhibitors of the metabolism of benzo[a]pyrene and 2-amino-1-methyl-6-phenylimido[4,5-b]pyridine by liver enzymes. The order of inhibitory effectiveness was bilirubin > protoporphyrin > biliverdin. Molecular modelling studies which examined the docking of the various BPs into the active sites of published crystal structures of the enzymes known to be responsible for the metabolism of the mutagens, suggested BPs could bind to the active sites of CYP1A1, 1A2, 1B1 and 3A4.

In summary, we conducted a series of experiments to evaluate the likely mechanisms of the inhibitory effects of BPs on known environmental mutagens. There are several theories postulated to explain the anti-mutagenic effects of BPs including the physical π -stacking driven aggregation of BPs with the polyaromatic mutagens, the chemical scavenging of BPs towards reactive metabolites, and the inhibition of BPs of the P450 mediated activation of the mutagens. We have systematically tested each of these and found that the latter appears to be the most likely mechanism to explain the effects reported. In broader terms, this research will aid in understanding how BPs inhibit mutagenesis and thus may lead to the development of synthetic compounds that could decrease the risk to humans exposed to these environmental mutagens.

Declaration by author

This thesis is composed of my original work, and contains no material previously published or written by another person except where due reference has been made in the text. I have clearly stated the contribution by others to jointly-authored works that I have included in my thesis.

I have clearly stated the contribution of others to my thesis as a whole, including statistical assistance, survey design, data analysis, significant technical procedures, professional editorial advice, and any other original research work used or reported in my thesis. The content of my thesis is the result of work I have carried out since the commencement of my research higher degree candidature and does not include a substantial part of work that has been submitted to qualify for the award of any other degree or diploma in any university or other tertiary institution. I have clearly stated which parts of my thesis, if any, have been submitted to qualify for another award.

I acknowledge that an electronic copy of my thesis must be lodged with the University Library and, subject to the policy and procedures of The University of Queensland, the thesis be made available for research and study in accordance with the Copyright Act 1968 unless a period of embargo has been approved by the Dean of the Graduate School.

I acknowledge that copyright of all material contained in my thesis resides with the copyright holder(s) of that material. Where appropriate I have obtained copyright permission from the copyright holder to reproduce material in this thesis.

Publications during candidature

Peer Reviewed Papers:

Mölzer, C.; Huber, H.; Steyrer, A.; Ziesel, G. V.; Wallner, M.; **Hong, H. T.**; Blanchfield, J. T.; Bulmer, A. C.; Wagner, K. H., Bilirubin and related tetrapyrroles inhibit food-borne mutagenesis: A mechanism for antigenotoxic action against a model epoxide. *J. Nat. Prod.* **2013**, 76 (10), 1958-1965.

Conference abstracts, poster and oral presentations:

Hung, H. T.; Wagner, K.H.; Bulmer, A.C. De Voss, J. J., Blanchfield, J. T., *The evaluation of physical and chemical interactions between bile pigments and polyaromatic mutagens*, 8th Annual Research Students Symposium School of Chemistry and Molecular Biosciences, The University of Queensland, Australia, November 2012. Abstract and poster presentation.

Hung, H. T.; Wagner, K.H.; Bulmer, A.C. De Voss, J. J., Blanchfield, J. T., *Mechanistic evaluation of chemical interactions between dipyrroles, tetrapyrroles and polyaromatic mutagens*. 9th Annual Research Students Symposium School of Chemistry and Molecular Biosciences, The University of Queensland, Australia, November 2013. Abstract and poster presentation.

Hung, H. T.; Wagner, K.H.; Bulmer, A.C. De Voss, J. J., Blanchfield, J. T., *Synthesis dipyrroles and the evaluation chemical interaction mechanisms between dipyrroles, tetrapyrroles and polyaromatic mutagens*, BBOCS 2013 - Brisbane Biological & Organic Chemistry Symposium, December 2013. Abstract and poster presentation.

Hung, H. T.; Wagner, K.H.; Bulmer, A.C. De Voss, J. J., Blanchfield, J. T., *Exploring the mechanism of tetrapyrroles' inhibition of environment mutagens*, Heterocyclic and synthetic conference, University of Florida, ARKAT USA, March 2014. Abstract and poster presentation.

Publications included in this thesis

Mölzer, C.; Huber, H.; Steyrer, A.; Ziesel, G. V.; Wallner, M.; **Hong, H. T.**; Blanchfield, J. T.; Bulmer, A. C.; Wagner, K. H., Bilirubin and related tetrapyrroles inhibit food-borne mutagenesis: A mechanism for antigenotoxic action against a model epoxide. *J. Nat. Prod.* **2013**, 76 (10), 1958-1965.

Included as Appendix-C. Chapter IV includes some of the work described in this publication.

Contributor	Statement of contribution
Hung H. T. (Candidate)	Designed experiments (50%) Wrote the paper (50%) Edited the paper (20%)
Mölzer, C.	Designed experiments (50%) Wrote and edited paper (50%) Edited the paper (40%)
Huber, H.	Supervision and discussions (5%) Edited the paper (2%)
Steyrer, A.	Supervision and discussions (5%) Edited the paper (2%)
Ziesel, G. V.	Supervision and discussions (5%) Edited the paper (2%)
Wallner, M.	Supervision and discussions (5%) Edited the paper (2%)
Blanchfield, J. T.	Supervision and discussions (50%) Edited the paper (12%)
Bulmer, A. C.	Supervision and discussions (10%) Edited the paper (10%)
Wagner, K. H.	Supervision and discussions (20%) Edited the paper (10%)

Contributions by others to the thesis

A/Prof. Joanne Blanchfield: Conception and design of the project, supervision, discussion, assistance with interpretation of data, and thesis editing;

Prof. James De Voss: Conception and design of the project, supervision, discussion, assistance with interpretation of data, and thesis editing;

Dr. Andrew Bulmer: Conception and design of chapter VI and chapter II, supervision, discussion, assistance with interpretation of data, and thesis editing;

Dr. Abu-Bakar, A'edah: Conception and design of chapter VI, supervision, discussion, assistance with interpretation of data, and thesis editing.

Statement of parts of the thesis submitted to qualify for the award of another degree

None

Acknowledgements

Firstly, I would like to thank my principal supervisor, Associate Professor Joanne Blanchfield who allowed me the opportunity to study in this interesting and challenging project. I am extremely grateful to you for your support in all aspects of my academic development. I especially appreciate your valuable criticism and expert guidance during my research candidature and assistance in editing this thesis.

I also wish to thank my co-advisor, Professor James De Voss who always provides useful advice and constructive criticism. James provided me with advanced facilities and also helped me to correct data analysis in my reports.

I sincerely wish to thank Dr Andrew Bulmer from the School of Medical Science, Griffith University and Dr Abu-Bakar A'edah from the National Centre for Environmental Toxicology for allowing me the opportunity to work in your laboratories. I am extremely grateful to you for your invaluable advice, editing my thesis, and the provision of technical support during my time working on the human liver S9 project. I am also grateful to Professor Mary Garson for her constructive criticism, knowledgeable feedback and helping me to develop critical thinking skills.

Thank you to past and present laboratory members and research groups, Joanne Blanchfield and James De Voss who provided much assistance during my working time in the laboratory. I would also like to thank Dr Tri Le and Mr Graham McFarlane for their NMR and MS expertise. Thank you to the general staff within SCMB and International Student Services who provided me with excellent service.

Very special thanks to my dear friends who have remained by my side during my study time at The University of Queensland.

Finally, warmest thanks and appreciation to my family, my college, the School of Chemistry and Molecular Biosciences and The University of Queensland for providing finance and supporting my spirit during my studies. I specially thank my wife, Anh, my dear little sons who have brought me great inspiration and motivation to complete my difficult project. I wish to express my deep gratitude to my mum and dad for unlimited encouragement and support for my studies at all levels.

Hung Trieu Hong

July, 2015

Keywords

Anti-mutagens, bile pigments, unconjugated bilirubin, styrene epoxide, caco-2 cell monolayer, chemical interactions, physical interactions, metabolism, inhibition.

Australian and New Zealand Standard Research Classifications (ANZSRC)

ANZSRC code: 030503, Organic Chemical Synthesis, 40%;

ANZSRC code: 030499, Medicinal and Biomolecular Chemistry not elsewhere classified, 50%;

ANZSRC code: 060199, Biochemistry and Cell Biology not elsewhere classified, 10%

Fields of Research (FoR) Classification

FoR code: 0305, Organic Chemical, 40%;

FoR code: 0304, Medicinal and Biomolecular Chemistry, 50%;

FoR code: 0601, Biochemistry and Cell Biology, 20%

Table of Contents

Abstract	ii
Declaration by author	iv
Publications during candidature	v
Publications included in this thesis	v
Contributions by others to the thesis	vii
Statement of parts of the thesis submitted to qualify for the award of another degree	vii
Acknowledgements	viii
Keywords	ix
Australian and New Zealand Standard Research Classifications (ANZSRC)	ix
List of Symbols and Abbreviations	xxv
Chapter 1: Introduction and literature review	1
1.1 Bile pigments.....	1
1.2 The biological properties of bile pigments and their derivatives	3
1.2.1 Anti-mutagenic effects of bile pigments	3
1.2.2 Physical interactions between mutagens and bile pigments	4
1.2.3 Bilirubin is substrate of cytochrome 1A2 (CYP 1A2), CYP 1A1, 2A6	5
1.3 Chemical studies of bile pigments.....	6
1.3.1 Unconjugated bilirubin-IX α	6
1.3.2 Biliverdin	10
1.3.3 Protoporphyrin	11
1.4 Mutagens	13
1.4.1 Benzo[α]pyrene	13
1.4.2 2-Aminofluorene	14
1.4.3 2-Amino-1-methyl-6-phenylimido[4,5-b]pyridine	15
1.5 Caco-2 cell monolayers	16

1.6	Conclusion and Hypothesis	17
1.7	Research Aims and Plans	18
1.8	Determining physical interactions between mutagens and bile pigments and their dimethyl esters	18
1.9	Determining chemical interactions between mutagens and bile pigments and their dimethyl esters	18
1.10	Investigating the inhibitory effects of BPs on the mechanism of mutagens in the human liver S9 fraction.....	18
Chapter 2: Physical interactions between bile pigments, biliverdin, unconjugated bilirubin, protoporphyrin and environmental mutagens, 2AF, PhIP, B[α]P.....		20
2.1	Introduction	20
2.2	Results and Discussion	23
2.2.1	Biliverdin and 2AF, PhIP, B α P	23
2.2.2	BRU and 2AF, PhiP, B α P.....	26
2.2.3	Protoporphyrin (2.1) and 2AF, PhiP, B α P	29
2.2.4	Dimethyl ester of BPs and 2AF, PhiP, B α P	31
2.3	Conclusion.....	31
2.4	Experimental.....	32
2.4.1	BV and 2AF, PhiP, B α P	33
2.4.2	BRU and 2AF, PhiP, B α P.....	35
2.4.3	PRO and 2AF, PhiP, B α P	36
2.4.4	Dimethyl ester of BPs and 2AF, PhiP, B α P	37
2.4.5	2AF and BV, BRU, PRO	39
2.4.6	PhiP and BV, BRU, PRO.....	39
2.4.7	B[α]P and BV, BRU, PRO	40
Chapter 3: Investigation of the effects of bile pigments on the permeability of PhIP across intestinal epithelial cells.....		41
3.1	Introduction	41

3.2	Results and discussion	43
3.2.1	Permeability of PhIP in the presence and absence of bile pigments	43
3.2.2	Permeability of benzo[α]pyrene in the presence and absence of bile pigments	49
3.3	Conclusion and future developments	50
3.4	Experimental.....	52
3.4.1	Chemicals and Biological Materials	52
3.4.2	Caco-2 cell culture	52
3.4.3	Caco-2 bioassay preparation and transport experiments.....	53
3.4.4	Preparation of Standard Solutions and Calibration Curves.....	54
3.4.5	Statistical analysis	56
Chapter 4:	Synthesis of pyrroles, dipyrroles and bile pigment esters.....	57
4.1	Introduction	57
4.2	Results and discussion.....	59
4.2.1	Synthesis of 2,3,4,5-tetramethylpyrrole (4.3)	59
4.2.2	Synthesis of substituted dipyrroles	60
4.2.3	Synthesis of dimethyl ester of BPs.....	65
4.3	Conclusion.....	71
4.4	Experimental.....	72
4.4.1	2,3,4,5-Tetramethyl pyrrole	72
4.4.2	Synthesis of dipyrroles	72
4.4.3	Synthesis of bilirubin-IX α dimethyl ester (4.11), biliverdin-IX α dimethyl ester (4.12), protoporphyrin-IX α dimethyl ester (4.13)	74
Chapter 5:	Model epoxide studies	76
5.1	Introduction	76
5.2	Results and discussion.....	79
5.2.1	Model reactions of indole, imidazole and guanine with styrene epoxide	79
5.2.2	The reactions of styrene epoxide with bile pigments and its derivatives.....	91
5.2.3	Competition reactions	102

5.3	Conclusions	103
5.4	Experimental.....	105
5.4.1	General materials and methods	105
5.4.2	Experimental	106
Chapter 6: Exploring the inhibitory effects of endogenous bile pigments on 2-Amino-1-methyl-6-phenylimidazo[4,5-b]pyridine and Benzo[α]Pyrene metabolic activation by cytochrome P450 enzymes.....		114
6.1	Introduction	114
6.2	Results and discussion.....	116
6.2.1	In vitro metabolism of 6.4 and 6.1 by a human liver S9 fraction	116
6.2.2	Inhibitory effects of bile pigments on 6.1 and 6.4 metabolism in the human liver S9 fraction.....	120
6.2.3	Docking simulation of 6.1, 6.4 and BPs on CYP1A1, 1A2 and 1B1 active sites....	125
6.3	Conclusions	134
6.4	Experimental.....	135
6.4.1	Metabolism of 6.4 and 6.1 in vitro.....	136
6.4.2	The inhibitory effects of BPs on 6.4 and 6.1 degradation in vitro.....	136
Chapter 7: Conclusion and future direction.....		137
References.....		141
Appendix-A.....		164
Appendix-B.....		169
Appendix-C.....		175
Appendix-D.....		179
Appendix-E.....		181

List of Figures

Figure 1.1: The metabolism of haem to form BPs (1.1 and 1.2) in mammals.....	1
Figure 1.2: Isomers of 1.2 (BV) produce from the breakdown of haem and the opening of protoporphyrin-IX at different carbon bridges by haem oxygenase. ⁷⁻⁹	2
Figure 1.3: The enantiomers of (4Z, 15Z)-bilirubin (<i>P</i> =plus, <i>M</i> =minus) demonstrate the presence of ‘ridge-tile’ conformers via the formation of six intramolecular hydrogen bonds. ^{58,59}	7
Figure 1.4: Configurational photo-isomerisation of (4Z,15Z)-bilirubin, leading to the formation of four isomers, (4 <i>E</i> ,15Z)-, (4Z,15 <i>E</i>)- and (4 <i>E</i> ,15 <i>E</i>)-bilirubin. ^{8,66,67}	8
Figure 1.5: The formation of adducts with the pyrrole rings nearby producing a new ring.	8
Figure 1.6: The isomerisation of 1.1 (UCB) in acid environment in which the protonation of carbons nearby C-10 to break the C-10 bridge covalent bond and produce four different dipyrrolic units and then randomly reassemble the C-10 covalent bond. ^{66,68,69,74}	9
Figure 1.7: The photooxidation products of 1.1 (UCB) in the exposure to air and light. ⁶⁶	10
Figure 1.8: Photoisomerisation of 1.2 (BV).....	11
Figure 1.9: Haem biosynthetic pathway from protoporphyrinogen IX. ⁸⁷	12
Figure 1.10: Products of the photooxidation of 1.3 (PRO) in the presence of light and oxygen.....	13
Figure 1.11: The metabolism of 1.7 (B α P) by P450 enzymes and the formation of products when benzo[α]pyrene-7,8-diol-9,10-epoxide reacts with DNA. ^{99,104}	14
Figure 1.12: The metabolism of 1.5 (2AF) by P450 enzymes and some nucleophilic positions of deoxyguanosine in DNA that can be attacked by oxidization products of 1.5 (2AF), N-acetyltransferase (NAT), sulfotransferase (ST). ^{105,108,109}	15
Figure 1.13: Proposed pathway of oxidization and DNA conjugation of PhIP.....	16
Figure 2.1: Overlay of the UV spectra of the mixtures of 2.9 (2AF, 1 μ M in methanol, 0.5 μ M in buffer) and varying concentrations of 2.2 (UCB, from 0.5 μ M to 2.5 μ M in methanol (left) and from 0.25 μ M to 0.5 μ M in buffer (right)). The red line close to the baseline (λ_{\max} 288 nm) was the UV spectra of 2.9 (2AF). The introduction of 2.2 (UCB, from 0.25 μ M to 2.5 μ M) in the mixture was detected by the increasing UV absorbance at 450 nm.	27
Figure 2.2: Overlay of the UV spectra of the mixtures of 2.9 (2AF, 1 μ M) and varying concentrations of 2.3 (BV, from 0.5 μ M to 0.75, 1, 1.5, 2 μ M) in methanol (left) and buffer (right). The red line with a signal peak at 288 nm was the UV spectra of 2.9 (2AF). The introduction of 2.3 (BV, from 0.5 μ M to 0.75, 1, 1.5, 2 μ M) in the mixture was detected by the increasing UV absorbance at 350 nm.....	33
Figure 2.3: Overlay of the UV spectra of the mixtures of 2.7 (PhIP, 1 μ M) and varying concentrations of 2.3 (BV, 1 μ M) in methanol (left) and buffer (right). The red line (right) and blue	

line (left) with signal peaks at 317 nm was the UV spectra of 2.7 (PhIP). The introduction of 2.3 (BV, from 1 μ M to 3 μ M) in the mixture was detected by the increasing UV absorbance at 350 nm.

.....33

Figure 2.4: Overlay of the UV spectra of the mixtures of 2.8 (B α P, 1 μ M) and varying concentrations of 2.3 (BV, 1 μ M) in methanol (left) and buffer (right). The red line that was in close proximity to baseline (λ_{max} 295 nm) was the UV spectra of 2.8 (B α P). The introduction of 2.3 (BV, from 1 μ M to 2 μ M) in the mixture was detected by the increasing UV absorbance at 350 nm. 34

Figure 2.5: Overlay of the ^1H NMR spectra of 2.9 (2AF, blue) and its mixtures with varying concentrations of 2.3 (BV) performed at 500MHz in Sol B. The molar ratios of 2.9 (2AF) and 2.3 (BV are 2:1 (pink), 1:1 (red), 1:2 (yellow), 1:0 (blue in the presence of HCl and acetic acid) and 1:2 (green in the presence of 10 μ L of LiOH). 34

Figure 2.6: Overlay of the ^1H NMR spectra of 2.8 (B α P, blue) and its mixtures with varying concentrations of 2.2 (UCB) performed at 500MHz in Sol B. The molar ratios of 2.8 (B α P) and 2.2 (UCB) are 2:1 (red), 1:1 (green), 1:2 (purple). 35

Figure 2.7: Overlay of the ^1H NMR spectra of 2.7 (PhIP, blue) and its mixtures with varying concentrations of 2.2 (UCB) performed at 500MHz in Sol B. The molar ratios of 2.7 (PhIP) and 2.2 (UCB) are 2:0.5 (red), 2:0.75 (green), 1:1.5 (purple). 35

Figure 2.8: Overlay of the ^1H NMR spectra of 2.9 (AF, blue) and its mixtures with varying concentrations of 2.2 (UCB) performed at 500MHz in Sol B. The molar ratios of 2.8 (B α P) and 2.2 (UCB) are 2:1 (red), 1:1 (green), 1:2 (purple). 36

Figure 2.9: The overlay of spectra of 2.8 (B α P, 1 μ M in methanol, 0.5 μ M in buffer) and varying concentrations of 2.1 (PRO, from 0.5 μ M to 3.0 μ M in methanol (left) and from 0.25 μ M to 0.75 μ M in buffer (right)). The red line (left) and black line (left) close to the baseline (λ_{max} 295 nm) was the UV spectra of 2.8 (B α P). The introduction of 2.1 (PRO, from 0.5 μ M to 3 μ M) in the mixture was detected by the increasing UV absorbance at 401 nm (left) and 385 nm (right). 36

Figure 2.10: Overlay of the ^1H NMR spectra of 2.9 (2AF, green) and its mixtures with varying concentrations of 2.1 (PRO) performed at 500MHz in Sol B. The molar ratios of 2.1 (PRO) and 2.7 (PhIP) are 1:1 (purple), 1:2 (blue). 37

Figure 2.11: Overlay of the ^1H NMR spectra of 2.7 (PhIP, green) and its mixtures with varying concentrations of 2.1 (PRO) performed at 500MHz in Sol B. The molar ratios of 2.1 (PRO) and 2.7 (PhIP) are 1:1 (purple, yellow), 1:2 (blue). 37

Figure 2.12: Overlay of the ^1H NMR spectra of 2.5 (UCBDE, yellow) and the mixtures of 2.8 (B α P) with varying concentrations of 2.5 (UCBDE, performed at 500MHz in Sol A. The molar ratios of 2.5 (UCBDE) and 2.8 B α P are 1:2 (blue), 1:1 (purple), 1:2 (green). 37

Figure 2.13: Overlay of the ¹ H NMR spectra of 2.5 (UCBDE, purple) and the mixtures of 2.9 (2AF) with varying concentrations of 2.5 (UCBDE, performed at 500MHz in Sol A. The molar ratios of 2.9 (2AF) and 2.5 (UCBDE) are 0.5:1 (green), 1:1 (brown).	38
Figure 2.14: Overlay of the ¹ H NMR spectra of 2.5 (UCBDE, blue) and its mixtures 2.7 (PhIP, performed at 500MHz in Sol A.....	38
Figure 3.1: Diagram of a well and an insert membrane used for culturing Caco-2 cell monolayers.	42
Figure 3.2: A comparison the percentage of 3.6 (PhIP) (10 μM) transported from AP to BL over 180 min in the absence and presence of 3.1 (PRO), 3.2 (UCB), 3.3 (BV) with 10 μM).	45
Figure 3.3: A comparison the percentage of 3.6 (PhIP) transported from AP to BL in the absence and presence of varying concentrations of 3.2 (UCB, from 5 μM to 20 μM) and 10 μM of 3.4 (UCBDE).	45
Figure 3.4: RPHPLC results of standard solution of 3.7 (BαP) at 0.5 μM, overlaid with the results from samples collected from the receiver chamber after 30, 60 and 90 min incubation	50
Figure 3.5: The standard curves for 3.6 (PhIP) and 3.7 (BαP) in HBSS were obtained from RPHPLC.....	55
Figure 4.1: Synthesis of 2,3,4,5-tetramethylpyrrole from butan-2-one (4.1) and diacetyl monoxime (4.2).....	59
Figure 4.2: The ¹ H NMR spectrum of 4.3 performed on a 500 MHz instrument in CDCl ₃ , the crossed peaks in the spectrum are the signals of ethanol which was difficult to fully remove from the compound.	60
Figure 4.3: The synthesis of 4.9 and 4.10 from the self-condensation of pyrrole-2-carboxylates in hydrobromic acid.	61
Figure 4.4: The synthetic route to 4.9 and 4.10 from ethyl 3-oxobutanoate (4.4).	61
Figure 4.5: The ¹ H NMR spectrum of 4.7a performed on a 500 MHz instrument in CDCl ₃	62
Figure 4.6: The HMBC correlations from protons of three methyl groups to tertiary carbons in pyrrole ring of 4.7b. Spectrum performed on a 500 MHz instrument in CDCl ₃	62
Figure 4.7: The ¹ H NMR spectrum of 4.7b performed on a 500 MHz instrument in CDCl ₃	63
Figure 4.8: The ¹ H NMR and HMBC spectra of 4.9 performed on a 500 MHz instrument in CDCl ₃	64
Figure 4.9: The ¹ H NMR spectrum of 4.10 performed on a 500 MHz instrument in CDCl ₃	64
Figure 4.10: The HMBC spectrum of 4.10 and the insert of the cross-peak from CH-bridge to C-3. All experiments were performed on a 500 MHz instrument in CDCl ₃	65
Figure 4.11: The ¹ H NMR spectrum of 4.11 performed on a 500 MHz instrument in DMSO- <i>d</i> ₆	68
Figure 4.12: The long range correlations (HMBC) between protons and carbons of 4.11. Spectrum performed on a 500 MHz instrument in DMSO- <i>d</i> ₆	69

Figure 4.13: The ^1H NMR spectrum of 4.12 performed on a 500 MHz instrument in $\text{DMSO-}d_6$	69
Figure 4.14: The ^1H NMR spectrum of 4.13 overlaid with ^1H NMR of protoporphyrin. Insert: an expanded region of the ^1H spectrum from 3.50 to 3.75 ppm. All experiments were performed on a 500 MHz instrument in $\text{DMSO-}d_6$	70
Figure 5.1 A simplified summary of the metabolism of 5.1 and 5.4 leading to DNA-adduct formation. Insert: the structure of 5.7 chosen as a mimic for 5.2 and 5.5 in the reactivity studies. ...	77
Figure 5.2: The structures of the BPs as well as that of imidazole (5.11) and indole (5.12) chosen as mimics for BPs in initial reactivity studies.	78
Figure 5.3: The mechanism of the reaction between 5.7 and 5.12 with silica. ²³⁴	79
Figure 5.4: The ^1H NMR spectra of three mono-phenylethanol substituted adducts of 5.12 and the spectrum of 5.12 is provided for comparison. All experiments performed at 500 MHz in $\text{DMSO-}d_6$	82
Figure 5.5: The ^1H NMR spectrum of five bis-phenylethanol substituted adducts of 5.12. All experiments were run on a 500 MHz machine in a mixture of $\text{DMSO-}d_6$	86
Figure 5.6: The RPHPLC trace of the methanol fraction from the reaction of 5.23 and 5.7 using gradients of 0.1% TFA in water (solvent A) and 0.1% TFA in MeCN (solvent B). Insert: The further resolution of major peak achieved using isocratic conditions of 8% solvent B.....	88
Figure 5.7: Positive ion mode MS/MS spectra of products from the reaction of 5.23 and 5.7 that consist of two units of phenylethanol and one of guanine.....	89
Figure 5.8: Positive ion mode MS/MS spectra of products from the reaction of 5.23 and 5.7 that consist of two three units of phenylethanol and one of guanine.	89
Figure 5.9 : An expanded region of the proton NMR spectrum of compounds (5.27, 5.28) performed at 500 MHz in $\text{DMSO-}d_6$	92
Figure 5.10: An expanded region of the proton NMR spectrum of 5.31 performed at 500 MHz in $\text{DMSO-}d_6$	93
Figure 5.11: An expanded region of the proton NMR spectrum of compounds (5.29, 5.30) performed at 500 MHz in $\text{DMSO-}d_6$	96
Figure 5.12: The structure of 5.32 and an expanded region of the HMBC spectrum of 5.32 showing the key correlations used to identify the structure. All experiments were performed at 500 MHz in $\text{DMSO-}d_6$	97
Figure 5.13: The negative ESIMS result of bilirubin mono phenylethanol ester.	99
Figure 5.14: The mixture of one to four units of 5.7 bonding to 5.9 (UCB) and 5.10 (BV) in the mixture reaction between 5.9 (UCB) and 5.7.	99
Figure 5.15: ESIMS spectrometry of two minor products in positive ion obtaining from the reaction between 5.8 and 5.7.....	111

Figure 5.16: ESIMS spectrometry of two minor products in positive ion obtaining from the reaction between 5.10 and 5.7.....	111
Figure 5.17: ESIMS spectrometry of the first fraction that was collected from the reaction between 5.35 and 5.7.....	112
Figure 5.18: ESIMS spectrometry of the second fraction that was collected from the reaction between 5.35 and 5.7.....	112
Figure 5.19: ESIMS spectrometry of a product obtained from the reaction between 5.37 and 5.7.	112
Figure 5.20: ESIMS/MS spectrometry of a product obtained from the reaction between 5.39 and 5.7.....	113
Figure 5.21: ESIMS spectrometry of a product obtained from the reaction between 5.38 and 5.7.	113
Figure 6.1: Metabolism of 6.1 and 6.4 by P450 enzymes leading to the formation of macromolecular adducts with DNA. ^{127,221,223}	114
Figure 6.2: Overlay of the HPLC chromatograms of 6.1 (B α P) analysis from metabolism experiments with the human liver S9 fraction from 0-45 min, λ_{max} 317 nm.	117
Figure 6.3: Overlay of the HPLC chromatograms of 6.4 (PhIP) analyses from metabolism experiments with the human liver S9 fractions at 0-45 min.	118
Figure 6.4: Kinetics of 6.1 (B α P) and 6.4 (PhIP) degradation by the human liver S9 fraction after 20 min of incubation (n = 3 per concentration).	119
Figure 6.5: Representative overlay of UV spectra of 6.4 (left-blue) and 6.1 (right-red) and its mixtures with various concentrations of 6.8.	120
Figure 6.6: Effects of bile pigments on the degradation of 6.4 in human liver S9 fraction (n = 3).	121
Figure 6.7: Effects of BPs on degradation of 6.1 (B α P) in human liver S9 fraction (n = 3).....	121
Figure 6.8: Configurational photo-isomerisation of 6.7 (UCB), leading to the formation of four isomers (4Z,15Z)-, (4E,15Z)-, (4Z,15E)-, (4E,15E).....	124
Figure 6.9: The enantiomers of (4Z, 15Z)-bilirubin (P=plus, M=minus) demonstrate the presence of ‘ridge-tile’ conformers via the formation of intramolecular hydrogen bonds. ^{58,59}	125
Figure 6.10: The docking of 6.1 (B α P) into the active site of CYP1A1 (a), CYP1B1 (b), CYP1A2 (c) and CYP3A4 (d). Simulations were performed using Molegro Virtual Docker.	129
Figure 6.11: The docking of 6.4 into the active site of CYP1A1(a), CYP1B1(b) and CYP1A2(c). Simulations were performed using Molegro Virtual Docker.....	129
Figure 6.12: The interactions of 6.7 (UCB) with amino acids on the active site of CYP1A1(a), CYP1A2(c), CYP1B1(b) and CYP3A4(d).	131
Figure 6.13: The interactions of 6.6 (PRO) with amino acids in the active site of CYP1A1(a), CYP1A2(c), CYP1B1(b) and CYP3A4(d).	132

Figure 6.14: The interactions of 6.8 (BV) with amino acids in the active site of CYP1A1(a), CYP1A2(c), CYP1B1(b) and CYP3A4 (d).	133
Figure 7.1: ¹ H NMR spectrum of 2.9 performed at 500 MHz in sol B.....	164
Figure 7.2: Overlay of the ¹ H NMR spectra of mixtures of 2.8 (blue) and its mixtures with varying concentrations of 2.1 performed at 500 MHz in Sol B, the mole ratio between 2.1 and 2.8 are 2:1 (red), 1:1 (green), 1:2 (puple), 1:2 (black-yellow in the presence of 1 drop of D ₂ O).....	164
Figure 7.3: Overlay of the ¹ H NMR spectra of 2.6 (brown) and its mixtures with 2.9 performed at 500 MHz in Sol A, the mole ratio between 2.6 and 2.9 are 2:1 (red), 1:1 (puple), 2:1 (blue).....	165
Figure 7.4: Overlay of the ¹ H NMR spectra of 2.6 (brown) and its mixtures with varying concentration of 2.8 performed at 500 MHz in Sol A, the mole ratio between 2.6 and 2.8 are 1:2 (puple), 1:1 (blue), 2:1 (green).....	165
Figure 7.5: Overlay of the ¹ H NMR spectra of 2.6 (brown) and its mixtures with 2.7 performed at 500 MHz in Sol A, the mole ratio between 2.6 and 2.7 are 1:1 (blue).	165
Figure 7.6: Overlay of the ¹ H NMR spectra of 2.4 (puple) and its mixtures with 2.9 performed at 500 MHz in Sol A, the mole ratio between 2.4 and 2.9 are 1:1 (green).	166
Figure 7.7: Overlay of the ¹ H NMR spectra of 2.4 (puple) and its mixtures with 2.8 performed at 500 MHz in Sol A, the mole ratio between 2.4 and 2.8 are 1:1 (green).	166
Figure 7.8: Overlay of the ¹ H NMR spectra of 2.4 (puple) and its mixtures with 2.7 performed at 500 MHz in Sol A, the mole ratio between 2.4 and 2.7 are 1:1 (brown).....	166
Figure 7.9: Overlay of the UV spectra of the mixture between 2.7 (0.5 μM in methanol (left)), 2.8 (0.5 μM in methanol (right) and varying concentrations of 2.2 (from 0.25 μM to 1.0 μM in methanol). The blue line (left) and red line (right) that were in close proximity to baseline (λ _{max} 317 nm 295 nm, respectively) were the UV spectra of 2.7 and 2.8. The introduction of 2.2 (from 0.25 μM to 1.0 μM) in the mixture was detected by the increasing UV absorbance at 450 nm in other overlaid spectra.	167
Figure 7.10: Overlay of the UV spectra of the mixture between 2.9 (1.0 μM in methanol (left) and 0.25 μM in buffer (right)) and varying concentrations of 2.1 (from 0.5 μM to 2.0 μM in methanol and from 0.25 μM to 1.5 μM). The black line (left) and blue line (right) that were in close proximity to baseline (λ _{max} 288 nm) were the UV spectra of 2.9. The introduction of 2.1 (from 0.5 μM to 2.0 μM) in the mixture was detected by the increasing UV absorbance at 401 nm and 385 nm in buffer nm in other overlaid spectra.....	167
Figure 7.11: Overlay of the UV spectra of the mixture between 2.7 (1.0 μM in methanol (left) and 1.0 μM in buffer (right)) and varying concentrations of 2.1 (from 0.5 μM to 2.5 μM in methanol and from 0.25 μM to 1.0 μM). The black line (right) and red line (right) that were in close proximity to baseline (λ _{max} 317 nm) were the UV spectra of 2.7. The introduction of 2.1 (from 0.5 μM to 2.0 μM)	

in the mixture was detected by the increasing UV absorbance at 401 nm in methanol and 385 nm in buffer nm in other overlaid spectra.	168
Figure 7.12: The HMBC correlations from protons to carbons of 4.12 performed on a 500 MHz instrument in DMSO- <i>d</i> ₆	175
Figure 7.13: The HMBC correlations from protons to carbons of 4.12 performed on a 500 MHz instrument in DMSO- <i>d</i> ₆	175
Figure 7.14: The ¹³ C NMR spectroscopy of 4.12 performed on a 500 MHz instrument in DMSO- <i>d</i> ₆	176
Figure 7.15: The HMBC correlations from protons to carbons of 4.11 performed on a 500 MHz instrument in DMSO- <i>d</i> ₆	176
Figure 7.16: The HMBC correlations from protons to carbons of 4.12 performed on a 500 MHz instrument in DMSO- <i>d</i> ₆	177
Figure 7.17: The HMBC correlations from protons to carbons of 4.13 performed on a 500 MHz instrument in DMSO- <i>d</i> ₆	177
Figure 7.18: The HMBC correlations from protons to carbons of 4.13 performed on a 500 MHz instrument in DMSO- <i>d</i> ₆	177
Figure 7.19: The HMBC correlations from protons to carbons of 4.13 performed on a 500 MHz instrument in DMSO- <i>d</i> ₆	178
Figure 7.20: The HMBC correlation from protons of three methyl groups to tertiary carbon in pyrrole ring of 8b performed on a 500 MHz instrument in CDCl ₃	178
Figure 7.21: ESI-MS spectrometry of unexpected products in positive ion obtaining from first fraction of the reaction between 5.10 and 5.7.	179
Figure 7.22: An expanded region of the HMBC spectrum of 5.13 showing the key correlations used to identify the structure. All experiments were performed at 500 MHz in DMSO- <i>d</i> ₆	179
Figure 7.23: An expanded region of the HMBC spectrum of 5.15 showing the key correlations used to identify the structure. All experiments were performed at 500 MHz in DMSO- <i>d</i> ₆	179
Figure 7.24: ESI-MS spectrometry of polymers in positive ion obtaining from first fraction of the reaction between 5.10 and 5.7.....	180
Figure 7.25: ESI-MS spectrometry of a fraction obtaining from the reaction between 5.9 and 5.7.	180
Figure 7.26: HRESI-MS spectra of compound 5.24, an example of a 1:1 adduct of 5.23 and 5.7..	180
Figure 7.27: Prism statistic applied for the data collected from the inhibition experiments of BPs to 6.4 using dose-response curves-inhibition for nonlinear regression.....	183
Figure 7.28: Prism statistic applied for the data collected from the inhibition experiments of BPs to 6.1 using dose-response curves-inhibition for nonlinear regression.....	184

Table of Tables

Table 2.1: A comparison of selected proton signals of 2.3 with different mutagens present.	24
Table 2.2: A comparison of selected proton signals of 2.3 in the absence and presence of 2.9 and CH ₃ NH ₂	25
Table 2.3: A comparison of selected proton signals of 2.2 with different mutagens present.	28
Table 2.4: A comparison of selected proton signals of 2.1 with different mutagens present.	30
Table 2.5: A comparison of selected proton signals of 2.9 with different BPs present.	39
Table 2.6: A comparison of selected proton signals of 2.7 with different BPs present.	39
Table 2.7: A comparison of selected proton signals of 2.8 with different BPs present.	40
Table 2.8: The pH of mutagens in the presence of BPs in sol A and sol B.	40
Table 3.1: Total amount of 3.6 transferred to BL and remained in the AP chamber and associated with the cell monolayers (nmol) from 0 to 180 min in control experiments (n = 3).	43
Table 3.2: Total amount of 3.6 transferred to BL and remained in the AP chamber and associated with the cell monolayers (nmol) in the presence of 3.4 from 0 to 180 min (n = 3).	44
Table 3.3: Total amount of 3.6 transferred to BL and remained in the AP chamber and associated with the cell monolayers (nmol) in the presence of 3.2 from 0 to 180 min (n = 3).	46
Table 3.4: Total amount of 3.6 transferred to BL and remained in the AP chamber and associated with the cell monolayers (nmol) in the presence of 3.3 from 0 to 180 min (n = 3).	48
Table 3.5 A comparison of P _{app} and the percentage of 3.6 remaining in AP, trapped in or on the cell monolayer and transported to BL over 180 min in the presence and absence of 3.1, 3.2, 3.3, 3.4, 3.5.	48
Table 3.6: TEER values were measured from the first plate before the experiment, immediately after and after 30 hours incubation after the experiments were completed.	54
Table 3.7: TEER values were measured from the first plate before the experiment, immediately after and after 30 hours incubation after the experiments were completed.	54
Table 3.8: The solutions of 3.6 and BPs prepared for the permeability assays.	55
Table 3.9: The solutions of 3.6 and varying concentrations of 3.2 prepared for permeability assays.	55
Table 3.10: The solutions of 3.7 and BPs prepared for the permeability assays.	55
Table 3.11: A summary of rules for combining standard deviation error. ¹⁷⁶	56
Table 4.1: ¹ H NMR and ¹³ C NMR of 4.11 performed in DMSO- <i>d</i> ₆ and the published data for the same compound. ^{210, 211}	67
Table 5.1: NMR Spectroscopic Data (500 MHz, DMSO- <i>d</i> ₆) for compound 5.13.....	80
Table 5.2: ¹ H and ¹³ C NMR data for compound (5.14, 5.15).	81
Table 5.3: ¹ H and ¹³ C NMR data for compound (5.16 and 5.19).	83

Table 5.4: ^1H and ^{13}C NMR data for compound (5.18 and 5.20).	84
Table 5.5: ^1H and ^{13}C NMR data for compound (5.17).	85
Table 5.6: ^1H and ^{13}C NMR data for 5.21 and 5.22.	87
Table 5.7: ^1H and ^{13}C NMR data for 3.24, 3.25 and 3.26.	90
Table 5.8: ^1H and ^{13}C NMR data for 5.27, 5.28, 5.29 and 5.30.	93
Table 5.9: ^1H and ^{13}C NMR data for 5.31 and 5.32.	97
Table 5.10: Ten minor products created from the reaction between 5.23 and 5.7 collected from RP-HPLC.	109
Table 6.1: Time-course of the in vitro degradation of 6.4 and 6.1 by human liver S9 (n = 3).	118
Table 6.2: Michaelis-Menten kinetics of 6.1 and 6.4 degradation by the human liver S9 fraction in the period of 20 min, EC_{50} is the concentration of mutagens at which the degradation rate achieves 50%.	119
Table 6.3: Potency of BPs inhibitory effects on 6.1 and 6.4 degradation in the human liver S9 fraction, IC_{50} values were derived from the GraphPad Prism using non-linear regression analysis (see Table 7.18 and Table 7.19 in Appendix-E)	122
Table 6.4: Effects of BPs (10 μM) on degradation rate of 6.1 (1.5 μM) and 6.4 (1.5 μM) in rat liver S9 fraction (n = 3).	123
Table 6.5: Effects of BPs (10 μM) on degradation rate of 6.1 (1.5 μM) and 6.4 (1.5 μM) in human liver S9 fraction (n = 3).	123
Table 6.6: Active site amino acid residues of human CYP 1A2 ²⁵⁸ , 1A1 ²⁵⁸ , 3A4 ²⁷⁷ and 1B1 ^{27,58} , Amino acid residues that are conserved in all four P450s are shown. Residues that interact with 6.1 are highlighted using a grey background.	126
Table 6.7: A comparison of the active site residues of CYP1A2 found within a range of 4 Å distance from ligands docked into the active site (Figure 6.10, Figure 6.14). The grey background shows the same amino acids residues of the active site were found in the docking of CYP 1A2 with α -naphthoflavone. ²⁷⁶	127
Table 7.1: The concentration of 3.6 collected from the AP and BL chamber of wells during the assays.	169
Table 7.2: The linear regression and P_{app} of 3.6 in the presence of 3.2 (5 μM).	170
Table 7.3: The concentration of 3.6 collected from the AP and BL chambers from 0 to 180 min..	170
Table 7.4: The linear regression and P_{app} of 3.6 in the presence of 3.2 (10 μM).	170
Table 7.5: The concentration of 3.6 collected from the AP and BL chambers from 0 to 180 min..	171
Table 7.6: The linear regression and P_{app} of 3.6 in the presence of 3.2 (20 μM).	171
Table 7.7: The concentration of 3.6 collected from the AP and BL chambers from 0 to 180 min..	171
Table 7.8: The linear regression and P_{app} of 3.6 in the presence of 3.4 (10 μM).	171

Table 7.9: The concentration of 3.6 collected from the AP and BL chambers from 0 to 180 min..	172
Table 7.10: The linear regression and P_{app} of 3.6 in the presence of 3.5 (10 μ M).....	172
Table 7.11: The concentration of 3.6 collected from the AP and BL chambers from 0 to 180 min.	172
Table 7.12: The linear regression and P_{app} of 3.6 in the presence of 3.3 (10 μ M).....	173
Table 7.13: The concentration of 3.6 collected from the AP and BL chambers from 0 to 180 min.	173
Table 7.14: The linear regression and P_{app} of 3.6 in control experiments.	174
Table 7.15: The concentration of 3.6 collected from the AP and BL chambers from 0 to 180 min.	174
Table 7.16: The linear regression and P_{app} of 3.6 in the presence of 3.1 (10 μ M).....	174
Table 7.17: A list of hepatic enzymes and the results of enzyme activity tests performed by Sigma- Aldrich upon analysis of S9 human liver.....	181
Table 7.18: Prism statistic applied for the data collected from the inhibition experiments of BPs to 6.1 using dose-response curves-inhibition for nonlinear regression.....	182
Table 7.19: Prism statistic applied for the data collected from the inhibition experiments of BPs to 6.4 using dose-response curves-inhibition for nonlinear regression.....	183

List of Symbols and Abbreviations

Å	angstrom(s)	2AF	2-aminofluorene
α	specific rotation	λ_{\max}	absorbance maximum
γ	gyromagnetic ratio	B[α]P	benzo[α]pyrene
δ	chemical shift (NMR)	BR	unconjugated bilirubin IX α
ϵ	molar extinction coefficient	brd	broad doublet
η	viscosity	brm	broad multiplet
λ	wavelength	brs	broad singlet
MeCN	acetonitrile	br	broad signal (NMR)
Ac ₂ O	acetic anhydride	brt	broad triplet
AcOH	acetic acid	BV	biliverdin IX α
BP	bile pigment	Caco-2	colorectal adenocarcinoma cell line
BPs	bile pigments	DNA	deoxyribonucleic acid
calc.	calculated	EDTA	ethylenediamine tetraacetic acid
CDCl ₃	deuterated chloroform	HBSS	Hank's buffered salt solution
(CD ₃) ₂ SO	deuterated dimethylsulphoxide	ID ₅₀	50% inhibition dose
conc.	concentrated	M+H ⁺	mass plus proton
COSY	correlation spectroscopy	Me	methyl group
d	doublet (NMR) or day(s)	n	number of observations
DCM	dichloromethane	NADP	nicotinamide adenine dinucleotide phosphate
DMF	<i>N,N</i> -dimethylformamide	P _{app}	apparent permeability coefficient
D ₂ O	deuterium oxide	PBS	phosphate buffered saline
Et ₃ N	triethylamine	rpm	revolutions per minute
Et ₂ O	diethyl ether	S9	microsomal liver preparation
EtOAc	ethyl acetate	TNFone	2,4,7 trinitrofluorenone
HMBC	heteronuclear multiple-bond correlation spectroscopy	UCB	unconjugated bilirubin
HPLC	high-performance liquid	DMSO-	deuterated dimethyl sulfoxide

	chromatography	<i>d</i> ₆	
HRESIMS	high-resolution ESI mass spectrometry	mol	mole(s)
HSQC	heteronuclear single quantum correlation spectroscopy	mp.	melting point
Hz	hertz	MS	mass spectrometry
IR	infrared spectroscopy	<i>m/z</i>	mass-to-charge ratio (MS)
<i>J</i>	coupling constant (NMR)	NMR	nuclear magnetic resonance
K	Kelvin	ppm	parts per million
Lit	literature		
M	molar (moles per litre)	q	quartet (NMR)
MeOH	methanol	<i>R_f</i>	retention factor
mg	milligram(s)	rt	room temperature
min	minute(s)	s	seconds (time); singlet (NMR)
mL	millilitre(s)	TFA	trifluoroacetic acid
SO	styrene epoxide	PhIP	2-amino-1-methyl-6-phenylimidazo[4,5-b]pyridine
tr	retention time	TLC	thin layer chromatography
UV-Vis	ultraviolet-visible	TOCSY	total correlation spectroscopy

Chapter 1: Introduction and literature review

1.1 Bile pigments

Bile pigments (BPs) are the main chemical components of animal bile and have been popularly used in traditional medicine for centuries.^{1,2} BPs are endogenous compounds that are produced in the metabolism of hemoglobin from red blood cells recycled in the liver. This class of compounds includes biliverdin (**1.2**, BV), produced from haem by the action of haem oxygenase and NADPH reductase with a release of carbon monoxide and iron. Unconjugated bilirubin (**1.1**, UCB) is a product of further reduction of **1.2** (BV) by biliverdin reductase (Figure 1.1).^{3,4} Unconjugated bilirubin (**1.1**, UCB) is a highly hydrophobic compound which is conjugated to glucose by UDP-glucuronosyl transferase to form bilirubin diglucuronide (a hydrophilic compound) and excreted from the body. The degradation of haem produces approximately 300 mg of **1.1** (UCB) per day.^{5,6}

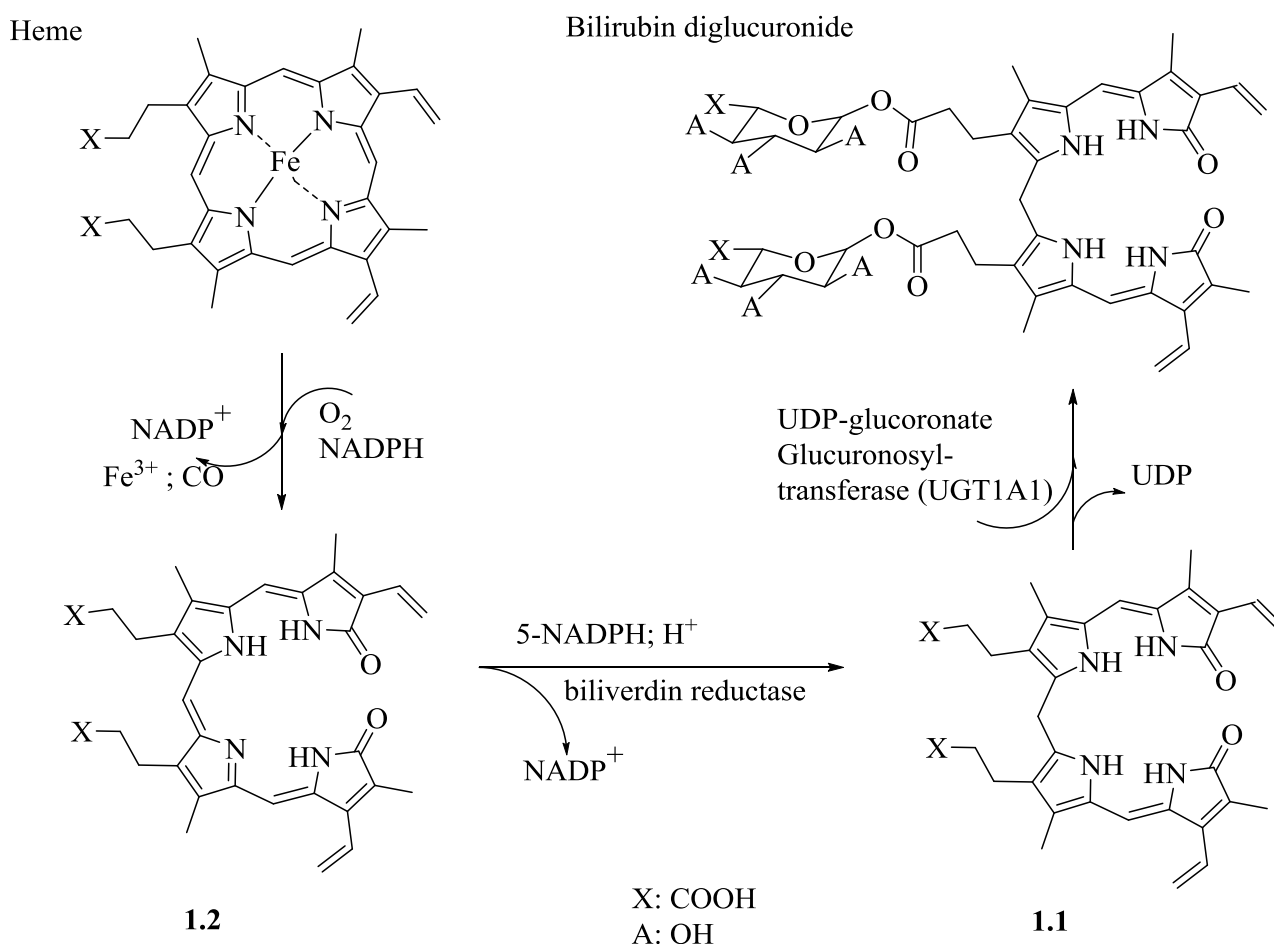


Figure 1.1: The metabolism of haem to form BPs (**1.1** and **1.2**) in mammals.

While senescent red blood cells release haemoglobin, enzymes open the protoporphyrin-IX (**1.3**, PRO) ring at different carbon bridge positions (α , β , γ , δ). These two processes create isomers of **1.2** (biliverdin IX α , IX β , IX γ , IX δ).^{7,8} These compounds were detected by HPLC in human serum from

jaundice patients by Adachi et al.⁸ Biliverdin IX β and IX α reductase then catalyses the reduction of biliverdin IX α (**1.2**, BV) and biliverdin IX β to the corresponding isomers of **1.1** (UCB) (Figure 1.2).^{7,9} Biliverdin isomers have identical polarity and are therefore very difficult to be isolated by column chromatography. To obtain pure **1.2** (BV), McDonagh conducted dehydrogenation of purified **1.1** (UCB) in DMSO solvent with 2,3-dichloro-5,6-dicyanobenzoquinone under argon atmosphere and obtained 70% yield.¹⁰

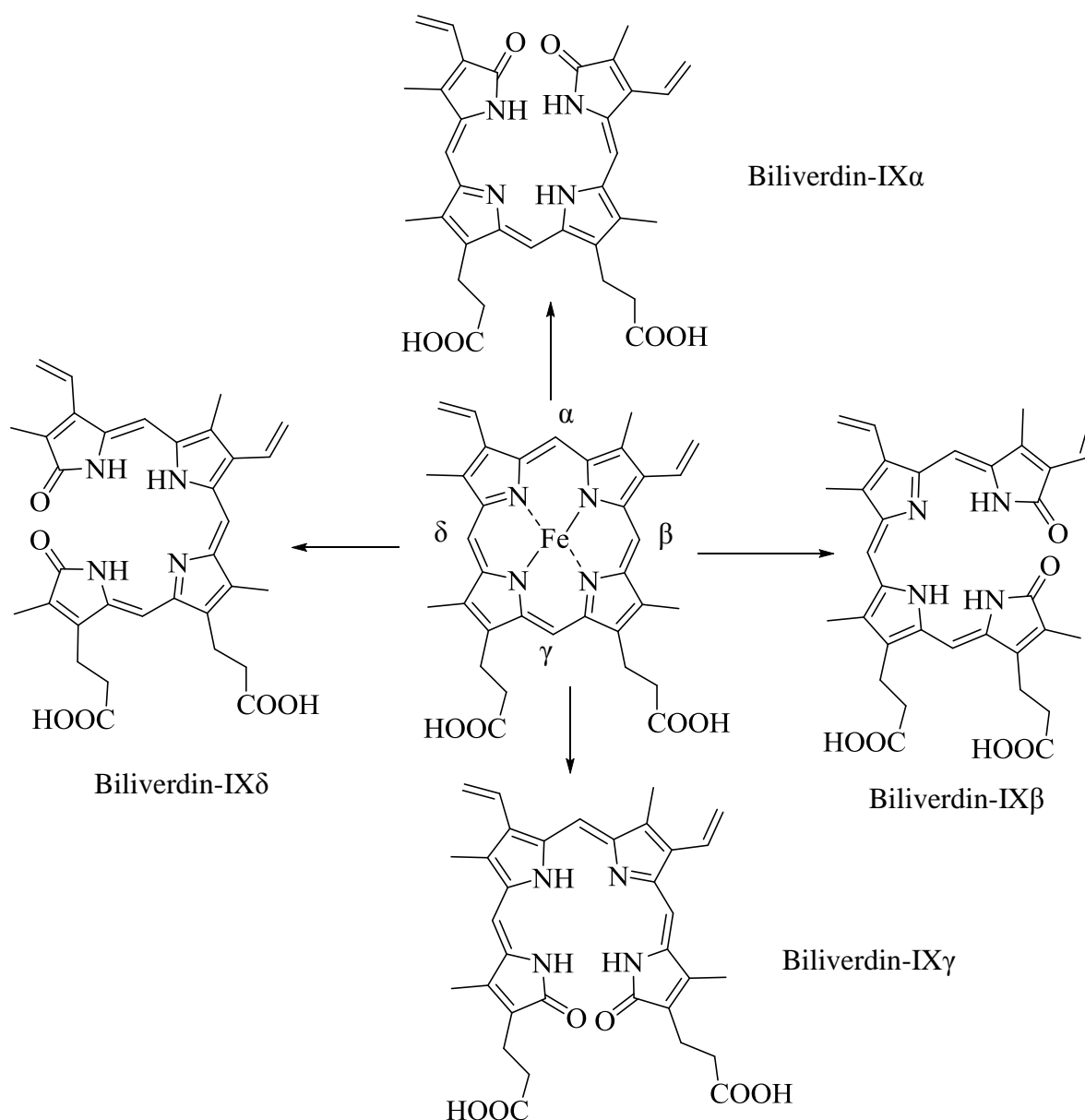


Figure 1.2: Isomers of **1.2** (BV) produce from the breakdown of haem and the opening of protoporphyrin-IX at different carbon bridges by haem oxygenase.⁷⁻⁹

Bile pigments (BPs), **1.1** (UCB), **1.2** (BV), and **1.3** (PRO) are biochemicals found in mammals. Unconjugated bilirubin and biliverdin are formed from the metabolism of haem and are the main components in animal bile¹ whereas **1.3** (PRO) is a biosynthetic intermediate in the production of haem and its synthesis is conserved in a wide range of organisms from bacteria to mammals.¹¹⁻¹³ All

of these compounds are often referred to as tetrapyrroles although compounds **1.1** (UCB) and **1.2** (BV) are in fact not tetrapyrroles as their structures consist of two conjugated pyrroles and two unsaturated lactam rings. As products of haem catabolism (**1.1** (UCB) and **1.2** (BV)) and a haem precursor **1.3** (PRO), we prefer to use BPs to refer to these three compounds throughout our studies. It is to be noted that these compounds will be differently numbered in each chapter.

1.2 The biological properties of bile pigments and their derivatives

Bile pigments (BPs) are known to be toxic to human beings at high concentrations,^{3,14,15} but are currently recognised as having potentially beneficial biological properties at low levels in blood.¹⁵⁻²¹ High concentrations of **1.1** (UCB) in the blood and bodily tissues leads to serious health problems such as jaundice, athetoid cerebral palsy, and hearing loss or deafness, particularly in newborn infants where the blood-brain barrier is not yet well formed and so may allow bilirubin to enter the brain.^{3,15} The beneficial biological effects of BPs and their derivatives have been of mounting interest recently as their potent anti-mutagenicity,^{15,18,19,21} and anti-oxidant properties^{18,22-28} come to light as well as their ability to bind to certain important enzymes.²⁹⁻³¹ The chemical details and their potential physiology properties will be reviewed in the following section.

1.2.1 Anti-mutagenic effects of bile pigments

Numerous studies have recently shown that BPs are important endogenous compounds with antioxidant, anti-mutagenic, and anti-cancer activities.^{14,17,22-28} Bulmer et al.^{15,18} showed that BPs effectively inhibited the genotoxic effects of tertiary-butyl hydroperoxide induced oxidative stress. Compound **1.1** (UCB) is proposed to act as an antioxidant by donation of a hydrogen radical from the C10-bridge^{15,18} or amide groups³² to free radicals to form stable carbon-centered radicals that then react with either other free radicals to form new covalent bonds or free oxygen.^{22,33}

The anti-mutagenic property of BPs was explored by Arimoto et al.^{34,35} who used benzo[α]pyrene (**1.7**) to promote the formation and development of revertants; in *Salmonella* strains TA100 and TA98 **1.1** (UCB), **1.2** (BV), **1.3** (PRO), and hemin were then used as inhibitors of the growth of these revertants. Manually counting and comparing the revertants formed in each experiment provided clear evidences to conclude the order of effectiveness of BPs on the B[α]P-induced mutagenesis: Hemin = **1.3** (PRO) > **1.1** (UCB) > **1.2** (BV). The same experiments were performed in the presence of a highly mutagenic metabolite of **1.7**, which showed the order of effectiveness at inhibiting DNA damage caused by mutagen: Hemin > **1.3** (PRO) > **1.1** (UCB) = **1.2**(BV). PhD work of our collaborator, Dr. Andrew Bulmer², studied the effects of BPs on the mutagenicity of some common environmental mutagens, **1.7**, 2,4,7-trinitro-9H-fluoren-9-one (**1.4**), and 2-

aminofluorene (**1.5**). The compounds were tested using the *Salmonella* reverse mutation assay using bacterial strains TA98, TA100, and TA102. The mutagens were used to promote revertant formation and growth on plates. The level of bacterial cell growth was determined by manual cell counting and the results for cells treated only with mutagens were compared to the results obtained from the same experiments with the addition of different BPs. The final results showed that the BPs were all effective at inhibiting the DNA damage caused by the mutagens and the order of effectiveness at inhibiting the mutagenic effects of **1.4** was: **1.1** (UCB) \geq bilirubin ditaurate (**1.6**) \geq **1.2** (BV); and the order of effectiveness against **1.5** was: **1.1** (UCB) \geq **1.2** (BV) \geq **1.6** in all strains (TA98, TA100, and TA102).¹⁸ Overall, the above-mentioned results indicated that **1.3** (PRO) has higher anti-mutagenic activation than **1.1** (UCB), followed by **1.2** (BV).

In a follow-up study, Molzer et al.,^{11,13} who used the same method, performed the experiments on *Salmonella Typhimurium* strains (TA102 and TA98) in the presence of rat liver S9 as a method of activating the mutagens. The study used aflatoxin B1 (AfB1) and 2-amino-1-methyl-6-phenylimidazo[4,5-b]pyridine (**1.8**) as environmental mutagens and a number of inhibitors such as **1.1** (UCB), **1.2** (BV), and **1.3** (PRO); bilirubin dimethyl ester (**1.9**); and biliverdin dimethyl ester (**1.10**) in order to test the promotion and inhibition of revertant growth. Comparing the number of revertant formation in each experiment indicated the order of effectiveness of the above inhibitors on the growth of mutagenesis in the presence of AfB1, to be **1.3** (PRO) $>$ **1.1** (UCB) = **1.6** $>$ **1.2** (BV) $>$ **1.9** $>$ **1.10** in strain TA102 and **1.10** $>$ **1.9** $>$ **1.3** (PRO) and **1.1** (UCB), **1.2** (BV), **1.6** did not inhibit any AfB1-induced mutagenesis in strain TA98. The studies also showed the order effectiveness of inhibitors on PhIP-induced mutagenesis was **1.3** (PRO) $>$ **1.1** (UCB) $>$ **1.2** (BV) $>$ **1.9** $>$ **1.6** $>$ **1.10** in strain TA98. It is concluded that the inhibitory action of these compounds depends on bacterial species, environmental mutagens, and the purity of inhibitors.

In general, the inhibitory effects of BPs on the revertant growth were investigated in many studies using bacteria.^{14,15,17,19,34,36,37} and all provided support for the powerful anti-mutagenicity of BPs. However, the mechanism by which this inhibition is achieved has not been elucidated. Understanding the inhibitory mechanism of BPs toward the action of environmental mutagens will greatly aid in our ability to combat these toxins

1.2.2 Physical interactions between mutagens and bile pigments

There have been many hypotheses put forward for the mechanism of action of BP's inhibition of mutagenesis. One such theory is that there are significant non-covalent attractive forces between the polyaromatic mutagens and the π -systems of the BPs resulting in aggregation. Although this is a

popular hypothesis,^{2,15,19,21} very few reports present evidence that these physical interactions contribute to the activity.^{21,38} Haino et al.³⁸ used variable temperature ¹H NMR in toluene-*d*₈ to detect stacked structures between 2,4,7-trinitro-9H-fluoren-9-one (**1.4**) and bisporphyrin, a compound belonging to the same class as BPs. Bulmer et al.^{15,18} recently hypothesised that physical interactions between BPs and mutagens may contribute to the inhibitory effects of BPs on environmental mutagens. In addition, Mölzer et al.²¹ used circular dichroism (CD) spectroscopy, vibrational circular dichroism (VCD), and infrared (IR) spectroscopy to explore the interactions between BPs and **1.4**. The spectra of some BPs and their derivatives in the presence and absence of **1.4** were compared. The results showed that the addition of **1.4** into the samples of BPs and their derivatives led to the variation of CD intensity of the blue band of BPs and significant changes in VCD and IR spectra. The studies suggested physical interactions between BPs and **1.4** are the cause of the modifications in CD, VCD, and IR spectra of BPs and their derivatives, and concluded that physical interactions could give rise to the anti-mutagenic actions of BPs.²¹

1.2.3 Bilirubin is substrate of cytochrome 1A2 (CYP 1A2), CYP 1A1, 2A6

Many previous studies have suggested that **1.1** (UCB) is a substrate for uridine 5'-diphosphoglucuronosyltransferase 1A1 (UGT-1A1)³⁹⁻⁴², CYP2A5⁴³, and some other enzymes, such as CYP 1A1,^{29,44-47} 1A2,^{44,48} and 2A6,^{30,31,49} that are responsible for the metabolism of mutagens. Phelan et al.²⁹ incubated guinea pig, rat, and human cells with 1 nM, 3 nM, and 5 nM of the environmental contaminant, 2,3,7,8-tetrachlorodibenzo-p-dioxin (TCDD), respectively and co-incubated with **1.1** (UCB) (50 µM) and **1.2** (BV) (50 µM) for 4 hours at 37 °C. TCDD is a substrate for CYP1A1 which converts it to reactive epoxide and then 8-OH-2,2,7-triCDD and 2-OH-1,3,7,8-tetraCDD.⁵⁰ Cells should increase the expression of this enzyme in response to exposure to TCDD or any of its other substrates. This was indeed found to be the case in these experiments. The study found the presence of **1.1** (UCB) (50 µM) can induce CYP1A1-luciferase to approximately 74%, 83%, and 100% of that induced from the activation of TCDD in the rat, guinea pig, and human cells respectively. The presence of **1.2** (BV) contributed to 80%, 76%, and 26% that of induced from TCDD. Therefore, the expression of the enzyme was also stimulated by the presence of **1.1** (UCB) and **1.2** (BV), with **1.1** (UCB) having a greater effect than **1.2** (BV). The study suggested that **1.1** (UCB) and **1.2** (BV) can act as competitive inhibitors of CYP1A1 slowing the metabolism of TCDD.²⁹

Christopher and John⁴⁵ determined the expression of CYP1A1 in Hepa 1c1c7 cell lines and recognised that the level of CYP1A1 increased significantly after 1 hour exposure to **1.1** (UCB) (100 µM) and **1.2** (BV) (100 µM), and after 2 hours exposure to hemin (100 µM). The presence of

1.1 (UCB) induced higher expression levels of CYP1A1 genes than **1.2** (BV) or hemin. Similarly to Phelan et al's study, **1.1** (UCB) and **1.2** (BV) were substrates of CYP1A1.⁴⁵ Kapitulnik and Gonzalez⁴⁷ measured the levels of CYP1A1 and 1A2 at 10 days to one month of age of non-jaundiced and jaundiced rats. The findings indicated that the levels of CYP1A1 and 1A2 were increased in jaundiced rats (high accumulation of **1.1** (UCB) in order to facilitate degradation of **1.1** (UCB) and elimination of the endogenously toxic chemical from the body of young rats.⁴⁷ All the above findings have been reviewed by Linh and Christopher⁵¹ and later by Bock.³⁹

Bilirubin was also believed to be a potent substrate for CYP2A6. Abu-Bakar et al.^{30,49} co-incubated **1.1** (UCB) and coumarin with CYP2A6 from mouse recombinant yeast microsomes and found that **1.1** (UCB) (at 10 μ M) can inhibit approximately 100% of coumarin 7-hydroxylation by CYP2A6. Similarly, Hiromi et al.³¹ conducted in vitro experiments with human hepatocytes within and without of 40 μ M of **1.1** (UCB) and found that the level of CYP2A6 increased to 1.7-fold compared to the control experiments. The study suggested **1.1** (UCB) induced CYP2A6 gene expression.³¹

In general, BPs could be inhibitors for a variety of enzymes that possess active functions for the metabolism of mutagens (see chapter IV for more details). Therefore, the presence of BPs could affect the rate of metabolism of mutagens.

1.3 Chemical studies of bile pigments

In order to understand how bile pigments (BPs) might interact with mutagens in biological systems, it is necessary to investigate the unique structures and physical and chemical properties of BPs. A summary of BPs' properties provides a useful background about the isomerization phenomenon and photooxidation of BPs facilitating further experimental designs.

The use of the terms biliverdin and bilirubin alone refer to biliverdin IX α and unconjugated bilirubin IX α . All their isomers for example; bilirubin included unconjugated bilirubin III α , XIII α , IX β , IX δ , and IX γ and the 4*E*,15*E*-; 4*E*,15*Z*-; 4*Z*,15*Z*-; 4*Z*,15*E*-configurational isomers and the enantiomers of (4*Z*, 15*Z*)-bilirubin IX α are denoted by their complete nomenclature.

1.3.1 Unconjugated bilirubin-IX α

Unconjugated bilirubin has long been considered only in terms of its toxicity. The accumulation of **1.1** (UCB) in mammalian blood leads to diseases such as jaundice which is the yellow colouration of the sclera of skin and eyes. Newborn infants might also be subjected to unconjugated hyperbilirubinaemia that leads to accumulation of bilirubin in the brain, resulting in serious neurological defects such as abnormal reflexes, eyes movements, seizures, permanent neurological

dysfunction, and encephalopathy.⁵² Studies have shown that the level of **1.1** (UCB) in the blood of a healthy human adult can vary from 1.7-20 μM .⁵³⁻⁵⁵ While the toxic effects of elevated levels of BPs are well documented, many papers recently reported that BPs are essential endogenous compounds that can inhibit the action of some mutagenic compounds, acting as anti-oxidants and having anti-inflammatory properties.^{14,27,56}

The presence of a saturated methylene group at the C10-bridge of **1.1** (UCB) blocks conjugation between the two halves of the molecule. Isomers of **1.1** (UCB) are described using notations such as IX α (Z,Z). The Greek letter (eg ‘ α ’) refers to the site of cleavage of the precursor protoporphyrin as discussed above. The ‘Z,Z’ refers to the configuration of the C4-C5 and C15-C16 double bonds.^{7,9,57} This Z,Z configuration allows intramolecular hydrogen bonding between nitrogens in the pyrrole rings and the carboxyl groups leading to folded structures with the lipophilic parts of the molecule exposed and the hydrophilicity of the molecule reduced.⁵⁷⁻⁵⁹ Thus, in spite of having two carboxyl groups and two lactam groups, (Z,Z)- **1.1** (UCB) is virtually insoluble in water. Its water solubility was assessed in a range of concentrations, from 7 nM to 70 nM.^{60,61} In general, six intramolecular hydrogen bonds of (Z,Z)- **1.1** (UCB) generate a number of conformational isomers that vary in their physical, chemical, and biological properties (Figure 1.5).^{57-59,62-64} (4Z, 15Z)- **1.1** (UCB), in which six intramolecular hydrogen bonds are formed between carboxylic acid and amide pyrrole N-H groups to create a ‘ridge-tile’ shape in the central molecule and form enantiomeric conformations (**M** and **P**).^{58-60,65}

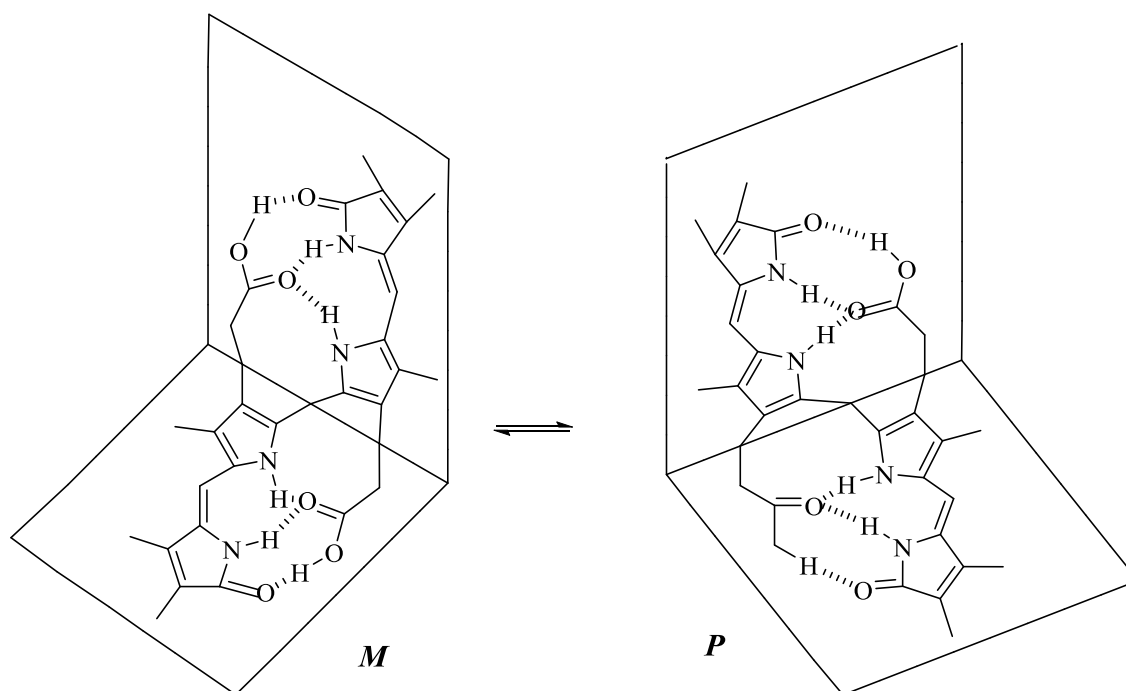


Figure 1.3: The enantiomers of (4Z, 15Z)-bilirubin (**P**=plus, **M**=minus) demonstrate the presence of ‘ridge-tile’ conformers via the formation of six intramolecular hydrogen bonds.^{58,59}

Photochemical isomerisation of unconjugated bilirubin

When (*Z,Z*)- **1.1** (UCB) is exposed to light, the *Z,Z* configuration is isomerised to (*Z,E*)-, (*E,Z*)-, (*E,E*)- **1.1** (UCB) (Figure 1.4).^{66,67} The mixture of photobilirubin isomers will convert back to the (*Z,Z*) isomer in the dark.⁶⁶ All bilirubin photoisomers were detected by HPLC analysis of the exposure of **1.1** (UCB) in DMSO to light for 60 min.⁸ Light also activates the π -bonds in the vinyl groups which leads to the formation of adducts with the pyrrole rings nearby and produces a new ring and releases one of the carboxyl groups which can now be deprotonated (Figure 1.4).^{68,69} As a result of this transformation, the polar groups (carboxylic and amide) are exposed and this leads to an increase in water solubility and the compound becomes easier to excrete through the urine and faeces.^{62,70,71}

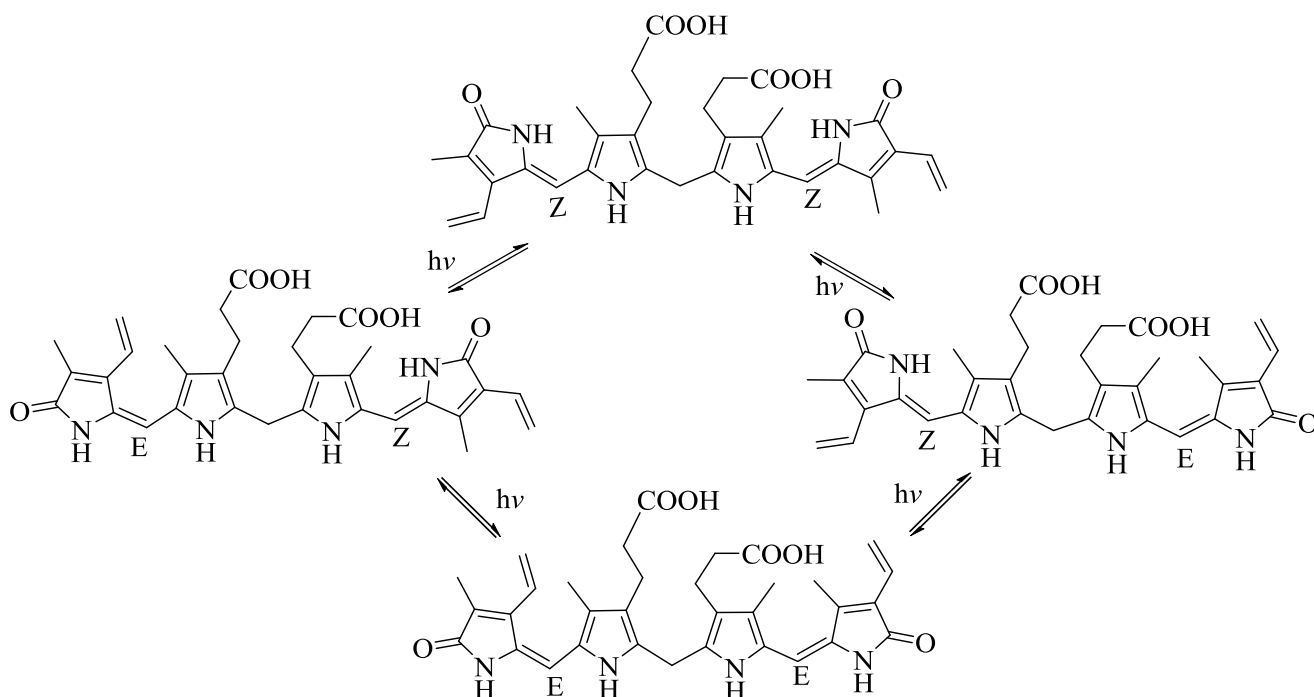


Figure 1.4: Configurational photo-isomerisation of (4*Z*,15*Z*)-bilirubin, leading to the formation of four isomers, (4*E*,15*Z*)-, (4*Z*,15*E*)- and (4*E*,15*E*)-bilirubin.^{8,66,67}

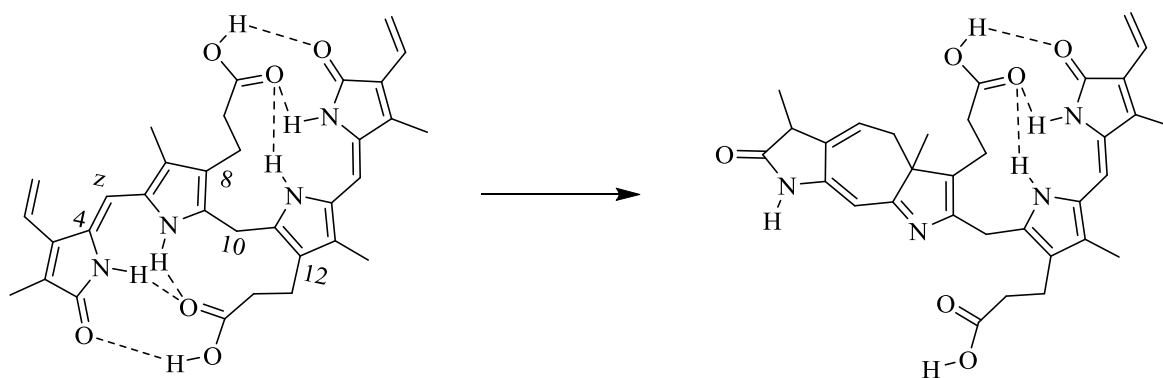


Figure 1.5: The formation of adducts with the pyrrole rings nearby producing a new ring.

Unconjugated bilirubin-IX α (**1.1**, UCB) is unstable to pH changes and isomerises to bilirubin-III α and XIII α in acid and alkaline solutions (Figure 1.6). The process of isomerisation starts with the dissociation of **1.1** (UCB) into four different dipyrrolic units which then randomly reassemble the C10 covalent bond between two symmetrical dipyrrolic units to create symmetric bilirubin-III α and XIII α .^{7,16,66,72,73} The photochemical isomers, bilirubin-XIII α , which exhibit no exo-vinyl groups, are more unstable than bilirubin-IX α which have one exo-vinyl and one endo-vinyl group and bilirubin-III α which contain two endo-vinyl group (Figure 1.6).⁶⁷ In a similar fashion to **1.1** (UCB), (Z,Z)-bilirubin-III α and XIII α isomerise in the presence of light to (Z,E)- and (E,E)-bilirubin-III α and XIII α .⁶⁷

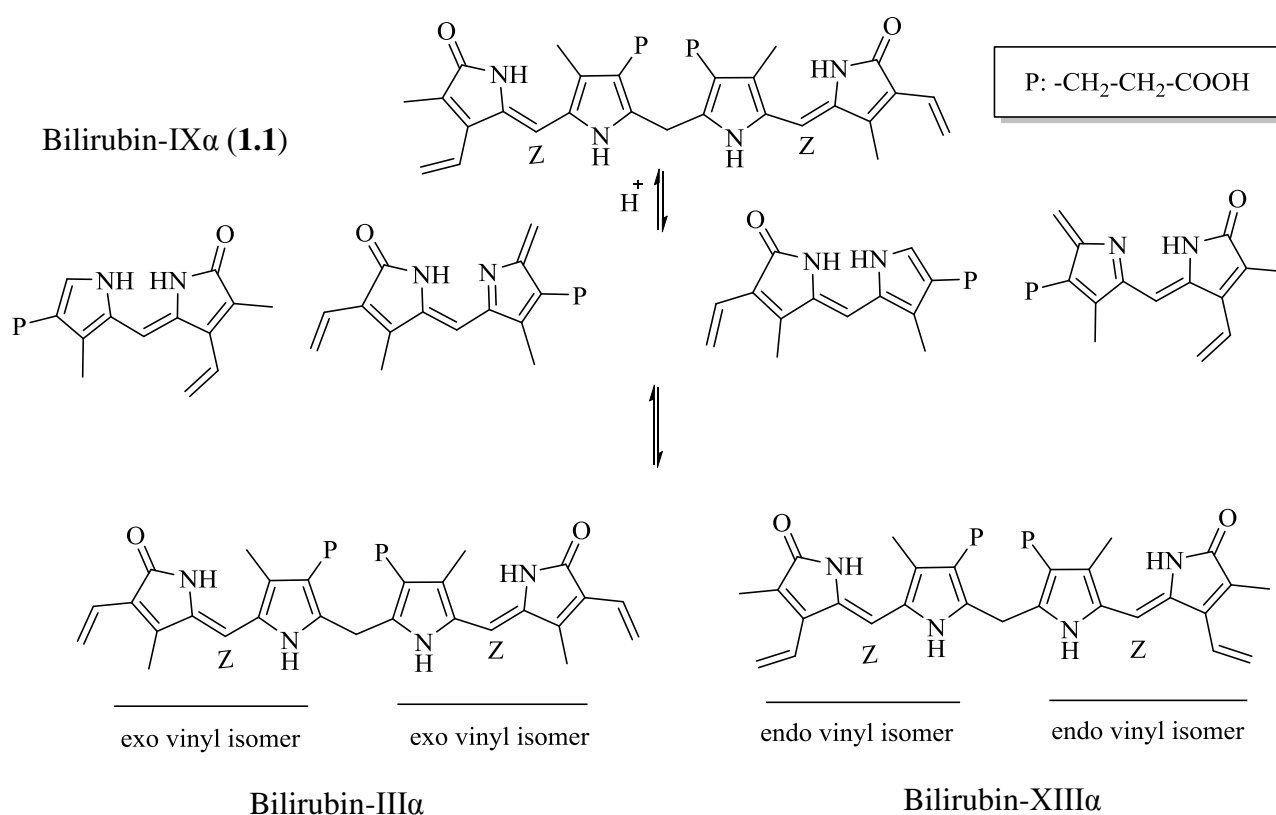


Figure 1.6: The isomerisation of **1.1** (UCB) in acidic environment in which the protonation of carbons nearby C10 to break the C10-bridge covalent bond and produce four different dipyrrolic units and then randomly reassemble the C10 covalent bond.^{66,68,69,74}

Adding to the complexity of the bilirubin family of compounds, bilirubin IX β , IX γ , and IX δ also photo-isomerize to produce a similar mixture of compounds. However, the principal BPs in human adult biles are **1.1** (UCB) with 95-97% and 3-5% of bilirubin-IX β .⁷⁵ The isomerisation reaction creates numerous bilirubin isomers in nature.

Photooxidation of unconjugated bilirubin

Bilirubin is not only complicated because of the formation of several isomers but is also unstable when exposed to air. Unconjugated bilirubin is oxidized to a variety of small molecules in the presence of light and oxygen. The oxidation reactions mainly occur at carbon-bridges including C5, C10, and C15 to produce substituted dipyrroles, pyrroles, and highly polar materials (Figure 1.7).⁶⁶

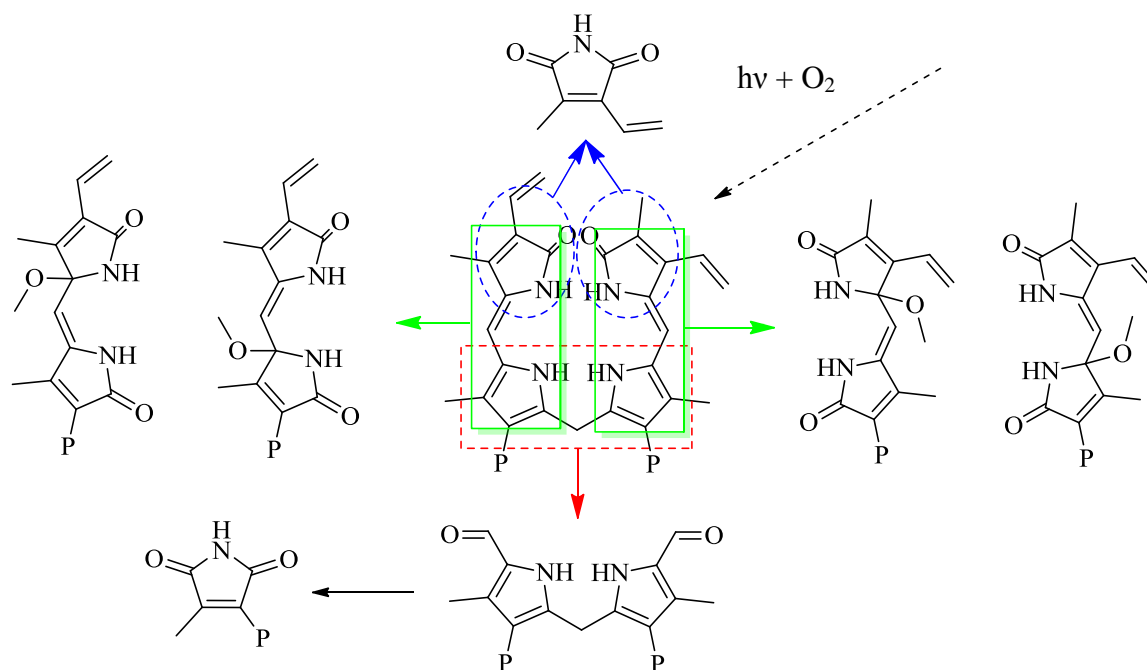


Figure 1.7: The photooxidation products of **1.1** (UCB) in the exposure to air and light.⁶⁶

Purification of bilirubin

The isomerization and instability of bilirubin's isomers result in difficulties in purifying the compound. Bilirubin-IX α is converted to **1.2** (BV) when in contact with silica (from column chromatography, see chapter III) and the compound is highly water insoluble and exhibits low solubility in organic solvents.^{76,77} It is, therefore, difficult to find suitable solvents for chromatography. The most efficient method for producing highly pure (4Z,15Z)-bilirubin is crystallisation by slow diffusion of n-hexane into chloroform or dichloromethane solution.^{58,78} (4E,15Z)-Bilirubin was obtained using this method in dim white light.⁵⁸

1.3.2 Biliverdin

Biliverdin IX α (**1.2**) and biliverdin IX β are major products obtained from the metabolism of haem in mammals or oxidization of **1.1** (UCB) and bilirubin-IX β at the C10-bridge.^{10,79} Biliverdin

contains a fully conjugated aromatic system bearing 26 electrons ($4n+2$). Biliverdin IX γ and IX δ are also formed from haem breakdown but are minor products (Figure 1.2).⁷⁻⁹ The C10 unsaturation of **1.2** (BV) and its derivatives prevent the dipyrrolic units from rotating freely around the C10-bridge. As a result, it does not form the complex hydrogen bonds system described for **1.1** (UCB) and so exhibits increased water solubility. Biliverdin not only has anti-mutagenic, and anti-oxidant properties^{80,81} but also inhibits vascular stenosis.⁸²

Biliverdin-IX α exposed to light can generate nine isomers; (Z,Z,Z)-, (Z,Z,E)-, (Z,E,Z), (Z,E,E)-, (E,Z,Z)-, (E,Z,E)-, (E,E,Z)-, (E,E,E)-biliverdin (Figure 1.8).^{66,83,84} These isomers exhibit very little differences in their solubilities and other properties as they are all planar structures. In comparison to **1.1** (UCB), **1.2** (BV) is more stable to light. However, **1.2** (BV) still loses about 7.1% at 4 °C over 20 days and can be stable at -80 C for a period of 40 days.⁷⁹

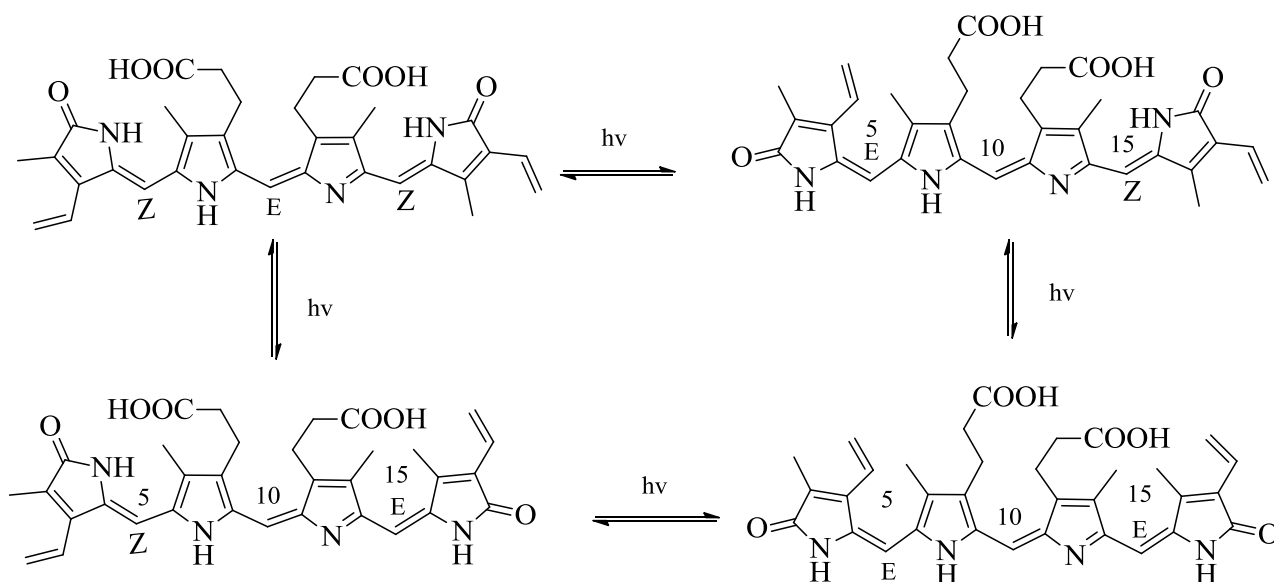


Figure 1.8: Photoisomerisation of **1.2** (BV).

1.3.3 Protoporphyrin

Protoporphyrin IX (**1.3**, PRO), a large macrocycle of the porphyrin moiety, has 26 π -electrons and 4 electrons from two of the pyrrole nitrogen atoms in conjugation creating a fully aromatic macrocycle. It is an important precursor of haem in biological systems and is biosynthesised from glycine and succinyl CoA or glutamate. Glycine combines with succinyl CoA under catalysis of aminolevulinic acid synthase to produce aminolevulinic acid.^{11,13,85,86} Aminolevulinic acid dehydratase converts aminolevulinic acid to porphobilinogen and then hydroxymethylbilane is produced by the action of porphobilinogen deaminase. Enzymes (uroporphyrinogen III synthase, uroporphyrinogen decarboxylase, and coproporphyrinogen oxidase) catalyze the formation of protoporphyrin IX from hydroxymethylbilane and then produce haem (Figure 1.9).^{11,13,85,86} The

compound was tested against a variety of tumor cell lines and exhibited strong anti-mutagenic properties.¹⁹

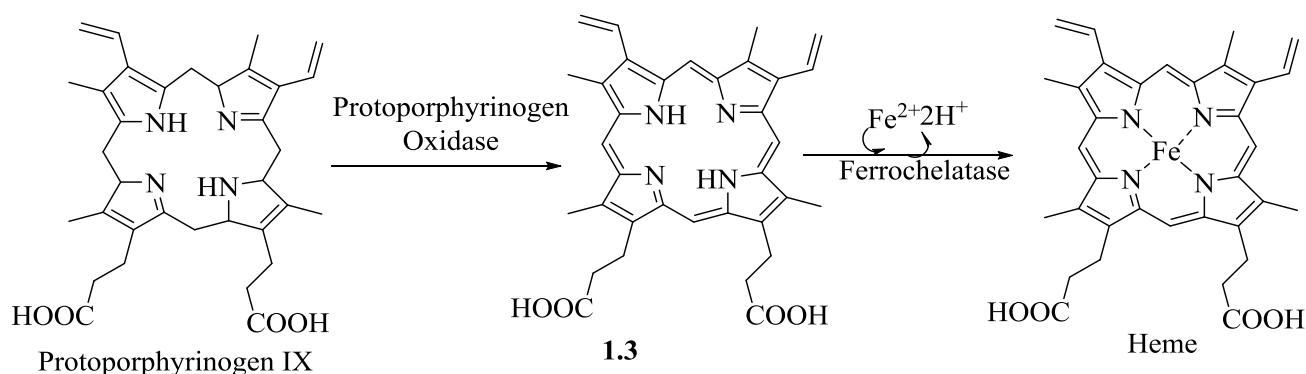


Figure 1.9: Haem biosynthetic pathway from protoporphyrinogen IX.⁸⁷

Chemistry of protoporphyrin IX:

A highly conjugated aromatic planar macrocycle, **1.3** (PRO) consists of four CH-bridges connecting four fully substituted pyrrolic rings exhibits unique physical and chemical properties. The formation of many stable metal complexes (with Mg^{2+} , Fe^{2+} , Cu^{2+} and Zn^{2+}) is one of the most important properties. ^1H NMR studies of **1.3** (PRO) show four proton signals corresponding to the CH-bridges very downfield (10.00 ppm) whereas the CH-bridge of dipyrrolic units exhibit a singlet signal in the aromatic region around 7.00 ppm (see Chapter II for more details). The unique in ^1H NMR spectrum of four CH-bridges indicate the low electron density of the positions and the high reactivity of the hydrogens. Protoporphyrin-IX and its derivatives exhibit strong intramolecular forces consisting of π - π stacking interactions, hydrogen bond, hydrophilic balance, charge transfer, and van der Waals forces with other chemicals.^{88,89}

In a similar manner to **1.1** (UCB) and **1.2** (BV) **1.3** (PRO) forms biproducts when exposed to light and oxygen. Specifically, the major photooxidation products are hydroxyaldehydes and mono and diformyldeuteroporphyrin (Figure 1.10).^{88,90} Therefore, Bhosale et al.⁸⁸ suggested that experiments involving in **1.3** (PRO) should be performed in the dark to avoid the formation of photooxidation products.

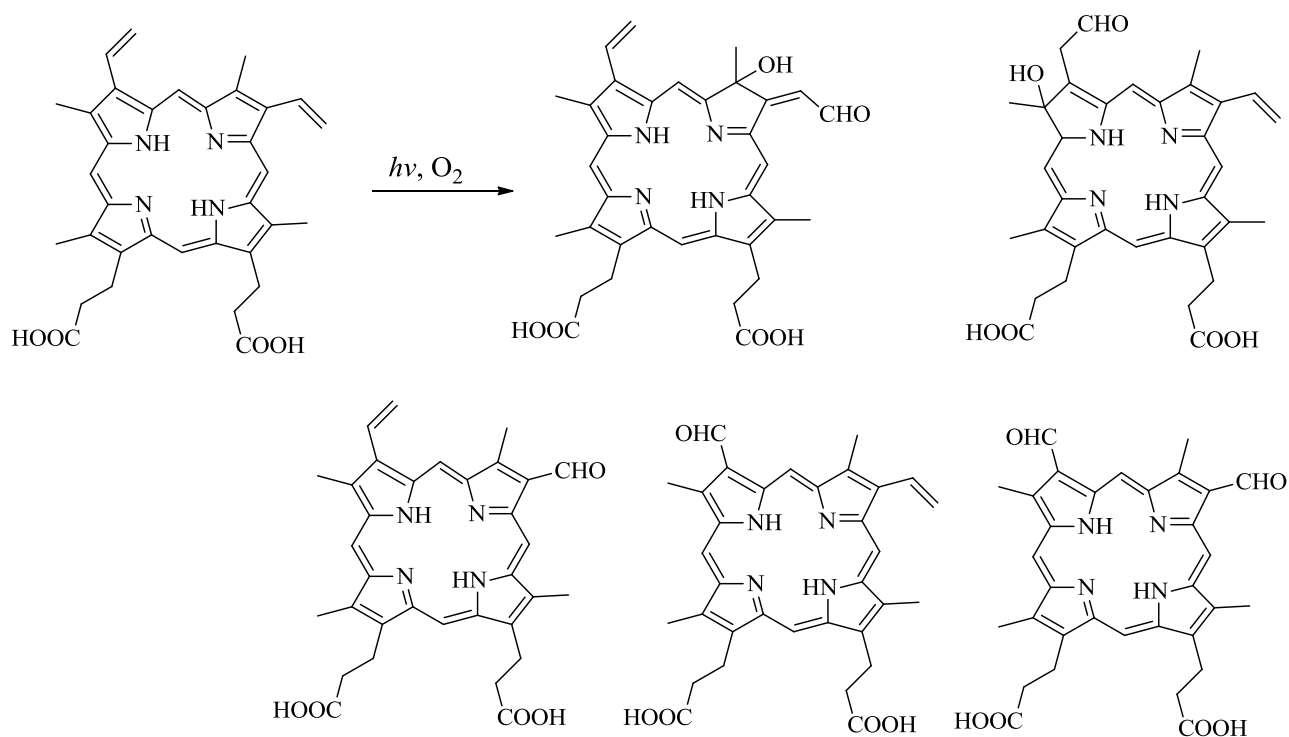


Figure 1.10: Products of the photooxidation of **1.3** (PRO) in the presence of light and oxygen.

In conclusion, BPs possess unique structures, physical and chemical properties which have led to the hypotheses that physical and chemical interactions between BPs and mutagens may be the key to the inhibitory effects of BPs on environmental mutagens. The mysterious mechanism of the inhibition needs to be explored.

1.4 Mutagens

1.4.1 Benzo[α]pyrene

Benzo[α]pyrene (BaP, **1.7**; C₂₀H₁₂; molecular weight: 252.31 g/mol) is a polycyclic aromatic hydrocarbon consisting of a planar five-ring aromatic system. The compound was discovered in 1933 in coal tar and automobile exhaust fumes from diesel engines being the main source. The combustion of organic materials (cigarette smoke, wood burning, incomplete combustion of meat between 300 °C and 600 °C) is the main source of **1.7** (BaP) in nature. Benzo[α]pyrene constitutes approximately 24.7 ng of a cigarette,⁹¹ 5.5 ng in each gram of fried chicken,⁹² and 62.6 ng in every gram of overcooked charcoal barbecued beef.⁹³ In the early 19th century in England an increased level of colon cancer⁹⁴ and high rates of skin cancers were reported among fuel industry workers and those who had been exposed to high levels of pollutants like **1.7** (BaP). Benzo[α]pyrene is metabolized in vivo by cytochrome P450 enzymes (CYP1A1 and 1B1) into a dangerous mutagen.⁹⁵⁻
⁹⁷ The mammal's body attempts to excrete the substance, so **1.7** (BaP) is oxidized to more polar

compounds, benzo[α]pyrene-7,8-dihydrodiol and then benzo[α]pyrene-7,8-dihydrodiol-9,10-epoxide, which are easier to eliminate from the body. However, benzo[α]pyrene-7,8-dihydrodiol-9,10-epoxide is not only more polar but also significantly more reactive. It can react with DNA leading to DNA damage and resulting in cancer (Figure 1.11).^{72,98-103} Thus, the International Agency for Research on Cancer (IARC) classified **1.7** (B α P) as a Group 1 carcinogen, a compound that has sufficient evidence to show causes cancer in humans. (carcinogenic to human).¹⁰³

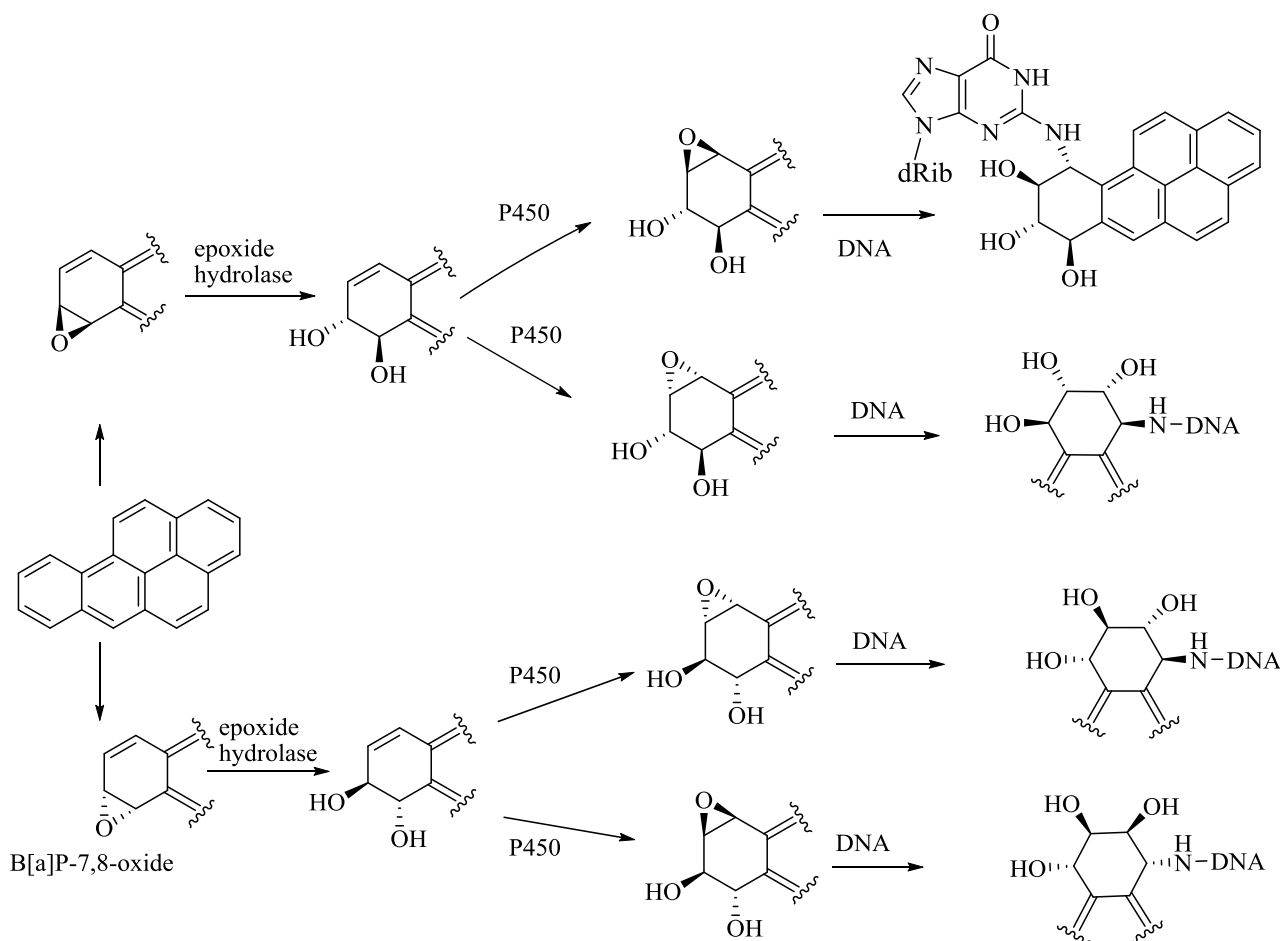


Figure 1.11: The metabolism of **1.7** (B α P) by P450 enzymes and the formation of products when benzo[α]pyrene-7,8-diol-9,10-epoxide reacts with DNA.^{99,104}

1.4.2 2-Aminofluorene

2-Aminofluorene (2AF, **1.5**) (C₁₃H₁₁N; formula weight: 181.23 g/mol) is a synthetic aromatic arylamine. It has been used in the laboratory as a research chemical and the metabolic activation of **1.5** (2AF) by cytochrome P450 enzymes is well studied. DNA-2AF adducts are found in some cancer cells particularly associated with deoxyguanosine.¹⁰⁵⁻¹⁰⁷ It is important to note that **1.5** (2AF) is oxidized by cytochrome P450 enzymes to the more active electrophilic agent, N-hydroxy-2-aminofluorene (N-OH-2-AF) and then HOSO₂O-NH-2-AF under the action of sulfotransferase or N-acyltransferase. They are both considered the most likely to attack the nucleophilic positions in

DNA such as C8-arylamine-dG, C8-arylamine-dA, and the amino group of deoxyguanosine as depicted in Figure 1.12.^{105,108-110} As a consequence of DNA modification, there are some changes in the cell's structure causing cancer.^{105,106,111,112}

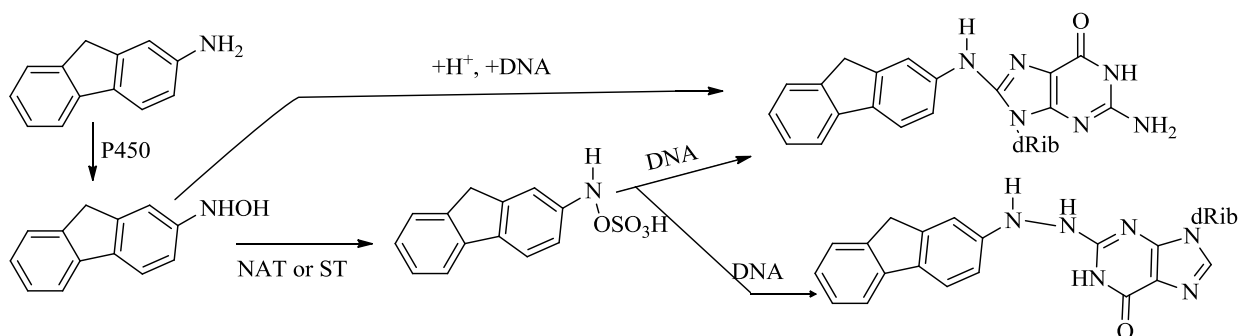


Figure 1.12: The metabolism of **1.5** (2AF) by P450 enzymes and some nucleophilic positions of deoxyguanosine in DNA that can be attacked by oxidation products of **1.5** (2AF), N-acyltransferase (NAT), sulfotransferase (ST).^{105,108,109}

1.4.3 2-Amino-1-methyl-6-phenylimido[4,5-b]pyridine

2-Amino-1-methyl-6-phenylimidazo[4,5-b]pyridine (PhIP, **1.8**) (C₁₃H₁₂N₄; formula weight: 224.26 g/mol) is a carcinogenic compound found in high-temperature-cooked meat and cigarette smoke. The level of **1.8** (PhIP) in food varies greatly depending on type of food and cooking method.¹¹³⁻¹¹⁷ Studies found high concentration of **1.8** (PhIP) in the urine of human volunteers who had eaten a normal diet but were cigarette smokers.¹¹⁸ The compound was also detected in breast, colon, and prostate tumors.^{114,115,117,119,120} This mutagenic chemical is believed to cause cell damage in humans by attacking and binding to guanine in DNA after being metabolized into bio-activated metabolites, N-hydroxy-PhIP and N-acetoxyl-PhIP by various cytochrome P450 enzymes, CYP1A1, 1A2, 1B1, N-acetyl transferases (NAT) and sulfotransferases (ST) in the liver.¹²¹⁻¹²⁵ Although many reports indicated that N-OH-PhIP is responsible for binding to DNA,^{105,108,109} it is thought that this compound requires further activation by the action of NAT and ST before attacking.^{120,126,127} Indeed, reports have recently found arylamine-DNA adducts (dG-C8-PhIP) in human tissues.^{124,125} For these reasons, **1.8** (PhIP) has been believed a potent carcinogen. The risk of cancer increases to those who frequently exposed to high levels of **1.8** (PhIP). Therefore, the International Agency for Research on Cancer (IARC) classified **1.8** (PhIP) as a Group 2B carcinogen (may be carcinogenic to human).¹⁰³

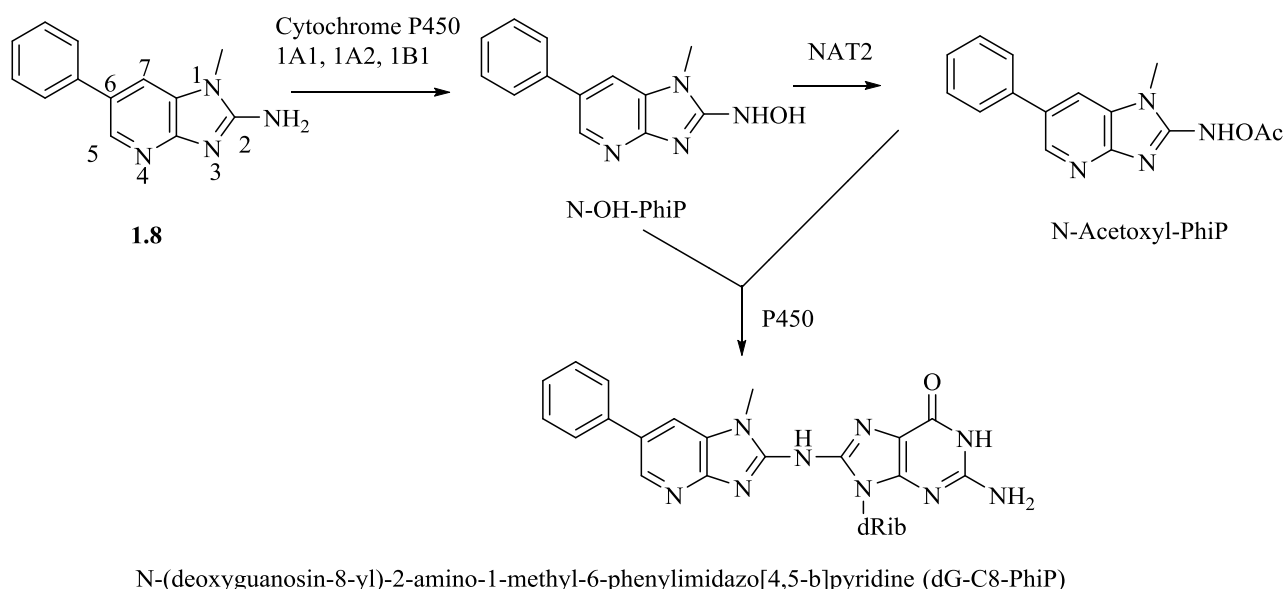


Figure 1.13: Proposed pathway of oxidation and DNA conjugation of PhIP.

1.5 Caco-2 cell monolayers

The human colonic adenocarcinoma (Caco-2) cell line has been developed from human large intestine cells by Jorgen and Trempe¹²⁸ at the Sloan-Kettering Institute Cancer Research, New York, The United States. During long-term culturing and passaging under specific conditions the cells differentiated into a polarized functional mimic of the small intestine.^{129,130} Caco-2 cell lines are seeded and cultured onto insert membranes in a well plate which divides the system into an apical chamber (AP) and a basolateral chamber (BL) and the cells are allowed to grow for at least 21 days when they are fully differentiated and provide the characteristic brush border of the small intestine epithelia. Caco-2 cell monolayers provide a physical and biochemical barrier for passing small molecules through a polarized epithelial cell.^{131,132} The AP represents the intestine and the BL mimics the blood supply. Caco-2 cells have been used as an *in vitro* model of the small intestinal epithelium for over a decade. The apparent permeability of compounds across the monolayer has been considered a good indication of the oral bioavailability of a compound.¹³³⁻¹³⁶ If the interactions between two compounds affect the permeability of any compound through the Caco-2 cells monolayers, this can be used as an indication that there may be similar effects occurring *in vivo*.^{130,133,137}

1.6 Conclusion and Hypothesis

In summary, the above pro-mutagenic environmental pollutants require metabolic activation from cytochrome P450 enzymes to be able to functionalize their carcinogenic activities. Their metabolites include hydrophobic and lipophilic parts with condensed planar aromatic rings. Many previous reports indicated that condensed aromatic hydrocarbons can form strong π - π stacking interactions.

These characteristics have led to the hypothesis that physical interactions in which the large lipophilic π -system of the BPs interacts with the lipophilic π -system of the polycyclic aromatic mutagens, causing aggregation of the molecules. This hypothesis is presented to explain the observed anti-mutagenic effects of BPs. These aggregates could then present the more polar groups (e.g. carboxyl groups in BPs and amine groups in the mutagens) to the outside surface which leads to increased hydrophilicity and more rapid excretion from the body through urine and faeces.

The second possible mechanism of inhibition is via chemical interactions. Mutagens of interest are oxidized in the liver by CYP P450 enzymes to produce more reactive agents that modify the DNA of cells by attaching to guanine and adenine bases. It is hypothesised that the electron rich aromatic system of BPs is more reactive towards these carcinogenic agents and thus act as scavengers of the mutagenic metabolites. Moreover, guanine and adenine bases in DNA are bound to sugars and phosphate groups which produce considerable crowd around the bases, while the BPs would offer a significantly less sterically crowded target for the electrophilic agents. The hydrogen bonding (H-bonding) of guanine and adenine with their based pair partners, cytosine, and thymine would also reduce their reactivity towards reactive carcinogenic agents compared to the pyrrole rings in BPs. Therefore, it is hypothesised that chemical interactions are a major contributing mechanism of inhibition of the mutagens by BPs.

The metabolism of mutagens such as **1.7** (B α P) and **1.8** (PhIP)^{5,70,98-100,105,111,138,139} by CYP enzymes have been well studied in relation to the mechanism of their mutagenicity.^{70,72,98,140} All of the environmental mutagens studied are in fact precursor molecules to the actual carcinogenic compounds which are formed by the action of CYP enzymes. Thus, another possible mechanism of inhibition may be that the BPs inhibit this conversion to carcinogenic metabolites. More work is required to fully understand the effect that BPs, bilirubin dimethyl ester, and biliverdin dimethyl ester might have on the metabolism of mutagens or on the reactive metabolites produced.

The hypothesis is that BPs are competitive inhibitors that have strong interactions with amino acid residues in the active site of enzymes. Bile pigments could also be non-competitive inhibitors with

strong binding to amino acids on the surface that modifies the active site of the enzymes. As a result, BPs inhibit the metabolic action of cytochrome P450 enzymes towards mutagens.

1.7 Research Aims and Plans

The inhibitory effects of BPs on the DNA modification activity of certain environmental mutagens are investigated. The most common hypotheses for the mechanism of inhibition were studied in an attempt to increase our understanding of the beneficial effects of BPs *in vivo*. This increased understanding may lead to further clinical studies on the use of BPs as dietary supplements.

1.8 Determining physical interactions between mutagens and bile pigments and their dimethyl esters

The study will identify whether the π -bond system of polyaromatic rings of mutagens participate in strong non-covalent interactions with BPs and their dimethyl esters. To achieve this, the experimental strategies involve three parts: 1) comparison of NMR spectra of mutagens alone with those of the mutagens in the presence of BPs; 2) documenting changes in the UV spectra of the mutagens upon addition of the BPs; and 3) using Caco-2 cell monolayers to measure and compare the apparent permeability of mutagens in the presence and absence of BPs and BPs dimethyl esters. The results obtained will clarify the physiological effects of BPs and provide evidence to support the beneficial effects of BPs in mammals.

1.9 Determining chemical interactions between mutagens and bile pigments and their dimethyl esters

Indole and imidazole will be used as the model of BPs and styrene epoxide as the model of the reactive epoxide metabolites of aflatoxin B1 and **1.7** (B α P), in order to identify the potential positions of indole and imidazole that can react with styrene epoxide. Then, the reaction between BPs and styrene epoxide will be conducted under the same conditions. Competitive reactions will then be conducted to evaluate the relative reactivity of indole, imidazole, BPs, BPs dimethyl ester, and guanine with styrene epoxide. The order of effectiveness of BPs on intercepting mutagens will be explored. The identification of the functional groups on BPs that are most likely to react with metabolites (epoxide) will be determined.

1.10 Investigating the inhibitory effects of BPs on the mechanism of mutagens in the human liver S9 fraction

The inhibitory effects of BPs on the metabolism of mutagens by cytochrome P450 enzymes are investigated. The comparison of results of the incubation between mutagens and the human liver S9

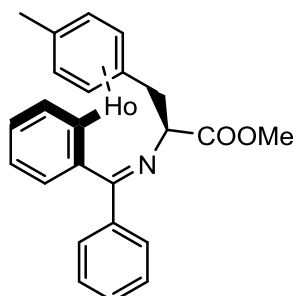
fraction in the presence and absence of BPs will postulate the role of BPs in inhibition of mutagenic metabolism. The docking studies of known enzymes' crystal structures from the protein data bank (PDB) with mutagens and BPs support these in vitro metabolism studies.

Chapter 2: Physical interactions between bile pigments, biliverdin, unconjugated bilirubin, protoporphyrin and environmental mutagens, 2AF, PhIP, B[α]P

2.1 Introduction

Intramolecular forces are the attractive and repulsive forces among molecules in close proximity. There are many types of non-covalent interactions such as ionic, hydrogen bonding, halogen bonding, dipole-dipole, dipole-induced dipole, London dispersion forces, π - π interactions, cation- π and anion- π interactions, polar- π and hydrophobic effects. They were classified into four categories of interactions: electrostatic, van der Waals forces, π -effects, and hydrophobic effects.¹⁴¹ Non-covalent interactions have apparently become important areas of study in recent years because of their importance in biochemical systems and materials chemistry.^{21,142-146} Physical interactions have been widely reported in both theoretical^{147,148} and experimental studies.¹⁴⁹⁻¹⁵¹ Particularly, attractive π -stacking forces occur between electron-rich and electron-deficient aromatic molecules when the delocalized p-orbitals of each aromatic molecule interact with an electron donor-acceptor fashion.^{145,152} Non-covalent interactions were also considered to be an important contribution for inhibitory action of bile pigments (BPs) to mutagens in biological systems.^{15,19,21}

The most common experimental methods that are applied to study physical interactions between chemical molecules are ^1H NMR^{149,150,153-155} and UV-Vis spectroscopies,^{149,154-157} CD spectroscopy,²¹ and X-ray techniques.^{149,158} For example, Jennings et al.¹⁵¹ used ^1H NMR and X-ray to explore the CH- π interactions in phenylalanine derivatives and observed that the proton signal of Ho (*ortho* proton) significantly shifted upfield from δ_{H} 7.14-7.17 to 5.5-5.8 in CD_2Cl_2 solvent as a result of these interactions. X-ray crystallography also showed evidence of CH- π interactions in phenylalanine derivatives with a distance of only 2.6 Å from Ho to the ring centroid.¹⁵¹



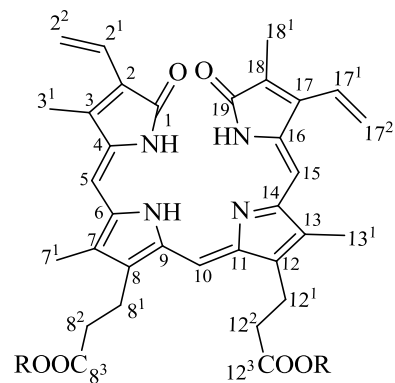
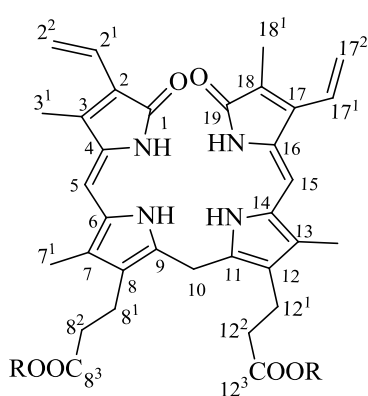
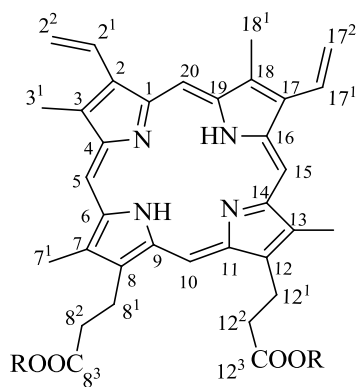
Sun et al.¹⁵³ used variable temperature (from 298 K to 213 K) for ^1H NMR spectroscopy to determine the aggregation of N,N'-di(n-butyl) quinacridone (DBQA) and its derivatives in CDCl_3 .

The study found the π - π interactions could be clearly observed at a temperature between 228 - 213 K by splitting of proton signals into new groups with different chemical shifts.

Ye et al.¹⁵⁷ described the π - π interactions between tetracationic porphyrins and graphene in aqueous medium using UV-Vis spectroscopy. The study found that $\Delta\lambda_{\max}$ of 5,10,15,20-tetra (4-pyridyl)-21H,23H-porphine was increased when the concentrations of carboxylic acid that modified graphene oxide, chemically converted graphene and graphene oxide increased.¹⁵⁷ Mölzer et al.²¹ suggested that one of the important factors that linked to the anti-mutagenicity of BPs was physical interactions occurring between BPs and 2,4,7-trinitro-9H-fluoren-9-one (TNFone). The π - π interactions were detected in aqueous solutions using CD and UV spectroscopy and confirmed by a negative VCD signal at 1620 cm^{-1} which ultimately indicated changes in the vibrations of C=C/C=N groups in the presence of TNFone.²¹

Bile pigments, especially protoporphyrin IX α (**2.1**, PRO), unconjugated bilirubin (**2.2**, UCB) and biliverdin (**2.3**, BV) have been recently reported to possess potential antioxidants and anti-mutagenic effects.^{14,19-21,34,36,37,159-161} Although various beneficial activities of BPs were discovered, a few studies suggested that the physical interactions between BPs and mutagens may be an important factor contributing to the inhibitory action of BPs.^{15,19,21} Therefore, exploration of physical interactions between BPs and polyaromatic environmental mutagens such as 2-Amino-1-methyl-6-phenylimidazo[4,5-b]pyridine (PhiP, **2.7**), benzopyrene (**2.8**, B α P), 2-aminofluorene (**2.9**, 2AF) and their likely contribution to the inhibition of mutagens is the aim of this chapter.

It is hypothesised that the intermolecular physical interactions between these compounds are stronger than in other compounds due to the unique aromatic surface of BPs and the electron rich polyaromatic nature of the environmental mutagens. Moreover, they have poor solubility in the aqueous biological environment due to their lipophilicity and so may aggregate to minimize exposure to water. Thus the physical interactions (non-covalent interactions, particularly π - π stacking) may be strong enough to change the λ_{\max} of the compounds and/or the chemical shifts of some of the protons in the structures.



R: H; protoporphyrin (2.1)

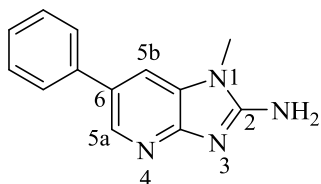
R: H; unconjugated bilirubin (2.2)

R: H; biliverdin (2.3)

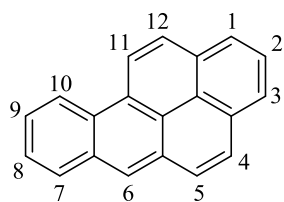
R: CH₃; (2.4)

R: CH₃; (2.5)

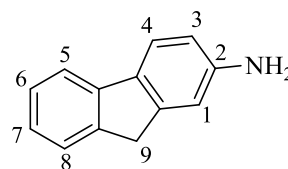
R: CH₃; (2.6)



PhIP (2.7)



BaP (2.8)



2AF (2.9)

2.2 Results and Discussion

2.2.1 Biliverdin and 2AF, PhIP, B α P

The studies were performed in methanol and repeated in aqueous phosphate buffer because aqueous phosphate more closely mimics biological conditions. Furthermore, since the polyaromatic mutagens and BPs have a lipophilic nature, they are more likely to aggregate in an aqueous environment in order to minimize exposure to the solution. The results showed that there was no change to the λ_{\max} of **2.7** (PhIP), **2.8** (B α P) or **2.9** (2AF) corresponding to 317 nm, 295 nm and 288 nm, respectively) upon addition of increasing amounts of **2.3** (BV). Likewise, the UV absorption spectrum of **2.3** (BV) remained unchanged ($\lambda_{\max} = 375$ nm) upon mixing with the polyaromatic mutagens (Figure 2.2, Figure 2.3 and Figure 2.4). It can be concluded that, in polar organic solvents with the polyaromatic mutagens examined, the π -system of **2.3** (BV) did not participate in π - π -interactions that are sufficiently strong to cause changes in the UV-absorbance spectrum of the compounds.

Possible interactions between **2.3** (BV) and **2.7** (PhIP), **2.8** (B α P), and **2.9** (2AF) were initially investigated using UV-spectroscopy. Indeed, the UV-Vis results did not show any evidence of strong interactions between the aromatic ring systems of **2.3** (BV) and mutagens. The second method was applied for this test in which solutions of **2.3** (BV) and the various mutagens were examined by ^1H NMR to determine whether or not there were detectable shifts in any of the signals which could be attributed to π -stacking interactions.

The ^1H NMR spectrum of **2.3** (BV) in neat DMSO- d_6 (Sol A) was used as the reference data for the experiments examining physical interactions between **2.3** (BV) and mutagens in 80% DMSO- d_6 and 20% D $_2$ O (Sol B). In order to increase the polarity of the solvent, which consequently stimulate aggregations of the lipophilic π -systems of both **2.3** (BV) and mutagens, D $_2$ O was added to the experiments.

^1H NMR results of **2.3** in Sol A and in Sol B indicated that all the proton chemical shifts of **2.3** (BV) shifted upfield in the presence of D $_2$ O, especially those corresponding to H-10, H-5, H-18 1 , H-17 1 , H-2, H-2 1 , H-2 2 (Table 2.1). This result indicated that these protons' chemical shifts are sensitive to the environmental change as D $_2$ O had a strong effect on these chemical shifts values. ^1H NMR of **2.3** (BV) in the presence of different mutagens showed that the chemical shifts of all BV's protons remained the same or changed slightly only in a narrow range of 0.15 ppm when in solution

with **2.8** (B α P). These data suggested that the wide aromatic surface of **2.8** (B α P) did not have any strong interactions with the π -bond aromatic system of **2.3** (BV).

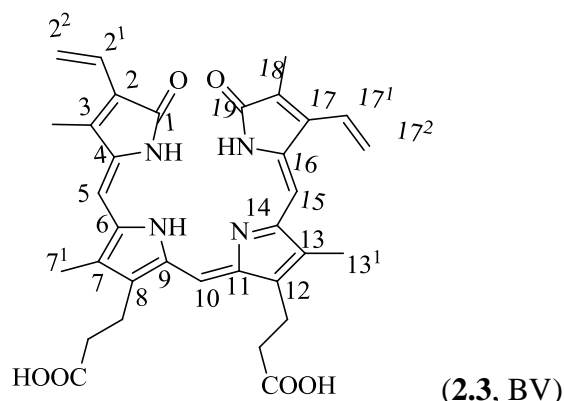


Table 2.1: A comparison of selected proton signals of **2.3** (BV) in the presence of different mutagens.

H	2.3 (Sol A) $\bar{\delta}_H$ (ppm), mult., J (Hz) ^a	2.3 (Sol B) $\bar{\delta}_H$ (ppm), mult., J (Hz) ^a	2.3+2.9 (Sol B) $\bar{\delta}_H$ (ppm), mult., J (Hz) ^a	2.3+2.7 (Sol B) $\bar{\delta}_H$ (ppm), mult., J (Hz) ^a	2.3+2.8 (Sol B) $\bar{\delta}_H$ (ppm), mult., J (Hz) ^a
2 ¹	6.89, dd, 17.5, 11.5	6.73, brt	6.67, dd, 17.5, 11.5	6.68, dd, 17.9, 12.0	6.78, dd, 17.5, 11.5
2 ²	5.53, d, 11.5	5.42, brd	5.36, brd	5.37, d, 12.0	5.46, brd
2 ^{2'}	6.30, d, 17.5	6.08, brd	5.92, brd	5.91, d, 17.9	6.14, brd
3 ¹	2.24, s	2.13, s	2.08, s	2.08, s	2.16, s
5	6.30, s	6.18, s	6.10, s	6.10, s	6.17, s
7 ¹	2.16, s	2.09, s	2.03, s	2.02, s	2.08, s
8 ¹	2.52, t, 7.2	2.50, brs	2.45, t, 7.0	2.43, t, 7.0	2.46, brs
8 ²	3.03, t, 7.2	2.95, brs	2.85, brs	2.81, brt	2.91, brs
10	7.54, s	7.41, brs	7.08, brs	6.98, s	7.26, brs
12 ¹	2.52, t, 7.2	2.50, brs	2.45, t, 7.0	2.43, t, 7.0	2.46, brs
12 ²	3.03, t, 7.2	2.95, brs	2.85, brs	2.81, brt	2.91, brs
13 ¹	2.14, s	2.06, s	2.00, s	1.99, s	2.05, s
15	6.28, s	6.18, s	6.10, s	6.10, s	6.17, s
17 ¹	6.66, dd, 17.5, 11.5	6.49, brt	6.43, brt	6.45, dd, 17.9, 12.0	6.55, dd, 17.5, 11.5
17 ²	5.77, d, 11.5	5.72, brt	5.64, d, 18.5	5.65, m	5.70, m
17 ^{2'}	5.77, d, 17.5	5.68, brt	5.67, d, 12.0	5.65, m	5.70, m
18 ¹	1.99, s	1.81, s	1.72, s	1.72, s	1.86, s

^aChemical shift (ppm) referenced to DMSO- H_6 δ_H 2.49 were taken from 1D NMR (DMSO- d_6 , 500 MHz).

In order to clarify the effect of the pH of the environment on the proton chemical shifts of both BPs and mutagens, a mixture of **2.3** (BV) and CH₃NH₂ in equal concentrations in Sol B was examined by ¹H NMR (Table 2.2).

Table 2.2: A comparison of selected proton signals of **2.3** (BV) in the absence and presence of **2.9** and CH₃NH₂.

H	2.3 (Sol B) δ_{H} (ppm), mult., J (Hz) ^a	2.3+2.9 (Sol B) δ_{H} (ppm), mult., J (Hz) ^a	2.3+CH₃NH₂ (Sol B) δ_{H} (ppm), mult., J (Hz) ^a
2 ¹	6.73, brt	6.67, dd, 17.5, 11.5	6.64, brs
2 ²	5.42, brd	5.36, brd	5.29, brs
2 ^{2'}	6.08, brd	5.92, brd	5.89, brs
3 ¹	2.13, s	2.08, s	2.06, s
5	6.18, s	6.10, s	6.10, s
7 ¹	2.09, s	2.03, s	2.06, s
8 ¹	2.50, brs	2.45, t, 7.0	2.46, brs
8 ²	2.95, brs	2.85, brs	2.90 brt
10	7.41, brs	7.08, brs	6.98, s
12 ¹	2.50, brs	2.45, t, 7.0	2.46, brs
12 ²	2.95, brs	2.85, brs	2.90 brt
13 ¹	2.06, s	2.00, s	2.01, s
15	6.18, s	6.10, s	6.10, s
17 ¹	6.49, brt	6.43, brt	6.36, brd
17 ²	5.72, brt	5.64, d, 18.5	5.61, m
17 ^{2'}	5.68, brt	5.67, d, 12.0	5.69, m
18 ¹	1.81, s	1.72, s	1.67, s

^aChemical shift (ppm) referenced to DMSO-*H*₆ δ_{H} 2.49 were taken from 1D NMR (DMSO-*d*₆, 500 MHz).

In contrast, all **2.3** (BV) proton signals shifted upfield in the presence of basic mutagens **2.9** (PhIP) and **2.7** (2AF). If the changes in the **2.3** (BV) spectrum were due to interactions of the π -systems, then we would expect to see the greatest shifts in the aromatic proton signals. However, the most significant shifts appeared in the signals corresponding to the protons in the carboxylic acid sidechains, H-8¹, H-8², H-12¹, and H-12² (Table 2.1). Both **2.9** (2AF) and **2.7** (PhIP) contain a basic amine group which can deprotonate the carboxylic acid groups of **2.3** (BV). Deprotonation causes an increase in pH of environment and this affects the chemical shifts of the protons in the tetrapyrrole and vinyl groups. ¹H NMR results of bilirubin dimethyl ester and biliverdin dimethyl

ester in chapter IV can clarify the hypothesis. This would explain the shifts that we observed: 1) H-10 was shielded from δ_{H} 7.41 to 7.08 and 6.98 in the mixture with **2.9** (2AF) and **2.7** (PhIP), respectively, 2) H-5 and H-15 were shielded from δ_{H} 6.18 to 6.10, and 3) H-12² and H-8² were shifted from δ_{H} 2.95 to 2.85 and 2.81, respectively (Table 2.1). All protons exhibiting a shift in their resonance frequency are in close proximity to the acidic or basic groups of **2.3** (BV). Thus, these mutagens may simply be participating in a simple acid-base reaction with the bile pigment. In order to test this hypothesis, the ¹H NMR spectrum of **2.3** (BV) in the presence of CH₃NH₂ was measured. The results showed extremely similar changes in the chemical shifts of the **2.3** (BV) protons to those seen in the presence of the basic mutagens (Table 2.2). These results indicated that the changes in the ¹H NMR signals in the presence of **2.7** (PhIP) and **2.9** (2AF) were predominately caused by deprotonation of **2.3** (BV) but not any significant π -stacking interactions.

In the presence of **2.3** (BV), the H-1 and H-3 signals of **2.9** (2AF) shifted slightly downfield (from δ_{H} 6.88 and 6.68 ppm to δ_{H} 7.01 and 6.82 ppm, respectively). Biliverdin hydrochloride was used to formulate the solution used in these experiments. As a result, there are two protonated carboxylic acid moieties and one molecule of HCl per molecule of biliverdin. This excess of acid would ensure that the amine group of **2.9** (2AF) was protonated to a NH₃⁺ group. The protonation of the amine group of **2.9** will result in less electron density to the aryl system and chemical shifts will move downfield. Another possible reason for the changes in the ¹H NMR signals is that the π -system of **2.3** (2AF) was interacting with the conjugated π -system of **2.9** (2AF). To evaluate how much of the changes to the NMR spectrum of **2.9** (2AF) were caused by the presence of acid, 10 μ L of LiOH (0.1 M) was added to the solutions. All the ¹H NMR signals corresponding to **2.9** (2AF) returned to the original values for **2.9** (2AF) in Sol B alone (Figure 2.5).

In order to further evaluate the effect of acid on **2.9** (2AF), the ¹H NMR of a mixture of **2.9** (2AF), acetic acid and HCl in a ratio of 1:2:1 was measured. This ratio was chosen to mimic the two carboxylic acid groups and one HCl moiety of the **2.3** (BV) solution. The evidence indicated that salt formation had a strong effect on proton chemical signals of **2.9** (2AF). In fact, all proton signals of **2.9** (2AF) shifted downfield in a similar fashion to that observed when **2.3** (BV) was added to **2.9** (2AF). This is in agreement with the pH data of mutagens and BPs collected in Sol A and Sol B (Table 2.8).

2.2.2 BRU and 2AF, PhiP, B α P

The UV results show that the λ_{\max} (450 nm) of **2.2** (UCB) did not change in the presence of **2.7** (PhIP), **2.8** (BoP) and **2.9** (2AF) in both methanol and phosphate buffer. Likewise, the UV absorbance spectra of the polyaromatic mutagens were not modified in the presence of increasing concentrations of **2.2** (UCB). This indicates that the π -bond systems in BPs and mutagens do not exhibit any strong physical interactions in both methanol and buffer.

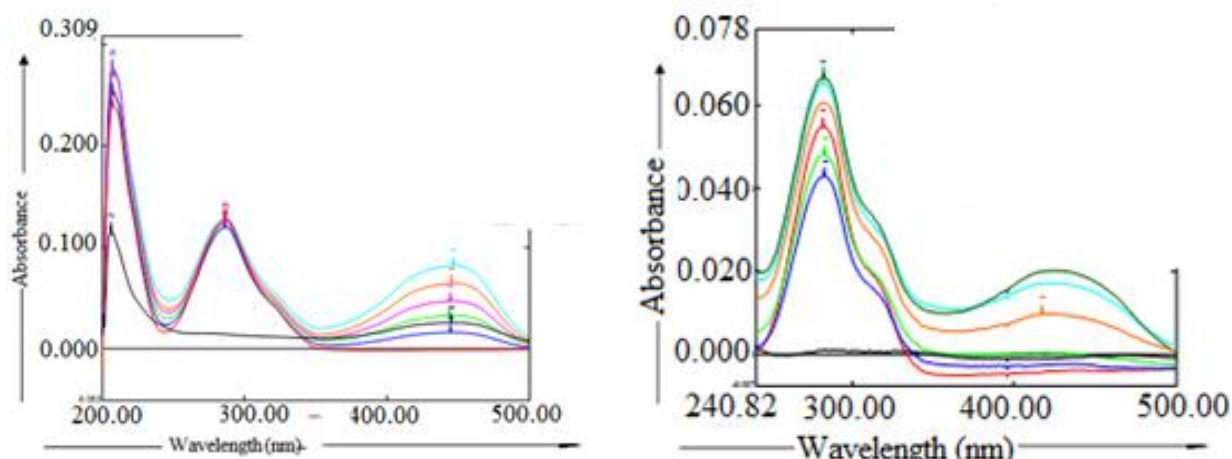
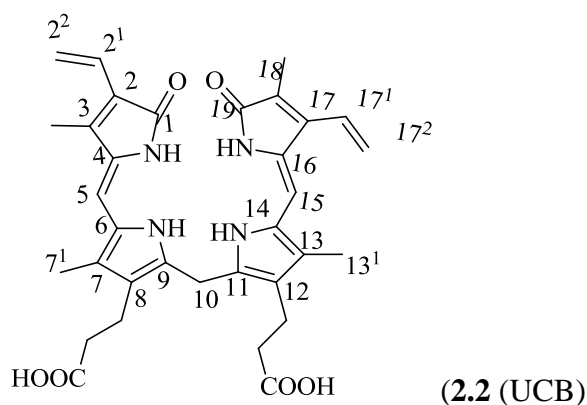


Figure 2.1: Overlay of the UV spectra of the mixtures of **2.9** (2AF, 1 μ M in methanol, 0.5 μ M in buffer) and varying concentrations of **2.2** (UCB, from 0.5 μ M to 2.5 μ M in methanol (left) and from 0.25 μ M to 0.5 μ M in buffer (right)). The red line close to the baseline (λ_{\max} 288 nm) was the UV spectra of **2.9** (2AF). The introduction of **2.2** (UCB, from 0.25 μ M to 2.5 μ M) in the mixture was detected by the increasing UV absorbance at 450 nm.

In order to verify the UV results, the mixtures of **2.2** (UCB) and mutagens were tested by ^1H NMR. A solution of Sol B was used to dissolve **2.2** (UCB) as well as the mutagens to produce a mixture in which the concentration of **2.2** (UCB) and mutagens were sufficient for NMR analyses. The above results were compared to ^1H NMR data of **2.2** (UCB) and mutagens only (control experiments) in Sol B and Sol A. It is important to compare the results from the control experiments performed in Sol A and Sol B to clarify the effect of water on the chemical shifts of the protons in the compounds which were being examined. ^1H NMR data collected in Sol B (Table 2.3) indicated that the addition of D_2O affected the chemical shifts of most of the protons in **2.2** (UCB). While most of the signals were shifted upfield when D_2O was added, the signals corresponding to H-2², H-5, H-15 and H-17² shifted slightly upfield. For example, slight changes to the signals belonging to H-17² (shifted from δ_{H} 6.16 to δ_{H} 6.10), H-2¹, H-17¹, and H-10 which respectively shifted from 0.06, 0.05, and 0.05 ppm upfield were observed. In contrast, addition of 20% D_2O resulted in signals for H-2², H-5, H-15, and H-17² shifting 0.01 ppm downfield. The results led us to the conclusion that the change of NMR solvent environment is the cause of a slight modification of the ^1H NMR spectrum of **2.2** (UCB). The conclusion was supported by the change of pH in the presence of D_2O and BPs (Table 2.8).

**Table 2.3:** A comparison of selected proton signals of **2.2** (UCB) with different mutagens present.

H	2.2 (Sol A) $\bar{\delta}_H$ (ppm), mult., J (Hz) ^a	2.2 (Sol B) $\bar{\delta}_H$ (ppm), mult., J (Hz) ^a	2.2+2.9 (Sol B) $\bar{\delta}_H$ (ppm), mult., J (Hz) ^a	2.2+2.7 (Sol B) $\bar{\delta}_H$ (ppm), mult., J (Hz) ^a	2.2+2.8 (Sol B) $\bar{\delta}_H$ (ppm), mult., J (Hz) ^a
2 ¹	6.81, dd, 17.5, 11.5	6.75, dd, 17.8, 11.5	6.73, dd, 17.8, (11.5)	6.74, dd, 17.5, 11.5	6.73, dd, 17.5, 11.5
2 ²	5.63, dd, 11.5, 1.6	5.59, d, 11.5	5.59, d, 11.5	5.58, d, 11.5	5.59, d, 11.5
2 ^{2'}	5.62, dd, 17.5, 1.6	5.63, d, 17.8	5.63, d, 17.9	5.63, d, 17.5	5.63, d, 17.5
3 ¹	2.15, s	2.11, s	2.11, s	2.11, s	2.11, s
5	6.08, s	6.09, s	6.10, s	6.10, s	6.10s
7 ¹	1.99, s	1.95, s	1.95, s	1.94, s	1.95, s
8 ¹	2.40, t, 7.5	2.40, brt	2.40, brt	2.38, brt	2.40, brt
8 ²	1.92, t, 8.0	1.91, brs	1.93, brs	1.89, brs	1.93, brs
10	3.98, s	3.93, s	3.69, s	3.56, s	3.92, s
12 ¹	2.40, t, 7.5	2.40, brs	2.40, m	2.38, s	2.40, m
12 ²	1.92, t, 8.0	1.91, brs	1.93, brs	1.89, m	1.93, m
13 ¹	2.02, s	1.98, s	1.98, s	1.98, s	1.98, s
15	6.08, s	6.09, s	6.10, s	6.10, s	6.10, s
17 ¹	6.57, dd, 17.5, 11.5	6.52, dd, 17.5, 11.5	6.52, dd, 17.5, 11.5	6.52, dd, 17.5, (11.5)	6.51, dd, 17.5, 11.5
17 ²	6.18, dd, 17.5, 2.8	6.10, d, 17.8	6.08, d, 17.9	6.08, d, 17.8	6.07, d, 17.5
17 ^{2'}	5.28, dd, 11.5,	5.29, d, 11.5	5.29, d, 11.5	5.29, d, (11.5)	5.29, d, 11.5

	2.8				
18 ¹	1.91, s	1.89, s	1.87, s	1.87, s	1.87, s

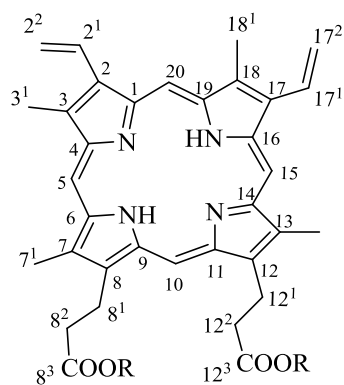
^aChemical shift (ppm) referenced to DMSO-*H*₆ δ_{H} 2.49 were taken from 1D NMR (DMSO-*d*₆, 500 MHz).

The mixture of **2.2** (UCB) and mutagens **2.7** (PhIP) and **2.9** (2AF) in Sol B showed that most of the proton chemical shifts of **2.2** (UCB) remained unchanged, except the H-10 signal which shifted considerably upfield from δ_{H} 3.93 ppm to 3.56 ppm (Table 2.3). In contrast, the signal of H-10 in the mixture with **2.8** (B α P) remained at δ_{H} 3.92. This observation suggested that H-10 is very susceptible to the changes in the pH of the solution because both **2.7** (PhIP) and **2.9** (2AF) are basic compounds. Proton chemical shifts of other positions only exhibited slight variations that are consistent with those observed in the control experiment. Likewise, only the proton signals corresponding to H-1 (δ_{H} 6.76) and H-3 (δ_{H} 6.58) in **2.9** (2AF) shifted downfield to δ_{H} 6.78 and δ_{H} 6.59, respectively, in the presence of **2.2** (UCB) (Figure 2.8 and Table 2.5). These protons are located ortho to the amine group of **2.9** (2AF) and so would be mostly affected by the protonation of the amine caused by the presence of **2.2** (UCB).

Not less changes were recognized in the ¹H NMR spectrum of **2.2** (UCB) in the presence of the mutagens than those of **2.3** (BV). It may be a result of unique dimensional isomers of **2.2** (UCB) present in solution (see Chapter 1 for details). The formation of these structures in solution significantly reduced the acidity of the carboxylic acid groups in **2.2** (UCB) due to their participation in intramolecular hydrogen bonds (see Chapter 1 for details). Thus, the NMR spectrum of the basic **2.7** (PhIP) was eventually unchanged in the presence of **2.2** (UCB) as was that of **2.8** (B α P) (Figure 2.6 and Figure 2.7). The NMR data combined with the UV-Vis results confirmed that physical interactions or π - π -stacking were not strong or did not occur between **2.2** (UCB) and the examined mutagens to a great enough extent to perturb the NMR or UV characteristics of **2.2** (UCB).

2.2.3 Protoporphyrin (2.1) and 2AF, PhiP, B α P

The interactions of **2.1** (PRO) with mutagens were also examined by UV-Vis spectroscopy in both methanol (λ_{max} of **2.1** = 401 nm) and aqueous phosphate buffer (λ_{max} of **2.1** = 386 nm). Once again, no changes to the UV absorbance of **2.1** (PRO) or the mutagens were observed in solutions that varied in the molar ratio of **2.1** (PRO) to mutagens from 1:1 to 3:1 (Figure 2.9).

**2.1 (PRO)****Table 2.4:** A comparison of selected proton signals of 2.1 with different mutagens present.

H	2.1 (Sol A) δ_{H} (ppm), mult., J (Hz) ^a	2.1 (Sol B) δ_{H} (ppm), mult., J (Hz) ^a	2.1+2.9 (Sol B) δ_{H} (ppm), mult., J (Hz) ^a	2.1+2.7 (Sol B) δ_{H} (ppm), mult., J (Hz) ^a	2.1+2.8 (Sol B) δ_{H} (ppm), mult., J (Hz) ^a
2 ¹	8.47, dd, 17.6, 11.6	8.33, brs	8.29, m	8.32, m	8.31, brs
2 ²	6.21, d, 11.6	6.20, brs	6.18, d, 11.5	6.19, d, 11.5	6.18, brs
2 ²	6.43, d, 17.6	6.38, brs	6.35, d, 17.5	6.37, d, 17.5	6.35, brs
3 ¹	3.71, s	3.60, brs	3.58, brs	3.61, brs	3.58, brs
5	10.21, brs	10.05, brs	9.96, brs	10.00, brs	9.96, brs
7 ¹	3.60, s	3.51, brs	3.49, brs	3.50, brs	3.49, brs
8 ¹	3.18, 7.2	3.09, brs	3.09, brs	3.13, brs	3.09, brs
8 ²	4.33, t, 7.2	4.24, brs	4.21, brs	4.23, brs	4.22, brs
10	10.21, brs	10.04, brs	9.96, brs	10.01, brs	9.96, brs
12 ¹	3.18, t, 7.2	3.09, brs	3.09, brs	3.13, brs	3.09, brs
12 ²	4.33, t, 7.2	4.24, brs	4.21, brs	4.23, brs	4.22, brs
13 ¹	3.61, s	3.51, brs	3.49, brs	3.50, brs	3.49, brs
15	10.19, brs	10.02, brs	9.93, brs	9.98, brs	9.93, brs
17 ¹	8.47, dd, 17.6, 11.6	8.28, brs	8.29, m	8.32, m	8.31, brs
17 ²	6.21, d, 11.6	6.20, brs	6.18, d, 11.5	6.18, d, 11.5	6.16, brs
17 ²	6.43, d, 17.6	6.38, brs	6.35, d, 17.5	6.37, d, 17.5	6.33, brs
20	10.26, brs	10.07, brs	9.97, brs	10.04, brs	9.97, brs
18 ¹	3.69 s	3.62, brs	3.56, brs	3.58, brs	3.56, brs

^aChemical shift (ppm) referenced to DMSO-*H*₆ δ_{H} 2.49 were taken from 1D NMR (DMSO-*d*₆, 500 MHz).

The UV results were again verified by examination of mixtures of **2.1** (PRO) and each mutagen in Sol B by ¹H NMR. The comparison of the NMR data of **2.1** (PRO) in Sol A and Sol B indicated

that D₂O had an effect on proton signals of **2.1** (PRO). Most of the proton chemical shifts moved upfield in the presence of D₂O, especially H-20 and H-17¹ which shifted 0.19 ppm from δ_{H} 10.26 and 8.47 ppm to δ_{H} 10.07 and 8.28 ppm, respectively, H-5 and H-10 which shifted 0.17 ppm from δ_{H} 10.19 and 10.21 to δ_{H} 10.02 and 10.04 ppm, and H-15 which shifted 0.16 ppm upfield.

In the presence of each mutagen (**2.7** (PhIP), **2.8** (B α P) and **2.9** (2AF) in Sol B, the changes in chemical shift values of **2.1** (PRO) were slightly again (Table 2.4). For example, H-2¹ and H-17¹ shifted from δ_{H} 8.29 to 8.33 and H-2² and H-17² shifted from δ_{H} 6.16 to δ_{H} 6.20. ¹H NMR results of each mutagen in the mixture were similar to those of the control experiments and thus were attributed to the increased concentration of D₂O in the samples and not to any substantial interactions with **2.1** (PRO). As seen in Figure 2.9, there were no significant differences in the NMR spectrum of **2.9** (2AF) in Sol B in the presence of increasing concentrations of **2.9** (2AF). Likewise, Figure 2.11 and Figure 7.2 (in appendix-A) demonstrate that the NMR spectra of **2.7** (PhIP) and **2.8** (B α P) did not change in the presence of **2.1** (PRO). These NMR data were in agreement with the UV results which indicated that there were no significant π - π -stacking interactions occurring between **2.1** (PRO) and the mutagens examined under the conditions of the experiments.

2.2.4 Dimethyl ester of BPs and 2AF, PhiP, B α P

¹H NMR showed that there were no changes in the spectra of the dimethyl esters of BPs (**2.4** (PRODE), **2.5** (UCBDE), **2.6** (BVDE)) in the presence of each mutagen (Figure 2.12-Figure 2.13 and Figure 7.4- 7.6 in appendix-A). Similarly, the addition of dimethyl ester of BPs did not modify the proton signals of **2.7** (PhIP), **2.8** (B α P) and **2.9** (2AF). The results suggested that the physical interactions between mutagens and dimethyl esters of BPs were not strong enough to create changes in the proton chemical shifts of the compounds, in Sol A.

2.3 Conclusion

It was hypothesized that polyaromatic mutagens and BPs would seek to minimize their exposure to water and other polar solvents by forming aggregates via π -stacking interactions. The UV and ¹H NMR spectra in the presence of water showed that the electron-rich aromatic surface of BPs and π system of mutagens did not have any strong π - π interactions that were sufficient to alter the UV- and ¹H NMR spectra of the compounds. It is unlikely, therefore, that physical interactions or aggregations are a major contributing mechanism to the anti-mutagenic effects of the BPs.

2.4 Experimental

Materials and Methods Solvents and mutagens were purchased from Sigma Aldrich Pty Ltd (Melbourne, Vic, Australia) and **2.7** (PhIP) from Wako pure chemical industries, Japan unless otherwise stated. Bile pigments were purchased from Frontier Scientific (Logan, UT, USA) unless otherwise stated. All bile pigments and mutagens are visualized with 254 nm UV light (λ_{max} : **2.2** (UCB) = 450 nm, **2.3** (BV) = 375 nm, **2.1** (PRO) = 409 nm, **2.6** (BVDE) = 375 nm, **2.5** (UCBDE) = 450 nm, **2.4** (PRODE) = 409 nm). 1D and 2D NMR experiments were performed on either a Bruker Advance 500 MHz spectrometer, with Topspin NMR and Mestranova 9.1 software. The solvents were DMSO- d_6 (δ_{H} 2.49 ppm and δ_{C} 35.95 ppm) and D₂O. Ultraviolet/Visible Spectroscopy was conducted using a Shimadzu UV-Vis Spectrophotometer Model UV-1600 for measuring absorbance with slit width 2.0 nm, light source change wavelength 340.8 nm. Measurement parameters included a λ_{max} range from 200 nm to 700 nm, fast speed, 0.5 of sampling interval, enabled or auto sampling interval and single scan mode.

The UV tests were performed in both methanol and aqueous phosphate buffer. Stock solutions of **2.7** (PhIP), **2.8** (B α P) and **2.9** (2AF) at concentrations of 1.0 mM were prepared in DMSO and 1 μL of each solution was added to 1 mL of methanol and phosphate buffer to provide solutions of 1.0 μM . The absorbance spectrum of each solution was measured from 200 nm to 700 nm. Solutions of **2.1** (PRO), **2.2** (UCB) and **2.3** (BV) in DMSO at concentrations of 1 mM, 2 mM, and 3 mM were prepared, and 1 μL of each bile pigment solution was added to a solution of a mutagen in order to have a final concentration of 0.25 μM , 0.5 μM , 1 μM , 1.5 μM , 2 μM , 3 μM (addition of the BPs solutions continued until the concentration of BPs was double or three times higher than that of the mutagen). All mixtures were measured and λ_{max} of both BPs and mutagens was recorded. Samples were then stored overnight at 4 °C before the UV spectrum was measured again.

The ¹H NMR spectrum of each mutagen and BP in Sol B was measured on a Bruker Advance 500 MHz spectrometer. A solution of the BPs being studied in Sol B was added to the mutagen sample in such a way that the molar ratio of BP to mutagen was raised from approximately 2:1 to 1:1 and then 1:2. The ¹H NMR spectra of these mixtures were then collected. Likewise, the experiments of dimethyl ester of BPs and mutagens were performed, however, instead of using Sol B, Sol A was utilized because dimethyl ester of BPs are sparingly soluble in the presence of D₂O.

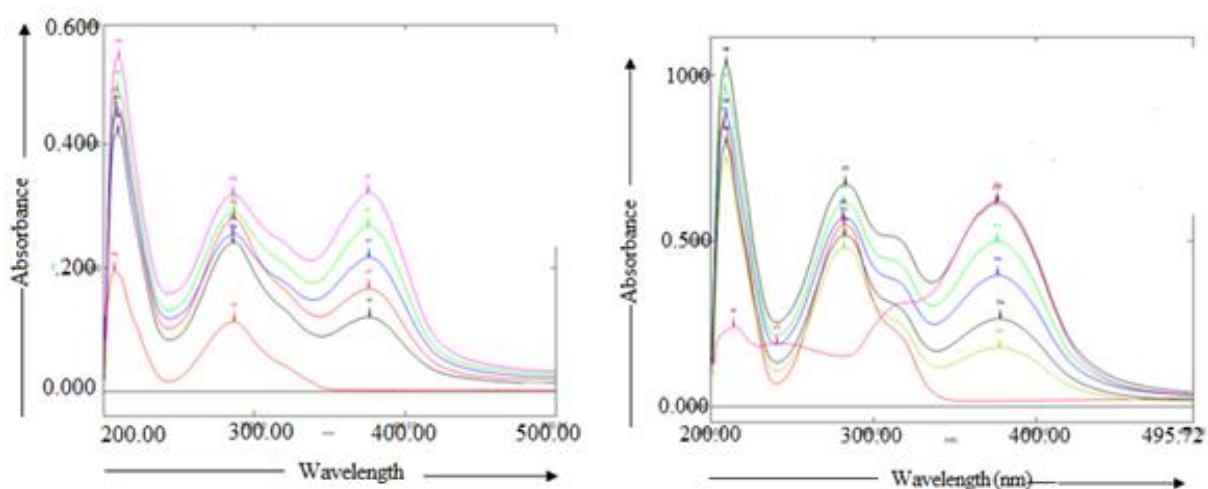
2.4.1 BV and 2AF, PhiP, B α P

Figure 2.2: Overlay of the UV spectra of the mixtures of **2.9** (2AF, 1 μ M) and varying concentrations of **2.3** (BV, from 0.5 μ M to 0.75, 1, 1.5, 2 μ M) in methanol (left) and buffer (right). The red line with a signal peak at 288 nm was the UV spectra of **2.9** (2AF). The introduction of **2.3** (BV, from 0.5 μ M to 0.75, 1, 1.5, 2 μ M) in the mixture was detected by the increasing UV absorbance at 350 nm.

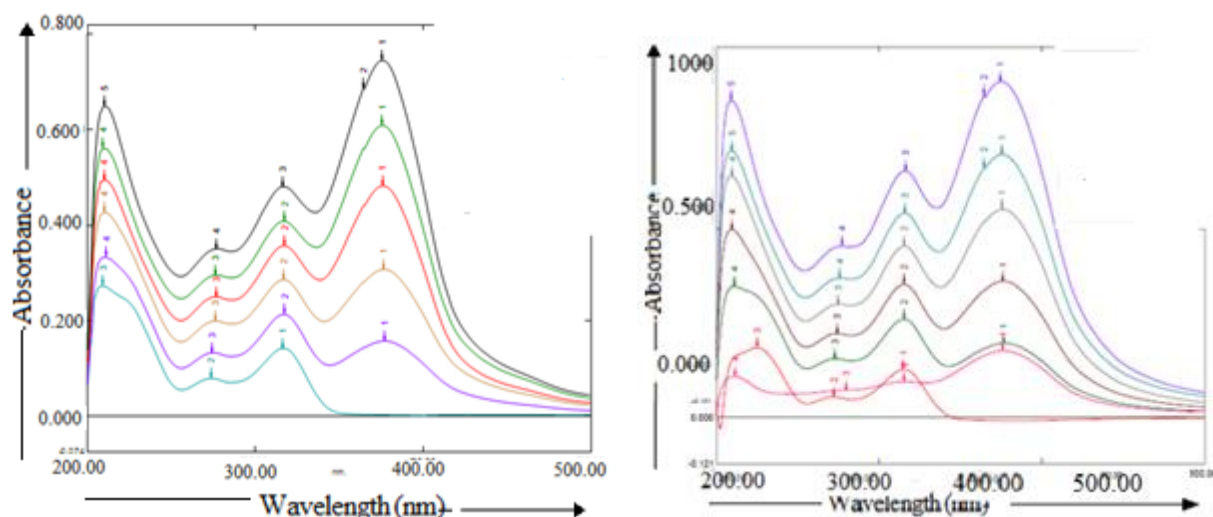


Figure 2.3: Overlay of the UV spectra of the mixtures of **2.7** (PhiP, 1 μ M) and varying concentrations of **2.3** (BV, 1 μ M) in methanol (left) and buffer (right). The red line (right) and blue line (left) with signal peaks at 317 nm was the UV spectra of **2.7** (PhiP). The introduction of **2.3** (BV, from 1 μ M to 3 μ M) in the mixture was detected by the increasing UV absorbance at 350 nm.

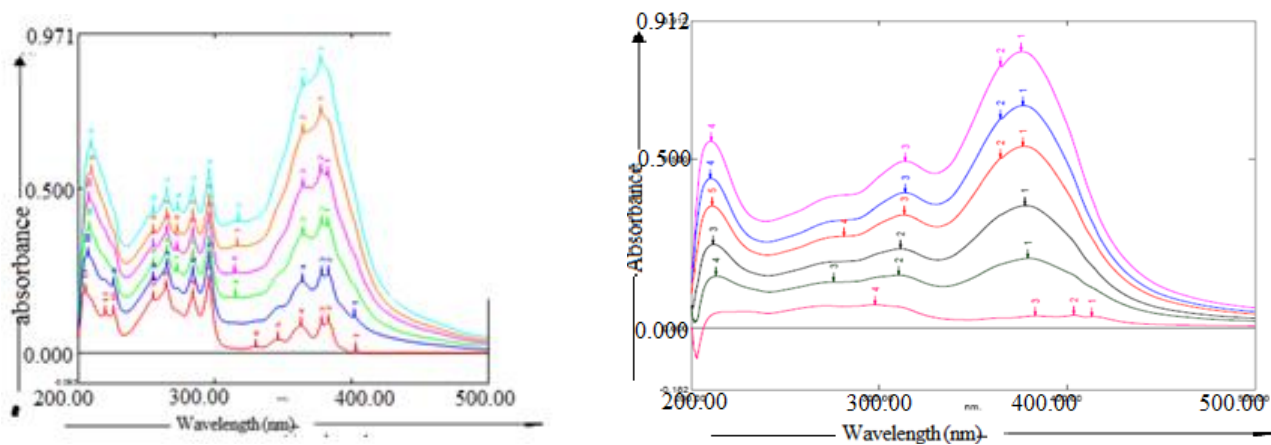


Figure 2.4: Overlay of the UV spectra of the mixtures of **2.8** (B α P, 1 μ M) and varying concentrations of **2.3** (BV, 1 μ M) in methanol (left) and buffer (right). The red line that was in close proximity to baseline (λ_{\max} 295 nm) was the UV spectra of **2.8** (B α P). The introduction of **2.3** (BV, from 1 μ M to 2 μ M) in the mixture was detected by the increasing UV absorbance at 350 nm.

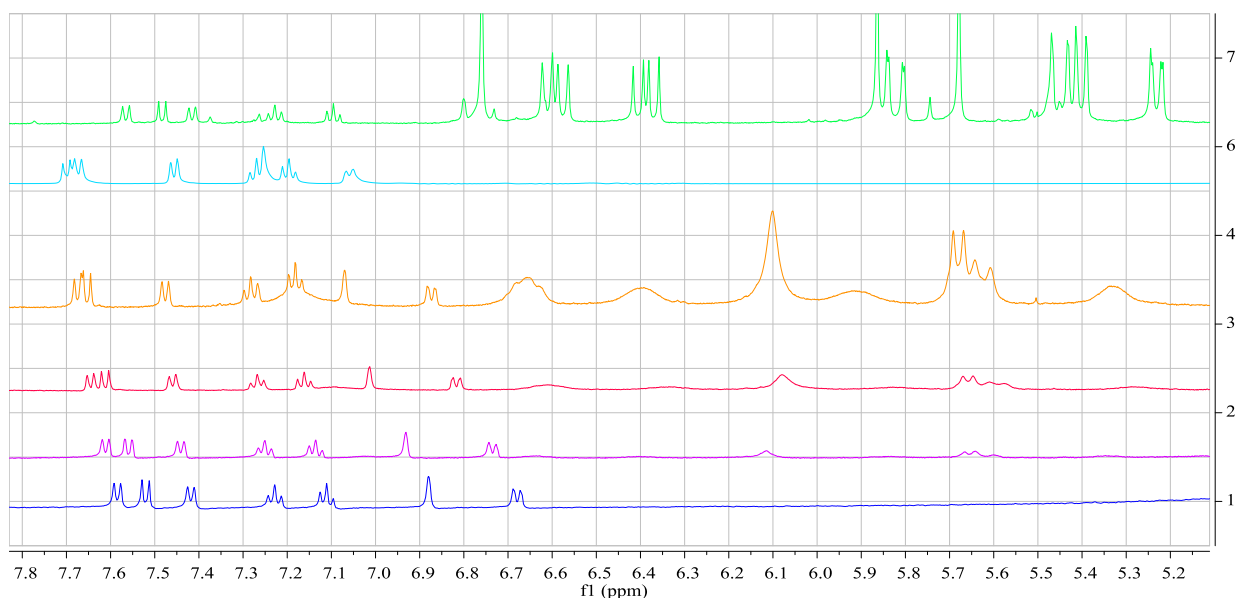


Figure 2.5: Overlay of the ^1H NMR spectra of **2.9** (2AF, blue) and its mixtures with varying concentrations of **2.3** (BV) performed at 500 MHz in Sol B. The molar ratios of **2.9** (2AF) and **2.3** (BV) are 2:1 (pink), 1:1 (red), 1:2 (yellow), 1:0 (blue in the presence of HCl and acetic acid) and 1:2 (green in the presence of 10 μ L of LiOH).

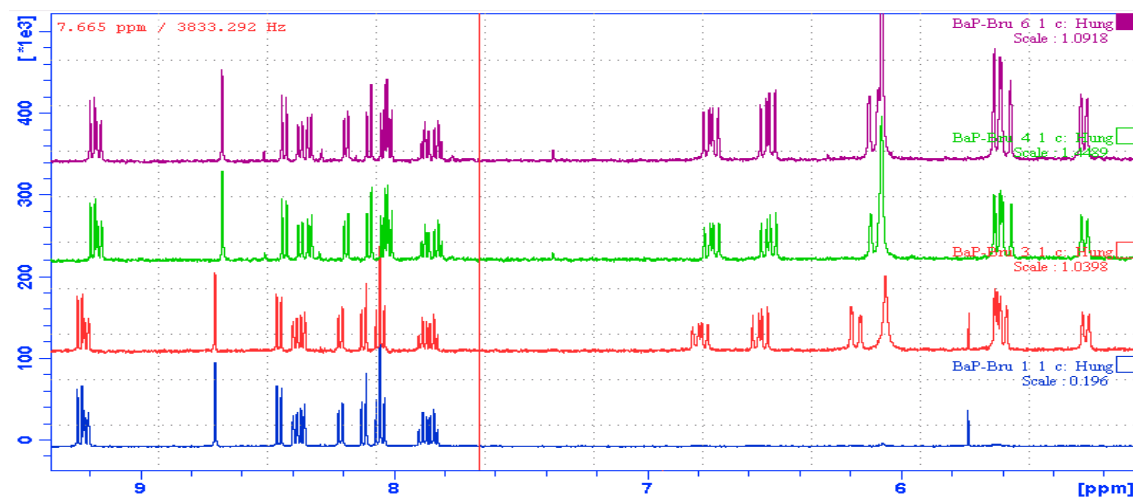
2.4.2 BRU and 2AF, PhiP, B α P

Figure 2.6: Overlay of the ^1H NMR spectra of **2.8** (BaP, blue) and its mixtures with varying concentrations of **2.2** (UCB) performed at 500 MHz in Sol B. The molar ratios of **2.8** (BaP) and **2.2** (UCB) are 2:1 (red), 1:1 (green), 1:2 (purple).

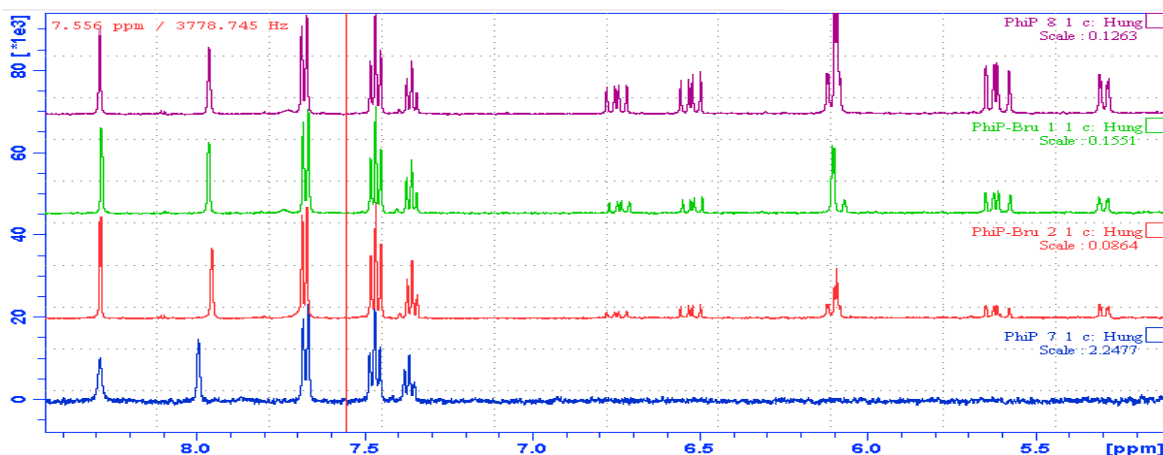


Figure 2.7: Overlay of the ^1H NMR spectra of **2.7** (PhiP, blue) and its mixtures with varying concentrations of **2.2** (UCB) performed at 500 MHz in Sol B. The molar ratios of **2.7** (PhiP) and **2.2** (UCB) are 2:0.5 (red), 2:0.75 (green), 1:1.5 (purple).

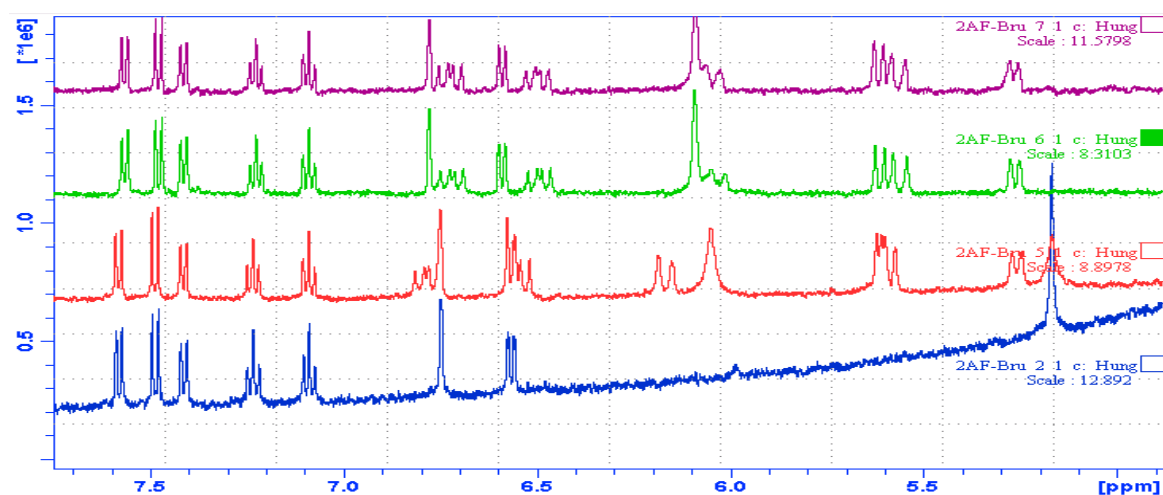


Figure 2.8: Overlay of the ^1H NMR spectra of **2.9** (AF, blue) and its mixtures with varying concentrations of **2.2** (UCB) performed at 500 MHz in Sol B. The molar ratios of **2.8** (B α P) and **2.2** (UCB) are 2:1 (red), 1:1 (green), 1:2 (purple).

2.4.3 PRO and 2AF, PhiP, B α P

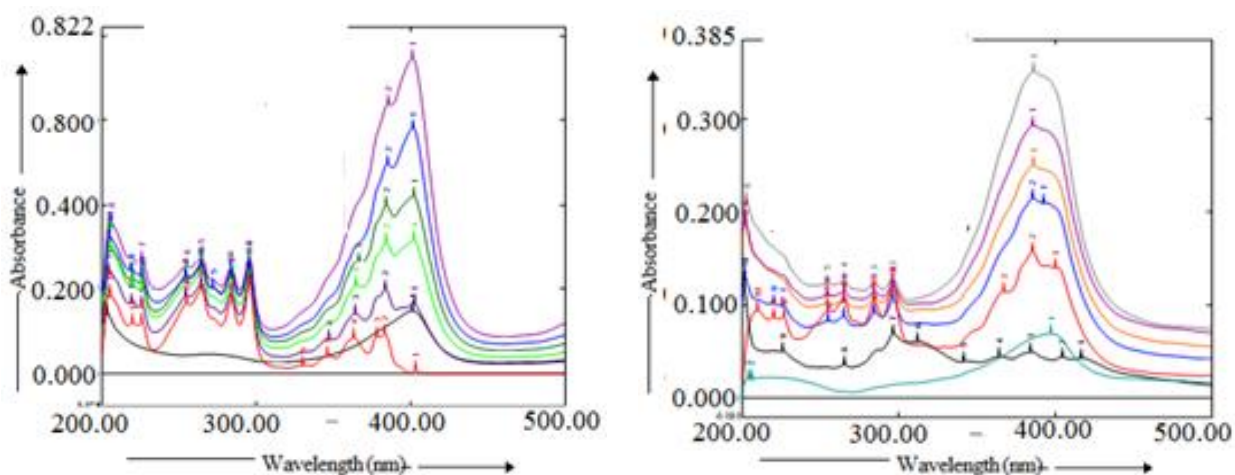


Figure 2.9: The overlay of spectra of **2.8** (B α P, 1 μM in methanol, 0.5 μM in buffer) and varying concentrations of **2.1** (PRO, from 0.5 μM to 3.0 μM in methanol (left) and from 0.25 μM to 0.75 μM in buffer (right)). The red line (left) and black line (left) close to the baseline (λ_{max} 295 nm) was the UV spectra of **2.8** (B α P). The introduction of **2.1** (PRO, from 0.5 μM to 3 μM) in the mixture was detected by the increasing UV absorbance at 401 nm (left) and 385 nm (right).

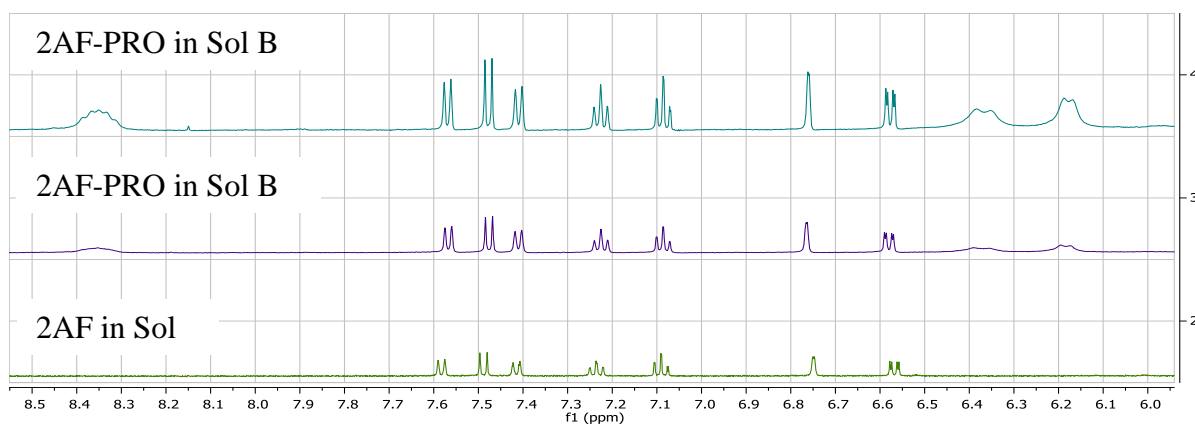


Figure 2.10: Overlay of the ¹H NMR spectra of **2.9** (2AF, green) and its mixtures with varying concentrations of **2.1** (PRO) performed at 500 MHz in Sol B. The molar ratios of **2.1** (PRO) and **2.7** (PhIP) are 1:1 (purple), 1:2 (blue).

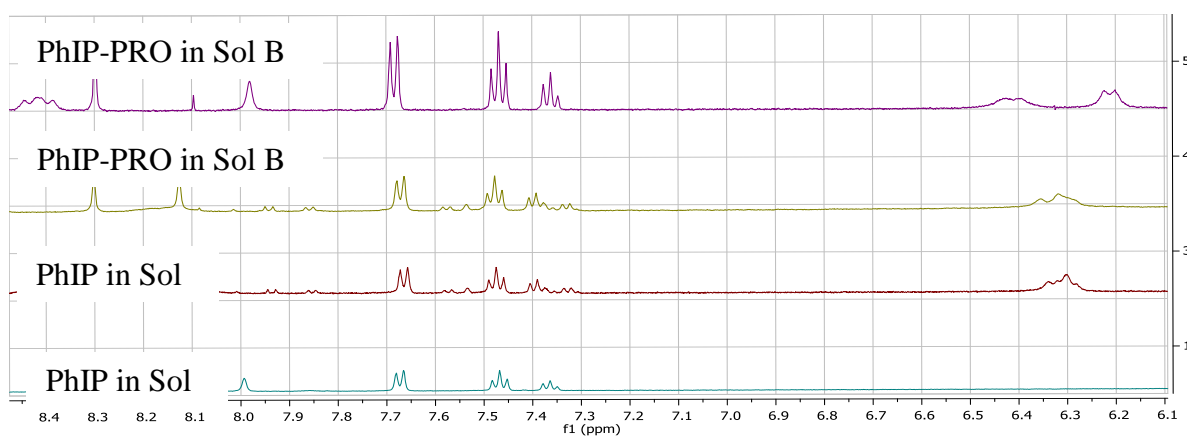


Figure 2.11: Overlay of the ¹H NMR spectra of **2.7** (PhIP, green) and its mixtures with varying concentrations of **2.1** (PRO) performed at 500 MHz in Sol B. The molar ratios of **2.1** (PRO) and **2.7** (PhIP) are 1:1 (purple, yellow), 1:2 (blue).

2.4.4 Dimethyl ester of BPs and 2AF, PhiP, BαP

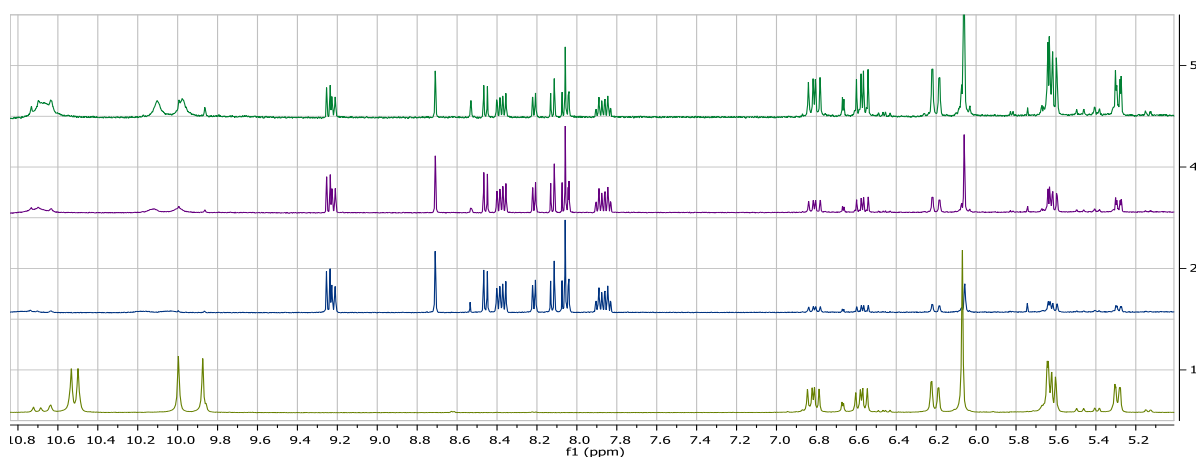


Figure 2.12: Overlay of the ¹H NMR spectra of **2.5** (UCBDE, yellow) and the mixtures of **2.8** (BαP) with varying concentrations of **2.5** (UCBDE, performed at 500 MHz in Sol A. The molar ratios of **2.5** (UCBDE) and **2.8** BαP are 1:2 (blue), 1:1 (purple), 1:2 (green).

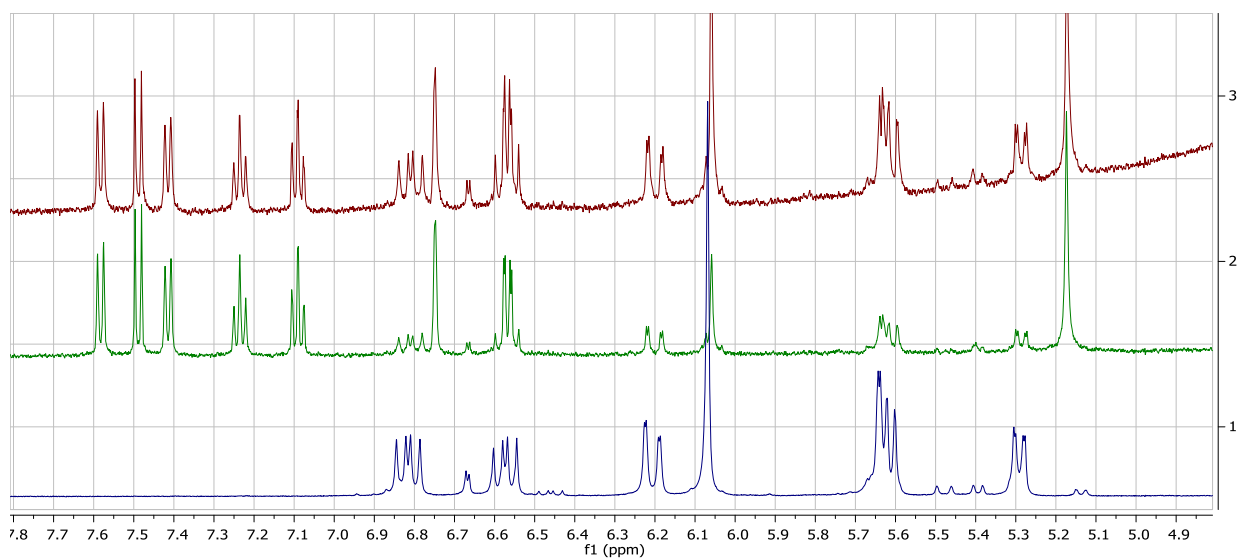


Figure 2.13: Overlay of the ¹H NMR spectra of **2.5** (UCBDE, purple) and the mixtures of **2.9** (2AF) with varying concentrations of **2.5** (UCBDE, performed at 500 MHz in Sol A). The molar ratios of **2.9** (2AF) and **2.5** (UCBDE) are 0.5:1 (green), 1:1 (brown).

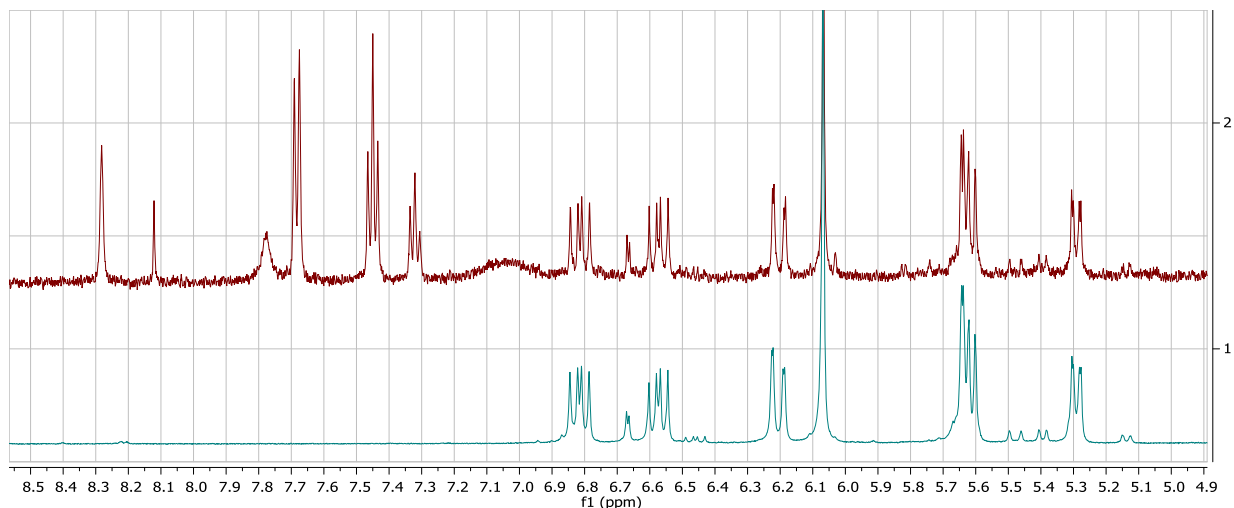


Figure 2.14: Overlay of the ¹H NMR spectra of **2.5** (UCBDE, blue) and its mixtures **2.7** (PhIP, performed at 500 MHz in Sol A).

2.4.5 2AF and BV, BRU, PRO

Table 2.5: A comparison of selected proton signals of **2.9** (2AF) with different BPs present.

	2.9 (Sol A)	2.9 (Sol B)	2.9+2.3 (Sol B)	2.9+2.1 (Sol B)	2.9+2.2 (Sol B)
H	$\overline{\delta_{\text{H}}}$ (ppm), mult., J (Hz) ^a	$\overline{\delta_{\text{H}}}$ (ppm), mult., J (Hz) ^a	$\overline{\delta_{\text{H}}}$ (ppm), mult., J (Hz) ^a	$\overline{\delta_{\text{H}}}$ (ppm), mult., J (Hz) ^a	$\overline{\delta_{\text{H}}}$ (ppm), mult., J (Hz) ^a
1	6.76, s	6.88, s	7.01 s	6.76, s	6.75, s
3	6.58, dd, 8.0, 2.0	6.68, dd, 8.0, 2.0	6.82, d, 8.0	6.58, dd, 8.0, 2.0	6.58, dd, 8.0, 2.0
4	7.50, d, 8.0	7.52, d, 8.0	7.61, d, 8.0	7.49, d, 8.0	7.49, d, 8.0
5	7.59, d, 7.5	7.58, d, 7.5	7.65, d, 7.5	7.58, d, 7.5	7.58, d, 7.5
6	7.24, t, 7.5	7.23, d, 7.5	7.27, t, 7.5	7.23, t, 7.5	7.23, t, 7.5
7	7.10, dt, 7.5, 1.0	7.11, d, 7.5	7.16, t, 7.5	7.09, t, 7.5	7.10, t, 7.5
8	7.42, d, 7.5	7.42, d, 7.5	7.45, d, 7.5	7.41, d, 7.5	7.41, d, 7.5
9	3.72, s	3.70, s	3.75, s	3.71, s	3.71, s

^aChemical shift (ppm) referenced to DMSO-*H*₆ δ_{H} 2.49 were taken from 1D NMR (DMSO-*d*₆, 500 MHz).

2.4.6 PhiP and BV, BRU, PRO

Table 2.6: A comparison of selected proton signals of **2.7** (PhiP) with different BPs present.

	2.7 (Sol A)	2.7 (Sol B)	2.7+2.3 (Sol B)	2.7+2.1 (Sol B)	2.7+2.2 (Sol B)
H	$\overline{\delta_{\text{H}}}$ (ppm), mult., J (Hz) ^a	$\overline{\delta_{\text{H}}}$ (ppm), mult., J (Hz) ^a	$\overline{\delta_{\text{H}}}$ (ppm), mult., J (Hz) ^a	$\overline{\delta_{\text{H}}}$ (ppm), mult., J (Hz) ^a	$\overline{\delta_{\text{H}}}$ (ppm), mult., J (Hz) ^a
1 ¹	3.66, s	3.57, s	3.54, s	3.55, s	3.57, s
2 ¹	8.53, brs				
5a	8.43, s	8.29, s	8.25, s	8.26, d, 2.0	8.28, d, 2.0
7	8.00, s	7.99, s	7.93, s	7.92, d, 2.0	7.93, d, 2.0
2 ²	7.76, d, 7.5	7.67, d, 7.5	7.65, d, 7.4	7.65, d, 7.5	7.67, d, 7.4
3 ²	7.51, t, 7.8	7.47, t, 7.8	7.46, t, 7.8	7.46, t, 7.8	7.46, t, 7.8
4 ²	7.42, t, 7.5	7.36, t, 7.5	7.35, t, 7.5	7.35, t, 7.5	7.35, t, 7.5
5 ²	7.51, t, 7.8	7.47, t, 7.8	7.46, t, 7.8	7.46, t, 7.8	7.46, t, 7.8
6 ²	7.76, d, 7.5	7.67, d, 7.5	7.65, d, 7.4	7.68, d, 7.5	7.67, d, 7.4

^aChemical shift (ppm) referenced to DMSO-*H*₆ δ_{H} 2.49 were taken from 1D NMR (DMSO-*d*₆, 500 MHz).

2.4.7 B[α]P and BV, BRU, PRO**Table 2.7:** A comparison of selected proton signals of **2.8** (B α P) in the presence of different BPs.

H	2.8 (Sol A)	2.8 (Sol B)	2.8+2.3 (Sol B)	2.8+2.1 (Sol B)	2.8+2.2 (Sol B)
	$\overline{\delta_H}$ (ppm), mult., J (Hz) ^a	$\overline{\delta_H}$ (ppm), mult., J (Hz) ^a	$\overline{\delta_H}$ (ppm), mult., J (Hz) ^a	$\overline{\delta_H}$ (ppm), mult., J (Hz) ^a	$\overline{\delta_H}$ (ppm), mult., J (Hz) ^a
1	8.36, d, 7.6	8.32, d, 7.8	8.33, d, 7.8	8.30, d, 7.8	8.33, d, 7.8
2	8.06, t, 7.5	8.03, d, 7.7	8.03, d, 7.7	8.02, d, 7.7	8.04, d, 7.7
3	8.21, d, 7.6	8.18, d, 7.4	8.18, d, 7.4	8.17, d, 7.4	8.19, d, 7.4
4	8.05, d, 9.1	8.01, d, 9.1	8.01, d, 9.1	7.99, d, 9.1	8.01, d, 9.1
5	8.12, d, 9.1	8.09, d, 9.1	8.09, d, 9.1	8.06, d, 9.1	8.10, d, 9.1
6	8.71, s	8.66, s	8.67, s	6.64, s	8.68, s
7	8.39, d, 8.0	8.36, d, 7.9	8.37, d, 7.9	8.35, d, 7.9	8.37, d, 7.9
8	7.84, m	7.82, m	7.82, t, 7.0	7.81, t, 7.0	7.83, m
9	7.89, m	7.87, m	7.87, m	7.86, t, 7.0	7.88, m
10	9.22, d, 8.5	9.14, d, 8.4	9.15, d, 8.4	9.12 brd	9.17, d, 8.4
11	9.24, d, 9.2	9.16, d, 9.2	9.18, d, 9.2	9.14 brd	9.19, d, 9.2
12	8.46, d, 9.2	8.42, d, 9.2	8.43, d, 9.2	8.40, d, 9.2	8.43, d, 9.2

^aChemical shift (ppm) referenced to DMSO- H_6 δ_H 2.49 were taken from 1D NMR (DMSO- d_6 , 500 MHz).

pH measurement:**Table 2.8:** The pH of mutagens in the presence of BPs in sol A and sol B.

Solution	pH		Solution	pH	
	Sol A	Sol B		Sol A	Sol B
2.1	8.8	6.2	2.1 + 2.7	8.2	7.9
2.2	8.2	6.9	2.1 + 2.8	8.0	6.3
2.3	4.0	3.8	2.1 + 2.9	8.2	7.2
2.7	8.0	8.9	2.2 + 2.7	8.2	7.8
2.8	7.3	6.9	2.2 + 2.8	8.3	7.1
2.9	7.6	8.1	2.2 + 2.9	8.0	8.0
2.3 + 2.7	5.9	4.9	2.3 + 2.9	4.9	5.0
2.3 + 2.8	4.4	3.9			

Chapter 3: Investigation of the effects of bile pigments on the permeability of PhIP across intestinal epithelial cells.

3.1 Introduction

Physical interactions between molecules, such as van der Waals forces, electrostatic forces, and π -stacking, play an important role in biology, biochemistry, and chemistry. These intermolecular interactions strongly affect the bioactivity of organic compounds *in vitro* and *in vivo*. Of these intermolecular interactions, the attractive forces between aromatic compounds, or π -stacking, have recently been the subject of a number of biochemical studies.^{21,143,149,151,153,162-165} Mölzer et al.²¹ and Bulmer et al.^{14,15} also hypothesised that π -stacking interactions were factors in the inhibitory action of BPs. All the above-mentioned findings hypothesised that physical interactions may have a significant contribution to the anti-mutagenic property of BPs.

The physical interactions between BPs and mutagens have been mentioned in a variety of biochemical studies.^{2,15,18,21,38} UV and ¹H NMR methods have also been used in other studies to determine the physical interactions between organic molecules.^{150,153,155} Our previous study (see Chapter II) used two methods (UV and ¹H NMR spectroscopy) to detect intermolecular interactions between mutagens (2-amino-1-methyl-6-phenylimidazo(4,5-b)pyridine (**3.6**, PhIP) and benzo[α]pyrene (**3.7**, B α P) and BPs (protoporphyrin IX α (**3.1**, PRO), unconjugated bilirubin IX α (**3.2**, UCB), biliverdin IX α (**3.3**, BV) bilirubin dimethyl ester (**3.4**, UCBDE), and biliverdin dimethyl ester (**3.5**, BVDE)). The results of the study were negative; no evidence was found in the ¹H NMR or UV spectra to indicate that strongly sustained π - π interactions were occurring. Some slight changes in the proton chemical shifts of the BPs were determined to be the result of changes in the protonation state of the compounds and not from π - π interactions. However, due to the low water solubility of the compounds, these studies were performed in organic solvents (DMSO, D₂O and MeOH), and therefore there remains some uncertainty about what might occur in a biological system. Furthermore, Mölzer et al.²¹ reported that the physical interactions between TNF α and BPs might result in the anti-mutagenicity of BPs. Therefore, it was necessary to discover another method to test the weaker physical interactions occurring between BPs and polycyclic aromatic mutagens

Caco-2 cells are derived from human colorectal carcinoma cells cultured under appropriate conditions to form fully functional polarised monolayers that mimic the small intestinal epithelia.^{129,130} The monolayers exhibit the brush border associated with the intestinal epithelia on the apical membrane and express most of the digestive enzymes and transporters present in the

small intestine.^{20,21} The apparent permeability (P_{app}) of small molecules across the monolayer has been shown to directly correlate to the compound's *in vivo* oral bioavailability.¹⁶⁶⁻¹⁷⁰

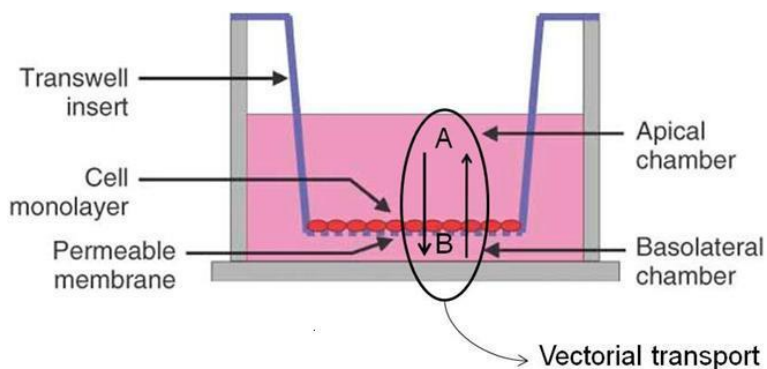
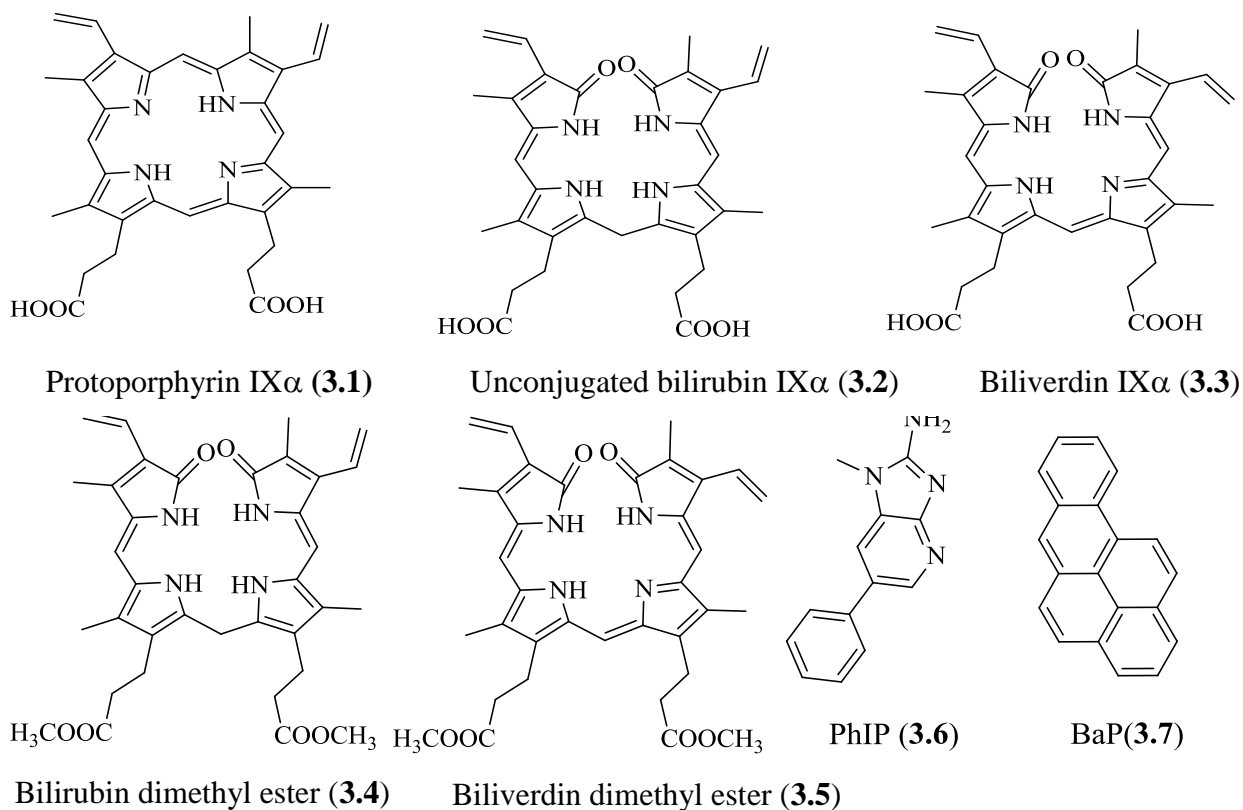


Figure 3.1: Diagram of a well and an insert membrane used for culturing Caco-2 cell monolayers.

Our hypothesis for this study was that if a molecule experiences significant physical interactions with another compound in the apical compartment of the transwell, its P_{app} and the fraction absorbed will be affected.^{136,171-173} Therefore, we used the Caco-2 cell monolayers to determine the effects of physical interactions between **3.6** (PhIP) and **3.7** (BaP) on their apparent permeability in the presence and absence of BPs.



3.2 Results and discussion

The experiments were conducted by placing a solution of the mutagen (10 μM) being examined in the apical chamber (AP) and placing fresh buffer in the basolateral chamber (BL) and taking samples from the BL every 30 min and determining the concentration of mutagen by analytical HPLC. Each experiment was performed in the presence of any BP and then with varying concentrations of BP (5 μM , 10 μM and 20 μM for **3.2** (UCB) and 10 μM for others) added to the AP with the mutagen at the start of the experiment.

3.2.1 Permeability of PhIP in the presence and absence of bile pigments.

At the conclusion of the experiments ($t = 180$ min), the number of moles of each of the compounds in the apical chamber (AP), and in the basolateral chamber (BL) was determined (Figure 3.1). If the total of these does not equate to the number of moles of compound initially added to the apical layer, it is assumed that the compound has been absorbed into, or adhered onto, the Caco-2 cell monolayers. This is known to be a significant issue when studying the permeability of very lipophilic compounds.^{174,175} The detailed data in Table 3.5 show the differences in the rate of absorbance, P_{app} , and transport of **3.6** (PhIP) in the presence of BPs and their dimethyl esters. The absorption of **3.6** (PhIP) across a confluent Caco-2 cell monolayer was measured in the absence of any other additive and it exhibited a very high rate of transport from AP to BL, with total amount increasing from 0 to 180 min and reaching nearly 70% of **3.6** (PhIP) crossing to the BL after 180 min and with a P_{app} of 1.74×10^{-5} cm/s (Table 3.1 and Table 3.5).

Table 3.1: Total amount of **3.6** (PhIP) transferred to BL and remained in the AP chamber and associated with the cell monolayers (nmol) from 0 to 180 min in control experiments ($n = 3$).

t (min)	Total amount transferred to receiver chamber (nmol)			Remained in apical chamber and associated with monolayers (nmol)		
	Well-1	Well-2	Well-3	Well-1	Well-2	Well-3
0	0	0	0	0.999	0.999	0.999
30	0.165	0.158	0.189	0.835	0.842	0.811
60	0.322	0.297	0.338	0.678	0.703	0.662
90	0.452	0.417	0.478	0.548	0.583	0.522
120	0.536	0.528	0.567	0.464	0.472	0.434
150	0.628	0.604	0.658	0.372	0.396	0.342
180	0.699	0.674	0.704	0.300	0.326	0.296

Figure 3.2 shows the permeability of **3.6** (PhIP) increased slightly in the presence of **3.3** (BV), **3.4** (UCBDE), and **3.5** (BVDE), with the total fraction transported across the monolayer in 180 min increasing, to 82.1%, 83.1%, and 79.9% respectively (Figure 3.2, Figure 3.3 and Table 3.5) (see appendix-B for more details). The total amount of **3.6** (PhIP) transferred to the BL in the presence of **3.4** (UCBDE) increased steadily over the incubation period from about 0.211 nmol after 30 min to just under 0.854 nmol after 180 min (Table 3.2). The amount transferred was slightly higher than that transferred in the control experiments (Table 3.1). In contrast, the total amount of **3.6** (PhIP) remained in the AP and associated with monolayers decreased significantly from 0.999 to 0.145 nmol (Table 3.2). This amount at 180 min was about 50% smaller than that of control reaction (0.145 compared to 0.326 nmol) (Table 3.1 and Table 3.2).

Table 3.2: Total amount of **3.6** (PhIP) transferred to BL and remained in the AP chamber and associated with the cell monolayers (nmol) in the presence of **3.4** (UCBDE) from 0 to 180 min (n = 3).

t (min)	Total amount of 3.6 in the presence of 3.4					
	transferred to receiver chamber (nmol)			Remained in apical chamber and associated with monolayers (nmol)		
	Well-1	Well-2	Well-3	Well-1	Well-2	Well-3
0	0	0	0	0.999	0.999	0.999
30	0.211	0.229	0.270	0.789	0.771	0.729
60	0.404	0.423	0.459	0.596	0.577	0.540
90	0.533	0.568	0.599	0.467	0.432	0.400
120	0.663	0.664	0.685	0.337	0.336	0.315
150	0.758	0.759	0.774	0.242	0.240	0.226
180	0.809	0.831	0.854	0.192	0.169	0.146

In the control experiment, 6.4% of **3.6** (PhIP) was assumed to be associated with the monolayer and this rate fell to 0% in the presence of **3.3** (BV), **3.5** (BVDE) and **3.4** (UCBDE) in Table 3.5). The P_{app} of **3.6** (PhIP) also underwent a considerable increase from 1.74×10^{-5} cm/s in the absence of BPs to approximately 2.27×10^{-5} cm/s in the presence of **3.3** (BV), **3.5** (BVDE) and **3.4** (UCBDE) in Table 3.5). Therefore, BPs (**3.3** (BV), **3.5** (BVDE) and **3.4** (UCBDE)) appeared to slightly support the transport of **3.6** (PhIP) across the cell monolayer which may be due to the effects of physical interactions between the compounds.

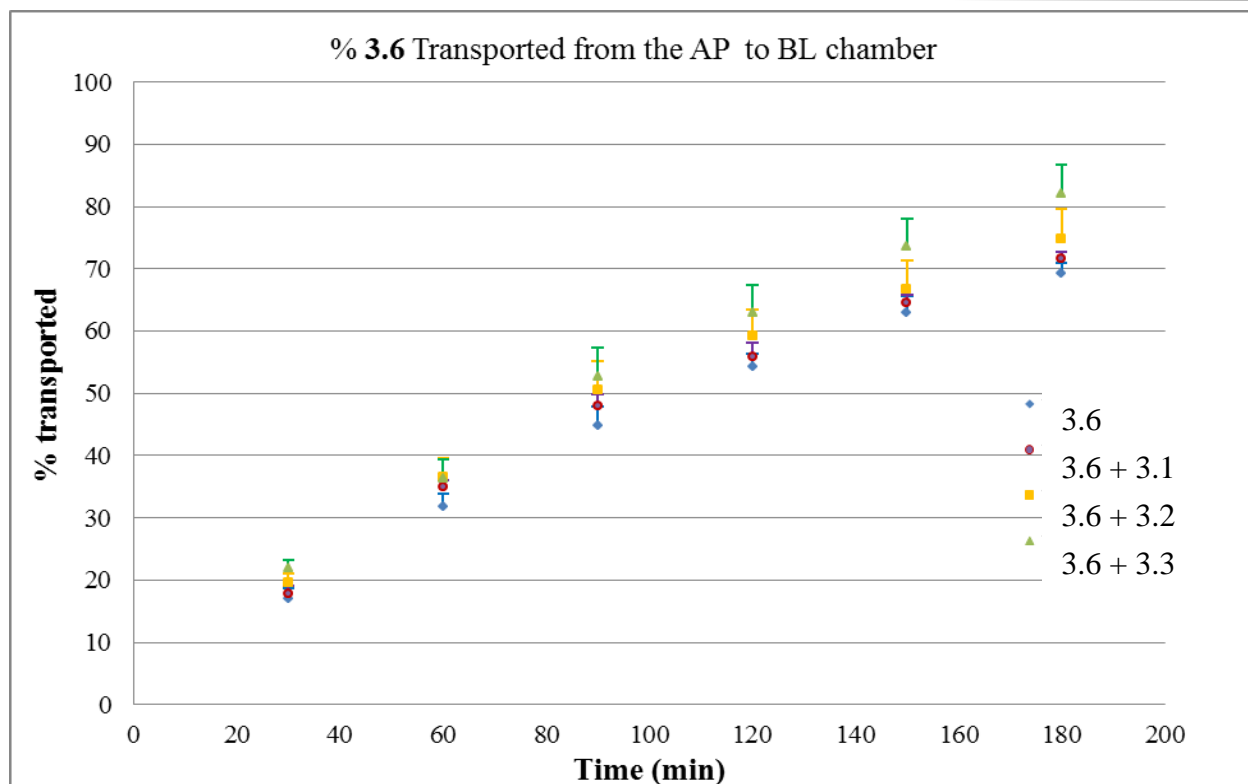


Figure 3.2: A comparison the percentage of **3.6** (PhIP) (10 μ M) transported from AP to BL over 180 min in the absence and presence of **3.1** (PRO), **3.2** (UCB), **3.3** (BV) with 10 μ M.

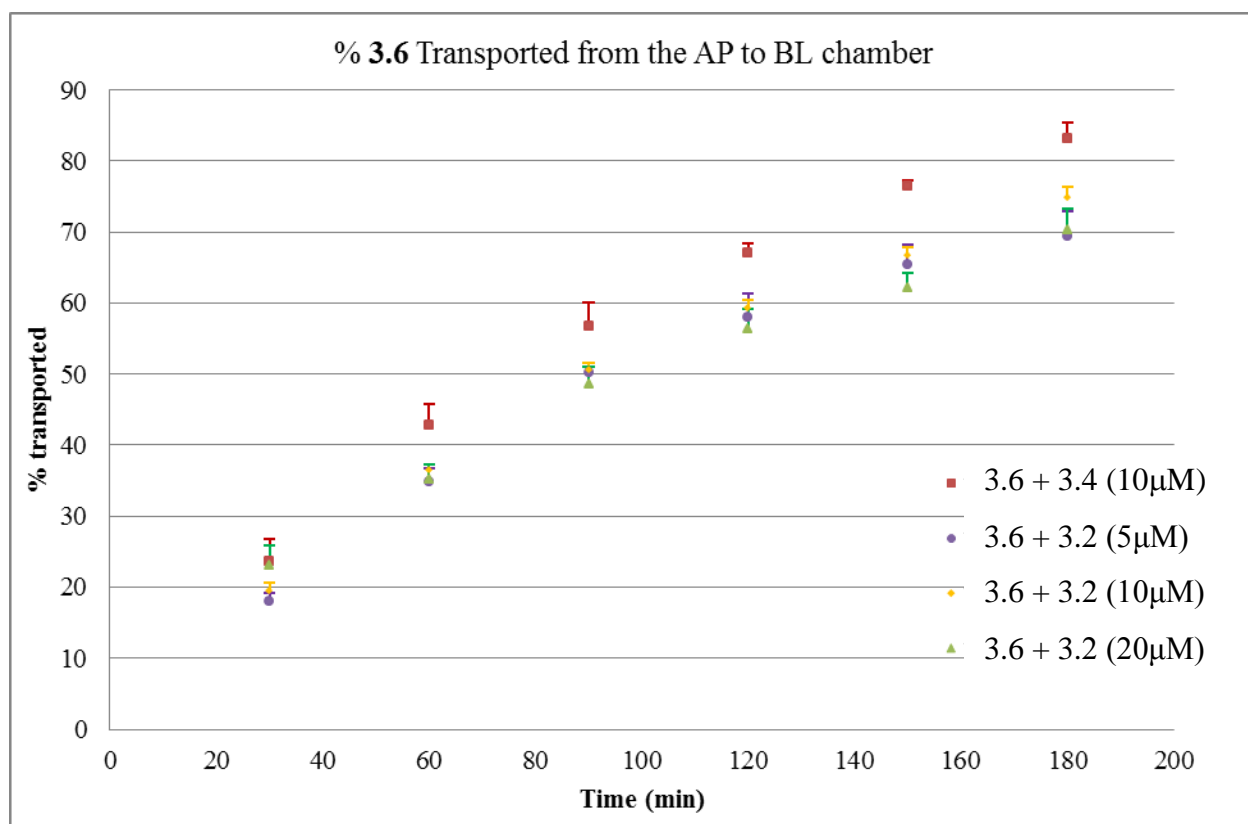


Figure 3.3: A comparison the percentage of **3.6** (PhIP) transported from AP to BL in the absence and presence of varying concentrations of **3.2** (UCB, from 5 μ M to 20 μ M) and 10 μ M of **3.4** (UCBDE).

Interestingly, there were differences in the transported rate of **3.6** (PhIP) in the presence of **3.2** (UCB) and **3.3** (BV). In the presence of **3.3** (BV), 82.1% of **3.6** (PhIP) was transported to the BL, while this was 70.4% with the addition **3.2** (UCB). The latter was not different from the amount of **3.6** transported in the control experiments indicating that **3.2** (UCB) did not affect the rate of transported of **3.6** (PhIP, Table 3.1 and Table 3.3). In contrast, the effects of **3.3** (BV) led to an increase of 13% in the amount of **3.6** (PhIP) transported rate. Furthermore, the percentage of **3.6** (PhIP) associated with the cell monolayers when no BPs were present was 6.4% while this increased to 12.6% in the presence of **3.2** (UCB) and decreased to 0% in the presence of **3.3** (BV, Table 3.5).

Table 3.3: Total amount of **3.6** (PhIP) transferred to BL and remained in the AP chamber and associated with the cell monolayers (nmol) in the presence of **3.2** (UCB) from 0 to 180 min (n = 3).

t (min)	Total amount of 3.6 (PhIP) in the presence of 3.2 (UCB)					
	transferred to receiver chamber (nmol)			Remained in apical chamber and associated with monolayers (nmol)		
	Well-1	Well-2	Well-3	Well-1	Well-2	Well-3
0	0	0	0	0.999	0.999	0.999
30	0.199	0.207	0.162	0.801	0.793	0.838
60	0.358	0.369	0.339	0.642	0.6.31	0.660
90	0.484	0.506	0.476	0.516	0.494	0.524
120	0.581	0.581	0.568	0.419	0.419	0.431
150	0.640	0.649	0.637	0.360	0.351	0.363
180	0.705	0.710	0.695	0.295	0.289	0.305

Moreover, the P_{app} of **3.6** (PhIP) fluctuated around 1.90×10^{-5} (cm/s) in the presence and absence of **3.1** (PRO) or **3.2** (UCB), whereas the addition of **3.3** (BV), **3.4** (UCBDE), and **3.5** (BVDE) led to an increase in the P_{app} of **3.6** (PhIP) to approximately 2.27×10^{-5} (cm/s). The variation in P_{app} , the percentage transferred, associated with the monolayers, and remaining in AP of **3.6** (PhIP) in the presence of BPs and their dimethyl esters may be the result of physical interactions between two classes of chemicals for the following reasons.

The differences in the fraction transported of **3.6** (PhIP) in the presence of **3.2** (UCB) and **3.3** (BV) may be the results of the differences in their structures. Although both structures of **3.2** (UCB) and **3.3** (BV) have the same carboxylic groups and similar conjugated aromatic ring systems, the unsaturated C10-bridge of **3.2** (UCB) causes a significant difference in the 3D structure of the compound compared to **3.3** (BV). This flexible bridge facilitates the free rotation of the two

carboxylic groups of **3.2** (UCB) to generate at least six stable isomers and a variety of transition structures in solution (for more details see Chapters I and V).^{58,59,62} The two propionic groups can freely rotate 360° and generate more interactions between **3.2** (UCB) and the polar cell surface. In contrast, **3.3** (BV) possesses a nearly planar, fully conjugated aromatic system that holds the two propionic groups on one side and is less able to interact with the cell surface of the monolayers.

Therefore, this led to a hypothesis that the lipophilic aromatic ring in **3.2** (UCB) interacted with **3.6** (PhIP) and the hydrophilic carboxylic acid groups then generated interactions with the polar surface of the cell monolayer to hold more **3.6** (PhIP) in the monolayers, thus causing the increase in the amount of **3.6** (PhIP) remaining associated with the cell monolayers (Table 3.3 and Table 3.5). In fact, **3.3** (BV) and **3.1** (PRO) showed less interactions with the cell surface, and the percentage of **3.6** (PhIP) associated with the monolayers was nearly 0%, while the presence of **3.2** (UCB) led to a significant increase of approximately 12% in the amount of **3.6** (PhIP) associated with the cells (Table 3.4 and Table 3.5). The hypothesis was also supported by the fact that 0% of **3.6** (PhIP) remained associated with the monolayers in the presence of **3.4** (UCBDE) and **3.5** (BVDE). These bile pigment derivatives have both carboxylate groups esterified and so would have reduced electrostatic interactions with the cell monolayer surface (Table 3.5). The results also indicated that BPs and their dimethyl esters supported the permeability of **3.6** (PhIP) through the Caco-2 cell monolayer.

The similar P_{app} of **3.6** (PhIP) in the presence of **3.4** (UCBDE) and **3.5** (BVDE) indicated that when carboxylic acid groups were converted to methyl esters (Table 3.5), there were equal interactions between **3.4** (UCBDE) and **3.5** (BVDE) to **3.6** (PhIP). The interactions with the methyl ester derivatives increased the P_{app} of **3.6** (PhIP) which suggests that the interactions between **3.6** (PhIP) and BPs are more likely to be associated with the aromatic rings systems of **3.3** (BV), **3.4** (UCBDE), **3.5** (BVDE) rather than electrostatic interactions with the carboxylate and carboxylic acid groups. The similar P_{app} and fraction absorbed of **3.6** (PhIP, $\sim 2.22 \times 10^{-5}$ cm/s and 80%, respectively) that were found in the presence of **3.3** (BV) its ester **3.5** (BVDE) supported the hypothesis that carboxylic groups have no effect on the permeability of **3.6** (PhIP).

Chapter III: Effect of bile pigments on the permeability of PhIP

Table 3.4: Total amount of **3.6** (PhIP) transferred to BL and remained in the AP and associated with the cell monolayers (nmol) in the presence of **3.3** (BV) from 0 to 180 min (n = 3).

t (min)	Total amount of 3.6 (PhIP) in the presence of 3.3 (BV)					
	transferred to receiver chamber (nmol)			Remained in apical chamber and associated with monolayers (nmol)		
	Well-1	Well-2	Well-3	Well-1	Well-2	Well-3
0	0	0	0	0.999	0.999	0.999
30	0.202	0.222	0.231	0.797	0.778	0.769
60	0.343	0.348	0.399	0.657	0.652	0.601
90	0.480	0.530	0.572	0.520	0.470	0.428
120	0.586	0.634	0.671	0.414	0.366	0.329
150	0.687	0.741	0.778	0.313	0.259	0.222
180	0.772	0.822	0.868	0.228	0.178	0.132

Furthermore, the similar absorption results for **3.6** (PhIP) in the presence of the methyl esters, **3.4** (UCBDE) and **3.5** (BVDE) indicated that when the carboxylic acid groups of **3.2** (UCB) were esterified, the presence of the unsaturated C10-bridge did not create any difference in the permeability of **3.6** (PhIP). Figure 3.3 shows the role of the carboxylic acid groups and the higher concentration of **3.2** (UCB) that can reduce the amount of **3.6** (PhIP) crossing the monolayers and increase the percentage of **3.6** (PhIP) that associated with the monolayer cells (Figure 3.3 and Table 3.5). The results indicate that addition of **3.1** (PRO) did not create any change in the permeability of **3.6** (PhIP). This suggests that **3.1** (PRO) did not interact strongly with **3.6** (PhIP, Table 3.5).

Table 3.5 A comparison of P_{app} and the percentage of **3.6** (PhIP) remaining in AP, trapped in or on the cell monolayer and transported to BL over 180 min in the presence and absence of **3.1** (PRO), **3.2** (UCB), **3.3** (BV), **3.4** (UCBDE), **3.5** (BVDE).

3.6 (10 μ M) added	P_{app} (cm/s)	% transferred to BL	% associated with monolayer	% remained in AP
Nil	$1.74 \times 10^{-5} \pm 1.59 \times 10^{-7}$	69.3 ± 1.9	6.4 ± 3.5	24.2 ± 2.9
3.1 (10 μ M)	$1.97 \times 10^{-5} \pm 2.59 \times 10^{-7}$	71.7 ± 1.6	2.7 ± 3.1	25.5 ± 2.7
3.2 (5 μ M)	$1.86 \times 10^{-5} \pm 5.41 \times 10^{-7}$	70.3 ± 3.1	11.4 ± 3.1	18.2 ± 0.3
3.2 (10 μ M)	$1.94 \times 10^{-5} \pm 1.48 \times 10^{-7}$	70.4 ± 1.5	12.6 ± 1.7	16.9 ± 0.8
3.2 (20 μ M)	$1.95 \times 10^{-5} \pm 9.29 \times 10^{-7}$	69.3 ± 3.8	14.0 ± 3.8	16.7 ± 0.4
3.3 (10 μ M)	$2.25 \times 10^{-5} \pm 1.32 \times 10^{-6}$	82.1 ± 1.8	0.0	17.3 ± 0.5
3.4 (10 μ M)	$2.27 \times 10^{-5} \pm 6.16 \times 10^{-8}$	83.1 ± 2.6	0.0	21.3 ± 1.6

3.5 (10 μ M)	$2.22 \times 10^{-5} \pm 5.82 \times 10^{-7}$	79.9 ± 3.3	0.0	21.2 ± 1.8
-------------------------	---	----------------	-----	----------------

When there was a high concentration of **3.2** (UCB) in the **3.6** (PhIP) assay, the percentage of **3.6** (PhIP) associated with the cell monolayers increased from 6.47% (without **3.2**) to 11.4% (5 μ M of **3.2**), 12.6% (10 μ M of **3.2**), and 14.0% (20 μ M of **3.2**) (Table 3.5). These results strongly support the hypothesis that carboxylic acid groups interact with the cell surface, and are in agreement with the literature, as reported by Phelan et al.²⁹ The amount of **3.6** (PhIP) remaining in the AP reduced from 24.2% (without **3.2**) to 16.7% (20 μ M of **3.2**) indicating that the interactions with **3.2** (UCB) supported the absorption of PhIP through the cell monolayers, and this is also true of **3.3** (BV) and **3.4** (UCBDE), **3.5** (BVDE) (Figure 3.3 and Figure 3.4).

The comparison of P_{app} , percent transferred to the BL, percent associated with monolayers and percent remaining in the AP between **3.2** (UCB) and **3.4** (UCBDE) provided more evidence to confirm that the difference in conformation of **3.2** (UCB) from **3.4** (UCBDE) caused the increase in percent transferred to the BL from 70.4 to 83.1%, respectively. There was a similar increase in the percent associated with the monolayers of **3.2** (UCB). When the carboxylic acid groups of **3.2** (UCB) are protected the complex H-bonding system that establishes the folded three dimensional conformation of UCB is disrupted and the molecule presumably adopts more open, less constrained conformations. Thus, the significant change we see in the Caco-2 cell monolayer permeability and interactions we observe between PhIP incubated with **3.2** (UCB) or the dimethyl ester derivative could be due to the loss of the carboxylate groups but may also be due to the change in overall conformation of the molecule. Since we do not observe the same large effects on the monolayers when BV is incubated with PhIP it could be argued that the presence or absence of carboxylic acid groups may not be the most important effects but the conformation change in **3.4** (UCBDE) may be the predominant effects.

The presence of BPs and their methyl esters increases the permeability of **3.6** (PhIP), with the exception of **3.1** (PRO). The BPs with free carboxylic acids also increased the amount of compounds that become associated with the Caco-2 cell monolayers. This led to a conclusion that it may be the physical interactions of the lipophilic parts of **3.1** (PRO), **3.2** (UCB), **3.3** (BV), **3.4** (UCBDE) and **3.5** (BVDE) with those of **3.6** (PhIP) which leads to the increase in electrostatic interactions with the cell surface that are responsible for the increased adsorption onto the cell surface.

3.2.2 Permeability of benzo[α]pyrene in the presence and absence of bile pigments

Benzo[α]pyrene (**3.7**, B α P) is insoluble in water and HBSS buffer. As a result, **3.7** (B α P) did not cross the cell monolayers in the experiments. Similarly, **3.7** (B α P) exhibited negligible permeability in the presence of BPs (Figure 3.4). Therefore, the permeability method could not be used to test the physical interactions between **3.7** (B α P) and BPs.

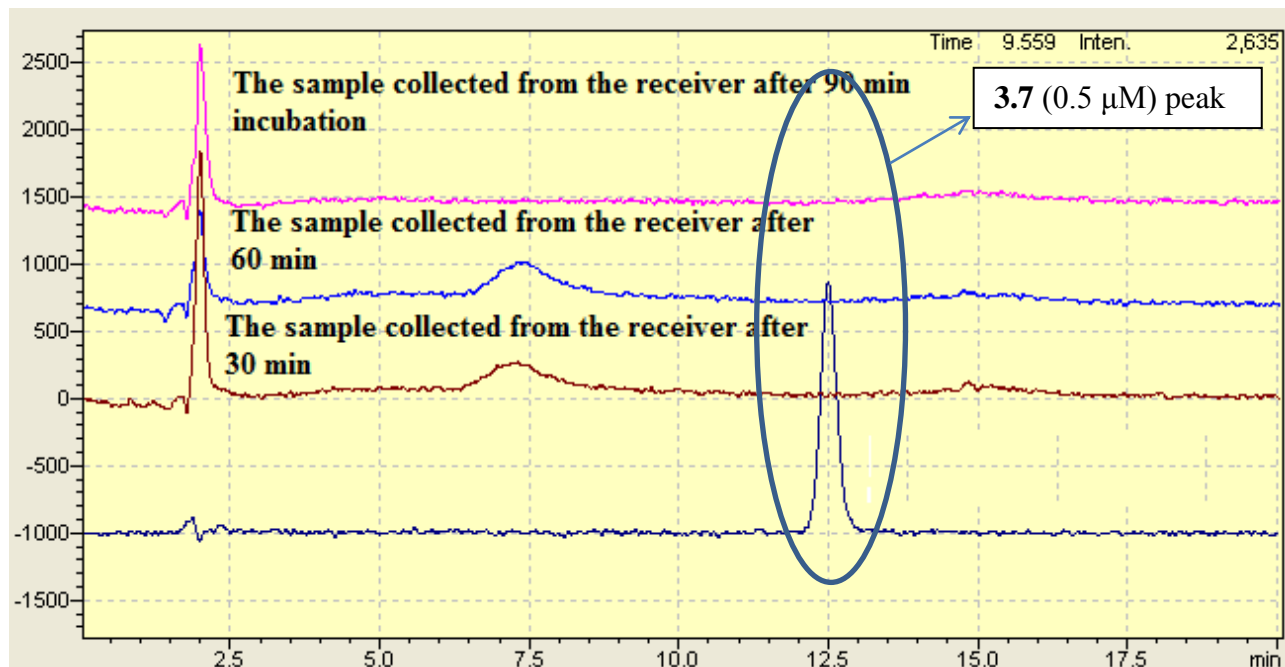


Figure 3.4: RPHPLC results of standard solution of **3.7** (B α P) at 0.5 μ M, overlaid with the results from samples collected from the receiver chamber after 30, 60 and 90 min incubation

3.3 Conclusion and future developments

The study was successful in using Caco-2 cell monolayers to determine the physical interactions between **3.6** (PhIP) and BPs, **3.4** (UCBDE), and **3.5** (BVDE). The study explored novel physical interactions occurring between the aromatic ring system of **3.6** (PhIP) and those of the BPs and their derivatives which resulted in a change of P_{app} of **3.6** (PhIP) through the Caco-2 cell monolayers. The larger amount of **3.6** (PhIP) remained either on or in the monolayers in the presence of **3.2** (UCB) suggested that carboxylic groups played an important role in the interactions between **3.2** (UCB) and the polar Caco-2 cell monolayer surface. As a consequence, when the carboxylic acid groups were protected as the dimethyl esters, the amount of compound associated with the cell monolayers dropped to 0% and the transported rate increased to just over 83%. Therefore, it led to a general conclusion that the physical interactions between aromatic rings in **3.2** (UCB), **3.3** (BV), their dimethyl esters and **3.6** (PhIP) affected the rate at which **3.6** (PhIP) crossed the cell monolayers.

These findings explored an important biological mechanism in which the lipophilic parts of **3.2** (UCB) and **3.3** (BV) interact with the lipophilic part of **3.6** (PhIP) to minimise its exposure in aqueous biological systems and maximise its hydrophilic properties. As a result of its increased hydrophilicity, pro-mutagen **3.6** (PhIP) bound to BPs (**3.2** (UCB) or **3.3** (BV) in biology system) becomes easy to excrete out of the body, thus minimising further chemical interactions with DNA.

This study also found that the presence of **3.1** (PRO) did not affect the apparent permeability of **3.6** (PhIP), as the two compounds did not interact strongly enough to affect the permeability of **3.6** (PhIP).

This study introduces a new key technique to explore the physical interactions occurring in biological systems that can be used for testing other mutagenic compounds (2-aminofluorene, aflatoxin B1, 2,4,7-TNFone...) with BPs and other potential inhibitors in the future.

3.4 Experimental

3.4.1 Chemicals and Biological Materials

BPs were purchased from Frontier Scientific, USA, and the dimethyl esters of the BPs (**3.4** (UCBDE), **3.5** (BVDE)) were synthesised (see the previous chapter) and used to test the physical interactions with **3.6** (PhIP) and **3.7** (B α P) obtained from Sigma Aldrich, Australia, together with Hanks Balance Salt Powder, DMSO and HEPES. The human cell line Caco-2/15 was obtained from American Type Cell Culture, Tockville VA. DMEM, FBS, and trypsin were purchased from Thermo Fisher Scientific, USA. Other solvents were of analytical and HPLC grade. Transwell permeable supports diameter 6.5 mm, 24 wells, insert membrane growth area 0.33 cm² were obtained from Lifesciences, USA. Transepithelial electrical resistance (TEER) was measured with an epithelial Volt-ohm-metre obtained from Millipore Millicell-ERS, USA.

Analytical reverse phase high performance liquid chromatography (RPHPLC) was performed using a Shimadzu system and LCsolution software and 3 μ m and 5 μ m Grace Vydac Denali C18 250 x 4.6 mm columns. Retention time (t_R) was obtained from the eluent gradient with mixtures of MQ-water (solvent A) and MeOH (solvent B – Sigma Aldrich, Sydney, Australia). MeOH and MQ-water were pumped at a standard flow rate of 1 ml/min. The gradient for PhIP was from 30% B to 70% B in 40 min. After injecting 5 samples, the HPLC analytical column was washed with 100% B for 1 hour to remove all remaining BPs from the column. Isocratic 90% B was used to elute **3.7**. Salt and BPs remaining in the column were also removed by 20% B for 15 min then increasing to 100% B over 20 min and held at 100% B for an hour. The eluent was detected on a UV detector set at 317 nm for **3.6** (PhIP) and 385 nm for **3.7** (B α P). Low resolution mass spectra were acquired on a Bruker Esquire HCT spectrometer (positive and negative ion ESI mode).

3.4.2 Caco-2 cell culture

Frozen Caco-2 cells were thawed in a water bath at 37 °C for 2 min before being transferred to a 10 mL centrifuge tube with 8 mL incomplete DMEM-10 (Dulbecco's Modified Essential Medium (DMEM) supplemented with 10% fetal bovine serum, 1% non-essential amino acids) (37 °C). The mixture was centrifuged for 5 min at 1000 rpm, the cell pellet was resuspended in 10 mL incomplete DMEM-10 and placed into 25 cm² tissue culture flask, stored in tissue culture incubator at 37 °C, 95% humidity, 5% CO₂.^{131,132} The media in the flask was changed every three days until the cells reached 70%-80% confluency (about 12-15 days after seeding). The cells were split by removing all old DMEM-10 and 5 mL of PBS solution was added at 37 °C. They were placed in the

incubator for 5 min before PBS was drawn and 3 mL trypsin solution at 37 °C was added and incubated for 4 min at 37 °C until all cells detached from the flask bottom. DMEM-10 (9 mL) was added to inhibit the action of the trypsin. The cells were centrifuged for 5 min at 150xg (1000 rpm) before DMEM-10 was aspirated and the cell pellet resuspended in 10 mL fresh DMEM-10. Cell density was counted under microscope before seeding at a density of about 1.3×10^4 cells/cm² to a new T-75 flask. The media was changed every other day until 80% confluency when the passaging procedure was repeated and cells were seeded onto wells membranes at a density of 2.5×10^5 cells/well. The media used for the wells was the same DMEM-10 media but with 1% penicillin added. The media in both the apical and basolateral chambers of the wells was changed every other day. From the 8th day, the apical side was changed every day and the basolateral side was changed every two days until the 28th day.

3.4.3 Caco-2 bioassay preparation and transport experiments

The monolayer integrity was monitored by measuring the transepithelial electrical resistance (TEER) after 22 days incubation. Wells having a resistance higher than 0.8 to 1.4 kΩ were selected and the wells with similar TEER values were used as replicates for the same compound or experiment. The apical and basolateral compartments of the wells were washed with PBS solution and then with Hanks Balance Salt solution (HBSS) with 25 mM HEPES buffer (twice). The Caco-2 cell monolayers were equilibrated in HBSS buffer for 30 min at 37 °C, then HBSS buffer was removed from both apical and basolateral sides and the basolateral sides were filled with 0.6 mL of fresh HBSS buffer. The apical sides were filled with 0.1 mL HBSS buffer containing 10 μM mutagen, **3.6** (PhIP) or **3.7** (BαP)), and varying concentrations of BPs from 0 μM (control experiments) to 20 μM. The experiments were performed in triplicate and data analysed using Microsoft Excel 2010. Samples (200 μL) were taken from the receiver (BL) compartment and replaced with 200 μL of fresh HBSS buffer every 30 min until the completion of the experiment at 180 min. At the end of each experiment, 80 μL HBSS of samples from the apical (AP) side was removed for analysis. All samples were centrifuged for 5 min at 1270xg (2800 rpm) and stored at -20 °C for RPHPLC analysis. At the end of the experiment the monolayers were washed with fresh HBSS before TEER values were measured again, and then they were incubated with medium. TEER values were measured every 12 hours until the values returned to the initial values (occurred after 24-36 hours). P_{app} values were determined using the following formula

$$P_{app} = \frac{\Delta C \cdot V}{\Delta t \cdot C_0 \cdot A}$$

Chapter III: Effect of bile pigments on the permeability of PhIP

Where ΔC is the concentration (μM) in the basolateral side; V is the volume of the basolateral chamber, Δt is the time for each transport experiment, C_0 is the concentration of mutagens in apical chamber at time 0, A is the membrane surface area.

Table 3.6: TEER values were measured from the first plate before the experiment, immediately after and after 30 hours incubation in DMEM-10 after the experiments were completed.

TEER ($\Omega \text{ cm}^2$) before assays					
1107	996	1001	1001	1027	1102
1097	998	1417	1103	1211	1026
TEER ($\Omega \text{ cm}^2$) after assays					
667	711	789	791	812	698
766	765	886	427	439	517
TEER ($\Omega \text{ cm}^2$) maintaining 30 hours after assays					
1118	1019	1177	1294	1201	965
1012	987	1278	977	987	955

Table 3.7: TEER values were measured from the first plate before the experiment, immediately after and after 30 hours incubation in DMEM-10 after the experiments were completed.

TEER ($\Omega \text{ cm}^2$) before assays					
967	996	925	981	1027	1010
1078	820	1210	999	1416	1026
TEER ($\Omega \text{ cm}^2$) after assays					
525	531	510	679	562	541
576	702	711	867	412	679
TEER ($\Omega \text{ cm}^2$) maintaining 30 hours after assays					
1008	856	988	978	867	1323
1022	1211	1099	1232	1321	1222

3.4.4 Preparation of Standard Solutions and Calibration Curves

Stock solutions of **3.1** (PRO), **3.2** (UCB), **3.3** (BV), **3.4** (UCBDE), **3.5** (BVDE), **3.6** (PhIP) and **3.7** (B α P) at 10 mM in DMSO were prepared and stored in a cold, dark place before another dilution in HBSS buffer to the final concentrations of 5 μM , 10 μM , 20 μM . Mutagenic standard solutions, 0.01 μM , 0.05 μM , 1.25 μM , 2.5 μM , 5 μM , 10 μM , 20 μM , were created from stock solutions and

Chapter III: Effect of bile pigments on the permeability of PhIP

analysed in triplicate by RPHPLC. Calibration curves were assembled using Microsoft Excel 2010.

The solutions to be tested were prepared as in Table 3.8 and Table 3.9.

Table 3.8: The solutions of **3.6** (PhIP) and BPs prepared for the permeability assays.

Test Mixtures		Test Mixtures	
1	3.6 (10 μ M) + HBSS buffer (control)	4	3.6 (10 μ M) + 3.2 (10 μ M) + HBSS buffer
2	3.6 (10 μ M) + HBSS buffer	5	3.6 (10 μ M) + 3.3 (10 μ M) + HBSS buffer
3	3.6 (10 μ M) + 3.1 (10 μ M) + HBSS buffer	6	3.6 (10 μ M) + 3.4 (10 μ M) + HBSS buffer

Table 3.9: The solutions of **3.6** (PhIP) and varying concentrations of **3.2** (UCB) prepared for permeability assays.

Test Mixtures		Test Mixtures	
1	3.6 (10 μ M) + HBSS buffer	3	3.6 (10 μ M) + 3.2 (5 μ M) + HBSS buffer
2	3.6 (10 μ M) + 3.5 (10 μ M) + HBSS buffer	4	3.6 (10 μ M) + 3.2 (10 μ M) + HBSS buffer
		5	3.6 (10 μ M) + 3.2 (20 μ M) + HBSS buffer

Table 3.10: The solutions of **3.7** (BaP) and BPs prepared for the permeability assays.

Test Mixtures		Test Mixtures	
1	3.7 (10 μ M) + HBSS buffer (control)	4	3.7 (10 μ M) + 3.2 (10 μ M) + HBSS buffer
2	3.7 (10 μ M) + HBSS buffer	5	3.7 (10 μ M) + 3.3 (10 μ M) + HBSS buffer
3	3.7 (10 μ M) + 3.1 (10 μ M) + HBSS buffer	6	3.7 (10 μ M) + 3.4 (10 μ M) + HBSS buffer

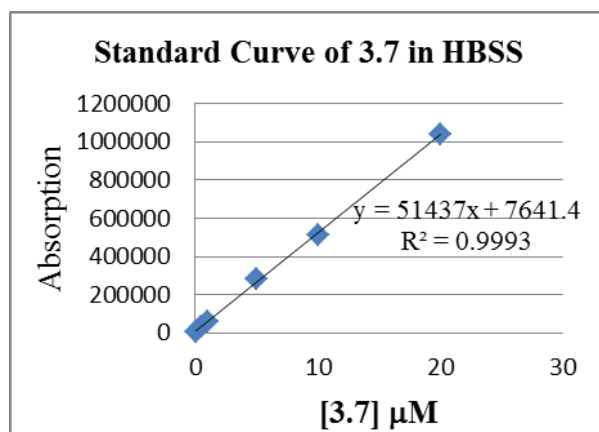
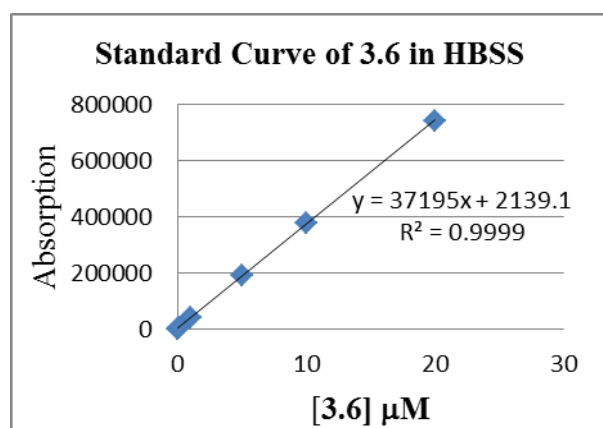


Figure 3.5: The standard curves for **3.6** (PhIP) and **3.7** (BaP) in HBSS were obtained from RPHPLC.

3.4.5 Statistical analysis

Table 3.11: A summary of rules for combining standard deviation error.¹⁷⁶

Relationship	Statistical uncertainty
$p=x+y$	$\Delta p = \sqrt{(\Delta x)^2 + (\Delta y)^2}$
$p=x-y$	$\Delta p = \sqrt{(\Delta x)^2 + (\Delta y)^2}$
$p=xy$	$\frac{\Delta p}{ p } = \sqrt{\left(\frac{\Delta x}{x}\right)^2 + \left(\frac{\Delta y}{y}\right)^2}$
$p=x/y$	$\frac{\Delta p}{ p } = \sqrt{\left(\frac{\Delta x}{x}\right)^2 + \left(\frac{\Delta y}{y}\right)^2}$

Chapter 4: Synthesis of pyrroles, dipyrroles and bile pigment esters

4.1 Introduction

Current investigations into the reactivity and biological activities of bile pigments (BPs) required substituted pyrroles and dipyrroles and BPs dimethyl esters as model compounds to determine the reactivity of various positions in the BP structures towards styrene epoxide (justification for synthesis of pyrroles and dipyrroles can be found in chapter V). We therefore endeavored to synthesise pyrroles, dipyrroles and BP dimethyl esters by published procedures, optimizing the efficiency of the syntheses where possible.

In addition, substituted pyrroles and dipyrroles exhibit a wide range of interesting physicochemical and biochemical properties. These properties have been exploited in nanomaterials comprising metal and BF₂ complexes of dipyrrolylmethenes (BODIPY)¹⁷⁷ which generate a strongly polarised π -electron system, and have proved useful as optical limiters,¹⁷⁸ sensors, fluorescent markers,^{179,180} photosensitisers,^{181,182} antioxidants,¹⁸³ and laser radiation limiters.^{184,185} Other important pyrrole containing compounds, for example, bile pigments and their dimethyl esters, are also reported in many reviews of their potential biological properties, such as antioxidant^{18-20,183} and anti-mutagenic activities^{15,18,19,186}. In spite of these promising properties and a variety of syntheses which aim to optimise the yield and efficiency, the need of pyrroles and dipyrroles for chemical interaction studies is not commercially available. Their production is still plagued by low yields, partly due to their instability, light sensitivity and reactivity with oxygen.^{66,187,188}

The classical syntheses of substituted pyrroles and dipyrroles were reported by German chemists Paal and Knorr,^{189,190} modified by MacDonald and Stedman¹⁹¹ and further developed by Kleinspehn.¹⁹² Cyclizations involving the acid-catalyzed condensation of a ketone and amine (Figure 4.1) have been a well-established synthetic approach to substituted pyrroles for over a century. However, the use of this method to synthesise substituted dipyrroles such as 4,4'-diethyl-3,3',5,5'-tetramethyldipyrromethene hydrobromide has produced yields ranging from 58% (Wood et al.¹⁹³) to 98% (Tsu et.al.¹⁹⁴), and 85% (Yutanova et al.¹⁹⁵), a fact perplexing to multiple reviewers.

In order to possess sufficient quantities of BPs dimethyl esters for the current project optimizing the efficiency and yield of the esterification reaction of BPs with diazomethane was another aim of this study. Moreover, after esterification of bilirubin-IX α , the complex 3D structure of bilirubin-IX α

with 6 intrahydrogen bonds forming between carboxylic groups and amides no longer exists. This simplified some aspects of the analysis of the assays and spectroscopic investigations.

4.2 Results and discussion

4.2.1 Synthesis of 2,3,4,5-tetramethylpyrrole (**4.3**)

Several previously published synthetic routes reported simple methods to synthesise 2,3,4,5-tetramethylpyrrole (**4.3**), including the treatment of racemate (*d,l*) of (3,4)-dimethyl-2,5-hexanedione in the presence of NH_3 in chloroform under an argon atmosphere for 18 hours at room temperature (rt).¹⁸⁸ By meticulously following the experimental procedure of Venkataraman et al.,¹⁸⁸ compound **4.3** was generated with 40% yield,¹⁸⁸ slightly better than the 35% yield reported by Juergen,¹⁹⁶ who used 1,2,3,4-tetramethylcyclobut-3-ene-1,2-diol in place of 3,4-dimethyl-2,5-hexanedione.¹⁹⁶ Although Juergen's method was simple, the yield was low and the reactants particularly expensive and so it was not attempted in this study. In another simple approach to achieve the desired compound, **4.3** in 44% yield was reported by Johnson and Price¹⁸⁷ via a different synthetic route in which diacetyl monoxime (**4.2**) was treated directly with 3-methyl-2,4-pentanedione (Figure 4.1).^{78,187} Therefore, in our experiments the desired compound **4.3** was synthesised directly in only two steps from butan-2-one (**4.1**), which was first treated with nitrous acid generated from the reaction of EtONO or NaONO and HCl at 0-5 °C overnight, to give diacetyl monoxime (**4.2**) in 92% yield. The second step was the reduction of **4.2** by zinc dust and glacial acetic acid at 40 °C to create the α -aminoketone. Then, in the presence of 3-methyl-2,4-pentanedione, α -aminoketone condensed to form the intermediate imine which then tautomerised to the enamine and cyclised to eliminate water and acetic acid and isomerised to the pyrrole (Figure 4.1).^{197,280}

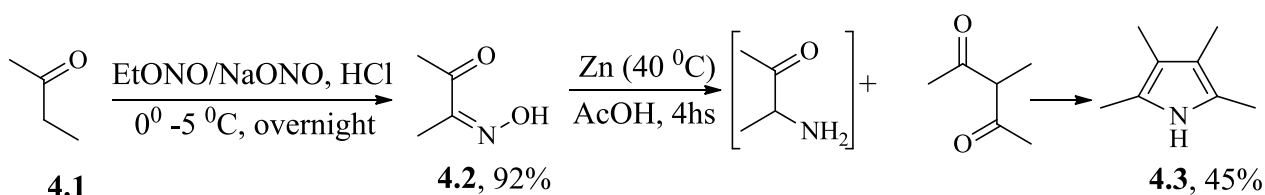


Figure 4.1: Synthesis of 2,3,4,5-tetramethylpyrrole from butan-2-one (**4.1**) and diacetyl monoxime (**4.2**)

The yield of **4.2** (92%) obtained from the procedure described in Figure 4.1 was similar to previous reports.^{198,199,200} Attempts were made to optimise the synthesis with a method in which Me_3SiCl and $\text{CHMe}_2\text{CH}_2\text{CH}_2\text{NO}_2$ in DCM were allowed to react at -20 °C for 3 hours, giving an 82% yield of **4.2**.²⁰¹ An attempt to generate **4.2** by treatment of **4.1** at 40-45 °C for 1 hour with NaONO and HCl also gave an 82% yield.²⁰² An attempt to synthesise **4.2** in KOH at rt overnight in the presence of NH_4OH gave only a 21% yield.¹⁹⁸ Thus, the conditions described in Figure 4.1 were deemed to be the most efficient in producing the diacetyl monoxime (**4.2**).

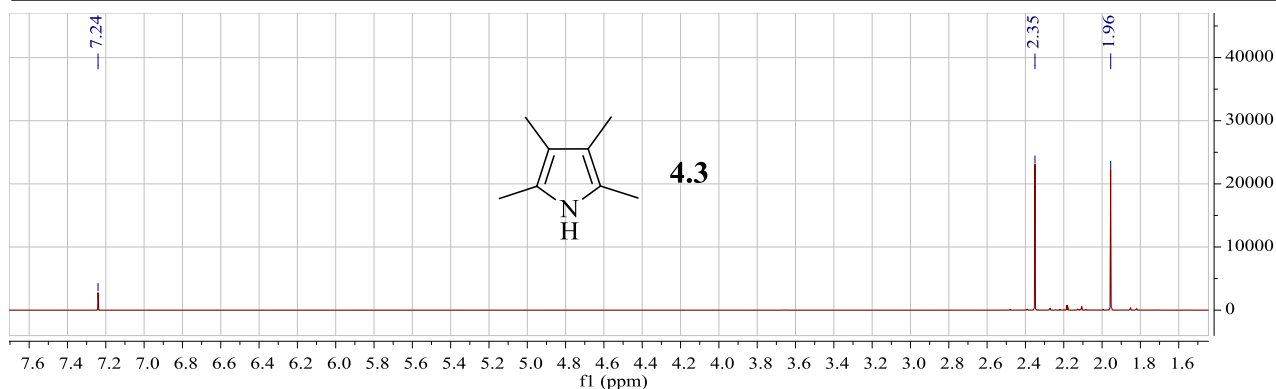


Figure 4.2: The ^1H NMR spectrum of **4.3** performed on a 500 MHz instrument in CDCl_3 .

The cyclisation of **4.2** to the pyrrole was less efficient, resulting in only a 30% yield. Compound **4.3** was identified by ^1H NMR with two singlets at δ_{H} 1.96 and δ_{H} 2.35 each integrated for 6 protons, suggesting two sets of equivalent methyl groups. Attempts to collect mass spectral data on this compound through ESIMS methods failed due to the instability of **4.3** and its reluctance to ionise. Compound **4.3** was rapidly oxidised in the presence of oxygen to an unidentified green compound.¹⁸⁷

4.2.2 Synthesis of substituted dipyrroles

Using an approach analogous to that described above (4.2.1) gave the desired substituted dipyrroles in moderate yields; however, there were large variations in the yields reported.¹⁹³⁻¹⁹⁵ The self-condensation of pyrrole-2-carboxylate derivatives such as 3,4,5-trimethylpyrrole-2-carboxylate (**4.7a**) and ethyl 4-ethyl-3,5-dimethylpyrrole-2-carboxylate (**4.7b**), by refluxing with formic acid in the presence of concentrated hydrobromic acid, produced dipyrrole products, 3,3',4,4',5,5'-hexamethyldipyrromethene (**4.9**) and 4,4'-diethyl-3,3',5,5'-tetramethyldipyrromethene (**4.10**) respectively (Figure 4.3).¹⁹³⁻¹⁹⁵ While Tu et al.¹⁹⁴ reported a 98% yield for this reaction, Yutanova et al.¹⁹⁵ and Wood et al.¹⁹³ reported yields of only 85% and 58% respectively. In addition, Omar et al.²⁰³ achieved the same condensation starting with 3-ethyl-2,4-dimethylpyrrole (**4.8b**) and acyl halides to obtain the desired dipyrrole, **4.10** with 93% yield.²⁰³ Another approach was reported by Semeikin et al.²⁰⁴ who used 2,3,4-trimethylpyrrole reacting with 3,4,5-trimethylpyrrole-2-carbaldehyde and gave only a 70% yield. The methods of Omar and Semeikin used starting materials that are not readily available in our laboratory. Tu's method for the synthesis of dipyrromethanes, **4.9** and **4.10** involved the self-condensation of pyrroles, **4.7a** or **4.7b** which we had synthesised previously. In this synthetic method, pyrrole-2-carboxylic acid was formed by the de-esterification of **4.7a** or **4.7b**, catalysed by strong acid HCl or HBr, followed by rapid decarboxylation to form 2-unsubstituted pyrrole which then reacts with formic acid under strongly

acidic conditions to release water and pyrrole-2-carboxaldehyde. Finally, the condensation of 2-unsubstituted pyrrole with pyrrole-2-carboxaldehyde produced dipyrromethanes (**4.9** and **4.10**) (Figure 4.3). The slow condensation of pyrrole-2-carboxaldehyde with 2-unsubstituted pyrrole is the rate determining step. Therefore, the use of less water and a strong acid speeds up the reaction. In fact, Tu et al.¹⁹⁴ and Yutanova et al.¹⁹⁵ used 98% formic acid and concentrated HBr or HCl for the reaction to obtain a greater than 90% yield.

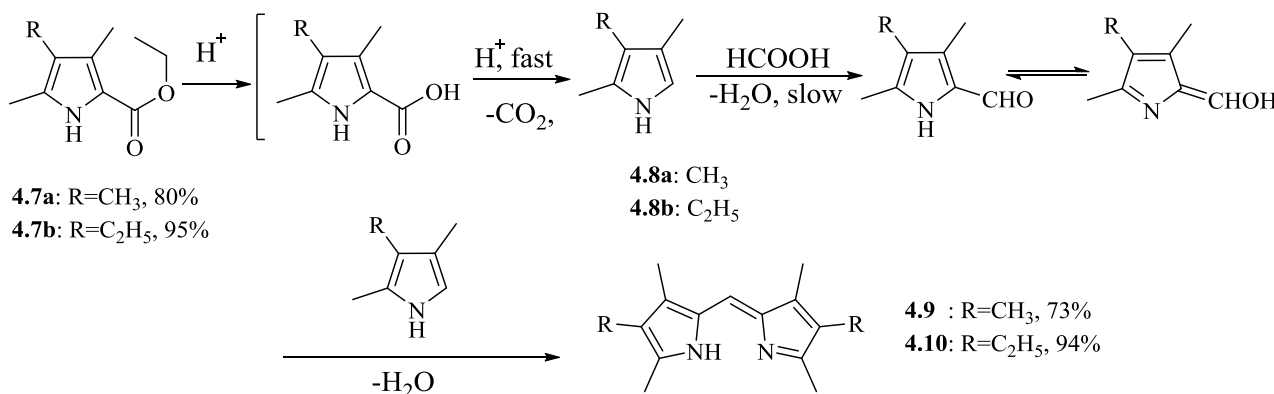


Figure 4.3: The synthesis of **4.9** and **4.10** from the self-condensation of pyrrole-2-carboxylates in hydrobromic acid.

One goal of this work was to find a simple method that has the efficiency and reproducibility of this reaction. We also aimed to link the previously described synthesis of pyrroles with this dipyrrole synthesis by starting with ethyl 3-oxobutanoate (**4.4**), producing ethyl 2-(hydroxyimino)-3-oxobutanoate (**4.5**) which can then be cyclised to give pyrrole carboxylate derivatives, **4.7a** and **4.7b**. These compounds can then be further elaborated to the corresponding dipyrroles (Figure 4.4).

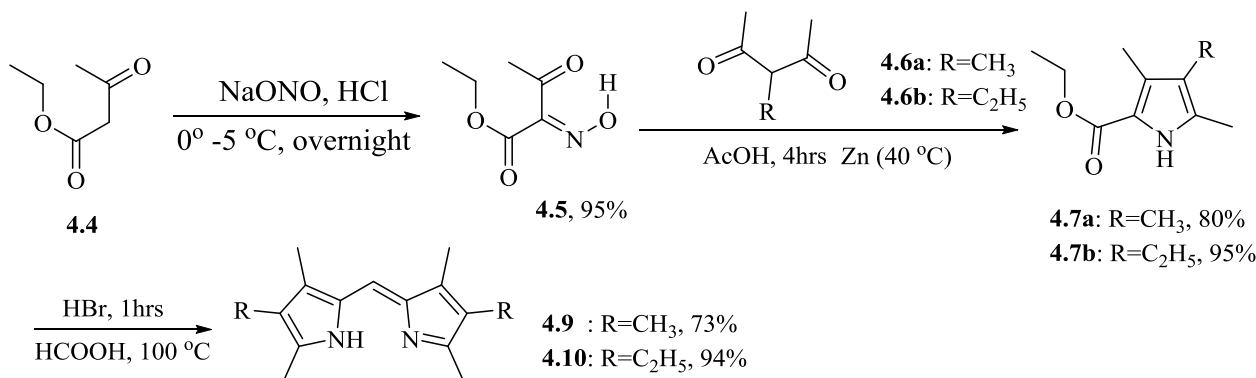


Figure 4.4: The synthetic route to **4.9** and **4.10** from ethyl 3-oxobutanoate (**4.4**).

Compounds **4.9** and **4.10** were synthesised in only three steps from **4.4** in high yields. The yields for the self-condensation reactions to produce **4.9** (73%) and **4.10** (94%) were in agreement with Yutanova et al.¹⁹⁵, Tu et al.¹⁹⁴ and Ali et al.²⁰³ The yield obtained was higher than that of the 58% reported by Wood et al.¹⁹³ who used cold methanol to wash the crystals of **4.9** and **4.10**. Our

synthesis found that the cold methanol still contained a large amount of these compounds. Therefore, the products were isolated from the methanol filtrate by column chromatography.

Analysis of **4.7a** by GC-MS showed the expected molecular ion (m/z 181 (M^+)) and the appearance of three singlet peaks at δ_H 2.25 (3H), 2.18 (3H), 1.91 (3H) in 1H NMR indicated three methyl groups having covalent bonds with the pyrrole ring. The presence of the ethyl ester was confirmed by the appearance of a 2H quartet at δ_H 4.49 and a 3H triplet at δ_H 1.34 (Figure 4.5).

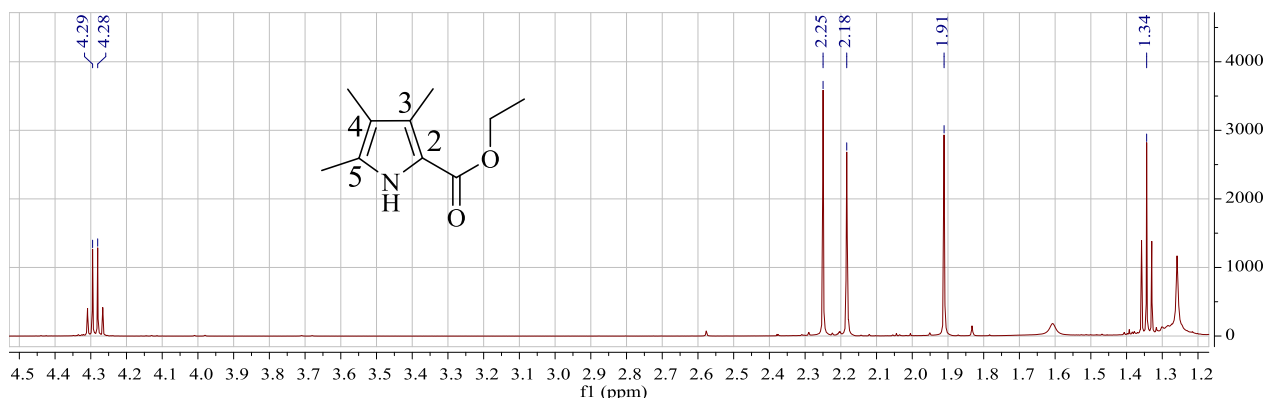


Figure 4.5: The 1H NMR spectrum of **4.7a** performed on a 500 MHz instrument in $CDCl_3$.

HMBC correlations from δ_C 117.2 to all three methyl signals suggested that this ^{13}C signal corresponded to C-4. The correlation from δ_H 1.91 to δ_C 129.4, 127.6 and 117.2 suggested that this 1H signal corresponded to the C-4- CH_3 group. Likewise, the HMBC spectrum showed correlations from δ_H 2.18 to only two carbon signals, δ_C 117.2 (C-4) and δ_C 129.1, assigning this 1H signal to the C-5- CH_3 group, and the signals at δ_C 129.1 and δ_H 2.25 to C-5 and C-3- CH_3 , respectively (Figure 4.5 and Figure 7.20 in appendix-C).

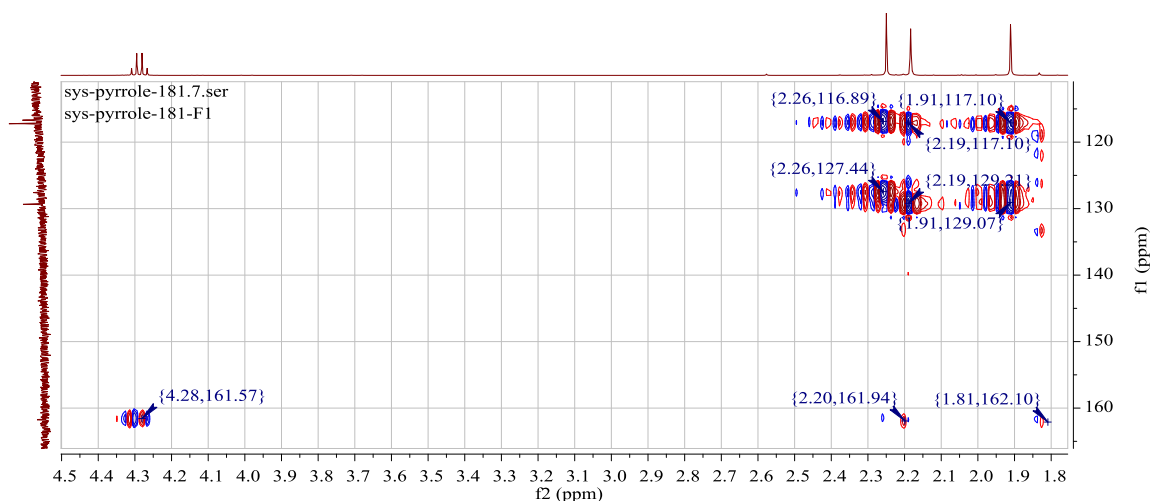


Figure 4.6: The HMBC correlations from protons of three methyl groups to tertiary carbons in pyrrole ring of **4.7b**. Spectrum performed on a 500 MHz instrument in $CDCl_3$

Compound **4.7b** was identified by GC-MS m/z 195 (M^+) and comparison of the ^1H NMR spectrum (Figure 4.7) with that of **4.7a**. The spectrum of **4.7b** showed two methyl singlets and two sets of coupled triplet-quartet signals. This confirmed the presence of two ethyl groups with one CH_2 signal shifted significantly downfield suggesting attachment to an oxygen atom.²⁰⁵

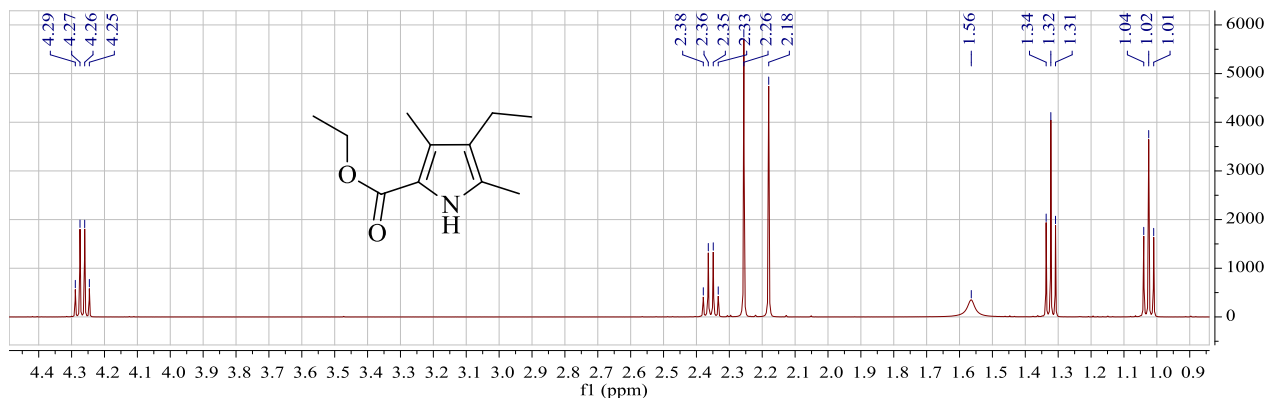


Figure 4.7: The ^1H NMR spectrum of **4.7b** performed on a 500 MHz instrument in CDCl_3 .

Compound **4.8b** is an unstable compound and it is a liquid at room temperature as its boiling point is $197\text{ }^\circ\text{C}$. That compound easily evaporates with the solvent under reduced pressure. Therefore, it was necessary to cool the solution in dry ice before removing the solvent under reduced pressure.

Compound **4.9** was identified by ESIMS m/z 229 $[\text{M}+\text{H}]^+$ and a simple ^1H NMR with three singlet peaks accounting for 18 protons from six methyl groups (δ_{H} 2.59, 2.21, 1.94) and a singlet at δ_{H} 6.95 belonging to the CH-bridge (Figure 4.8). The HMBC correlation from δ_{H} 6.95 to δ_{C} 141.8 suggested that this ^{13}C signal could be assigned to C-3, 3'. The correlation from δ_{H} 2.59 to δ_{C} 154.0 and δ_{C} 124.1 allowed assignment of these carbon signals to C-5, 5' and C-4, 4', respectively and the proton signal to $\text{CH}_3\text{-C-5}'$. The proton signal of $\text{CH}_3\text{-C-4, 4}'$ was identified by the cross-peaks between δ_{H} 1.94 and δ_{C} 124.1 (C-4, 4'), δ_{C} 142.8 (C-3, 3') and a three-bond coupling to δ_{C} 154.0 (C-5, 5'). The cross-peaks from δ_{H} 2.21 ($\text{CH}_3\text{-C-3, 3}'$) to δ_{C} 124.1 (C-4, 4'), 141.8 (C-3, 3') and δ_{C} 126.1 confirmed the assignment of the C-2, 2' signal (Figure 4.8). The ^1H NMR data were in agreement with the published data for this compound.¹⁹⁵

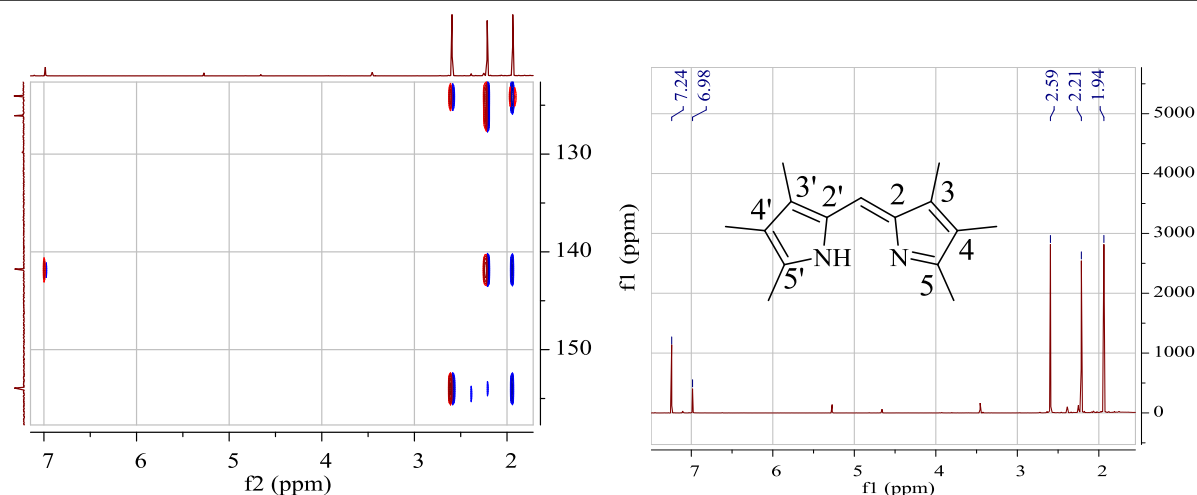


Figure 4.8: The ^1H NMR and HMBC spectra of **4.9** performed on a 500 MHz instrument in CDCl_3 .

Compound **4.10** was identified by ESIMS m/z 257 $[\text{M}+\text{H}]^+$ and the absence of a singlet signal of H-4' at δ_{H} 1.94 in comparison to ^1H NMR of **4.9**. In addition, the presence of an ethyl group was indicated by the appearance of quartet signal at δ_{H} 2.42 and a triplet signal at δ_{H} 1.07 (Figure 4.9). The HMBC correlations from δ_{H} 2.42 ($\text{CH}_3\text{-CH}_2\text{-C-4, 4'}$) to δ_{C} 130.4 (C-4, 4'), 153.6 (C-5, 5') and δ_{C} 141.0 suggested this latter signal corresponded to the C-3, 3' positions in the pyrrole ring. The HMBC correlation from δ_{H} 7.01 to δ_{C} 141.0 (C-3,3') suggested this proton signal corresponded to the CH-bridge, δ_{H} 2.26 ($\text{CH}_3\text{-C-3, 3'}$) to δ_{C} 130.4 (C-4, 4'), δ_{C} 141.0 (C-3, 3') and δ_{C} 126.2 identified the latter ^{13}C signal as that corresponding to the tertiary carbon of C-2, 2' (Figure 4.10). All remaining proton data were in agreement with the literature.^{195,203,206-208}

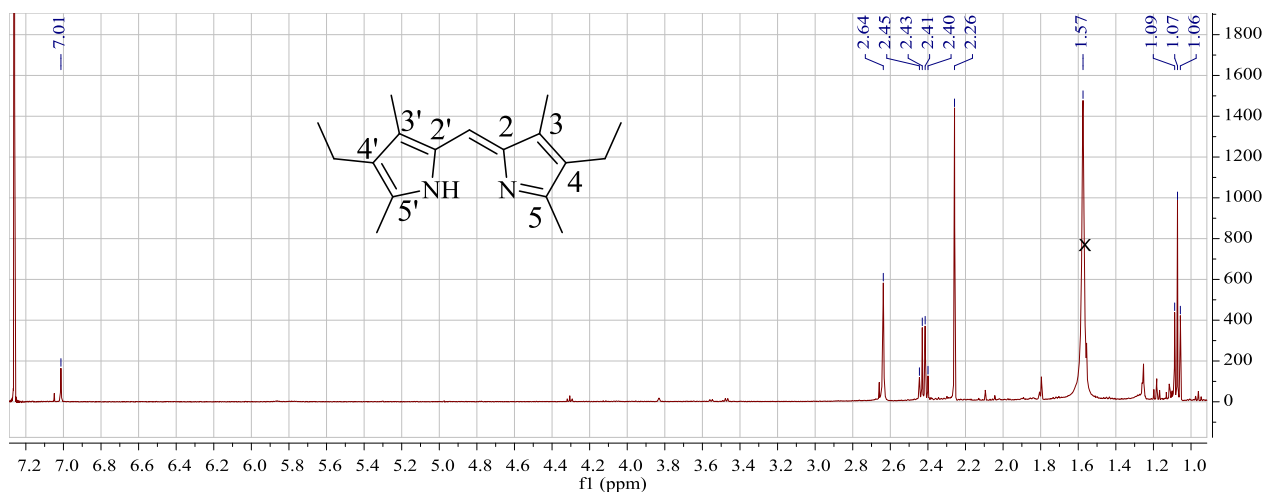


Figure 4.9: The ^1H NMR spectrum of **4.10** performed on a 500 MHz instrument in CDCl_3 .

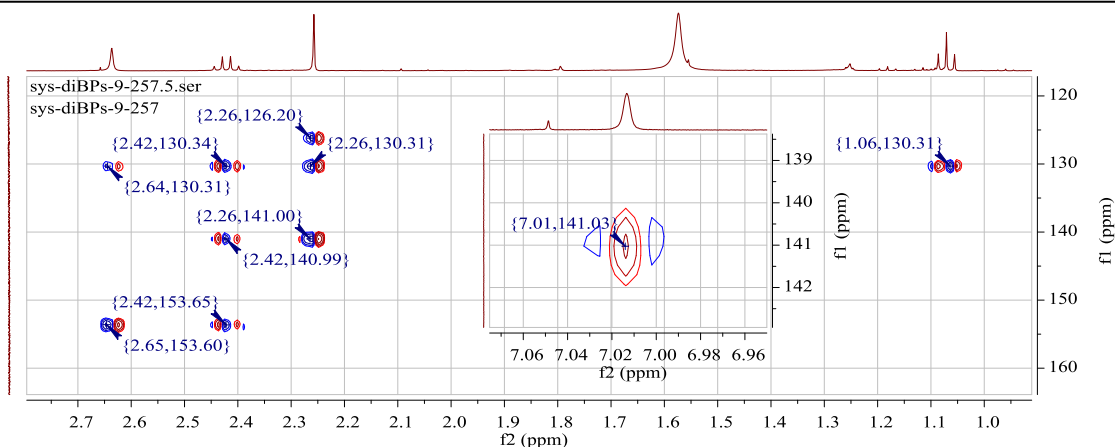
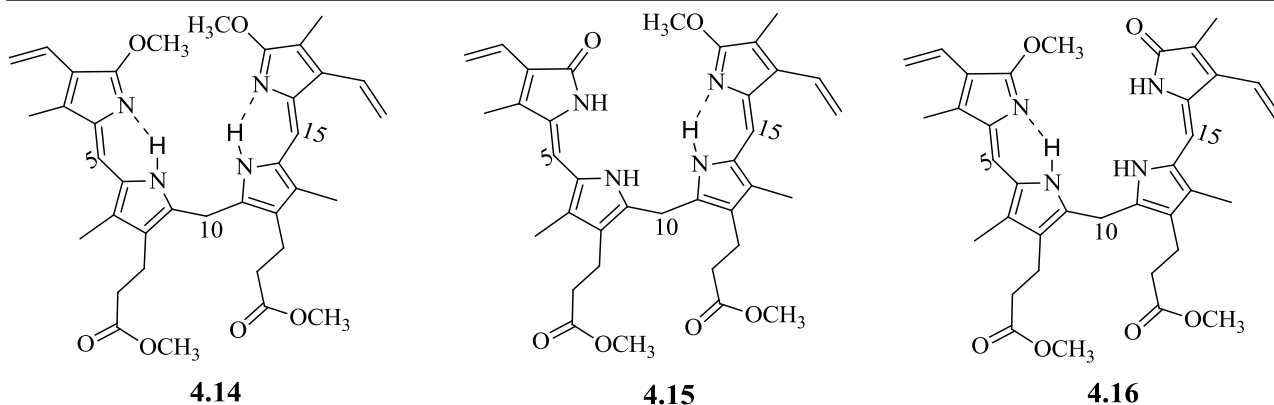


Figure 4.10: The HMBC spectrum of **4.10** and the insert of the cross-peak from CH-bridge to C-3. All experiments were performed on a 500 MHz instrument in CDCl_3 .

4.2.3 Synthesis of dimethyl ester of BPs

Synthesis of bilirubin-IX α dimethyl ester: Although bilirubin- IX α dimethyl ester (**4.11**) is a well-known photochemical, there are currently only a few methods to synthesize **4.11** from bilirubin- IX α and the yields reported are low due to the instability and light sensitivity of both the free acid and the esters.²⁰⁹⁻²¹³ Lightner et al.²¹² esterified bilirubin- IX α by treatment with Me_2CO and MeI and reported 12.4% yield of **4.11** and 86% yield of bilirubin monomethyl ester.²¹² The report also indicated that the esterification rate of the first propionic acid group was higher than the second. In contrast, Nichol and Morell²¹⁰ esterified bilirubin- IX α with methanol in hydrochloric acid or sulfuric acid and obtained only **4.11** in about 9% yield. Nichol and Morell²¹⁰ also treated bilirubin- IX α with diazomethane in MeOH in chloroform and isolated **4.11** in 12% yield. Bilirubin- IX α monomethyl ester was not isolated from either reaction.²¹⁰ Kuenzle²⁰⁹, performing the esterification of Bilirubin- IX α with diazomethane in chloroform and ethyl ether, obtained only 2% yield of **4.11** and 23% yield of monomethoxybilirubin dimethyl ester (**4.15**, **4.16**) and dimethoxybilirubin dimethyl ester (**4.14**).²⁰⁹ Using a different method, Hutchinson et al.²¹¹ treated bilirubin- IX α in chloroform with 1-methyl-3-p-tolyltriazene at room temperature for 12 hours and obtained 46% of **4.11** and less than 15% of other isomers.^{211,213} Lightner's method was the only one of the above literature procedures in which bilirubin- IX α monomethyl ester was isolated.



In summary, while successful in producing **4.11**, the above methods gave a low yield and produced biproducts such as bilirubin-IX α monomethyl ester, **4.14**, **4.15** and **4.16** which make purification of **4.11** difficult. Therefore, a modification of Kuenzle's method²⁰⁹ was developed to provide a higher yielding and more reliable synthesis of **4.11**.

Diazomethane is an extremely sensitive and a highly reactive reagent used in a number of reactions, especially for esterification of carboxylic acids in high yields. However, the reagent can also react with other groups such as amide or vinyl groups, to produce unexpected products such as the formation of **4.14**, **4.15** and **4.16** as seen in Kuenzle's reports.²⁰⁹ The mechanism of methyl ester formation of UCB begins with the deprotonation of carboxylic acid groups by the diazomethane which makes the methyl groups of the protonated diazomethane reactive to attack by the carboxylate anion to form the ester. The highly reactive protonated diazo intermediate can also be attacked by other nucleophilic groups in UCB and although neutral amides are not as reactive as the carboxylate anion, literature reports indicate that the products of amide methylation are isolated in small quantities when the reaction was performed at room temperature. By reducing the temperature of the reaction to $-20\text{ }^{\circ}\text{C}$ we have successfully slowed the reactions sufficiently that the competing amide methylation no longer occurs.

In order to minimize the reactions of diazomethane with other groups in BPs, the reactions were performed at low temperatures ($-20\text{ }^{\circ}\text{C}$ and then $-80\text{ }^{\circ}\text{C}$). The yields of **4.11** from the reaction conducted at $-80\text{ }^{\circ}\text{C}$ was 44% and at the reaction performed at $-20\text{ }^{\circ}\text{C}$ gave a 35% yield. These compared well to the 12% yield of the previously published procedures performed at room temperature and $4\text{ }^{\circ}\text{C}$ ²¹⁰.

The formation of **4.11** was supported by ESIMS m/z 613 $[\text{M}+\text{H}]^+$ and the presence of new singlet proton signals in the ^1H NMR at δ_{H} 3.42 (s, O-CH₃, 3H) and δ_{H} 3.41 (s, O-CH₃, 3H) in comparison to the ^1H NMR spectrum of bilirubin-IX α (Figure 4.11). HMBC correlations from δ_{H} 3.42 and δ_{H} 3.41 to the carboxylate carbon signal at δ_{C} 173.1 (C-12³, C-8³) suggested the successful

esterification of bilirubin-IX α (Figure 4.12). The proton chemical shifts were slightly different to Hutchinson et al.²¹¹ and Kuenzle's results⁴⁶, however these differences may be explained by the use of different solvents (literature spectra performed in CDCl₃) and a lower field spectrometer. There is also evidence in the published spectra of contamination of the samples with possible reaction byproducts.^{209,211}

Table 4.1: ¹H NMR and ¹³C NMR of **4.11** performed in DMSO-*d*₆ and the published data for the same compound.^{210, 211}

C	4.11		Data reported by Nichol ²¹⁰ and Hutchinson ²¹¹	
	δ_C (ppm) ^a	δ_H (ppm), mult., <i>J</i> (Hz) ^b	δ_H (ppm), mult. ^c	δ_H (ppm), mult. ^d
1	170.9	--		
2	122.6	--		
2 ¹	127.5	6,57, dd, 11.5, 17.5	6.47, m	4.72-6.68, m
2 ²	117.6	5.29, dd, 11.5, 2.5 6.21, dd, 17.5, 2.5	6.06, m	4.72-6.68, m
3	128.7	--		
3 ¹	9.7	2.15, s	2.08, s	1.73-2.08, s
4	142.5	--		
5	99.7	6.07, brs	5.54, s	4.72-6.68, m
6	122.5	--		
7	124.7	--		
7 ¹	9.5	2.01, d	2.08, s	1.73-2.08, s
8	120.0	--		
8 ¹	19.7	2.46, t, 8.0	2.76, m	2.68
8 ²	34.2	1.90, m	2.47, m	2.68
8 ³	173.3	--		
8 ⁴	51.5	3.43, s	3.65, s	3.69, s
9	131.3	--		
10	116.0	3.98, s	4.13, s	4.16, s
11	131.3	--		
12	119.8.0	--		
12 ¹	19.7	2.46, t, 8.0	2.76, m	2.68
12 ²	34.2	1.90, m	2.47, m	2.68
12 ³	172.0	--		
12 ⁴	51.5	3.43, s	3.65, s	3.69, s

13	124.0	--		
13 ¹	9.5	1.97, s	1.96, s	1.73-2.08, s
14	122.6	--		
15	97.0	6.07, s	5.89, s	4.72-6.68, m
16	141.0	--		
17	123.8	--		
17 ¹	126.8	6.81, dd, 17.5, 11.5	6.47, m	4.72-6.68, m
17 ²	122.5	5.63, d, 11.5 5.62, d, 17.5	5.28, m	4.72-6.68, m
18	128.0	--		
18 ¹	9.9	1.92, s	1.72, s	1.73-2.08, s
19	171.9	--		
20	--	--		

^aChemical shift (ppm) referenced to DMSO-*H*₆ δ_C 39.5 were taken from 1D and 2D NMR (DMSO-*d*₆, 500 MHz);

^bChemical shift (ppm) referenced to DMSO-*H*₆ δ_H 2.49 were taken from ¹H NMR (DMSO-*d*₆, 500 MHz);

^cChemical shift (ppm) referenced to CDCl₃ δ_H 7.26 from literature²¹⁰

^dChemical shift (ppm) referenced to CDCl₃ δ_H 7.26 from literature²¹¹

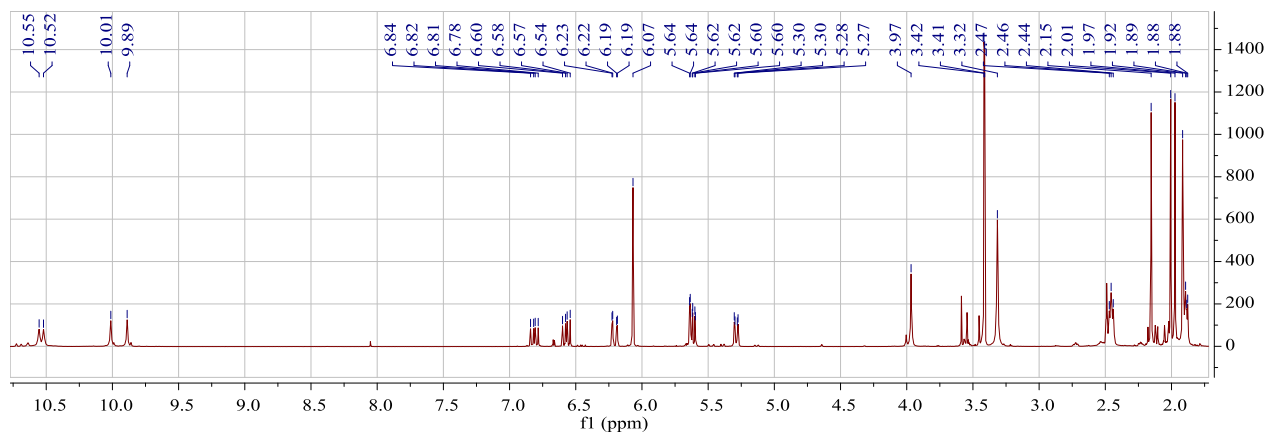


Figure 4.11: The ¹H NMR spectrum of **4.11** performed on a 500 MHz instrument in DMSO-*d*₆

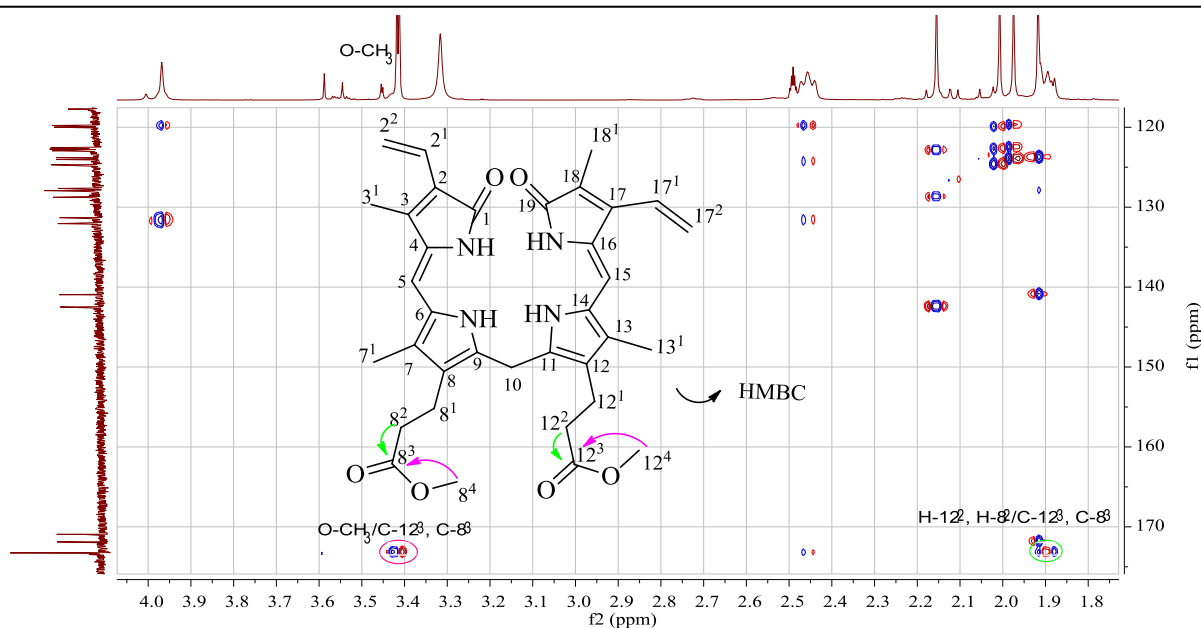


Figure 4.12: The long range correlations (HMBC) between protons and carbons of **4.11**. Spectrum performed on a 500 MHz instrument in DMSO- d_6 .

Synthesis of biliverdin-IX α dimethyl ester (4.12): The diazomethane esterification methods were applied to the synthesis of **4.12**, and gave 45% yield at $-20\text{ }^\circ\text{C}$ and 56% yield at $-80\text{ }^\circ\text{C}$. Compound **4.12** was identified by ESIMS (m/z 611 $[\text{M}+\text{H}]^+$ and 609 $[\text{M}-\text{H}]^-$) and the presence of a new singlet signal in the ^1H NMR spectrum at δ_{H} 3.58 integrating to six protons (Figure 4.13). The HMBC correlations from δ_{H} 3.58 to the carboxylate carbon signal at δ_{C} 172.7 confirmed the formation of the methyl esters (Figure 7.12 and Figure 7.13 in appendix-C).

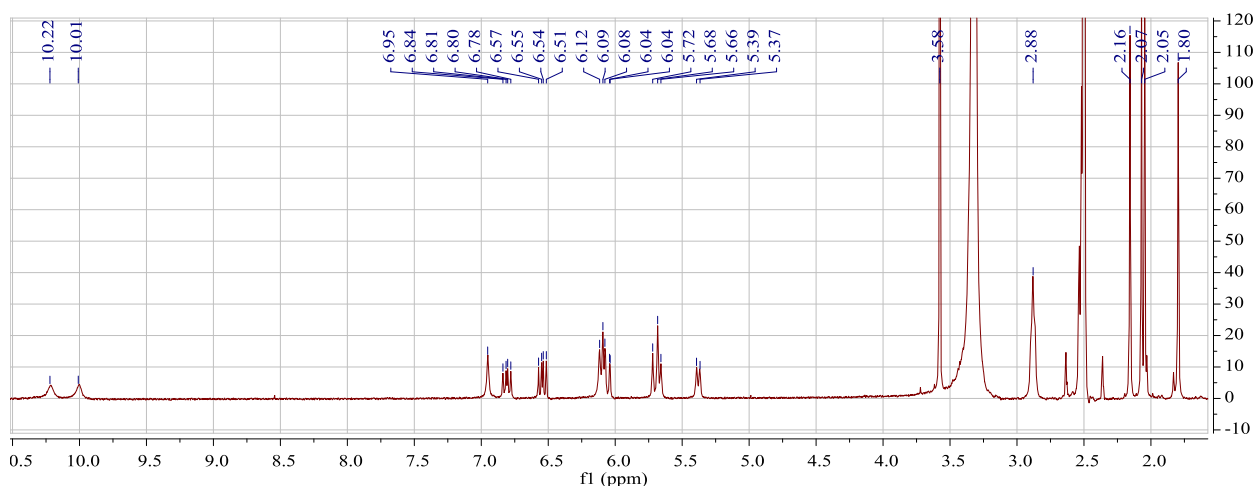


Figure 4.13: The ^1H NMR spectrum of **4.12** performed on a 500 MHz instrument in DMSO- d_6

Synthesis of protoporphyrin-IX α dimethyl ester: Protoporphyrin-IX α dimethyl ester (**4.13**) was synthesized using the same method. The results indicated no difference in the yield obtained at $-80\text{ }^\circ\text{C}$ and $-20\text{ }^\circ\text{C}$ (83%). ESIMS analysis of **4.13** supported the introduction of two methyl groups in

place of two hydrogen atoms, m/z 591 $[M+H]^+$. The ^1H NMR spectra showed two new singlet peaks at δ_{H} 3.56 and 3.55 corresponding to the methyl esters (Figure 4.14). The HMBC correlations from carbonyl signal at δ_{C} 173.2 to δ_{H} 4.33 (H-8¹, H-12¹), 3.24 (H-8², H-12²) and δ_{H} 3.56, 3.55 confirmed the formation of **4.13** (Figure 7.17, Figure 7.18 and Figure 7.19 in appendix-C).

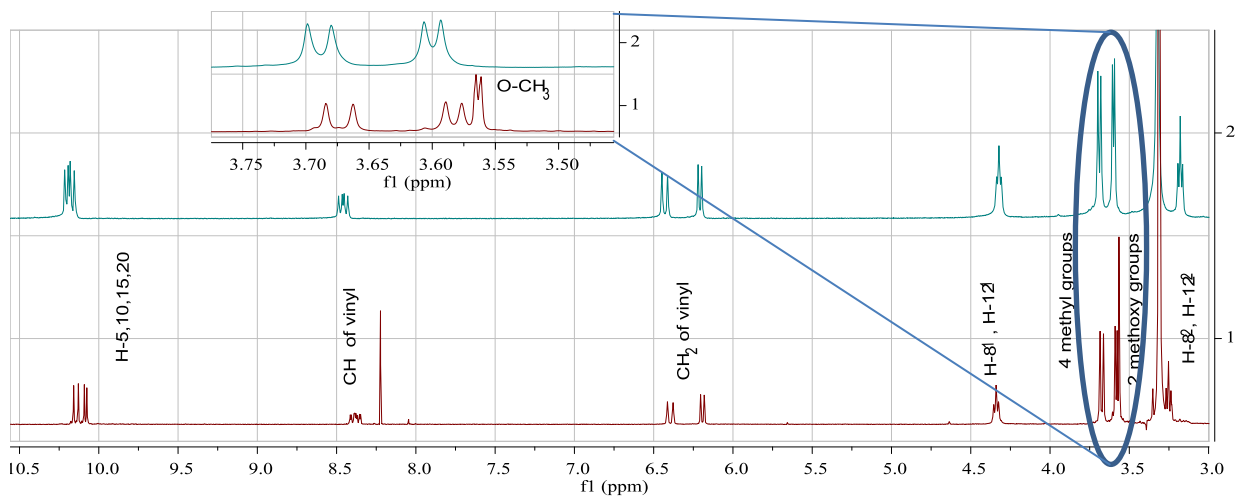


Figure 4.14: The ^1H NMR spectra of **4.13** overlaid with ^1H NMR of protoporphyrin. Insert: an expanded region of the ^1H spectrum from 3.50 to 3.75 ppm. All experiments were performed on a 500 MHz instrument in $\text{DMSO-}d_6$.

4.3 Conclusion

This chapter outlined the successful synthesis and characterization of a series of substituted pyrroles, dipyrroles via the Knorr pyrrole synthesis. The study indicated that the cold methanol filtrates of the crystals of **4.9** and **4.10** contained a high concentration of those compounds, explaining the low yield reported by Wood et al. (58%). Changes to the published syntheses were also reported which improved efficiency of the synthesis of **4.9** and **4.10**. The synthesis of the dimethyl ester of the BPs used in this research program via diazomethane esterification was also reported.

We have been successful in synthesizing a number compounds critical for our studies into the chemical reactivity of bile pigments and related pyrrole derivatives. Compounds **4.3**, **4.9**, **4.10**, **4.11**, **4.12**, **4.13** were characterized by ^1H NMR, ^{13}C NMR, ^1H - ^1H COSY, HSQC, HMBC, mp, ESIMS, TLC, GC-MS and UV spectroscopy. The full assignment of the ^1H and ^{13}C NMR characteristics of **4.11**, **4.12** and **4.13** will provide valuable guidance in NMR studies of BPs and their derivatives.

4.4 Experimental

4.4.1 2,3,4,5-Tetramethyl pyrrole

Butanone (302 mg, 4.2 mmol) was kept in ice to maintain the temperature between 0 to 5 °C, 50 mL MQ-water and 870 mg (12.6 mmol) of NaONO was added via a dropping funnel with 20 mL HCl (1.0 M) then added slowly under nitrogen gas. The reaction vessel was sealed and protected from light and stirred overnight allowing the reaction to reach room temperature. Saturated Na₂CO₃ was added to neutralize to the reaction, bringing the pH to 7-8. Compound **4.2** was extracted into ether before purifying by column chromatography with hexane and EtOAc (from 100% of hexane to 50% hexane) as the eluent to obtain a white solid (390 mg, 92%), R_f 0.5 (TLC 80% hexane/EtOAc), mp 73-76 °C (Lit.,²¹⁴ 75-78 °C); ¹H NMR (500 MHz, C₅D₅N) δ_H 2.18 (s, H-1, 3H), 2.46 (s, H-4, 3H), ¹³C NMR (500 MHz, C₅D₅N) δ_C 8.2 (CH₃-CN), 24.9 (CH₃-CO), 156.1 (C=N), 197.2 (C=O).²¹⁵

A solution of 1,1-diacetyethane (342 mg, 3 mmol), zinc dust (1170 mg, 18 mmol) and **4.2** (200 mg, 0.2 mmol) in MQ-water (30 mL) was heated to 40 °C and glacial acetic acid (9.0 mL, 10M) added via a dropping funnel. The reaction was then stirred under a nitrogen atmosphere for 4 hours protected from light. Saturated Na₂CO₃ was added to neutralize the reaction and bring the pH to 7-8. The product was extracted into hexane and then purified using flash silica column chromatography with hexane as the eluent containing increasing quantities of ethyl acetate. Compound **4.3** eluted in 95% hexane/EtOAc and was dried to give a yellow solid (110 mg, 45%), R_f 0.61 (TLC 80% hexane/EtOAc), Rt (GC) 6.26 min, mp 107 °C, ¹H NMR (500 MHz, CDCl₃) δ_H 1.96 (s, 2CH₃, 6H), 2.35 (s, CH₃, 6H), ¹³C NMR (500 MHz, CDCl₃) δ_C 8.0 (CH₃-C-3, CH₃-C-4), 25.1 (CH₃-C-2, CH₃-C-5), GC-MS *m/z* 123 (M⁺). Compound **4.3** was light sensitive and oxidized readily to red and then green components in the presence of air.^{187,188}

4.4.2 Synthesis of dipyrroles

Ethyl 2-(hydroxyimino)-3-oxobutanoate (4.5)

Ethyl 3-oxobutanoate (**4.4**) (390 mg, 3 mmol) was cooled to between 0 and 5 °C by placing the reaction vessel in ice. MQ-water (40 mL) and 621 mg (9 mmol) of NaONO were added followed by 10 mL HCl (1.0 M) via a dropping funnel under a nitrogen atmosphere. The vessel was protected from light and allowed to stir overnight such that the temperature increased to rt. To neutralize free acid in the reaction mixture, saturated Na₂CO₃ solution was added until pH = 7-8. Compound **4.5** was extracted into ether and isolated from a silica flash column using 70% hexane/ EtOAc as the

eluent. The fraction was dried to give a white solid (453 mg, 95%). R_f 0.2 (TLC 50% hexane/EtOAc), R_t (GC) 8.0 min, mp 43-45 °C (Lit.,²¹⁶ 45-47 °C), ^1H NMR (500 MHz, CDCl_3) δ_{H} 1.44 (t, $J = 7.1$ Hz, $\text{CH}_2\text{-CH}_3$, 3H), 2.79 (s, CH_3 , 3H), 4.49 (q, $J = 7.1$ Hz, $\text{CH}_2\text{-CH}_3$, 2H), ^{13}C NMR (500 MHz, CDCl_3) δ_{C} 14.3 ($\text{CH}_2\text{-CH}_3$), 22.5 ($\text{CH}_3\text{-CO}$), 62.6 ($\text{CH}_2\text{-CH}_3$), 151.4 (C=N), 161.8 (COO), 193.9 (C=O); GC-MS m/z 159 (M^+), 131 ($\text{M-C}_2\text{H}_4$), 113 ($\text{M-C}_2\text{H}_5\text{O}$), ESIMS m/z 158 [M-H] $^-$.

Ethyl 3,4,5-trimethylpyrrole-2-carboxylate (4.7a) and Synthesis of ethyl 4-ethyl-3,5-dimethylpyrrole-2-carboxylate (4.7b)

Ethyl 2-(hydroxyimino)-3-oxobutanoate (**4.5**) (318 mg, 2 mmol), compound **4.6a** (342 mg, 3 mmol) or compound **4.6b** (384 mg, 3 mmol) and zinc dust (1170 mg, 18 mmol) were heated to 40 °C, then glacial acetic acid (9 mL, 10M) was added via a dropping funnel. The reaction was protected from light and stirred for 4 hours under nitrogen gas. Saturated Na_2CO_3 was added until pH = 7-8 and the product extracted into ether and then purified by flash silica column chromatography with hexane and EtOAc (from 100% -50% hexane) as the eluent. Compound **4.7a** was eluted in 95% hexane/EtOAc and was dried to give a white solid (290 mg, 80%). R_f 0.80 (TLC 50% hexane/EtOAc), R_t (GC) 9.90 min, mp 119-120 °C (Lit.,²¹⁷ 125-125 °C), ^1H NMR (500 MHz, CDCl_3) δ_{H} 1.34 (t, $J = 7.1$ Hz, $\text{CH}_3\text{-CH}_2$, 3H), 1.91 (s, $\text{CH}_3\text{-C-4}$, 3H), 2.18 (s, $\text{CH}_3\text{-C-5}$, 3H), 2.25 (s, $\text{CH}_3\text{-C-3}$, 3H), 4.29 (q, $J = 7.1$ Hz, $\text{CH}_2\text{-CH}_3$, 2H), ^{13}C NMR (500 MHz, CDCl_3) δ_{C} 8.7 ($\text{CH}_3\text{-C-4}$), 10.6 ($\text{CH}_3\text{-C-5}$), 11.4 ($\text{CH}_3\text{-C-3}$), 14.5 ($\text{CH}_3\text{-CH}_2$), 59.6 ($\text{CH}_3\text{-CH}_2$), 116.9 (C-2), 117.3 (C-4), 127.4 (C-3), 129.2 (C-5) and 161.8 (C=O), GC-MS m/z 181 (M^+), 152 ($\text{M-C}_2\text{H}_5$), 136 ($\text{M-C}_2\text{H}_5\text{O}$).

Compound **4.7b** was obtained in 95% hexane/EtOAc and dried to give a white solid (370 mg, 95%). R_f 0.83 (TLC 50% hexane/EtOAc), R_t (GC) 10.39 min, mp 101-105 °C (Lit.,²¹⁸ 88-89 °C), ^1H NMR (500 MHz, CDCl_3) δ_{H} 1.04 (t, $J = 7.6$ Hz, $\text{CH}_3\text{-CH}_2\text{-C-4}$, 3H), 1.34 (t, $J = 7.1$ Hz, $\text{CH}_3\text{-CH}_2\text{-O}$, 3H), 2.20 (s, $\text{CH}_3\text{-C-3}$), 2.28 (s, $\text{CH}_3\text{-C-5}$), 2.38 (q, $J = 7.6$ Hz, $\text{CH}_3\text{-CH}_2\text{-C-4}$, 2H), 4.29 (q, $J = 7.1$ Hz, $\text{CH}_3\text{-CH}_2\text{-O}$, 3H); GC-MS m/z 195 (M^+), 180 (M-CH_3), 166 ($\text{M-C}_2\text{H}_5$), ESIMS m/z 196 [M+H] $^+$, 218 [M+Na] $^+$.

2,3,4-Trimethyl-5-(3,4,5-trimethylpyrrole-2-ylidene)methylpyrrole (4.9) and 3-ethyl-5-((4-ethyl-3,5-dimethylpyrrole-2-ylidene)methyl)-1,2-dimethylpyrrole (4.10)

A solution of **4.8a** (181 mg, 1 mmol) or **4.8b** (195 mg, 1 mmol) in a mixture of 0.2 mL of concentrated HBr and 10 mL of 96% formic acid was refluxed under Ar atmosphere for 1 hour. The reaction vessel was cooled to rt and then to 4 °C before washing the solid with ice cold

methanol to obtain a yellow solid, 137 mg for **4.9** and 219 mg for **4.10**. The methanol filtrates were evaporated to dryness and the residue redissolved in ether. The ether solution was then washed with water, dried over MgSO₄ and the ether removed under reduced pressure. The compounds were then purified by flash silica column chromatography with hexane and EtOAc. Compounds **4.9** and **4.10** were eluted in 30% hexane/EtOAc. This provided a further 30 mg of **4.9** and 21 mg of **4.10**. Compound **4.9** was further purified by column chromatography using 95% DCM/MeOH which provided a yellow solid (167 mg, 73%); R_f 0.33 (TLC 95% DCM/MeOH), mp 125-130 °C, ¹H NMR (500 MHz, CDCl₃) δ_H 1.94 (s, CH₃-C-3, 6H), 2.21 (s, CH₃-C-4, 6H), 2.59 (s, CH₃-C-5, 6H), 6.95 (s, =CH-, 1H), ¹³C NMR (500 MHz, CDCl₃) δ_C 118.6 (C-bridge), 124.1 (C-4), 126.1 (C-2), 141.8 (C-3), 154.0 (C-5); ESIMS *m/z* 229 [M+H]⁺, HRESIMS *m/z* 229.1703 [M+H]⁺ (calcd for C₁₇H₂₄N₂, 229.1699).

Compound **4.10** (240 mg, 94%); R_f 0.61 (TLC, EtOAc), mp 130-132 °C, ¹H NMR (500 MHz, CDCl₃) δ_H 1.07 (t, *J* = 7.1 Hz, CH₃-CH₂, 6H), 2.26 (s, CH₃-C-3, 3', 6H), 2.43 (q, *J* = 7.1 Hz, CH₃-CH₂, 4H), 2.64 (s, CH₃-C-5, 5'), 7.01 (s, CH=C-2, 2'), ¹³C NMR (500 MHz, CDCl₃) δ_C 9.9 (CH₃-C-3), 12.7 (CH₃-C-5), 14.2 (CH₂-CH₃), 17.0 (CH₂-CH₃), 126.2 (C-2, 2'), 130.4 (C-4, 4'), 141.0 (C-4, 4'), 153.6 (C-5, 5'); ESIMS *m/z* 257 [M+H]⁺, HRESIMS *m/z* 257.2016 [M+H]⁺ (calcd for C₁₇H₂₄N₂, 257.2012).

3-Ethyl-2,3,5-trimethylpyrrole (4.8b)

A solution of **4.7b** (780 mg, 4 mmol) in 48 mL of ethylene glycol and 600 mg NaOH was sealed into a reaction vessel and protected from light before refluxing for 1 hour under Ar gas. The product was extracted into hexane and washed three times with saturated Na₂CO₃ then dried at low temperature (-20 °C) by rotary evaporation to give a white solid (a yellow liquid at room temperature, 248 mg, 50%), R_f 0.67 (TLC 80% hexane/EtOAc), R_t (GC) 6.03 min, ¹H NMR (500 MHz, CDCl₃) δ_H 1.11 (m, CH₃-CH₂, 3H), 2.06 (s, CH₃-C-4, 3H), 2.19 (s, CH₃-C-3, 2H), 2.41 (m, CH₃-CH₂, 2H), 6.41 (s, H-5), 7.50 (s, N-H), GC-MS *m/z* 123 (M⁺).

4.4.3 Synthesis of bilirubin-IX α dimethyl ester (4.11), biliverdin-IX α dimethyl ester (4.12), protoporphyrin-IX α dimethyl ester (4.13)

A reaction vessel containing diazomethane (17 mg, 0.4 mmol) in 4 mL ether was kept at -20 °C (dry ice/ Oxylen) or -80 °C (dry ice/ acetone) under Ar gas. The vessel was sealed and protected from light before bilirubin (117 mg, 0.2 mmol) for synthesis of **4.11** or biliverdin (116 mg, 0.2 mmol) for

synthesis of **4.12** or protoporphyrin (113 mg, 0.2 mmol) for synthesis of **4.13** was added and the mixture stirred for 2 hours before slowly increasing to rt overnight.

The reaction's mixture was dried before purifying quickly by column chromatography with DCM/MeOH as the eluent to achieve a yellow solid at 98% DCM/MeOH (compound **4.11**, 64 mg, 44%), R_f 0.23 (TLC 99% DCM/MeOH), mp 197-200 °C, λ_{abs} (MeOH) 450 nm, ^1H NMR (500 MHz, $(\text{CD}_3)_2\text{OS}$) and ^{13}C NMR (500 MHz, $(\text{CD}_3)_2\text{OS}$) (Table 4.1 in discussion section), ESIMS m/z 613 $[\text{M}+\text{H}]^+$.

The reaction's mixture of biliverdin was purified by column chromatography to achieve a green solid (**4.12**, 68 mg, 56%), R_f 0.20 (TLC 30% hexane/EtOAc), mp 195-210 °C, λ_{abs} (MeOH) 375 nm, ^1H NMR (500 MHz, $(\text{CD}_3)_2\text{OS}$) δ_{H} 1.79 (s, $\text{CH}_3\text{-C-18}$, 3H), 2.02 (s, $\text{CH}_3\text{-C-13}$, 3H), 2.06 (s, $\text{CH}_3\text{-C-7}$, 3H), 2.15 (s, $\text{CH}_3\text{-C-3}$, 3H), 2.51 (brs, $\text{CH}_2\text{-CH}_2\text{-CO}$, 4H), 2.88 (brs, $\text{CH}_2\text{-CH}_2\text{-CO}$, 4H), 3.58 (s, $\text{CH}_3\text{-O}$, 6H), 5.37 (d, $J = 11.5$ Hz, $\text{CH}_2=\text{CH-C-2}$, 1H), 5.67 (dd, $J = 17.5, 11.5$ Hz, $\text{CH}_2=\text{CH-C-17}$, 2H), 6.05 (dd, $J = 17.5, 2.0$ Hz, $\text{CH}_2=\text{CH-C-2}$, 1H), 6.08-6.11 (s, H-5, H-15, 2H), 6.55 (dd, $J = 17.5, 11.5$ Hz, $\text{CH}_2=\text{CH-C-17}$, 1H), 6.81 (dd, $J = 17.5, 11.5$ Hz, $\text{CH}_2=\text{CH-C-2}$, 1H), 6.95 (s, H-10, 1H), 10.01-10.22 (s, NH-CO, 2H); ^{13}C NMR (500 MHz, $(\text{CD}_3)_2\text{OS}$) δ_{C} 9.1 (C-13¹, C-7¹, C-3¹), 9.5 (C-18¹), 19.3 (C-8², C-12²), 34.9 (C-8¹, C-12¹), 51.3 ($\text{CH}_3\text{-O}$), 97.3 (C-5, C-15), 116.0 (C-10), 119.2 (C-2²), 122.5 (C-17²), 126.6 (C-17¹), 126.8 (C-2¹), 128.2 (C-18), 137.2 (C-12, C-8), 139.2 (C-17), 139.6 (C-7, C-13), 141.1 (C-9, C-11), 141.3 (C-2), 141.4 (C-4), 171.7 (C-1, C-19), 172.6 (C-8³, C-12³), ESIMS m/z 611 $[\text{M}+\text{H}]^+$, ESIMS m/z 609 $[\text{M}+\text{H}]$.

The dimethyl ester of protoporphyrin in the mixture after reaction was purified by column chromatography with hexane and EtOAc to give a red solid at 80% EtOAc/hexane fraction (**4.13**, 98 mg, 83%). R_f 0.79 (TLC EtOAc), mp 215-220 °C, λ_{abs} (MeOH) 410 nm, ^1H NMR (500 MHz, $(\text{CD}_3)_2\text{OS}$) δ_{H} 3.56-3.57 (2s, $\text{CH}_3\text{-O}$, 6H), 3.58-3.59 (2s, H-3¹, H-18¹, 6H), 3.66-3.68 (2s, H-7¹, H-13¹, 6H), 4.34 (t, $J = 7.7$ Hz, H-8¹, H-12¹, 4H), 6.19 (d, $J = 11.5$ Hz, H-17², H-2², 2H), 6.40 (d, $J = 17.5$ Hz, H-17², H-2², 2H), 8.38 (ddd, $J = 17.5$ Hz, 11.5 Hz, 3.5 Hz, H-2¹, H-17¹, 2H), 10.08 (s, H-10), 10.09-10.13 (2s, H-5, H-15, 2H), 10.16 (H-20), ^{13}C NMR (500 MHz, $(\text{CD}_3)_2\text{OS}$) δ_{C} 11.8-13.0 (C-3¹, C-7¹, C-13¹, C-18¹), 36.9 (C-8², C-12²), 36.9 (C-8¹, C-12¹), 51.8 ($\text{CH}_3\text{-O}$), 97.8 (C-5, C-10, C-15, C-20), 121.5 (C-2², C-17²), 130.5 (C-2¹, C-17¹), 136.6 (C-2, C-17), 137.5 (C-7, C-13), 139.5 (C-8, C-12), ESIMS m/z 591 $[\text{M}+\text{H}]^+$.

Chapter 5: Model epoxide studies

5.1 Introduction

A leading cause of DNA modification and mutation, resulting in cancerous cells, is the attack of environmental carcinogens and mutagens. Therefore, elucidation of the mechanisms by which these mutagens react with DNA has become a key interest in biochemistry. One of the most common environmental pollutants is benzo[α]pyrene (**5.1**, B α P) but research has shown that the compound responsible for DNA damage is the metabolite, benzo[α]pyrene-7,8-dihydrodiol-9,10-epoxide (**5.2**)^{95,219,220} produced by the action of human cytochrome P450 enzymes (hCYP1A1, hCYP1B1 and hCYP3A4) on **5.1** (Figure 5.1).^{219,221-223} The highly reactive epoxide **5.2** attacks DNA bases, particularly guanine, to produce covalent DNA adducts.^{95,101} Similarly, the action of liver enzymes (CYP3A4 and CYP1A2) on Aflatoxin B1 (AFB1) (**5.4**) produces a reactive epoxide, AFB1-8,9-epoxide (**5.5**) that is a highly mutagenic agent which can modify DNA by binding to guanine nucleotides (Figure 5.1).²²⁴⁻²²⁶ One possible way of reducing the impact of these environment mutagens is to provide alternate ‘scavenger’ compounds to react with the mutagenic metabolites before they react with DNA. BPs, especially unconjugated bilirubin IX α (**5.9**), biliverdin IX α (**5.10**) and protoporphyrin IX α (**5.8**), have been the focus of some attention in this area, due to their highly anti-mutagenic^{2,18,19,186,227}, anti-cancer^{17,18} and antioxidant properties.^{18,27,28,30,33} To date, however, little is known about the mechanisms by which BPs exhibit these properties and thus, the focus of the research detailed in this chapter was to investigate if the BPs’ anti-mutagenic properties were a result of covalent adduct formation between the reactive epoxide metabolites and the BPs.

A key concern in our research is that both epoxides **5.2** and **5.5** are toxic to humans, unstable and not commercially available. Styrene epoxide (**5.7**) is a commercially available aromatic epoxide that has previously been demonstrated to be mutagenic in mammalian cells, binding to DNA at the N-7 position of guanine, and subsequently modifying DNA.^{228,229} This reaction between **5.7** and guanine is analogous to the epoxide-opening reaction which occurs between **5.5**^{230,231} and **5.2** and the N-2 of guanine.^{101,102} Styrene epoxide (**5.7**) was therefore chosen as a model for **5.2** and **5.5** in studies on the reactivity of mutagens towards BPs and their derivatives (Figure 5.2).

In an effort to evaluate the ability of BPs (poly-heterocyclic compounds) to inhibit the reaction of aromatic epoxides with guanine in DNA, we initially studied the reactivity of cheaper, simpler and more stable heterocyclic compounds such as indole (**5.12**) and imidazole (**5.11**) with model epoxide **5.7**. While aqueous phosphate buffer would be the ideal medium for model reactions to mimic

biological conditions, none of the BPs dissolve in aqueous solvents and thus, CHCl_3 and DCM were chosen as solvents for the reactions.⁷⁶ Addition of silica to the reactions as a catalyst had a crucial role in activating **5.7** to nucleophilic attack,^{232,233} replacing the hydrogen bonding role of water molecules in an aqueous medium.²³⁴ The experiments aimed to assess the reactivity of the pyrrole ring, as well as other nitrogen containing aromatic rings, toward activated epoxides. They represented preliminary examination of the mechanism of reactions that may contribute to the inhibition of mutagenic epoxide agents by natural BPs.

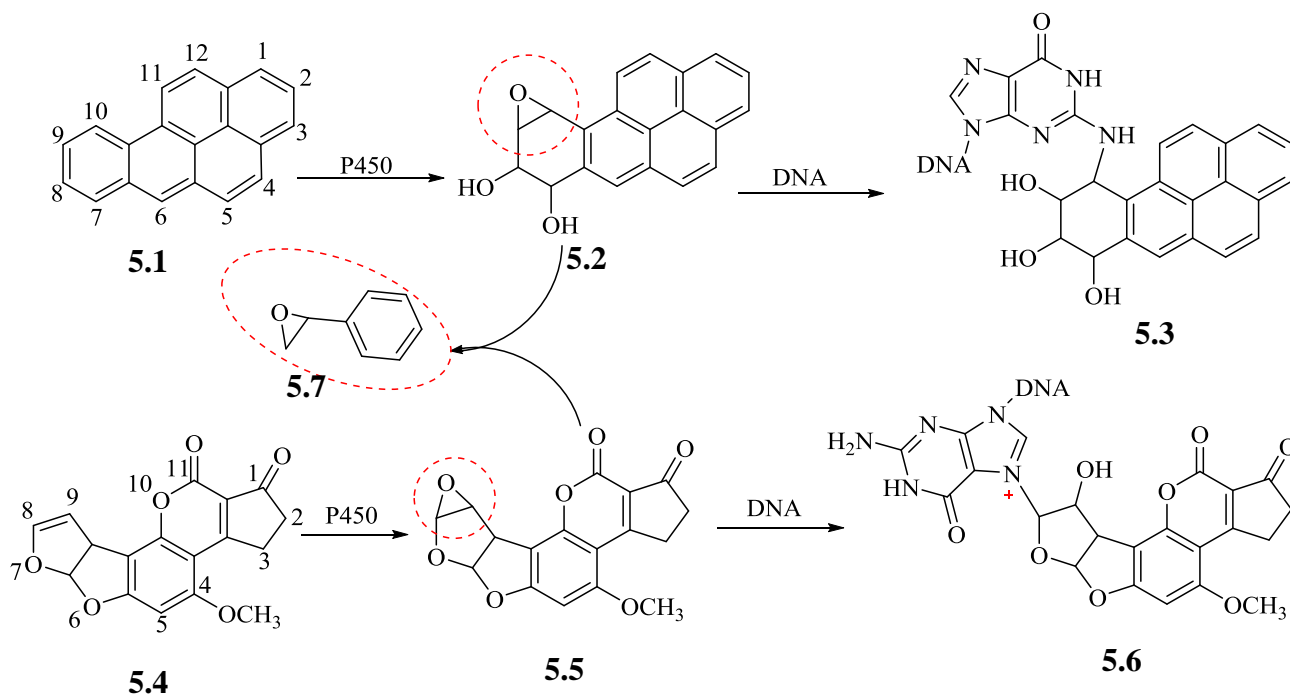


Figure 5.1 A simplified summary of the metabolism of **5.1** and **5.4** leading to DNA-adduct formation. Insert: the structure of **5.7** chosen as a mimic for **5.2** and **5.5** in the reactivity studies.

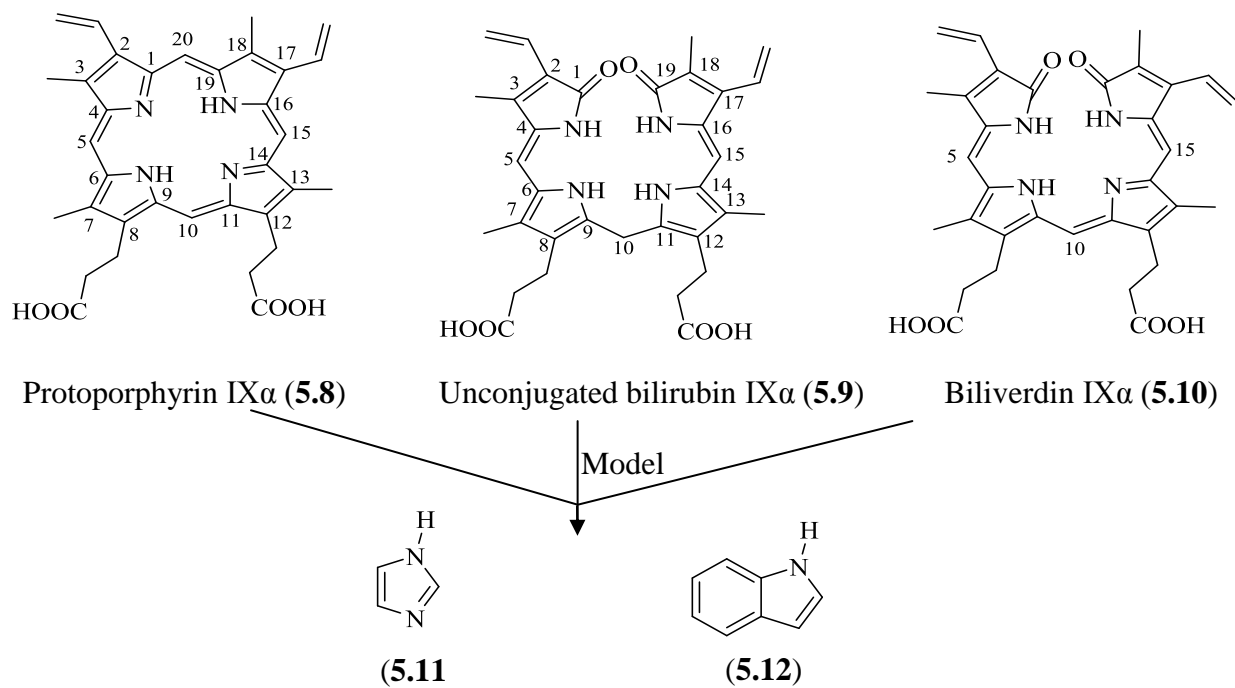


Figure 5.2: The structures of the BPs as well as that of imidazole (5.11) and indole (5.12) chosen as mimics for BPs in initial reactivity studies.

5.2 Results and discussion

5.2.1 Model reactions of indole, imidazole and guanine with styrene epoxide

5.2.1.1: Reaction of indole with styrene epoxide

The experiments performed in DCM gave polymers of styrene epoxide as the main products. Reactions performed in neat chloroform gave very low yields of any products. Therefore, the experiments were performed in 50% DCM and 50% chloroform in the presence of silica. The analysis of covalent conjugates from the reaction of **5.7** and **5.12** indicated that silica is an effective catalyst for activation of **5.7** to attack by nucleophilic agents. This confirmed similar observations by Kotsuki et al. who also used silica in DCM at rt to study the reaction of **5.7** with **5.12**. Kotsuki et al. found that 88% of **5.12** was converted to 2-(3'-indolyl)-2-phenylethanol (**5.13**), however they do not report any other minor products.²³⁴ Similarly, we found **5.13** to be the major product of our reaction between **5.7** and **5.12**, being isolated in 80% yield but the overall yield of conjugates from the reaction was 97% with the remaining 17% being made up of minor products resulting from attachment of **5.7** to other sites around the heterocycle. GC/MS, one- and two- dimensional NMR spectroscopy, TLC, LRESIMS, HRESIMS, and melting point analysis were used to identify eight products from the reaction of **5.7** and **5.12**.

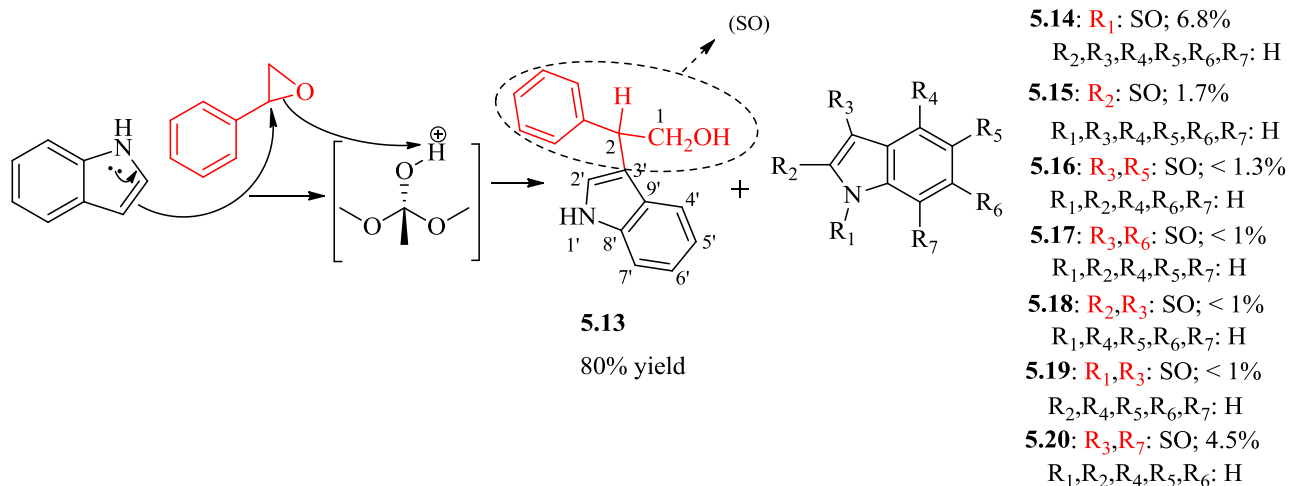


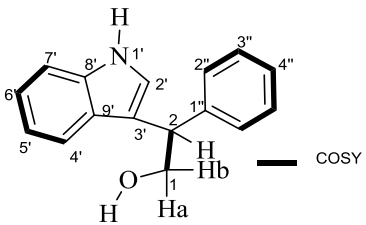
Figure 5.3: The mechanism of the reaction between **5.7** and **5.12** with silica.²³⁴

The main product from the reaction of **5.12** with **5.7** was 2-(3'-indolyl)-2-phenylethanol (**5.13**) as determined by MS (EIMS m/z 237 $[M]^+$, m/z 206 $[M-CH_2OH]^+$, LRESIMS m/z 260.1 $[M+Na]^+$, m/z 276.1 $[M+K]^+$), 1H NMR and ^{13}C NMR spectroscopy (Table 5.1). The 1H spectrum indicated the H-3' of the pyrrole ring was no longer present and a doublet at δ_H 7.27, which exhibited the

characteristic shift for H-2', had a long-range HMBC coupling to a benzylic carbon assigned to C-2 (δ_C 45.5) (See Figure 5.3 and Figure 7.22 (2D) of appendix-D). The HMBC experiment also showed correlations from proton signals associated with a primary alcohol assigned as δ_H 4.07 and 4.01 (H-1) to δ_C 115.9 (C-3') of the indole ring and the regiochemistry of the substitution of **5.12** with one unit of **5.7** was further supported by correlations from H-2 to C-2', C-4' and C-3' (HMBC spectra can be viewed in Figure 7.22 of appendix-D).

A regioisomer of **5.13**, **5.15** was identified as the next most abundant product being isolated in 6.8% yield and possessed MS data consistent with the addition of a unit of **5.7**, EIMS m/z 237 $[M]^+$, ESI-MS m/z 260 $[M+Na]^+$, 276 $[M+K]^+$. The structure of **5.15** was elucidated using NMR spectroscopy (Table 3.2). In particular the absence of the H-2' signal and the presence of a doublet corresponding to H-3' at δ_H 6.22 (d, $J = 1.5$ Hz) were keys in its structure determination. The $J = 1.5$ Hz coupling is the result of an allylic coupling from H-3' to H-2. The HMBC experiment confirmed the 1H NMR results showing correlations from δ_H 4.19 (H-2) to δ_C 141.1 (C-2') and δ_C 99.0 (C3') (See Figure 5.4 for 1H NMR spectrum and HMBC spectra can be viewed in Figure 7.23 of appendix-D). A minor product (1.7% yield, MS m/z 237 $[M]^+$, ESI-MS m/z 260 $[M+Na]^+$, 276 $[M+K]^+$) was isolated and identified as **5.14** by the absence of the N₁-H signal and HMBC correlations from δ_H 5.64 (H-2) to δ_C 126.4 (C-2'). The 1H , ^{13}C NMR data for **5.14** is presented in Table 5.2 and the 1H spectrum in Figure 5.4.

Table 5.1: NMR Spectroscopic Data (DMSO- d_6 , 500 MHz) for compound **5.13**.



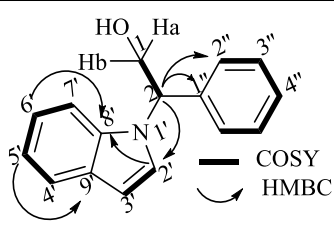
#	δ_C (ppm) ^a	δ_H (ppm), mult., J (Hz) ^b	1H - ^{13}C HMBC ^{ab}
1	63.4	4.07, m 4.01, m	C2, C1'', C3' C2, C1'', C3'
2	45.5	4.33, (dd, J 7.3 Hz, H-2),	C1, C3', C2'C1'', C2'', C4'
1'	-	10.90, brs	C3', C2', C9', C8'
2'	122.2	7.27, d, 2.4	C3', C8', C9'
3'	115.9	-	-
4'	118.7	7.37, m	C5', C3', C6', C9', C8'
5'	118.3	6.90, ddd, 7.8, 7.9, 1.1	C6', C7', C9'

6'	121.0	7.04, ddd, 7.6, 8.1, 1.0	C4', C8'
7'	111.4	7.35, m	C9', C5'
8'	127.0	-	-
9'	136.3	-	-
1''	144.0	-	-
2''	128.3	7.34, dd, 8.0, 0.9	C3'', C4''
3''	128.0	7.24, dd, 7.8, 7.5	C2'', C4''
4''	125.9	7.14, t, 7.5	C2''

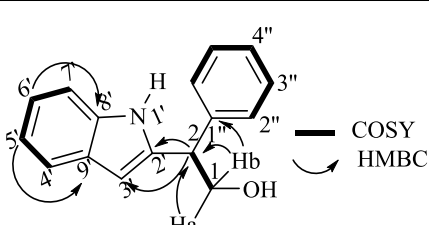
^aChemical shift (ppm) referenced to DMSO-*H*₆ δ_C 39.5 were taken from 1D and 2D NMR (500 MHz, DMSO-*d*₆);

^bChemical shift (ppm) referenced to DMSO-*H*₆ δ_H 2.49. HMBC correlations, optimized for 8 Hz, are from proton(s) stated to the indicated carbon.

Table 5.2: ¹H and ¹³C NMR data for compound (5.14, 5.15).



5.14



5.15

C	5.14		5.15	
	δ _C (ppm) ^a	δ _H (ppm), mult., <i>J</i> (Hz) ^b	δ _C (ppm) ^a	δ _H (ppm), mult., <i>J</i> (Hz) ^b
1	61.5	4.06, dd, 11.6, 5.0 4.23, m	64.8	3.92, m 4.04, m
2	63.2	5.64, dd, 8.4, 5.1,	48.2	4.19, t, 7.0
1'	--	--	--	--
2'	126.4	7.68, d, 3.3	141.1	
3'	101.0	6.49, d, 3.2	99.0	6.22, d, 1.5
4'	120.4	7.52, d, 7.8	119.8	7.4, brd, 7.8
5'	119.2	6.97, ddd, 7.0, 8.2, 0.9	119.2	6.91, ddd, 7.6, 7.5, 1.0
6'	121.1	7.03, ddd, 7.5, 7.8, 0.9	120.7	6.97, ddd, 7.8, 7.5, 1.0
7'	110.2	7.35, d, 8.2	111.3	7.25, brd, 7.6
8'	136.2	--	136.4	--
9'	128.3	--	128.4	--
1''	139.7	--	142.3	--
2''	126.9	7.24, m	126.6	7.29, m

3''	128.5	7.26, m	128.6	7.28, m
4''	127.6	7.21, m	126.8	7.19, m

^aChemical shift (ppm) referenced to DMSO-*H*₆ δ_C 39.5 were taken from 1D and 2D NMR (DMSO-*d*₆, 500 MHz);

^bChemical shift (ppm) referenced to DMSO-*H*₆ δ_H 2.49

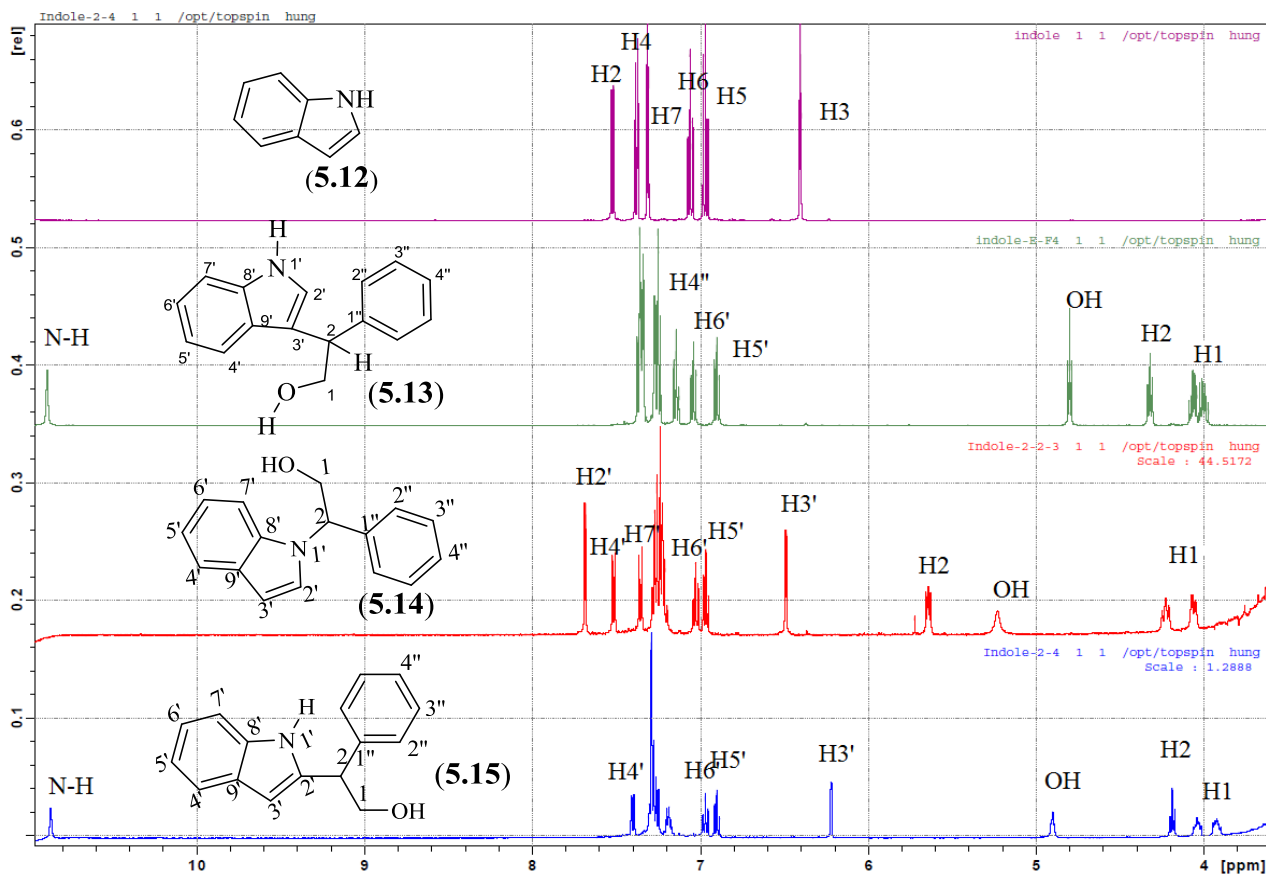
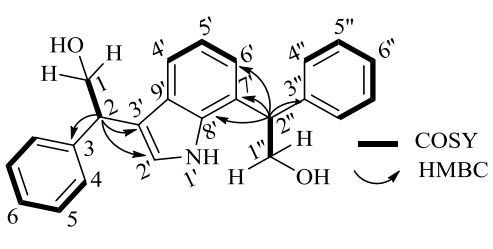


Figure 5.4: The ¹H NMR spectra of three mono-phenylethanol substituted adducts of **5.12** and the spectrum of **5.12** is provided for comparison. All experiments performed at 500 MHz in DMSO-*d*₆.

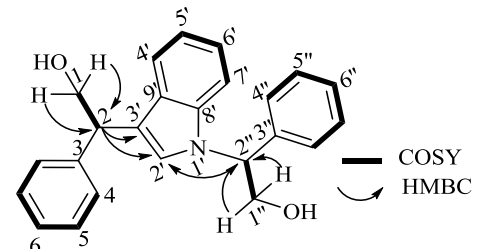
Five minor products (8.5% yield in total) possessed MS data consistent with the addition of two phenylethanol groups attached to two different positions of the indole ring were also isolated from the reaction. The presence of two phenylethanol groups was suggested by the presence of a *m/z* 380 signal of [M+Na]⁺ in the mass spectra of these compounds. The locations of the substituents were determined by ¹H, ¹³C and HMBC NMR. Compound **5.16**, the third major product, was isolated in 4.5% yield, and was identified by the absence of H-3 and H-7 in the ¹H NMR spectrum and a downfield doublet signal at δ_H 7.19 (d, *J* = 2.4 Hz) that had a long range correlation to δ_C 135.1 (C-8') and δ_C 116.3 (C-3'). The HSQC correlation showed the cross-peak between the proton signal at δ_H 7.19 and a carbon at δ_C 122.0. The HMBC correlation from δ_C 122.0 to δ_H 10.82 (s, H-1') identified the C-2' signal as that at δ_C 122.0 and H-2' at δ_H 7.19. Another deshielded signal at δ_H 7.00 (d, *J* = 7.1 Hz) was identified as the signal of H-6' and showed an HMBC correlation to δ_C

47.8 (C-2'') (Table 5.3). In addition, the absence of H-3' and H-7' signals in the ^1H NMR of **5.16** suggested the location of the substituents (Figure 5.4). Moreover, the HMBC correlations from δ_{H} 4.53 (H-2'') to δ_{C} 135.1 (C-8'), δ_{C} 126.0 (C-7') and δ_{C} 118.5 (C-6') (Table 5.3) confirmed the substitution of C-3' and C-7' of **5.12** with two phenylethanol units. Compound **5.19** accounted for approximately 1% yield, MS (m/z 357 (M^+), ESIMS m/z 380 [$\text{M}+\text{Na}^+$], 396 [$\text{M}+\text{K}^+$]) and was identified due to the absence of H-3' and H-1' signals in the ^1H NMR (Table 5.3). The HMBC spectrum showed interactions from δ_{H} 4.08 (H-2) and δ_{H} 5.62 (H-2'') to δ_{C} 123.1 (C-2') (Table 5.3). Other minor isomers, compounds **5.17**, **5.18**, **5.20** were similarly identified by 1D and 2D NMR spectroscopy as showed in Table 5.4 and Table 5.5 and Figure 5.5.

Table 5.3: ^1H and ^{13}C NMR data for compound (**5.16** and **5.19**).



5.16



5.19

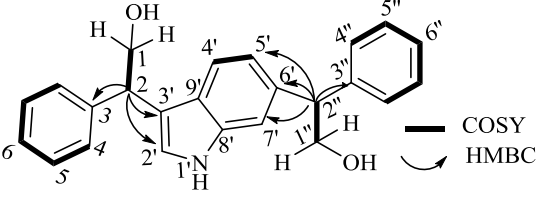
C	5.16		5.19	
	δ_{C} (ppm) ^a	δ_{H} (ppm), mult., J (Hz) ^b	δ_{C} (ppm) ^a	δ_{H} (ppm), mult., J (Hz) ^b
1	65.2	3.97, m 3.92, m	65.3	3.98, m 4.06, m
2	45.4	4.21, dd, 7.2, 7.3	45.5	4.08, m
3	143.9	-	143.8	--
4	128.2	7.30, dd, 8.2, 15	128.3	7.33, m
5	128.0	7.22, m	127.9	7.24, m
6	125.8	7.12, m	125.8	7.13, t, 7.5
1'	-	10.82, brs	--	--
2'	122.0	7.19, d, 2.4	123.1	7.69, s
3'	116.3	-	115.5	--
4'	111.6	7.15, d, 7.8	118.8	7.28, m
5'	118.8	6.84, t, 7.7	118.5	6.85, t, 7.0
6'	118.5	7.00, dd, 7.1	120.9	6.97, t, 7.5
7'	126.0	-	110.0	7.30, m
8'	135.1	-	136.4	--
9'	127.1	-	127.5	--

1''	64.1	4.03, m	63.2	4.25, m
		4.02, m		4.08, m
2''	47.8	4.53, m	61.0	5.62, dd, 8.5, 5.0
3''	142.7	-	139.7	--
4''	128.3	7.39, dd, 8.2, 1.5	126.8	7.30, m
5''	128.0	7.22, m	128.3	7.25, m
6''	126.1	7.12, m	127.4	7.21, m

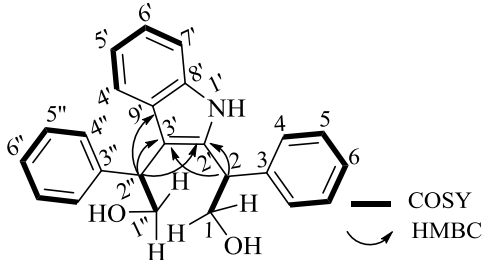
^aChemical shift (ppm) referenced to DMSO-*H*₆ δ_C 39.5 were taken from 1D and 2D NMR (DMSO-*d*₆, 500 MHz);

^bChemical shift (ppm) referenced to DMSO-*H*₆ δ_H 2.49

Table 5.4: ¹H and ¹³C NMR data for compound (5.18 and 5.20).



5.18



5.20

C	δ _C (ppm) ^a	δ _H (ppm), mult., <i>J</i> (Hz) ^b	δ _C (ppm) ^a	δ _H (ppm), mult., <i>J</i> (Hz) ^b
1	64.8	3.91, m 3.95, m	63.8	3.79, m 4.26, m
2	45.5	4.29, t, 7.0	45.2	4.44, dd, 9.0, 6.0
3	143.9	--	143.5	--
4	128.2	7.20, m	128.3	7.31, d, 7.5
5	128.0	7.24, m	127.8	7.24, t, 7.5
6	125.8	7.11, m	126.3	7.16, t, 7.5
1'	--	10.70, brs	--	10.71, s
2'	121.8	7.14, s	136.0	--
3'	115.6	--	112.4	--
4'	118.4	7.17, d, 8.0	119.2	7.21, m
5'	119.1	6.77, m	118.1	6.75, td, 7.5, 1.0
6'	135.8	--	120.2	6.90, td, 7.0, 1.0
7'	110.5	7.13, m	111.0	7.23, m
8'	136.4	--	136.5	--

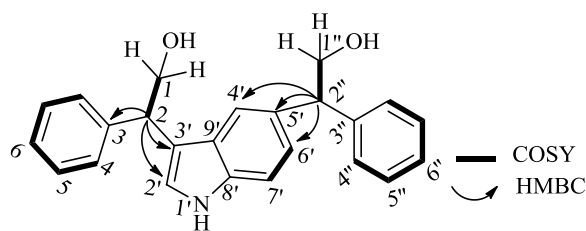
Chapter V: Model epoxide studies

9'	125.3	--	126.9	--
1''	65.1	3.92, m 3.96, m	63.4	4.05, m 4.05, m
2''	53.6	4.08, t, 7.0	44.2	4.49, t, 7.5
3''	143.8	--	141.7	--
4''	127.9	7.20, m	128.5	7.38, d, 7.5
5''	128.0	7.24, m	128.2	7.20, t, 7.5
6''	125.7	7.11, m	125.5	7.09, t, 7.0

^aChemical shift (ppm) referenced to DMSO-*H*₆ δ_C 39.5 were taken from 1D and 2D NMR (DMSO-*d*₆, 500 MHz);

^bChemical shift (ppm) referenced to DMSO-*H*₆ δ_H 2.49

Table 5.5: ¹H and ¹³C NMR data for compound (5.17).



C	δ _C (ppm) ^a	δ _H (ppm), mult., <i>J</i> (Hz) ^b	¹ H- ¹³ C HMBC ^{ab}
1	65.1	3.87-3.97, m	C2
2	45.4	4.22, t, 7.0	C1, C3', C9', C4, C3 C2'
3	143.9	--	--
4	128.2	7.22, m	C2, C6
5	128.0	7.22, m	C3
6	125.8	7.14, m	C4
1'	--	10.72, brs	C8', C9', C3', C2'
2'	122.3	7.14, s	C8', C9'
3'	115.6	--	--
4'	117.5	7.22, m	C6', C3', C8'
5'	132.7	--	--
6'	121.5	6.90, dd, 8.5, 1.5	C8', C4'
7'	110.0	7.18, m	C5', C9'
8'	134.8	--	--
9'	126.9	--	--
1''	65.1	3.87-3.97, m	C2''
2''	53.6	4.02, t, 7.0	C6', C4', C5', C3'', C4''
3''	143.8	--	--

4''	127.9	7.18, m	C2'', C6''
5''	128.0	7.24, m	C3''
6''	125.7	7.11, m	C4''

^aChemical shift (ppm) referenced to DMSO-*H*₆ δ_C 39.5 were taken from 1D and 2D NMR (DMSO-*d*₆, 500 MHz);

^bChemical shift (ppm) referenced to DMSO-*H*₆ δ_H 2.49

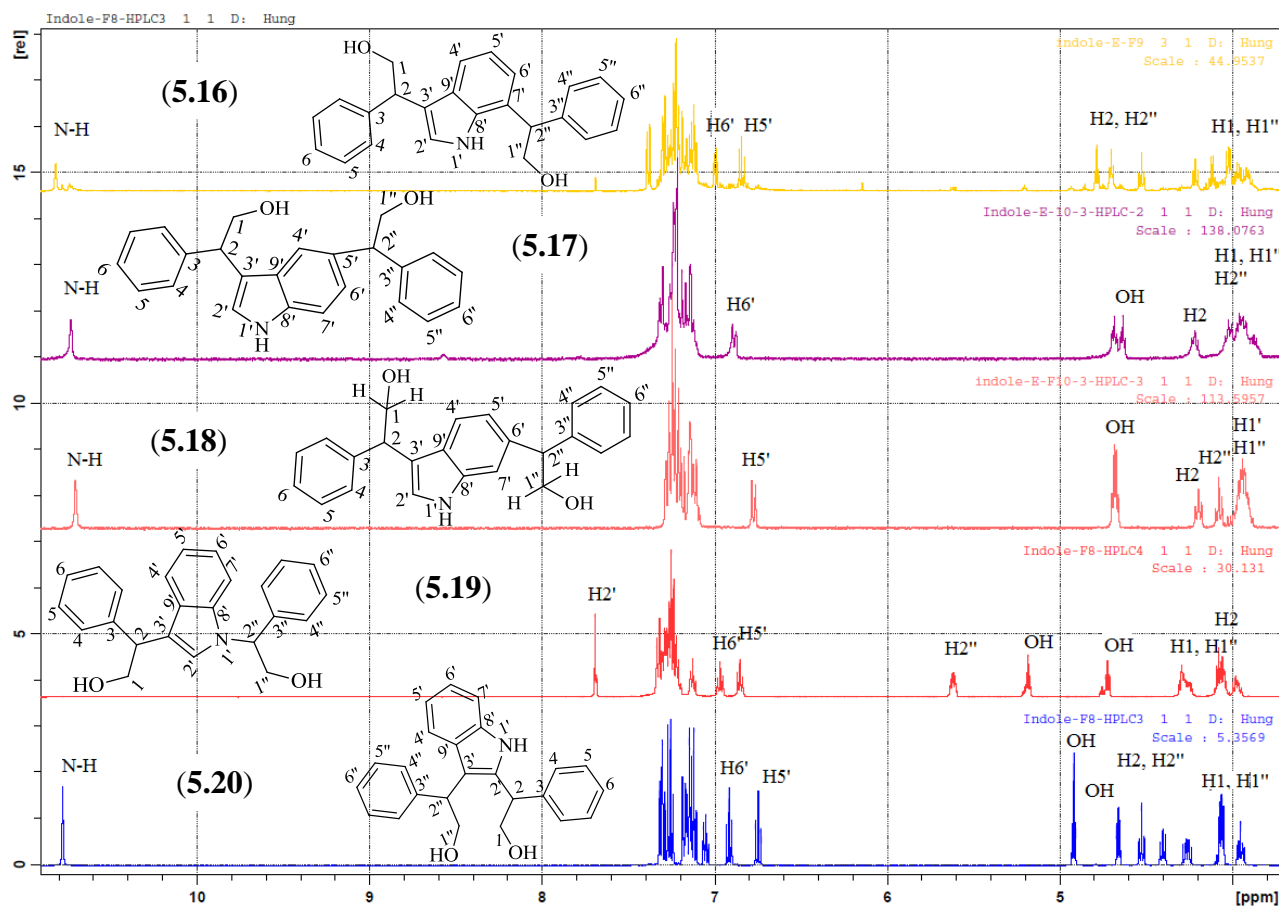



Figure 5.5: The ¹H NMR spectrum of five bis-phenylethanol substituted adducts of **5.12**. All experiments were run on a 500 MHz machine in a mixture of DMSO-*d*₆.

5.2.1.2: Reaction of imidazole with styrene epoxide

Imidazole (**5.11**) was allowed to react with **5.7** in the presence of silica under the conditions described above. The reactions produced a 1:1 ratio of compounds **5.21** and **5.22** in a total yield of 44%. The likely mechanism of this reaction is detailed in Figure 5.3, in which silica activated **5.7** in order to facilitate nucleophilic attack of the imidazole to the epoxide ring. 2-(Imidazole-1-yl)-1-phenylethanol (**5.21**) was characterized by a ¹H-¹H-COSY correlation from the δ_H 5.69 (O-H) signal to a methine signal at δ_H 4.80²³⁵ (H-2) indicating a secondary alcohol and the HMBC correlations from the methylene proton signals at δ_H 4.02 and δ_H 4.12²³⁵ (H-2) to δ_C 127.7 (C-5') and δ_C 137.9 (C-2') indicating a new bond between C-2 of the phenylethanol unit and N-1' of **5.11** (Table 5.6).

Similarly, the identity of the primary alcohol (**5.22**) was determined by the correlations from δ_{H} 5.36 (H-2) to δ_{C} 128.2 (C-5') and δ_{C} 136.9 (C-2').

Table 5.6: ^1H and ^{13}C NMR data for **5.21** and **5.22**.



C	5.21		5.22	
	δ_{C} (ppm) ^a	δ_{H} (ppm), mult., <i>J</i> (Hz) ^b	δ_{C} (ppm) ^a	δ_{H} (ppm), mult., <i>J</i> (Hz) ^b
1	72.1	4.80, dd, 4.1, 8.0	63.3	3.97, m 4.08, m
2	53.6	4.02, dd, 8.0, 13.9 4.12, dd, 4.1, 13.9	62.6	5.36, dd, 5.0, 8.0
1'	--	--	--	--
2'	137.9	7.51, brs	136.9	7.81, brs
3'	--	--	--	--
4'	120.2	7.12, brs	120.2	6.91, brs
5'	127.7	6.84, brs	128.2	7.27, brs
1''	142.7	--	139.1	--
2''	126.0	7.33, m	127.0	7.30, m
3''	128.1	7.32, m	128.3	7.31, m
4''	127.4	7.25, m	127.9	7.21, m

^aChemical shift (ppm) referenced to DMSO- H_6 δ_{C} 39.5 were taken from 1D and 2D NMR (DMSO- d_6 , 500 MHz);

^bChemical shift (ppm) referenced to DMSO- H_6 δ_{H} 2.49

5.2.1.3 Reaction of guanine with styrene epoxide

Styrene epoxide was reported to modify DNA by reacting predominately with guanine (**5.23**).²³⁶⁻²³⁹

In order to evaluate the ability of **5.11** and **5.12** to compete with the reaction of **5.23** with reactive epoxides such as **5.7**, it was necessary to confirm that **5.23** reacts with **5.7** under the conditions used in these model reactions and that covalent adducts can be isolated. Guanine and **5.7** were treated under two different reaction conditions. Method A employed those conditions used for the previous experiments involving indole (**5.12**) and imidazole (**5.11**) and involved allowing the reactions to occur in a mixture of 50% CHCl_3 and 50% DCM with silica presence to activate the epoxide. As guanine exhibited better water solubility than the previous reactants, Method B used 50%

ethanol/water to mimic a better biological condition for the reaction between **5.7** and **5.23**²³⁷ (for more details about method A and B, see experimental). The total yield of covalent adducts isolated under the two conditions was nearly the same. However, analytical RPHPLC of the MeOH fraction revealed that the relative abundance of the various products differed from Method A to Method B. Figure 5.6 shows the RPHPLC analysis of the MeOH fraction after removed starting materials. Mass spectrometric analysis of the collected HPLC products indicated the presence of at least three compounds having m/z 272 $[M+H]^+$ (Figure 7.26), corresponding to compounds formed from one molecule of **5.7** and one of **5.23**, six minor components having m/z 392 $[M+H]^+$ suggesting compounds consisting of two units of **5.7** and one of **5.23** which was supported by MS/MS analysis (Figure 5.7), and four minor components having m/z 512 $[M+H]^+$ suggesting three units of **5.7** have reacted with one molecule of **5.23** (Figure 5.8). These adducts were isolated in a total yield of 11% after the reaction was allowed to proceed for seven days. The results indicated that all nucleophilic positions in **5.23** are reactive to **5.7** under both sets of reaction conditions.

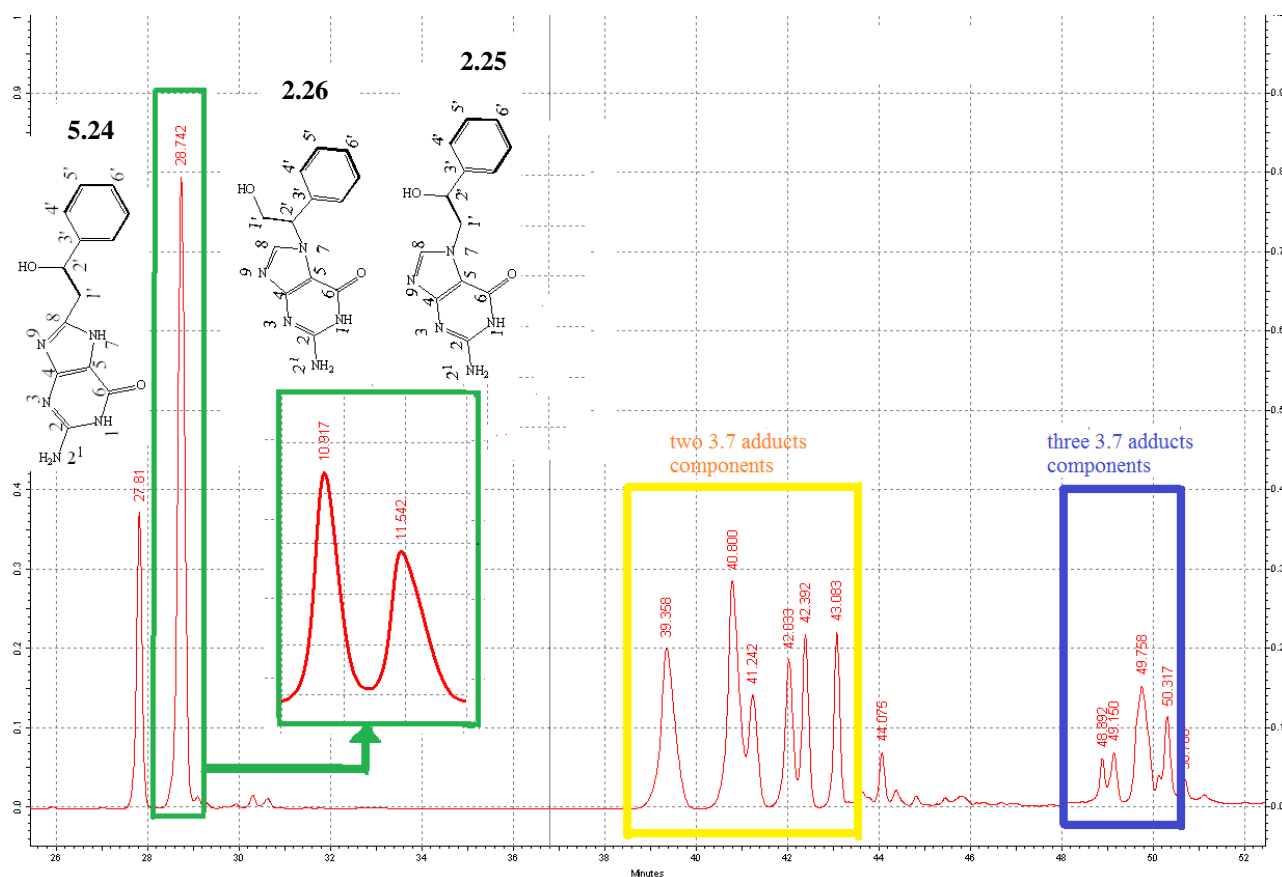


Figure 5.6: The RPHPLC trace of the methanol fraction from the reaction of **5.23** and **5.7** using gradients of 0.1% TFA in water (solvent A) and 0.1% TFA in MeCN (solvent B). Insert: The further resolution of major peak achieved using isocratic conditions of 8% solvent B.

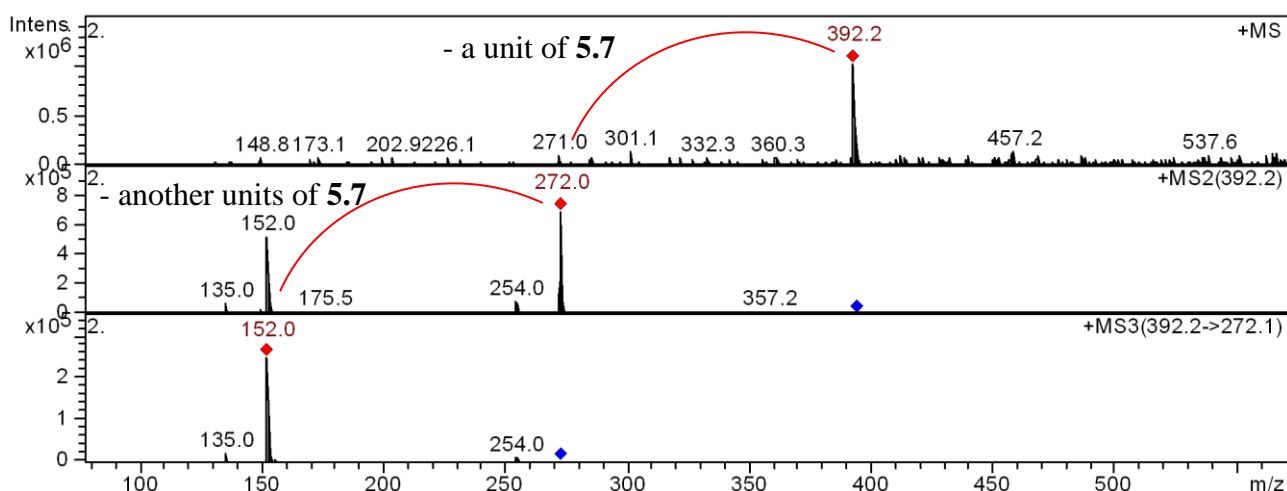


Figure 5.7: Positive ion mode MS/MS spectra of products from the reaction of **5.23** and **5.7** that consist of two units of phenylethanol and one of guanine.

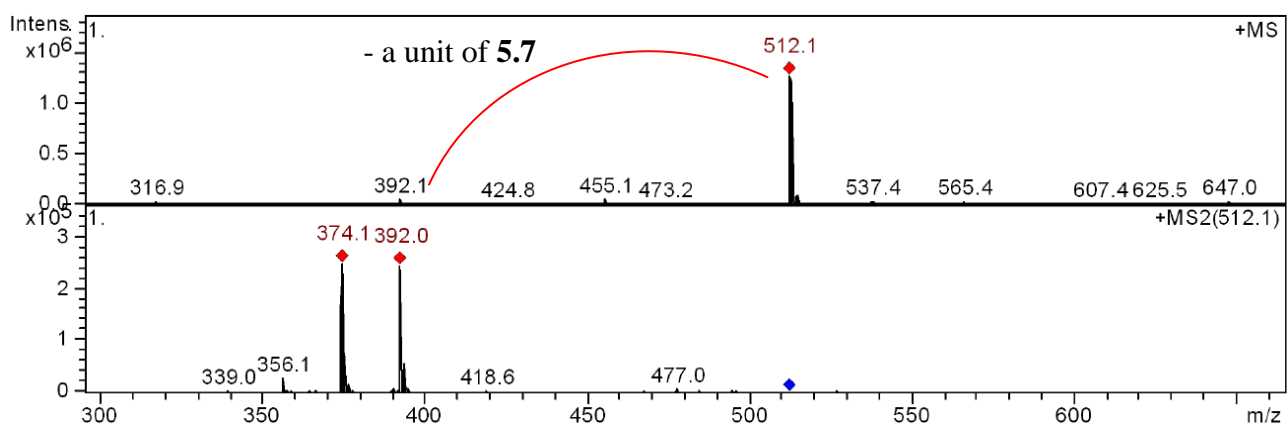


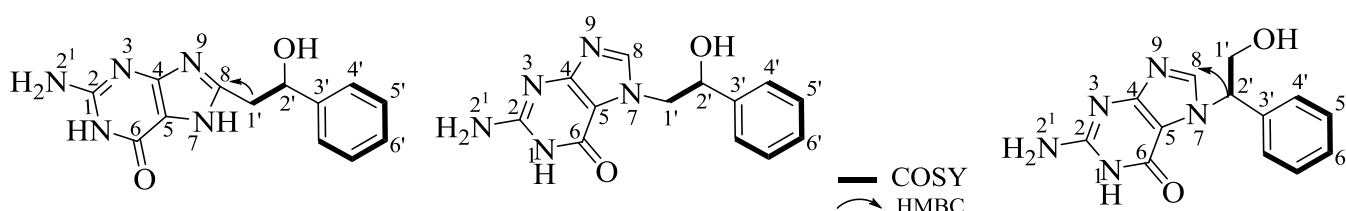
Figure 5.8: Positive ion mode MS/MS spectra of products from the reaction of **5.23** and **5.7** that consist of three units of phenylethanol and one of guanine.

The structures of DNA-**5.7** adducts have previously been proposed based on LCMS, UV and EIMS analyses, therefore lacking evidence to confirm the precise structures.^{229,239-241} Heminki et al. proposed N-7, N-2 and O-6 of guanine were the main sites for **5.7** attacking, based only on the mass spectrometric analysis of modified DNA.²³⁵ Further compounds **5.25** and **5.26** were synthesized and their structures confirmed by Novák et al. using ^1H NMR and ^{13}C NMR.²⁴² In our experiments, we were able to isolate sufficient quantities of products to perform NMR analysis. The formation of O-6 adducts would cause significant changes to the ^1H and ^{13}C NMR spectra compared to other adducts due to the CH_2 forming a covalent bond with oxygen, leading to a modified amide group in guanine. However, none of the products we isolated exhibited NMR characteristics that would suggest an O⁶-linked adduct. The ^1H NMR and HMBC analysis of the three major products isolated from our reactions between **5.23** and **5.7** indicated that the N-7 and C-8 positions of guanine were functionalized with a phenylethanol unit.

Compound **5.25** (Figure 5.6) was obtained as a white powder, ESIMS m/z 272 $[M+H]^+$ and identified as the adduct formed when N-7 of **5.23** attacks the terminal carbon of the epoxide of **5.7**. ^1H NMR shows a signal at δ_{H} 4.96 (dd, $J = 3.5, 9.0$ Hz, H-2') integrating to a proton in a CH group connected to the δ_{H} 4.45 (dd, $J = 3.5, 13.0$ Hz) and δ_{H} 4.22 (dd, $J = 9.0, 13.0$ Hz) CH_2 group (the findings were confirmed by COSY and HMBC). HMBC correlations indicated the new covalent bond forming between **5.7** and **5.23** by the cross-peaks for nuclei interacting from δ_{H} 4.96 (H-2') to δ_{C} 141.8 (C-8). The findings were in agreement with Novák. J^{242} who synthesized **5.25** from **5.7** and one of reaction pathways proposed by Vodicka et al.²³⁸ and Hemminki et al.²³⁹

Similarly, compound **5.24** was identified by ESIMS m/z 272 $[M+H]^+$ and the absence of H-8 at δ_{H} 7.58 in ^1H NMR spectra suggesting the substitution of H-8 by a phenylethanol moiety. The HMBC correlations confirmed the new covalent bond by the cross-peaks from δ_{H} 4.12 and δ_{H} 4.09 (H-1') to δ_{C} 151.0 (C-8).

Table 5.7: ^1H and ^{13}C NMR data for **5.24**, **5.25** and **5.26**.



	5.24	5.25	5.26
H	δ_{H} (ppm),mult., J (Hz)	δ_{H} (ppm),mult., J (Hz)	δ_{H} (ppm),mult., J (Hz)
1'	4.12, dd, 8.5, 13.5 4.09, dd, 4.0, 13.5	4.45, dd, 3.5, 13.0 4.22, dd, 9.0, 13.0	4.22, dd, 9.0, 12.0 4.00, dd, 5.5, 12.0
2'	4.92, dd, 4.0, 8.5	4.96, dd, 3.5, 9.0	5.46, dd, 5.5, 9.0
1	10.67, s	--	10.54, s
2	--	--	--
2 ¹	6.67, brs	6.79, brs	6.39, brs
7	8.14, brs	--	--
8	--	8.46, s	8.02, s
4'	7.36, m	7.37, m	7.33, m
5'	7.35, m	7.39, m	7.28, m
6'	7.28, m	7.35, m	7.25, m

Chemical shift (ppm) referenced to DMSO- H_6 δ_{H} 2.49 were taken from 1D and 2D NMR (DMSO- d_6 , 500 MHz).

The absence of an H-7 signal in the ^1H NMR of **5.26** and ESIMS m/z 272 $[\text{M}+\text{H}]^+$ suggested a connection between a unit of phenylethanol and the N-7 of guanine.²⁴³ A one proton signal at δ_{H} 5.46 (dd, $J = 5.5, 9.0$ Hz) suggested a CH group bound to a N-atom adjacent to a CH_2 group (δ_{H} 4.22 (dd, $J = 9.0, 12$ Hz), δ_{H} 4.00 (dd, $J = 5.5, 12$ Hz)) and ^{13}C NMR spectrum shown δ 59.5 (PhCH), 62.4 (CH_2OH). These results are in agreement with Novak's finding²⁴². As a result of the attachment directly to N, the CH signal was deshielded compared with the same proton signal in compounds **5.24** and **5.25** observed at δ_{H} 4.92 and δ_{H} 4.96 respectively. This N-linked adduct is analogous to compound **5.21** (Scheme 3.1) with the chemical shift and coupling constants of the methylene protons in **5.21** (δ_{H} 4.02 (dd, $J = 8.0, 13.9$ Hz), 4.12 (dd, $J = 4.1, 13.9$ Hz)) being similar to those of **5.25**. Signals at δ_{H} 4.22 (dd, $J = 9.0, 13.0$ Hz), 4.45 (dd, 3.5, 13.0 Hz) and a ^{13}C NMR signal at δ_{C} 51.4 were assigned to the CH_2OH carbon. Similar NMR data for this compound were reported by Novak²⁴².

3.2.1.4 *The competitive reactions between guanine and indole or imidazole with styrene epoxide*

The experiments were conducted in the presence of **5.23** (guanine), **5.7** (styrene epoxide) and **5.11** (imidazole) or **5.12** (indole) under the same conditions as previous reactions of **5.23**. The products obtained from the competitive reactions were all products associated with the reaction of **5.7** with indole, (**5.13** (2-(3-indolyl)-2-phenylethanol), **5.14** (2-(1-indolyl)-2-phenylethanol), **5.15** (2-(2-indolyl)-2-phenylethanol), **5.16** (2,2''-(indole-1',7'-diyl)bis(2-phenylethanol)), **5.17** (2,2''-(indole-3',5'-diyl)bis(2-phenylethanol)), **5.18** (2,2''-(indole-3',6'-diyl)bis(2-phenylethanol)), **5.19** (2,2''-(indole-1',3'-diyl)bis(2-phenylethanol)), **5.20** (2,2''-(indole-2',3'-diyl)bis(2-phenylethanol)), and with imidazole (**5.12**), **5.21** (2-(imidazole-1-yl)-1-phenylethanol), **5.22** (2-(imidazole-1-yl)-2-phenylethanol)). No products of the reaction of **5.23** and **5.7** were found in the experiments suggesting that indole (**5.12**) and imidazole (**5.11**) are more reactive towards the activated epoxide than guanine (**5.23**).

5.2.2 The reactions of styrene epoxide with bile pigments and its derivatives

5.2.2.1 *The reaction of styrene epoxide with bile pigments*

With the model studies indicating that N-heterocycles of **5.11** and **5.12** can efficiently compete with guanine in the reaction with activated epoxides in the competitive reactions, attention turned to the reactions of BPs (**5.8**, **5.9**, **5.10**) with **5.7**. Biliverdin (**5.10**, BV) was allowed to react with **5.7** in the presence of silica in 50:50 DCM/chloroform for one week. Two major products were isolated and

their structures (Figure 5.9 and Table 5.8) identified by 1D and 2D NMR. The first fraction exhibited an ESIMS m/z 703 $[M+H]^+$ indicating one unit of **5.7** had reacted with **5.10** (BV). The ^1H NMR spectrum of the product showed a two-proton signal, at δ_{H} 4.04 coupled with a proton signal at δ_{H} 4.75 which was consistent with the $\text{CH}_2\text{-CH-OH}$ group resulting from the opening of the epoxide ring of **5.7** by a carboxylic acid group of **5.10** (BV). A very downfield signal at δ_{H} 12.10 integrating to one proton indicated that one of the carboxylic acid moieties of **5.10** (BV) was unreacted (Figure 5.9). The HMBC correlations from δ_{H} 4.04 (H-1') to a carboxyl carbon signal at δ_{C} 172.0 confirmed the formation of a phenylethanyl ester (Table 5.8). It is not possible to distinguish between esters **5.27** and **5.28** spectroscopically. Compound **5.10** (BV) is pseudo-symmetrical, differing only in the substitution pattern of the two lactam rings. The NMR spectra for **5.10** (BV) shows slight differences for the signals associated with the two lactam rings but identical signals for the two indole rings and the methyl and carboxylic acid substituents of these rings. It is logical to assume therefore, that both esters **5.27** and **5.28** would give essentially identical spectra. The two carboxylic acid groups would have similar reactivity and thus it is likely that the mono-ester product isolated from this reaction is in fact an indistinguishable mixture of **5.27** and **5.28**.

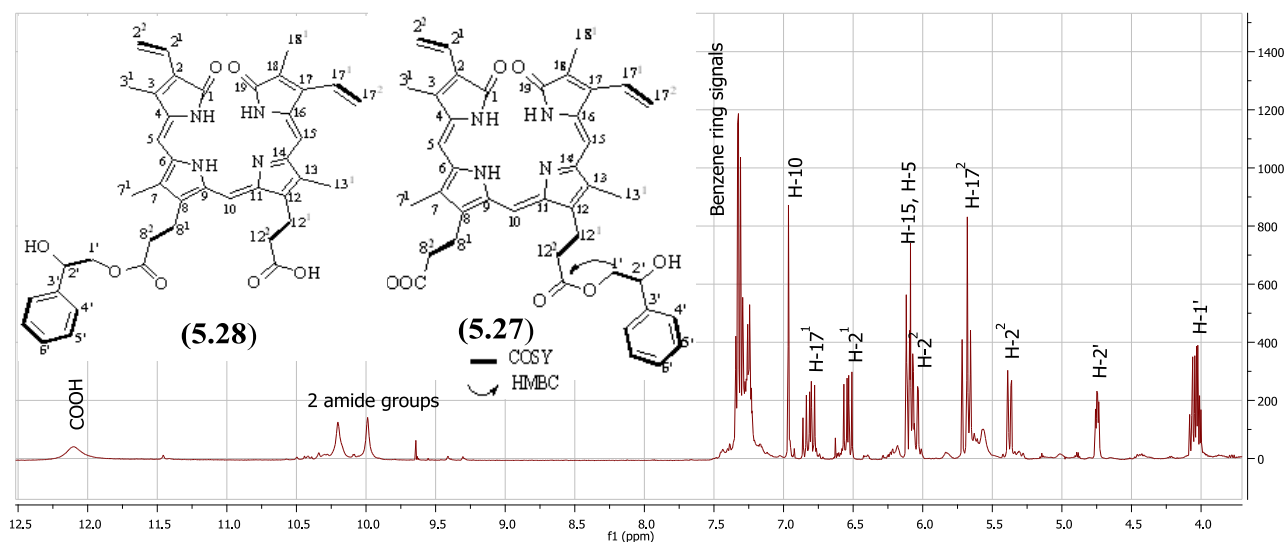


Figure 5.9 : An expanded region of the proton NMR spectrum of compounds (**5.27**, **5.28**) performed at 500 MHz in $\text{DMSO-}d_6$.

The second fraction contained a single third major product of the reaction was the di-ester, **5.31** which was characterized initially by the ESIMS m/z 823 $[M+H]^+$. The structure was confirmed by the absence of ^1H NMR signals around δ_{H} 12.00 and the fact that the aromatic proton signals now integrated to 10 protons (benzene ring signals). The signal assigned to H-2', H-2'' was defined as two protons at δ_{H} 4.74 and δ_{H} 4.04 integrated to 4 protons exhibited proton signals of methylene groups, H-1' and H-1'', (Figure 5.10). The structure of the ester was confirmed by HMBC

correlations from δ_{H} 4.04 (H-1'' and H-1') to δ_{C} 172.0 (C-12³ and C-8³) and to the unprotonated aromatic carbons, δ_{C} 147.0 (C-3'' and C-3').

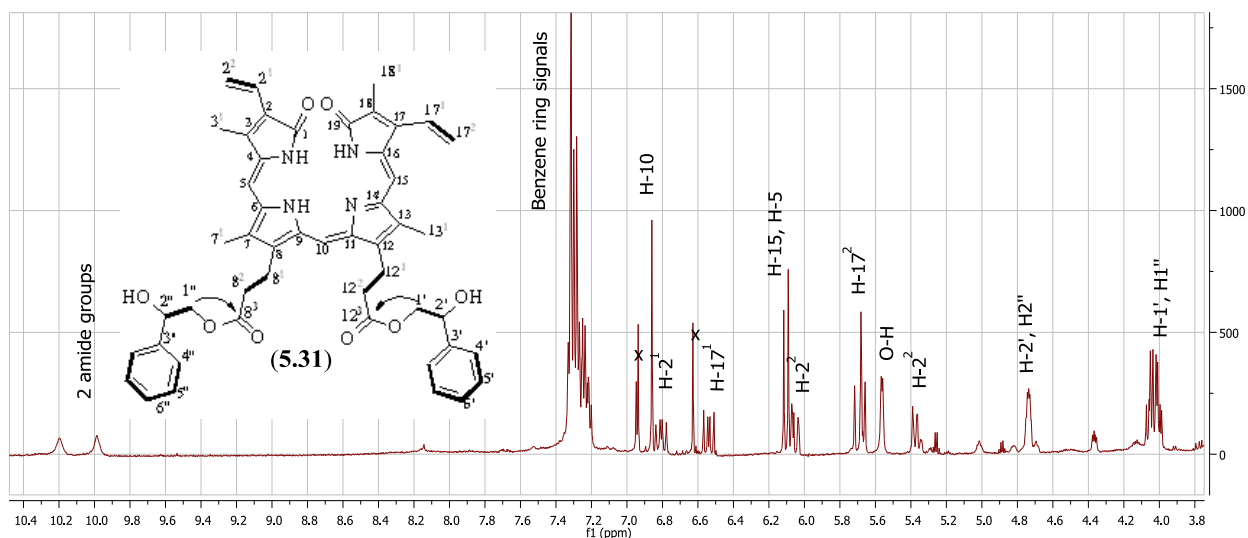
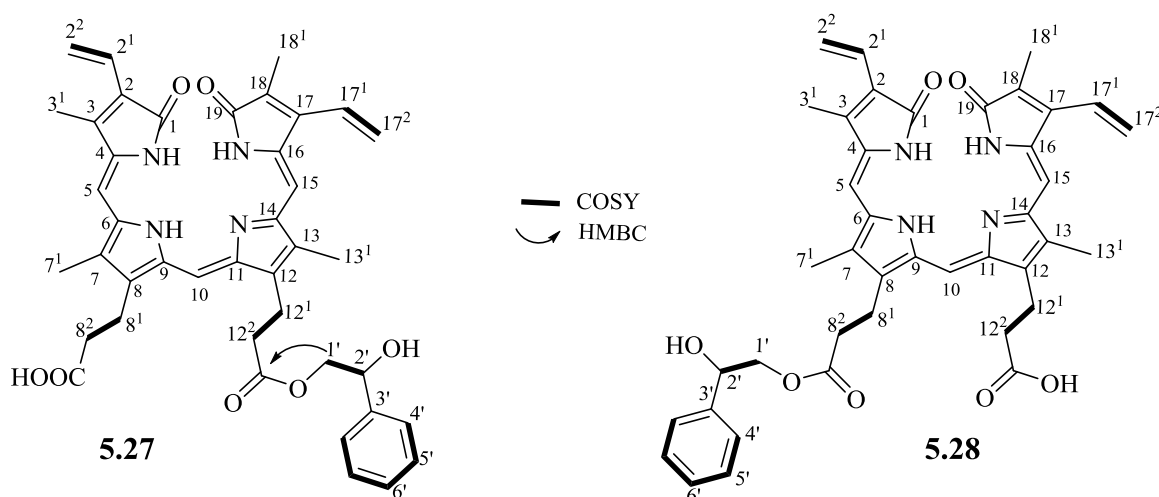
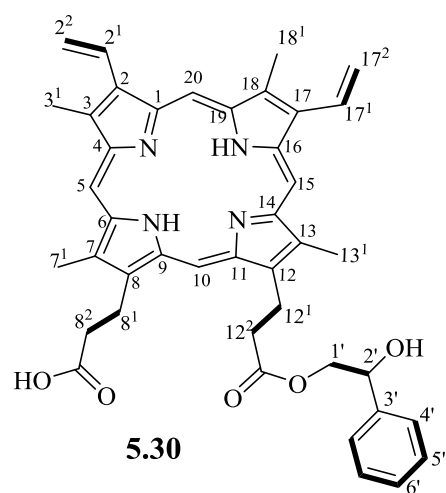
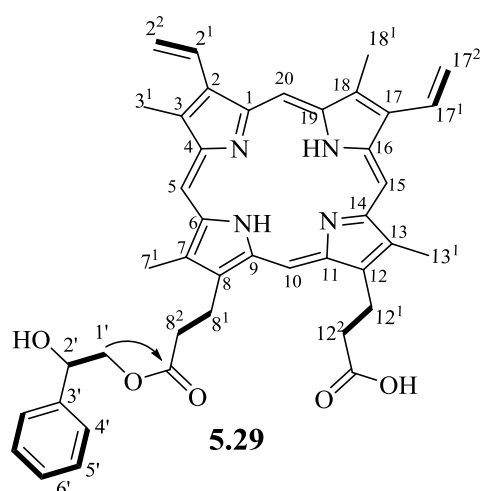


Figure 5.10: An expanded region of the proton NMR spectrum of **5.31** performed at 500 MHz in DMSO-*d*₆.

The reaction between **5.8** (PRO) and styrene epoxide (**5.7**) also yielded an inseparable mixture of mono-esters, **5.29** and **5.30** (Figure 5.11) as the major products. The identity of **5.29** and **5.30** were identified by ESIMS (m/z 683 [M+H]⁺) and the appearance of aromatic signals and the hydroxylated methylene group in the ¹H NMR. The structures of the esters were confirmed by HMBC correlations from δ_{H} 4.00 and δ_{H} 4.08 (m, H-1') to δ_{C} 172.4 (C-12³ or 8³).

Table 5.8: ¹H and ¹³C NMR data for **5.27**, **5.28**, **5.29** and **5.30**.





C	5.27;	5.28	5.29;	5.30
	δ_C (ppm) ^a	δ_H (ppm), mult., <i>J</i> (Hz) ^b	δ_C (ppm) ^a	δ_H (ppm), mult., <i>J</i> (Hz) ^b
1	170.9	--	136.9	--
2	126.1	--	136.9	--
2 ¹	126.2	6,54, dd, 11.5, 17.5	130.1	8.38, m
2 ²	119.2	5.38, dd, 11.5, 2.5	120.9	6.16, m
		6.05, dd, 17.5, 2.5	--	6.37, m
3	139.8	--	136.9	--
3 ¹	9.0	2.15, s	12.4	3.59, s
4	141.3	--	136.9	--
5	97.7	6.09, d, 2.0	97.0	9.96, s
6	127.5	--	137.0	--
7	137.7	--	137.0	--
7 ¹	9.0	2.06, d	11.1	3.51, s
8	138.5	--	138.9	--
8 ¹ (12 ¹)	19.2	2.84, m	21.0	4.28, t, 7.0
8 ² (12 ²)	34.9	2.41, t, 7.5	36.5	3.22, t, 7.5
8 ³ (12 ³)	173.6	--	172.4	--
9	141.0	--	138.9	--
10	116.0	6.96, s	97.0	10.02, s
11	139.5	--	139.1	--
12	137.5	--	139.1	--
12 ¹ (8 ¹)	19.2	2.84, m	21.0	4.27, t, 7.0
12 ² (8 ²)	35.2	2.49, t, 7.5	36.6	3.13, t, 7.5

Chapter V: Model epoxide studies

12 ³ (8 ³)	172.0	--	174.0	--
13	128.4	--	137.0	--
13 ¹	9.0	2.04, s	11.1	3.54, s
14	128.5	--	137.0	--
15	97.0	6.11, d, 2.5	97.0	10.02, s
16	140.0	--	136.9	--
17	128.1	--	136.9	--
17 ¹	126.8	6.81, dd, 17.5, 11.5	130.1	8.38, m
17 ²	122.5	5.70, d, 17.5 5.66, d, 11.5	120.9	6.16, m 6.37, m
18	139.2	--	136.9	--
18 ¹	9.3	1.79, s	12.4	3.59, s
19	171.5	--	136.9	--
20	--	--	97.0	9.96, s
1'	68.7	4.04, m	68.8	4.00, m 4.08, m
2'	70.2	4.75, dd, 7.5, 5.0	7.01	4.57, m
3'	141.8	--	141.7	--
4'	126.2	7.32, m	126.1	7.13, m
5'	128.0	7.3, m	127.9	7.08, m
6'	127.3	7.24, m	127.2	7.05, m

^aChemical shift (ppm) referenced to DMSO-*H*₆ δ_C 39.5 were taken from 1D and 2D NMR (500 MHz, DMSO-*d*₆);

^bChemical shift (ppm) referenced to DMSO-*H*₆ δ_H 2.49

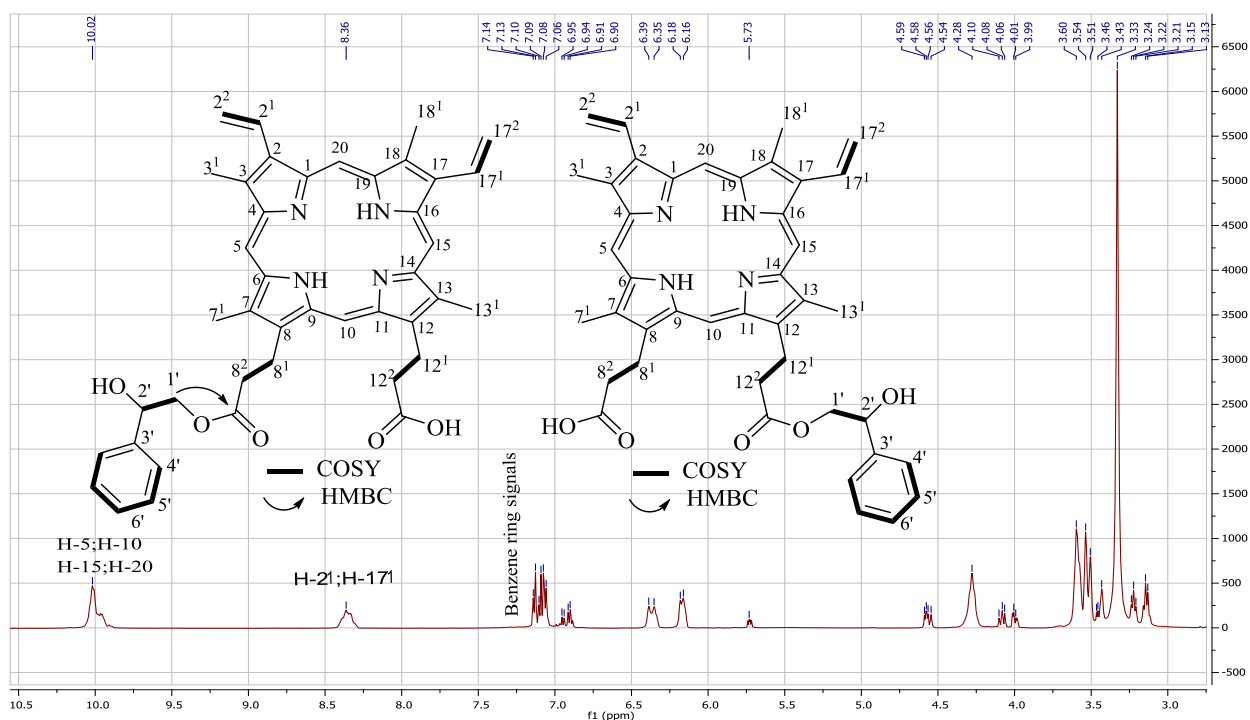


Figure 5.11: An expanded region of the proton NMR spectrum of compounds (**5.29**, **5.30**) performed at 500 MHz in $\text{DMSO-}d_6$.

The next most abundant product isolated from the reaction was the diester, **5.32** and again identified by the ESIMS data (m/z 803 $[\text{M}+\text{H}]^+$) and the appearance of a two-proton signal at δ_{H} 4.56 assigned to two saturated methine groups and a four-proton signal at δ_{H} 3.98 and δ_{H} 4.07 assigned to two methylene groups of **5.7**. The presence of aromatic hydrocarbon signals at 7.35 ppm integrated to 10 protons was benzene ring signals. The HMBC spectra for both the mono and diester products showed the expected correlations from the methylene's protons δ_{H} 4.07 and δ_{H} 3.98 (H-1', H-1'') to the carboxyl carbon signal δ_{H} 172.4 (C-8³ and C-12³) (Figure 5.12 and Table 5.9).

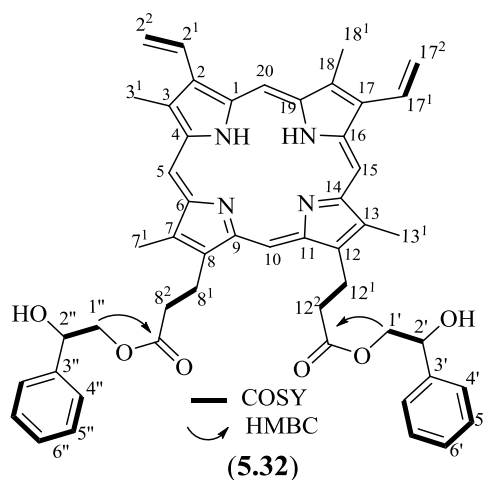
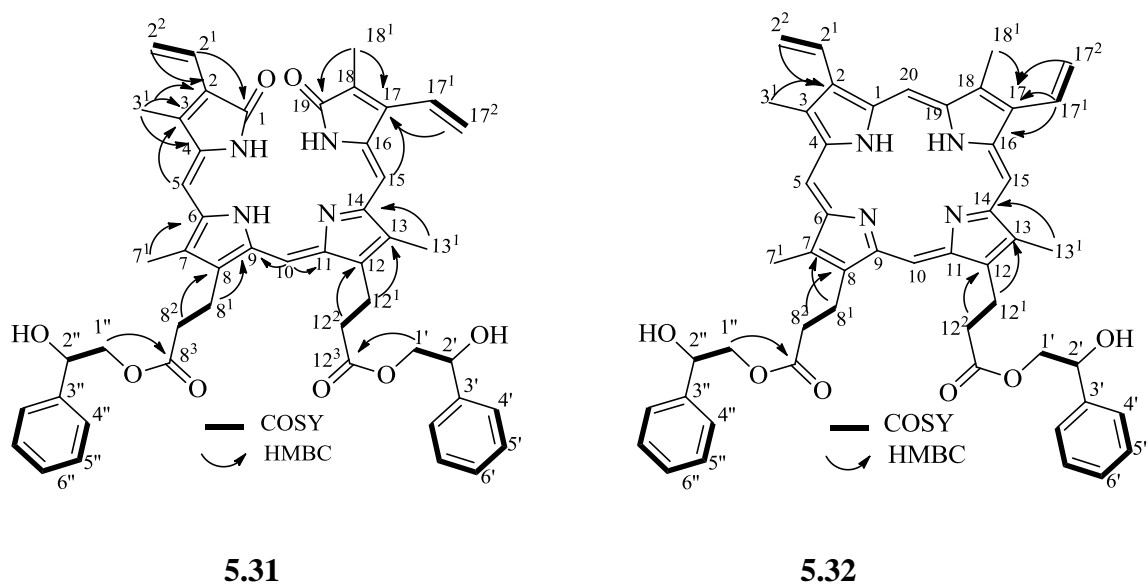


Figure 5.12: The structure of **5.32** and an expanded region of the HMBC spectrum of **5.32** showing the key correlations used to identify the structure. All experiments were performed at 500 MHz in DMSO- d_6 .

Table 5.9: ^1H and ^{13}C NMR data for **5.31** and **5.32**.



C	δ_{C} (ppm) ^a	δ_{H} (ppm), mult., J (Hz) ^b	δ_{C} (ppm) ^a	δ_{H} (ppm), mult., J (Hz) ^b
1	171.5	--	136.3	--
2	140.0	--	136.1	--
2 ¹	127.3	6.81, dd, 17.5, 11.5	130.0	8.37, dd, 18.5, 11.5
2 ²	119.6	6.05, dd, 17.5, 2.0 5.37, dd, 11.5, 2.0	121.0	6.37, dd, 18.5, 0.9 6.17, dd, 11.5, 0.9
3	141.5	--	137.2	--
3 ¹	9.6	2.15, s	11.30	3.53, s
4	126.0	--	136.1	--

Chapter V: Model epoxide studies

5	97.5	6.10, s	97.1	10.05
6	148.0	--	137.2	--
7	128.0	--	137.2	--
7 ¹	9.5	2.05, s	11.3	3.53, s
8	137.0	--	137.0	--
8 ¹	19.5	2.50, m	36.5	4.30, t, 7.0
8 ²	35.5	2.84, m	21.1	3.22, t, 7.5
8 ³	172.2	--	172.4	--
9	137.2	--	137.2	--
10	116.4	6.94, s	96.6	10.02, s
11	138.2	--	139.0	--
12	138.5	--	139.0	--
12 ¹	35.5	2.50, m	36.5	3.22, t, 7.0
12 ²	19.5	28.4, m	21.1	4.30, t, 7.5
12 ³	172.2	--	172.4	--
13	128.2	--	137.0	--
13 ¹	9.5	2.03, s	12.5	3.53, s
14	151.0	--	137.2	--
15	98.0	6.11, s	97.0	9.99, s
16	139.0	--	136.1	--
17	139.8	--	136.1	--
17 ¹	127.1	6.54, dd, 17.5, 11.5	130.0	8.37, dd, 18.5, 11.5
17 ²	123.0	5.70, d, 17.5 5.70, d, 11.5	121.0	6.37, dd, 18.5, 0.9 6.17, dd, 18.5, 0.9
18	128.2	--	137.2	--
18 ¹	10.0	1.79	12.5	3.62, s
19	171.6	--	136.1	--
20			97.1	10.04, s
1',1''	6.92	4.04, m	70.1	4.07, m 3.98, m
2',2''	71.5	4.74, brs	68.8	4.56, m
3',3''	147.0	--	141.7	--
4',4''	126.8	7.31, m	126.1	7.06, m
5',5''	128.5	7.28, m	127.9	7.11, m
6',6''	127.2	7.21, m	127.2	7.08, m

^aChemical shift (ppm) referenced to DMSO-*H*₆ δ_C 39.5 were taken from 1D and 2D NMR (500 MHz, DMSO-*d*₆);

^bChemical shift (ppm) referenced to DMSO-*H*₆ δ_H 2.49

The products of the reaction of **5.9** (UCB) with **5.7** were unstable and light sensitive, therefore they were not isolable. However, the ESIMS analysis of the crude reaction mixture indicated an m/z 703 [M-H]⁻ (Figure 7.22) and m/z 823 [M-H]⁻ which corresponded to the mono- and diphenylethanol esters which would be expected based on the results of the reactions of **5.10** (BV) and **5.8** (PRO). The ESIMS analysis also indicated the presence of **5.10** (PRO) and the mono-phenylethanol and diphenylethanol esters of **5.10** (PRO) (Figure 5.14). The reaction's mixture was turned from yellow to green over the course of the reaction which also indicates the conversion of **5.9** (UCB) to **5.10** (BV).

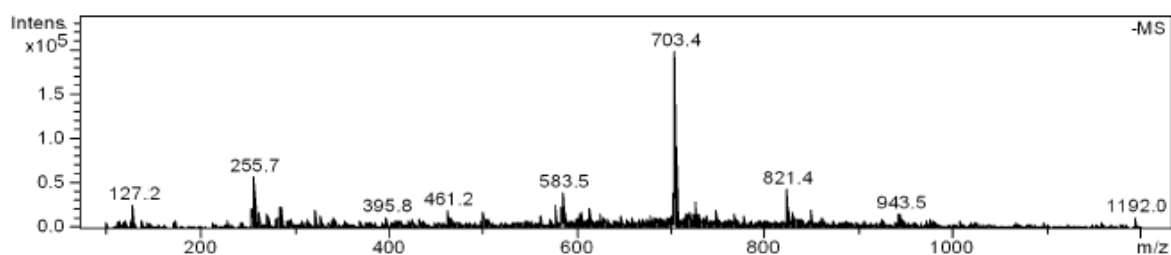


Figure 5.13: The negative ESIMS result of bilirubin mono phenylethanol ester.

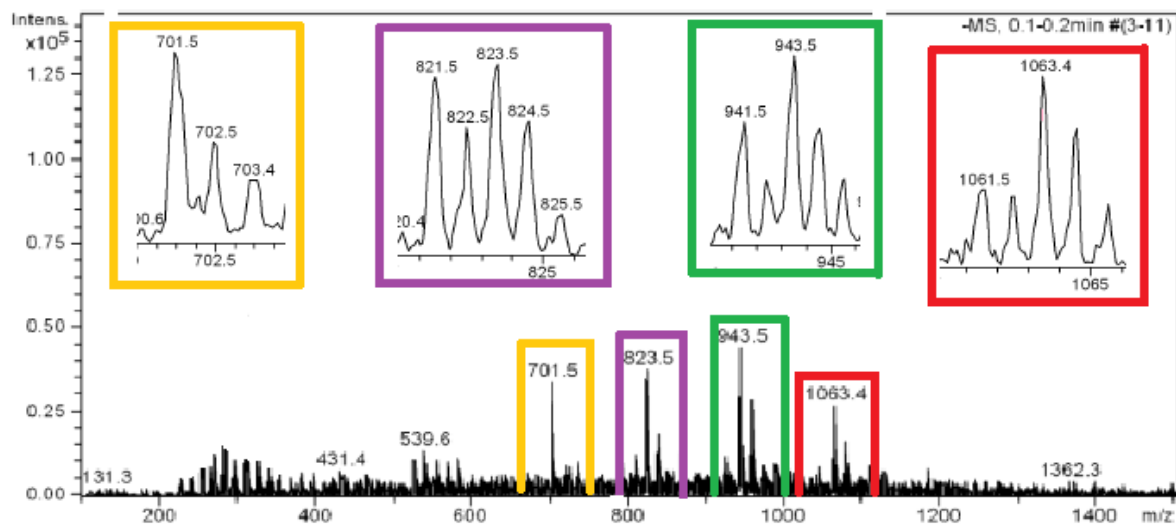


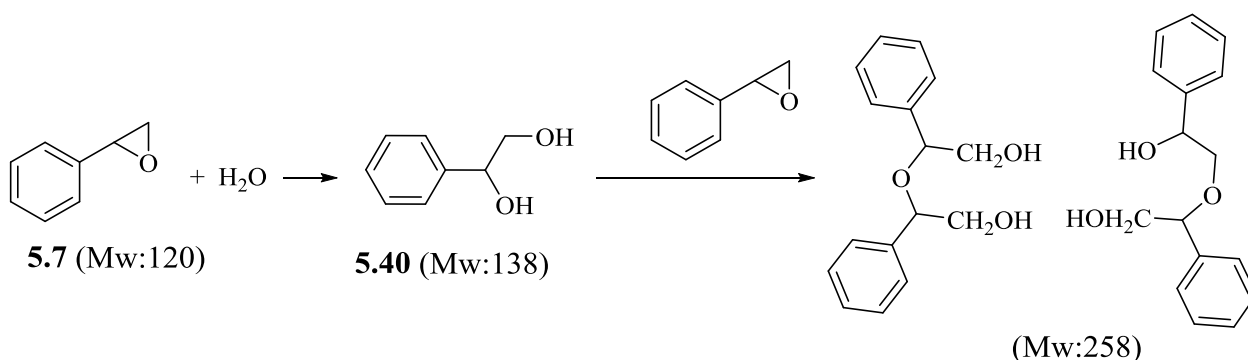
Figure 5.14: The mixture of one to four units of **5.7** bonding to **5.9** (UCB) and **5.10** (BV) in the reaction's mixture between **5.9** (UCB) and **5.7**.

The conversion of **5.9** (UCB) to **5.10** (BV) in the presence of silica is a spontaneous oxidation that is unavoidable over the time of the experiment (the findings were identified in a control reaction and it was also found in vitro studies by Abu-Bakar et al.³⁰). Detailed analysis of the MS results from the reaction mixture reveal that the ratio of biliverdin-monoester (m/z 701) to bilirubin-monoester (m/z 703) is 8:2. However the ratio of the two diesters is ~1:1 while the bilirubin adducts bearing three and four units of **5.7** are more abundant than the equivalent biliverdin adducts (m/z 941:943 = 3:7, m/z 1061:1063 = 2:8, Figure 5.14). These data suggest that reaction with **5.7** to form

an ester is somehow stabilizing to **5.9** (UCB) and the initial adduct can continue to react with other units of **5.7** without oxidation to **5.10** (BV). It also suggests that **5.9** (UCB) is more reactive to **5.7** than **5.10** (BV) and has additional sites of the reaction after the two carboxylic acid groups have been esterified.

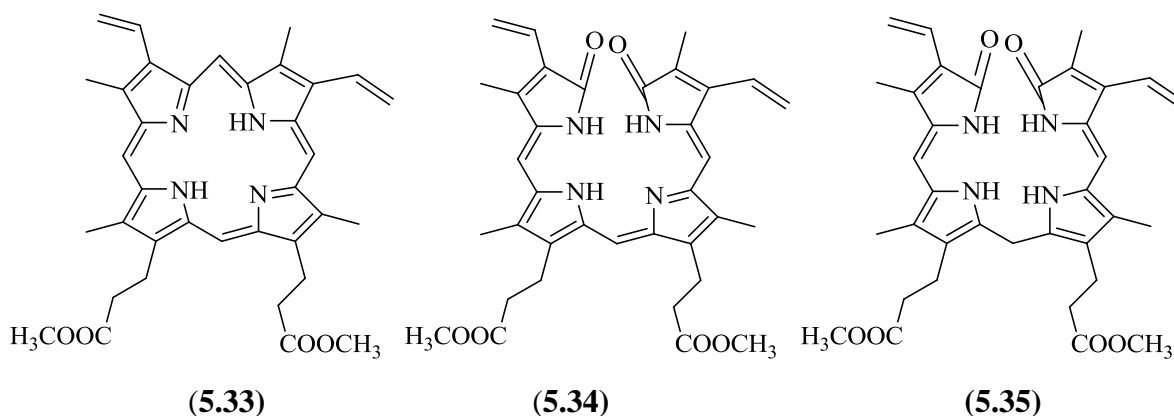
5.2.2.2 The oligimerisation of styrene epoxide

In reactions of **5.7** with all other compounds, major isolated products were polymers of **5.7** and the hydrolysed product **5.40**. They were detected by ESIMS (m/z 161 $[M+Na]^+$ (**5.40**)) with dimers (m/z 281 $[M+Na]^+$), trimers (m/z 401 $[M+Na]^+$) and sequential oligomers of **5.7** (see Figure 7.21 in appendix-D).²⁴³⁻²⁴⁵



5.2.2.3 Reaction between bile pigment dimethyl esters and substituted pyrrole and dipyrroles with styrene epoxide

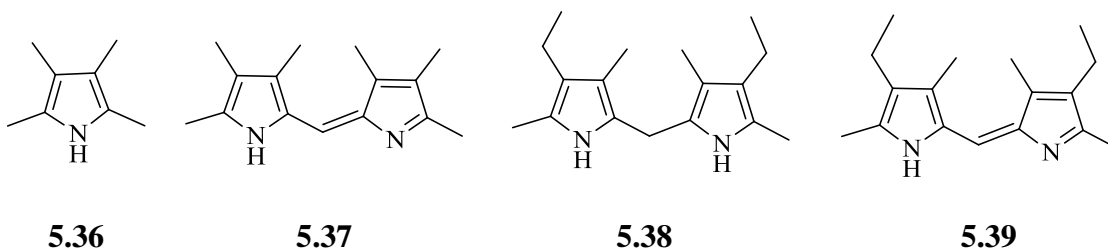
The ESIMS results show that all BPs (**5.8**, **5.9**, **5.10**) can react with more than four units of **5.7**. However, only the mono- and di- phenylethanol esters were isolable from **5.8** (PRO) and **5.10** (BV). There are two hypotheses that could explain these high molecular weight products. The first is that the secondary alcohol of the phenylethanol attacks an additional molecule of **5.7** resulting in oligomeric chains forming from the initial esters. This hypothesis is supported by the above mentioned formation of oligomers of **5.7**. The second hypothesis is that other nucleophilic positions on BPs are capable of reacting with **5.7**. In order to test these hypotheses, the dimethyl esters of the BPs (**5.33**, **5.34**, **5.35**) were synthesized and treated with **5.7** under the reaction conditions previously described.



Guanine adducts were not found in the competitive reactions of **5.33**, **5.34** and **5.35** with **5.7** in the presence of **5.23** suggesting that **5.33**, **5.34** and **5.35** still intercepted the reaction of **5.7** with **5.23** (more details can be found in experimental section). However, products of **5.33** with **5.7** were not found and the reaction of compound **5.34** and **5.7** produced minor unstable products having $m/z = 731 [M+H]^+$, $851 [M+H]^+$ and $971 [M+H]^+$ accounting for one, two and three units of **5.7** binding to **5.34**. The starting materials (**5.33** and **5.34**) in competitive reactions decomposed to give yellow, pink, blue, and yellow components while in the control reactions the **5.33** and **5.34** were stable. The esterification of these BPs may react with **5.7** to produce very unstable components. This hypothesis is supported by the detection of unstable products bearing more than two units of **5.7** in the reactions of **5.7** with **5.8** (PRO) and **5.10** (BV).

In contrast, ESIMS analysis of the reaction of **5.35** with **5.7** showed evidence that the products of one unit of **5.7** with **5.35** had a violet colour, $m/z 755 [M+Na]^+$ and two and three units of **5.7** with **5.35** were violet-yellow, with $m/z 853 [M+Na]^+$ and $m/z 973 [M+Na]^+$, respectively. These products constituted approximately 15% of the starting material (Figure 5.17, Figure 5.18 in experimental section). Although the fraction containing the mono-adduct ($m/z 755$) appeared to be pure by ESIMS, it is a mixture by ^1H NMR. Therefore, all attempts to isolate the product failed. However, given the documented higher reactivity of **5.35** to **5.7** than that of **5.34** and **5.33** suggested the unconjugated C10-bridge may play an important role in the increase of the reactivity of **5.35**.

In order to investigate the role of C10-bridge group in bilirubin, the substituted pyrrole **5.36** and dipyrroles **5.37-5.39** were synthesized and reacted with **5.7** under the same conditions as previously described.



Compounds **5.36** showed no reaction with **5.7** which eliminated the possibility that the reaction with the epoxide occurs at saturated methyl groups. Compound **5.37** and **5.39** reacted with **5.7** to produce minor unstable products, (m/z 469 $[M+H]^+$) and (m/z 497 $[M+H]^+$) respectively. In addition, **5.38** having a saturated carbon bridge similar to C10-bridge of **5.9** and **5.35**, reacted with **5.7** to form a yellow product having m/z 512 $[M+Na]^+$ (**5.38** + 2 units of **5.7**) which appeared to constitute up to approximately 22% of the starting material. Once again, this product was too unstable to be isolated. Therefore, the structure was not identified by NMR. However, these results suggested that the aromatic ring-system of bilirubin and its derivatives may be additional sites of reaction with activated epoxides.

5.2.3 Competition reactions

The reactions of **5.23** with **5.7** in the presence of **5.8** (PRO), **5.9** (UCB), **5.10** (BV), **5.33**, **5.34**, **5.35**, **5.36**, **5.37**, **5.38** and **5.39** clearly indicated that none of the products of the reaction of **5.7** with **5.23** that were isolated previously were present in these competition reactions. The results suggested that **5.9** (UCB), **5.10** (BV), **5.33**, **5.34**, **5.35**, **5.36**, **5.37**, **5.38** and **5.39** were very effective inhibitors of the reaction of **5.7** with **5.23**. In spite of no products forming between **5.36** or **5.33** and **5.7** after reactions, those compounds were decomposed in the presence of **5.7**. All cases, isolated adducts and the ratio of products were identical to those isolated from the reactions of **5.9** (UCB), **5.10** (BV), **5.33**, **5.34**, **5.35**, **5.36**, **5.37**, **5.38** and **5.39** conducted in the absence of **5.23**.

5.3 Conclusions

Although the inhibitory effects of BPs (**5.8**, **5.9**, **5.10**) on environmental mutagens (**5.1**, **5.4**) has been reported in a variety of studies,^{14,17,19,35,186} the inhibition mechanism has not been explored. Therefore, the investigation of possible chemical reactions between activated mutagens and BPs is a focus of our study to elucidate the mechanism of this inhibition. Reactions between these two classes of compounds performed in biological systems both in vitro and in vivo produce very tiny amounts of products that can only be analysed by MS.^{121,122,222,272} Having a larger amount of products for structure analyses has been a challenge for biological studies. Therefore, developing and using a mimic of the biological conditions and using more readily available compounds as mimics for the biologically generated compounds is a vital strategy in our study into the chemical interactions of BPs and mutagens. This study was successful in developing a set of conditions to mimic the biological conditions.

This chapter also explored some important novel aspects. Firstly, indole and imidazole possess higher reactivity to the activated epoxide than guanine. The chemical interactions of BPs with **5.7**, the epoxide chosen to mimic the reactive epoxide metabolites of B α P and Aflatoxin B, were investigated. Our studies showed that the carboxylic groups on the BPs were the main sites of reaction with **5.7**. In addition, nitrogen atoms and the methylene C10-bridge in BPs may also have made a minor contribution to the reactions of **5.7** with BPs which may contribute to their inhibition of the reaction of **5.7** with guanine. Our results clearly demonstrated that, under our in vitro reaction conditions, indole, imidazole, and all of BPs studied totally inhibited the reaction of **5.7** with guanine.

The reactions of **5.7** with the various substrates gave rise to 14 new compounds (2-(1-Indolyl)-2-phenylethanol (**5.14**), 2-(2-Indolyl)-2-phenylethanol (**5.15**), 2,2''-(Indole-1',7'-diyl)bis(2-phenylethanol) (**5.16**), 2,2''-(Indole-3',5'-diyl)bis(2-phenylethanol) (**5.17**), 2,2''-(Indole-3',6'-diyl)bis(2-phenylethanol) (**5.18**), 2,2''-(Indole-1',3'-diyl)bis(2-phenylethanol) (**5.19**), 2,2''-(Indole-2',3'-diyl)bis(2-phenylethanol) (**5.20**), 8-(2-Hydroxy-2-phenylethyl)guanine (**5.24**), **5.27**, **5.28**, **5.29**, **5.30**, **5.31**, **5.32**) and five known compounds (2-(3-Indolyl)-2-phenylethanol (**5.13**), 2-(Imidazole-1-yl)-1-phenylethanol (**5.21**), 2-(Imidazole-1-yl)-2-phenylethanol (**5.22**), 7-(2-Hydroxy-1-phenylethyl)guanine (**5.25**), 7-(2-Hydroxy-2-phenylethyl)guanine (**5.26**)) which were isolated and characterised by TLC, mp, HPLC, UV, GC/MS, ESIMS, ¹H NMR and ¹³C NMR. In addition, 11 components were detected from the products of guanine, BPs, BP dimethyl esters and substituted dipyrroles with **5.7** by ESI-MS.

The major finding in our study of the reactions of BPs and **5.7** was that the sites of reactions of BPs with the epoxide is the carboxylic acid groups and other groups such as tertiary amines or C10-bridge may play a minor role. However, despite being poorly reactive toward the model epoxide, the dimethyl esters of the BPs completely protected guanine from reactions with the activated epoxide in competition reactions. This is in agreement with recent studies that have clearly shown that the bile pigment dimethyl esters are as effective inhibitors of mutagens in some biological systems as the parent BPs.^{19,186} Free carboxylic acid groups are ubiquitous in biological systems thus it seems unlikely that this reaction is a major contributor to the unique inhibition activity exhibited by BPs towards the mutagenic effects of activated epoxides.

5.4 Experimental

5.4.1 General materials and methods

Solvents, mutagens and reagents were purchased from Sigma Aldrich Pty Ltd (Melbourne, Vic, Australia). Bile pigments were purchased from Frontier Scientific (Logan, UT, USA) unless otherwise stated. Thin layer chromatography (TLC) was performed on Merck Silica 60 F₂₅₄ sheets. Flash column chromatography was performed on Lom silica 60 (0.04-0.06 mm; 230-400 mesh). All bile pigments and mutagens were visualized with 254 nm UV light (λ_{max} bilirubin = 450 nm, biliverdin = 375 nm, protoporphyrin = 409 nm, biliverdin dimethyl ester = 375 nm, bilirubin dimethyl ester = 450 nm, protoporphyrin dimethyl ester = 409 nm). Analytical reverse phase high performance liquid chromatography (RPHPLC) was performed using a Shimadzu system and running Shimadzu CLASS VP, LCsolution software and using a Waters 3.5 μm C18 column (150 x 4.6 mm), 3 μm and 5 μm Grace Vydac Denali C18 250x4.6 mm and 250x10 mm columns. Analytical analyses (t_{R}) was performed using gradient mixtures of water and MeOH. The eluent was monitored using a dual wavelength UV detector set at 214 nm and the second wavelength was varied depending on which BP was used and other compounds in the experiments. UV-Visible absorption measurements were recorded on a Perkin Elmer Lambda 35 Spectrometer.

¹H, ¹³C, DEPT, COSY, HSQC, and HMBC NMR spectra were recorded on either Bruker AV400 or a Bruker AV500 spectrometer with CDCl₃ (99.8 atom %D), CD₃OD (99.8 atom %D) or DMSO (99.8 atom %D) used as solvents. ¹H and ¹³C signals are recorded in parts per million (ppm) on the δ scale referenced to residual CHCl₃ at δ_{H} 7.24 and CDCl₃ at δ_{C} 77.0 ppm; DMSO: δ_{H} 2.49 and δ_{C} 35.9; CD₃OD: δ_{H} 3.30 and δ_{C} 49.0. GC/MS analyses (positive ion EI mode) were performed on a Shimadzu GC/MS QP2010-plus, gas chromatograph mass spectrometer, operating at 70 eV, connected to a GC-2010 Standard GC/MS programs: Shimadzu GC/MS, ZB-5MS column (length 30.0, thickness 0.25 μm , diameter 0.25mm) : split mode; column flow 3.14 ml min⁻¹; total flow 97.5 ml min⁻¹; injector 250 °C; detector 250 °C; oven 50 °C (2.0 min equilibration) held for 14.0 min, ramp 50 °C min⁻¹ to 250° C and held for 4.0 min (total program time 20.0 min). Melting points were recorded on a Buchi Dr Tottoli apparatus and were uncorrected. Low resolution mass spectra were acquired on a Bruker Esquire HCT spectrometer (positive and negative ion ESI mode). High resolution mass spectra were recorded on a Bruker micrOTOF-Q spectrometer (positive ion ESI mode) or on a Finnigan MAT 900XL Trap instrument (positive ion EI mode, 70eV) at the Mass Spectrometry Facility, School of Chemistry and Molecular Biosciences, at the University of Queensland.

5.4.2 Experimental

5.4.2.1 Reaction of indole (5.12) with styrene epoxide (5.7) in the presence and absence of guanine (3.35)

The experiments were conducted in a mixed solvent consisting of 50% CH₂Cl₂ and 50% CHCl₃ (150 mL). Silica (500 mg) was suspended in the solvent. Compound **5.12** (117 mg, 1 mmol) was dissolved into the solvent and **5.7** (360 mg, 3 mmol) was added and the reaction held at 37 °C under argon atmosphere for one week. The competition experiments were performed as above with the addition of **5.23** (151 mg, 1 mmol). The stability of **5.11** and **5.12** under current reaction conditions were also determined in the control experiments in the absence of **5.7** and **5.23** by TLC analysis every 24 hours. The result from TLC analysis showed that **5.11** and **5.12** were stable with single spot being observed.

At the conclusion of the reactions, the solvents were removed under reduced pressure to provide products adsorbed onto silica that were purified by flash chromatography (hexane/EtOAc from 9:1 to 0:10) Compounds **5.13**, **5.14**, **5.15** and **5.16** were isolated. Compounds **5.17**, **5.18**, **5.19**, **5.20** remained as an intractable mixture in EtOAc fraction which was separated by RPHPLC using a gradient from 38% MeOH in water to 53% MeOH over 15 min then increasing to 65% MeOH in 25 min and holding at 65% MeOH for 10 min.

2-(3-Indolyl)-2-phenylethanol (5.13): White solid (189.6 mg, 80%), R_f 0.44 (TLC 50% hexane/EtOAc), Rt (GC) 5.22 min, mp 98-100 °C, UV (methanol) λ_{max} 229 nm, GCMS *m/z* 237 (M⁺), *m/z* 206 [M-CH₂OH]⁺, ESIMS *m/z* 260.1 [M+Na]⁺, *m/z* 276.1 [M+K]⁺, HRESIMS *m/z* 260.1053 [M+Na]⁺ (calcd for C₁₆H₁₅NNaO, 260.1046)

2-(1-Indolyl)-2-phenylethanol (5.14): White solid (4.0 mg, 1.7%) R_f 0.64 (TLC 50% hexane/EtOAc), Rt (GC) 4.2 min, UV (methanol) λ_{max} 220 nm, GCMS *m/z* 237 (M⁺), ESIMS *m/z* 260 [M+Na]⁺, 276 [M+K]⁺, HRESIMS *m/z* 260.1056 [M+Na]⁺ (calcd for C₁₆H₁₅NNaO, 260.1046).

2-(2-Indolyl)-2-phenylethanol (5.15): White solid (16.1 mg, 6.8%), R_f 0.56 (TLC 50% hexane/EtOAc), Rt (GC) 5.0 min, UV (methanol) λ_{max} 224 nm, GCMS *m/z* 237 (M⁺), ESIMS *m/z* 260 [M+Na]⁺, 276 [M+K]⁺.

2,2''-(Indole-1',7'-diyl)bis(2-phenylethanol) (5.16): White solid (17.4 mg, 4.5%), mp 118 °C, R_f 0.3 (TLC 50% hexane/EtOAc), Rt (GC) 11.42 min, UV (methanol) λ_{max} 222 nm, GCMS *m/z* 357

(M⁺), ESIMS m/z 380 [M+Na]⁺, 396 [M+K]⁺, HRESIMS m/z 380.1628 [M+Na]⁺ (calcd for C₂₄H₂₂NNaO₂, 380.1621).

2,2''-(Indole-1',3'-diyl)bis(2-phenylethanol) (5.19): White solid (3.6 mg, 1%), R_f 0.4 (TLC 50% hexane/EtOAc), Rt (GC) 10.0 min, t_R (RPHPLC) 15.2 min, UV (methanol) λ_{max} 224 nm, GCMS m/z 357 (M)⁺, ESIMS m/z 380 [M+Na]⁺, 396 [M+K]⁺, HRESIMS m/z 380.1616 [M+Na]⁺ (calcd for C₂₄H₂₂NNaO₂, 380.1621).

2,2''-(Indole-3',6'-diyl)bis(2-phenylethanol) (5.18): Yellow solid (3.5 mg, <1%), R_f 0.44 (TLC 50% hexane/EtOAc), Rt (GC) 14.6 min, t_R (RPHPLC) 16.8 min, UV (methanol) λ_{max} 229 nm, GCMS m/z 357 (M⁺), 326 (M-CH₂OH), 295 (M-2CH₂OH), ESIMS m/z 380 [M+Na]⁺, 396 [M+K]⁺, HRESIMS m/z 380.1611 [M+Na]⁺ (calcd for C₂₄H₂₂NNaO₂, 380.1621).

2,2''-(Indole-2',3'-diyl)bis(2-phenylethanol) (5.20): Yellow solid (3.3 mg, <1%), R_f 0.43 (TLC 50% hexane/EtOAc), Rt (GC) 9.8, t_R (RPHPLC) 18.6 min, UV (methanol) λ_{max} 229 nm, GCMS m/z 357 (M⁺), ESIMS m/z 380 [M+Na]⁺, 396 [M+K]⁺, HRESIMS m/z 380.1619 [M+Na]⁺ (calcd for C₂₄H₂₂NNaO₂, 380.1621).

2,2''-(Indole-3',5'-diyl)bis(2-phenylethanol) (5.17): Yellow solid (4.2 mg, 1.2%), R_f 0.42 (TLC 50% EtOAc/hexane), Rt (GC) 9.2 min, t_R (RPHPLC) 19.5 min, UV (methanol) λ_{max} 229 nm, GCMS m/z 357 (M⁺), 326 (M-CH₂OH), 295 (M-2CH₂OH), ESIMS m/z 380 [M+Na]⁺, 396 [M+K]⁺, HRESIMS m/z 380.1608 [M+Na]⁺ (calcd for C₂₄H₂₂NNaO₂, 380.1621).

5.4.2.2 Reaction of imidazole with styrene epoxide in the presence and absence of guanine

The reaction between of **5.11** (68 mg, 1 mmol) and **5.7** (360 mg, 3 mmol) was performed in 6 mL DCM/CHCl₃ (1:1) under Ar gas in the presence of silica (1 g) at 37 °C for 1 week. The competition reaction was performed under the same conditions with the addition of **5.23** (151 mg, 1 mmol). At the end of the reaction the solvent was removed, isolated **3.7** and its polymers by extracting with ether, then a mixture of products was isolated from column chromatography using AcOEt/MeOH (9:1) as the eluting solvent. These two compounds, **5.21** and **5.22**, were separated by RPHPLC using an isocratic elution solvent method (35% MeOH /H₂O) and a flow rate of 4 mL/min.

2-(Imidazole-1-yl)-1-phenylethanol (5.21), White solid (39.5 mg, 21%), R_f 0.27 (TLC 90% EtOAc/MeOH), (GC) 2.77 min, t_R (RPHPLC) 15.94 min, mp 138 °C, UV (methanol) λ_{max} 270 nm, GCMS m/z 188 (M⁺), 82 (M-C₇H₆O), ESIMS m/z 189.1 [M+H]⁺, HRESIMS m/z 189.1027 [M+H]⁺ (calcd for C₁₁H₁₂N₂O, 189.1022).

2-(Imidazole-1-yl)-2-phenylethanol (5.22), White solid (43.2 mg, 23%), R_f 0.27 (TLC 90% EtOAc/MeOH), t_R (RPHPLC) 17.23 min, R_t (GC) 2.85 min, UV (methanol) λ_{\max} 212 nm, GCMS m/z 188 (M^+), 157 ($M-CH_2OH$), ESIMS m/z 189 [$M+H$] $^+$, HRESIMS m/z 189.1025 [$M+H$] $^+$ (calcd for $C_{11}H_{12}N_2O$, 189.1022).

5.4.2.3 Reaction of 5.23 with 5.7

Method A: Silica (1g) was suspended in a mixture of 50% $CHCl_3$ and 50% CH_2Cl_2 and **5.23** (151 mg, 1 mmol) and **5.7** (360 mg, 3 mmol) were added and incubated under Ar gas at 37 °C for a week. The crude reaction mixture was then dried under nitrogen gas, resuspended in methanol/DCM (3:7) and filtered, dried and then resuspended again in methanol/water (7:3). This methanol solution was extracted with hexane to eliminate compound **5.7** and its polymers.

Method B: Compound **5.23** (151 mg, 1 mmol) of and **5.7** (360 mg, 3 mmol) were dissolved in ethanol : water (1:1) at 37 °C under Ar gas and allowed to react for one week (method based on published procedure of Wolfgang and Michael²³⁷). The crude reaction mixture was dried under nitrogen gas before being redissolved in 70% methanol and extracted with hexane to eliminate compound **5.7** and its polymers.

The methanol fractions from both methods were filtered for HPLC analysis. The mobile phases were gradients of 0.1% TFA in water (solvent A) and 0.1% TFA in MeCN (solvent B) and the stationary phase was a Grace Vydac C18 monomeric, 120 Å column (250 x 4.6 mm). The UV detector was set at 214 and 257 nm and the analytical RPHPLC elution gradient began at 18% B for 10 min, increasing to 20% B over 20 min and continuing to 50% B over the next 10 min. At this point the solvent was held at 50% B for 10 min before increasing to 90% B in 10 min and held for 10 min. A fraction collected at 28.7 min was subjected to further resolution by RPHPLC (isocratic conditions of 8% B) to give two compounds, **5.25** and **5.26**. Ten other minor products were collected from the initial HPLC purification in the later part of the HPLC spectrum (Figure 5.6). The same products were detected in from two different methods however, the total yield of 25% obtained from method B was more than double that obtained from method A (11% yield).

8-(2-Hydroxy-2-phenylethyl)guanine (5.24): White solid (1.9 mg, 1%), t_R (RPHPLC) 27.8 min, 1H NMR (500 MHz, $(CD_3)_2OS$) δ_H 4.09 (dd, $J = 4.0, 13.5$ Hz, H_{1a}), 4.12 (dd, $J = 8.5, 13.5$ Hz, H_{1b}), 4.92 (dd, $J = 4.0, 8.5$ Hz, H_2), 6.67 (brs, NH_2-C_2), 7.28-7.36 (m, Ph), 8.14 (brs, $NH-C_8$), 10.67 (s, $NH-C_6$), ^{13}C NMR obtained from HSQC and HMBC spectra (500 MHz, $(CD_3)_2OS$) δ_C 50.3 (C_1), 70.3, (C_2), 125.8 (C_4), 127.6 (C_6), 128.1 (C_5), 142.0 (C_3), UV (methanol) λ_{\max} 278 nm,

ESIMS m/z 272 $[M+H]^+$, HRESI-MS m/z 272.1150 $[M+H]^+$ (calcd for $C_{13}H_{14}N_5O_2$, 272.1142), 294.0961 $[M+Na]^+$ (calcd for $C_{13}H_{13}N_5O_2Na$, 294.0966), 301.0710 $[M+K]^+$ (calcd for $C_{13}H_{13}N_5O_2K$ 301.0701).

7-(2-Hydroxy-1-phenylethyl)guanine (5.25): White solid (2.8 mg, 1.5%), t_R (RPHPLC) 10.9 min, 1H NMR (500MHz, $(CD_3)_2OS$) δ_H 4.22 (dd, $J = 9.0, 13.0$ Hz, $H_{1a'}$), 4.45 (dd, $J = 3.5, 13.0$ Hz, $H_{1b'}$), 4.96 (dd, $J = 3.5, 9.0$ Hz, H_2'), 6.79 (brs, NH_2-C_2), 7.35-7.39 (m, Ph), 8.46 (brs, H_8), ^{13}C NMR obtained from HSQC and HMBC spectra (500 MHz, $(CD_3)_2OS$) δ_C 54.4 (C_1'), 70.8, (C_2'), 125.6 (C_4'), 127.6 (C_6'), 128.2 (C_5'), 140.9 (C_3'), UV (methanol) λ_{max} 278 nm, ESIMS m/z 272 $[M+H]^+$, HRESIMS m/z 272.1148 $[M+H]^+$ (calcd for $C_{13}H_{14}N_5O_2$, 272.1142).

7-(2-Hydroxy-2-phenylethyl)guanine (5.26): White solid (2.9 mg, 1.5%), t_R (RPHPLC) 11.5 min, 1H NMR (500MHz, $(CD_3)_2OS$) δ_H 4.00 (dd, $J = 5.5, 12.0$ Hz, $H_{1a'}$), 4.22 (dd, $J = 9.0, 12.0$ Hz, $H_{1b'}$), 5.46 (dd, $J = 5.5, 9.0$ Hz, H_2'), 6.39 (brs, NH_2-C_2), 7.25-7.33 (m, Ph), 8.02 (brs, H_8), ^{13}C NMR obtained from HSQC and HMBC spectra (500 MHz, $(CD_3)_2OS$) δ_C 59.5 (C_2'), 62.4, (C_1'), 126.7 (C_4'), 127.6 (C_6'), 128.4 (C_5'), 138.2 (C_3'), UV (methanol) λ_{max} 278 nm, ESIMS m/z 272 $[M+H]^+$, HRESI-MS m/z 272.1143 $[M+H]^+$ (calcd for $C_{13}H_{14}N_5O_2$, 272.1142).

Table 5.10: Ten minor products created from the reaction between **5.23** and **5.7** collected from RPHPLC.

Compounds	Rt (RP-HPLC) (min)	LRESI-MS $[M+H]^+$	HRESI-MS (calcd) $[M+H]^+$	HRESI-MS (found)
5.39	39.36	392	392.1717	392.1707
5.40	40.80	392	392.1717	392.1715
5.41	41.24	392	392.1717	392.1719
5.42	42.00	392	392.1717	392.1710
5.43	42.39	392	392.1717	392.1724
5.44	43.08	392	392.1717	392.1711
5.45	48.89	512	--	--
5.46	49.15	512	--	--
5.47	49.76	512	--	--
5.48	50.32	512	--	--

5.4.2.4 The reaction of styrene epoxide with bile pigments

In these experiments, each BPs (**5.9**, **5.10**, **5.8**) (0.1 mmol) was added to a 100 ml flask containing a 50/50 mixture of $CHCl_3$ and CH_2Cl_2 (50 mL), **5.7** (0.3 mmol) and silica (10 mg). The reactions

were placed under Ar gas and incubated for a week at 37 °C. The control and the competitive reactions were also performed under the same conditions. The products of the experiments were isolated by flash chromatography using hexane/EtOAc/MeOH (from 9:1:0 to 0:10:0 then 0:8:2, in v/v) then DCM/MeOH (from 10:0 to 7:3) and finally toluene/acetone (from 10:0 to 5:5) as eluting solvents. Compounds **5.27**, **5.28**, **5.29**, **5.30**, **5.31**, **5.32** were isolated.

Products from reaction of protoporphryn and styrene epoxide

Compounds **5.29** and **5.30** were isolated as a red solid (15 mg, 22%) which was an inseparable mixture that the compounds were visible as a broad spot on thin layer chromatography, R_f 0.16-0.28 (TLC, EtOAc) but gave one set of ^1H NMR signals (Table 3.8), UV (methanol) λ_{max} 400 nm, ESIMS m/z 683 $[\text{M}+\text{H}]^+$, HRESIMS m/z 683.3237 $[\text{M}+\text{H}]^+$ (calcd for $\text{C}_{42}\text{H}_{43}\text{N}_4\text{O}_5$, 683.3228).

Compound **5.32** presented as a red solid (7 mg, 8.7%), R_f 0.57-0.67 (TLC EtOAc), UV (methanol) λ_{max} 399 nm, ESIMS m/z 803 $[\text{M}+\text{H}]^+$, HRESIMS m/z 803.3785 $[\text{M}+\text{H}]^+$ (calcd for $\text{C}_{42}\text{H}_{43}\text{N}_4\text{O}_5$, 803.3803), 825.3602 $[\text{M}+\text{Na}]^+$ (calcd for $\text{C}_{42}\text{H}_{43}\text{N}_4\text{O}_5$, 825.3623).

Products from reaction of biliverdin and styrene epoxide

Compounds **5.27**, **5.28** were isolated as a green solid (14 mg, 20%) which is assumed to be an inseparable mixture of compounds that give identical ^1H NMR proton data (Table 5.8), R_f (100% EtOAc) 0.41-0.48, UV (methanol) λ_{max} , nm: 381, ESIMS m/z 703 $[\text{M}+\text{H}]^+$, HRESIMS m/z : $[\text{M}+\text{H}]^+$ calcd for $\text{C}_{41}\text{H}_{43}\text{N}_4\text{O}_7$, 703.31263; found, 703.31419).

Compound **5.31** was isolated as a green solid (10 mg, 12%), R_f 0.68-0.75 (TLC EtOAc), UV (methanol) λ_{max} 380 nm, ESIMS m/z 823 $[\text{M}+\text{H}]^+$, HRESIMS m/z 823.3686 $[\text{M}+\text{H}]^+$ (calcd for $\text{C}_{49}\text{H}_{51}\text{N}_4\text{O}_8$, 823.3701).

Four minor inseparable and unstable products from the reactions of **5.8** (PRO) and **5.10** (BV) with **5.7** were detected on UV (methanol) λ_{max} 400 nm, ESIMS m/z 923.4 $[\text{M}+\text{H}]^+$, 921.4 $[\text{M}-\text{H}]^-$, m/z 1043.5 $[\text{M}+\text{H}]^+$, 1041.4 $[\text{M}-\text{H}]^-$ and m/z 943.4 $[\text{M}+\text{H}]^+$, 941.4 $[\text{M}-\text{H}]^-$; m/z 1063.5 $[\text{M}+\text{H}]^+$, 1061.5 $[\text{M}-\text{H}]^-$ respectively (Figure 5.15 and Figure 5.16). The reaction between **5.9** (UCB) and **5.7** also produced eight very unstable components possessing ESIMS m/z 701.5 $[\text{M}-\text{H}]^-$, 703.4 $[\text{M}-\text{H}]^-$, 821.5 $[\text{M}-\text{H}]^-$, 823.5 $[\text{M}-\text{H}]^-$, 941.5 $[\text{M}-\text{H}]^-$, 943.5 $[\text{M}-\text{H}]^-$, 1061.5 $[\text{M}-\text{H}]^-$, 1063.4 $[\text{M}-\text{H}]^-$ (Figure 7.25).

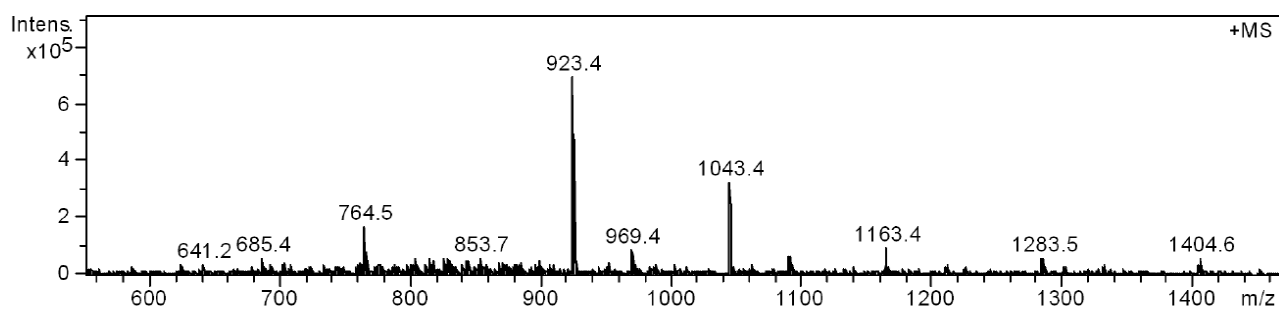


Figure 5.15: ESIMS spectrometry of two minor products in positive ion obtaining from the reaction between **5.8** and **5.7**.

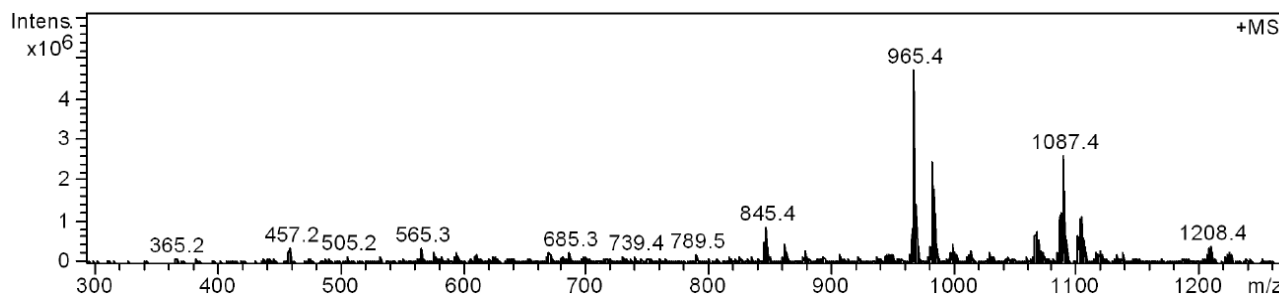


Figure 5.16: ESIMS spectrometry of two minor products in positive ion obtaining from the reaction between **5.10** and **5.7**.

5.4.2.5 Reactions between dimethyl ester of BPs with *SO*

The dimethyl esters of BPs (**5.33**, **5.34**, **5.35**) (0.01 mmol) were treated with **5.7** (0.03 mmol) under the conditions outlined above. The products were purified by flash chromatography and ESIMS/MS method was applied to identify the products. While neither no product of **5.33** and **5.7** was found nor the majority was not decomposed, more than half of **5.34** was decomposed and very small mixture of products (m/z 731 $[M+H]^+$, 851 $[M+H]^+$ and 971 $[M+H]^+$ and polymers of **5.7**) (See Figure 7.24 of appendix-D) were found detected by ESIMS. In contrast, the reaction between **5.35** and **5.7** occurred quite efficiently with at least three unstable components were detected. The main product had violet colour in methanol, UV (methanol) λ_{\max} 337 nm, m/z 733.2 $[M+H]^+$, 755.2 $[M+Na]^+$, ESIMS m/z 853.3 $[M+H]^+$ or 875.3 $[M+Na]^+$, 891.2 $[M+K]^+$ and ESIMS m/z 973.3 $[M+H]^+$ (Figure 5.17 and Figure 5.18). In the competitive reactions with the presence of **5.23**, the products of **5.23** were not detected while the products of dimethyl ester of BPs and **3.7** were found.

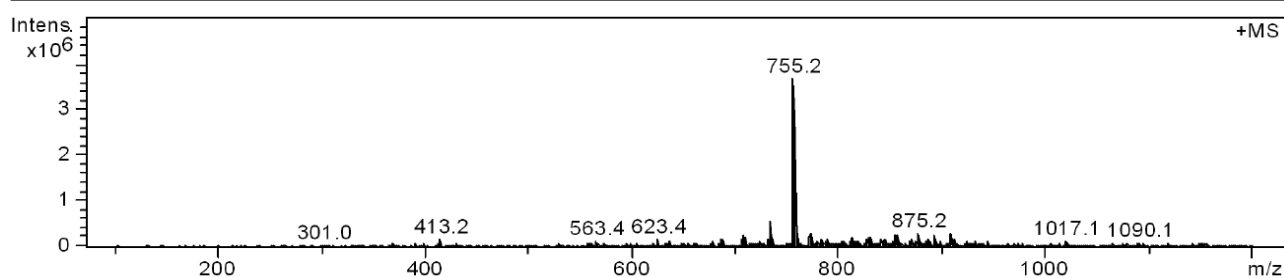


Figure 5.17: ESIMS spectrometry of the first fraction that was collected from the reaction between **5.35** and **5.7**.

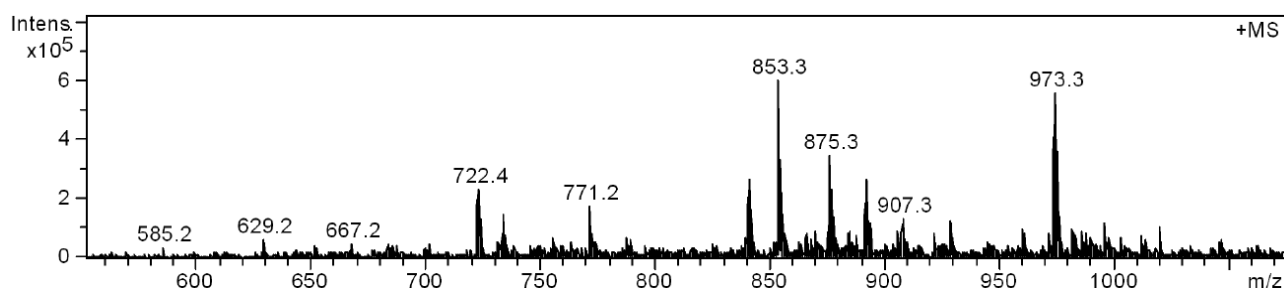


Figure 5.18: ESIMS spectrometry of the second fraction that was collected from the reaction between **5.35** and **5.7**.

5.4.2.6 Substituted dipyrroles and substituted pyrroles with styrene epoxide

The synthetic compounds **5.36**, **5.37**, **5.38**, **5.39** were reacted with **5.7** under the condition described above. The mixtures were monitored by TLC every 24 hours for up to a week. The appearance of a new compound at R_f 0.32 was observed, compared to 0.35 belonging to compound **5.38** in 100% EtOAc. The solvents were removed before column chromatography using EtOAc and hexane as the eluting solvents, and ESIMS was applied to detect the new product m/z 523.2 $[M+Na]^+$ (Figure 5.21). Although no a formation product between compound **5.36** and **5.7** was detected, the starting material (**5.36**) was decomposed in the presence of **5.7**. Compound **5.37** and **5.39** reacted with **5.7** to produce minor unstable 2 unit-SO products, ESIMS m/z 469 $[M+H]^+$ and m/z 497 $[M+H]^+$ respectively (Figure 5.19 and Figure 5.20).

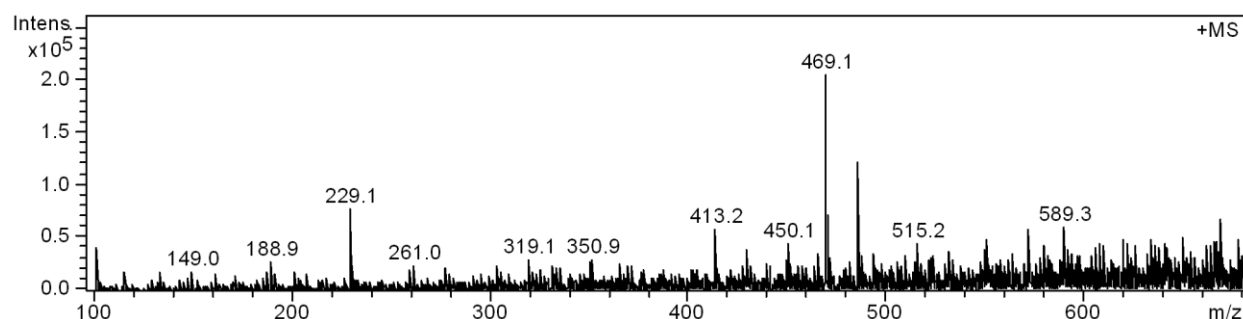


Figure 5.19: ESIMS spectrometry of a product obtained from the reaction between **5.37** and **5.7**.

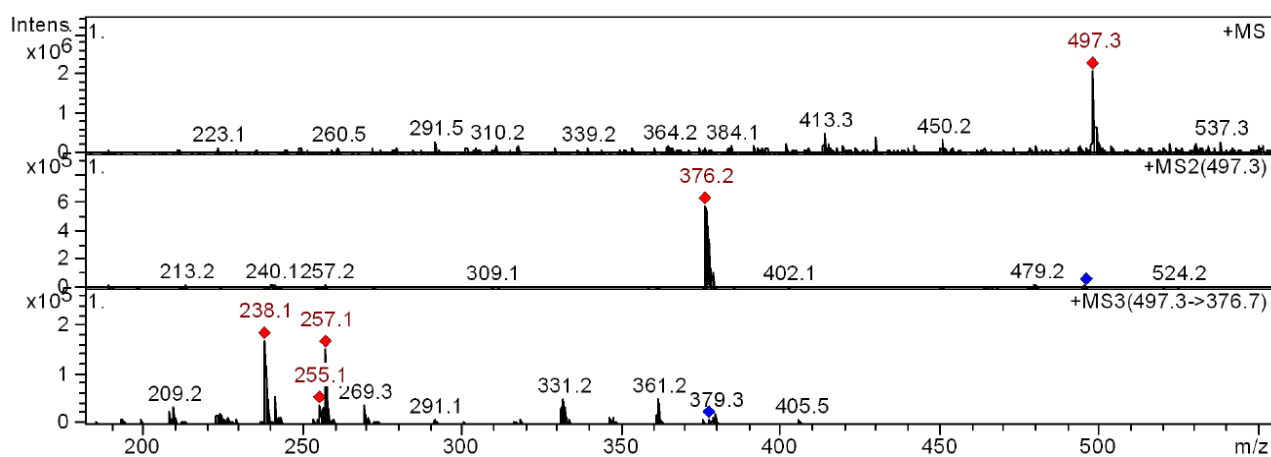


Figure 5.20: ESIMS/MS spectrometry of a product obtained from the reaction between **5.39** and **5.7**.

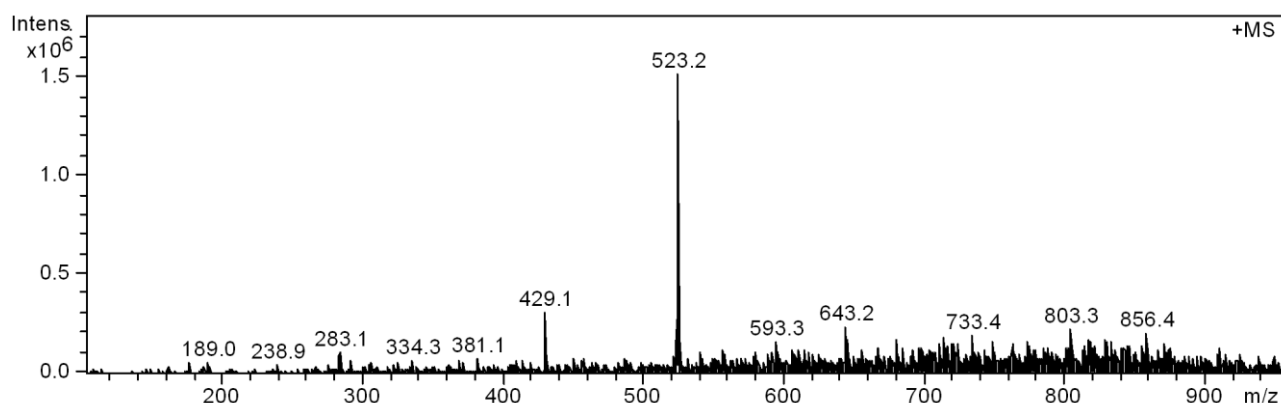


Figure 5.21: ESIMS spectrometry of a product obtained from the reaction between **5.38** and **5.7**.

5.4.2.7 The competition reactions

Compounds of **5.8** (PRO), **5.9** (UCB), **5.10** (BV), **5.11**, **5.12**, **5.33**, **5.34**, **5.35**, **5.36**, **5.37**, **5.38** and **5.39** were incubated with **5.7**, silica in the presence of guanine (**5.23**) at 37 °C in CHCl₃/DCM (1:1) for a week. The reaction mixtures were examined by TLC every 24 hours. The mixtures were separated by column chromatography using the same method as each above compounds reacting with **5.7**. The fractions obtaining after purification were analysed by GCMS, ESIMS, RPHPLC and ¹H NMR to determine the products of each compound with **5.7**. No products of the reaction of **5.7** with **5.23** were detected and all products isolated were identical to those isolated from the reactions of **5.7** and the test compounds in question in the absence of **5.23**.

Chapter 6: Exploring the inhibitory effects of endogenous bile pigments on 2-Amino-1-methyl-6-phenylimidazo[4,5-b]pyridine and Benzo[α]Pyrene metabolic activation by cytochrome P450 enzymes

6.1 Introduction

Benzo[α]pyrene (**6.1**, B α P), a polycyclic aromatic hydrocarbon found in coal tar, automobile exhaust fumes, cigarette smoke, cooked meat products and charbroiled food²⁴⁶⁻²⁴⁸, is classified as a Group 1 carcinogen by the International Agency for Research on Cancer (IARC)¹⁰³. The carcinogenicity of **6.1** is attributed to its oxidation to benzo[α]pyrene diol epoxide (**6.3**), a reaction catalysed by cytochrome P450 1A (CYP1A1), CYP1B1 (reviewed in Badal et al.²²¹) and CYP3A^{222,223} (Figure 6.1). Benzo[α]pyrene diol epoxide is highly carcinogenic, attacking guanine residues in DNA, generating DNA adducts and genetic damage in cells, which can lead to the development of lung cancer.^{104,249,250} The afore-mentioned CYP enzymes are also known to catalyse the hydroxylation of 2-amino-1-methyl-6-phenylimidazo[4,5-b]pyridine (**6.4**, PhIP), the most abundant heterocyclic amine in food which has also been classified by IARC as a Group 2B carcinogen,¹⁰³ leading to the formation of 4'-hydroxy of **6.4** and N²-hydroxy of **6.4** (**6.5**) (Figure 6.1). There is also strong evidence to support the harmful effects of **6.5** in human cells, which are linked to the development of cancer.^{127,251-253} Generally, the metabolism of **6.1** and **6.4** produces highly reactive metabolites that form DNA adducts that can result in the transformation of a cell into a cancer cell.^{127,221}

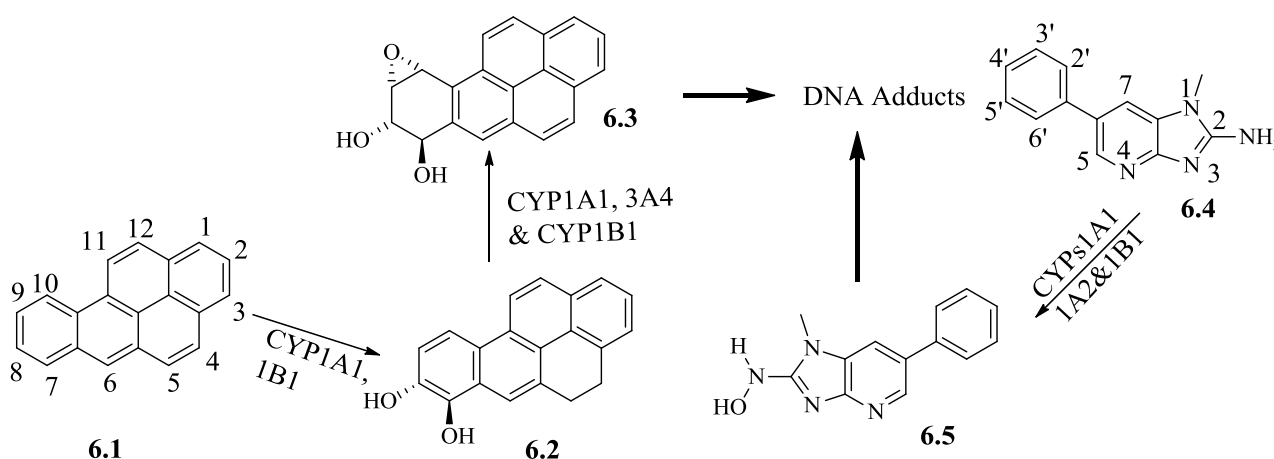
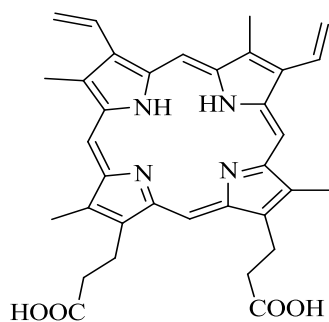
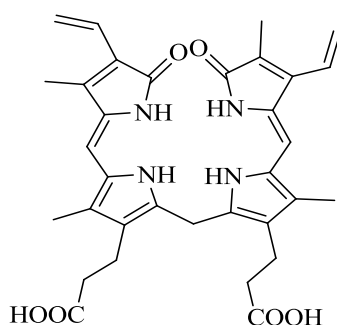
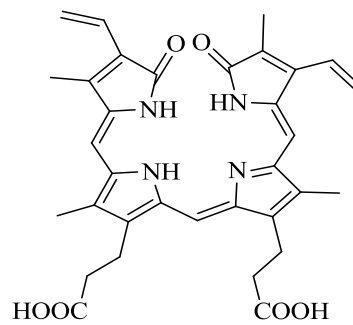


Figure 6.1: Metabolism of **6.1** and **6.4** by P450 enzymes leading to the formation of macromolecular adducts with DNA.^{127,221,223}

Potential endogenous bile pigments (BPs), such as protoporphyrin IX α (**6.6**, PRO), Unconjugated bilirubin IX α (**6.7**, UCB) and biliverdin IX α (**6.8**, BV) effectively inhibit bacterial DNA mutation

upon exposure to environmental mutagens, such as **6.1** (B α P) and **6.4** (PhIP), and oxidative stress.^{14,15,19,20,186} Furthermore, recent studies report that **6.7** (UCB) is a potent inhibitor of cytochrome P450 2A activities,^{30,254} which is also known to contribute to the activation of some environmental carcinogens^{36,255,256}. Bulmer et al.¹⁴ used the S9 fraction of rat liver homogenate and bacterial cultures to test the anti-mutagenic properties of **6.7** (UCB) and **6.8** (BV) and showed that both compounds efficiently inhibited revertant growth. Investigators from the same group later tested the anti-mutagenic effects of a wide range BPs including **6.7** (UCB), **6.8** (BV) and **6.6** (PRO) and reported that they potentially inhibited food derived mutagens (aflatoxin B1 and **6.4**) induced mutation.¹⁹ Despite these encouraging observations, the mechanisms contributing to BPs anti-mutagenic effects remain unknown. Interestingly, **6.7** (UCB) has recently shown to be an endogenous substrate for CYP2A enzymes.^{30,254} In studies using recombinant human CYP2A6 protein and mouse liver microsomes with induced CYP2A5 activity, **6.7** (UCB) inhibited CYP2A-dependent hydroxylation of coumarin by almost 100% with a K_i value in the range of the K_m for coumarin (0.5 to 2.5 μ M).^{30,254} Incubation of recombinant CYP2A6 and CYP2A5 with **6.7** (UCB) in the presence of NADPH produced **6.8** (BV) and some dipyrroles.^{30,254} Bilirubin IX α (**6.7**, UCB) also interacts with key amino acid residues within the CYP2A6 active site.³⁰ Collectively, these observations indicate that **6.7** (UCB) is a high affinity substrate of CYP2A. Interestingly, **6.7** (UCB) maximally inhibited CYP1A1 and CYP1A2 activities by 30%.⁴³ CYP1A1 and 1A2 catalyse the activation of **6.4** (PhIP) to mutagenic **6.5** and **6.1** (B α P) to **6.2** and **6.3**,²²¹ whilst CYP2A6 catalyses the transformation of **6.9** to mutagenic AFB $_1$ -8,9-epoxide.²⁵⁷ Another human P450 catalysing the N-hydroxylation of **6.4** (PhIP) is CYP1B1. Given that the active site cavities of CYP1A2 and CYP1B1 are 50% larger than that of the CYP2A6,²⁵⁸ and that the CYP1A activity is partially inhibited by **6.7** (UCB),^[25] it is plausible that **6.7** (UCB) and other BPs potentially inhibit activation of procarcinogens by these CYP enzymes. Thus, the aims of this study were to explore the potential of **6.6** (PRO), **6.7** (UCB) and **6.8** (BV) to inhibit the activation of mammalian liver S9 fractions on procarcinogenic mutagens (**6.4** and **6.1**).

**6.6** (PRO)**6.7** (UCB)**6.8** (BV)

6.2 Results and discussion

6.2.1 In vitro metabolism of **6.4** (PhIP) and **6.1** (B α P) by a human liver S9 fraction

Optimization of incubation parameters with the human liver S9 fraction

The activation of procarcinogens (**6.1**, **6.4**) by human cytochrome P450 enzymes has been extensively studied, with most research focusing on CYP1A1, CYP1A2, CYP3A4 and CYP1B1,^{127,221,252} which are also contained within the human liver S9 fraction. As a general rule for most biochemical reactions, the longer an enzyme is incubated with its substrate and necessary co-factors, the greater the amount of products is formed.²⁵⁹ Many in vitro studies investigating cytochrome P450 metabolism have been performed by using incubation periods varying from 10 to 60 min.^{30,254,260-270} In general, the incubation time chosen depend upon enzyme used, temperature and pH of the environment. Therefore, it is necessary to determine the most efficient incubation time for the human liver S9 enzymes for use in future metabolism and inhibition experiments in our laboratory. In an effort to determine the most efficient incubation period of **6.4** (PhIP) and **6.1** (B α P) metabolism by the human liver S9 fraction, experiments were conducted under the same conditions (see Section 6.3 experimental for details) and samples were taken at baseline (0 min) and every 15 min for 45 min to analyse the presence of **6.4** (PhIP) and **6.1** (B α P).

Figure 6.2 shows a distinct **6.1** (B α P) peak in baseline samples (t_R 13.8 min) which decreased over time to a point where the peak was almost undetectable after 45 min of incubation. At 15 min of incubation, the metabolism of the **6.1** (B α P) peak coincided with the appearance of a smaller peak (t_R 11.7 min), which then decreased after 30 min of incubation. The new product (t_R 11.7 min) was hypothesized to be a more polar metabolite of **6.1** given the shorter retention time in RPHPLC. It is plausible that this peak represented that of benzo[a]pyrene-9,10-diol or benzo[α]pyrene -7,8-diol,^{271,272} which are oxidized further to more polar compounds (such as benzo[α]pyrene-7,8,9,10-tetraol) formed from **6.1** (B α P) by CYPs.^{95,104,271,272}

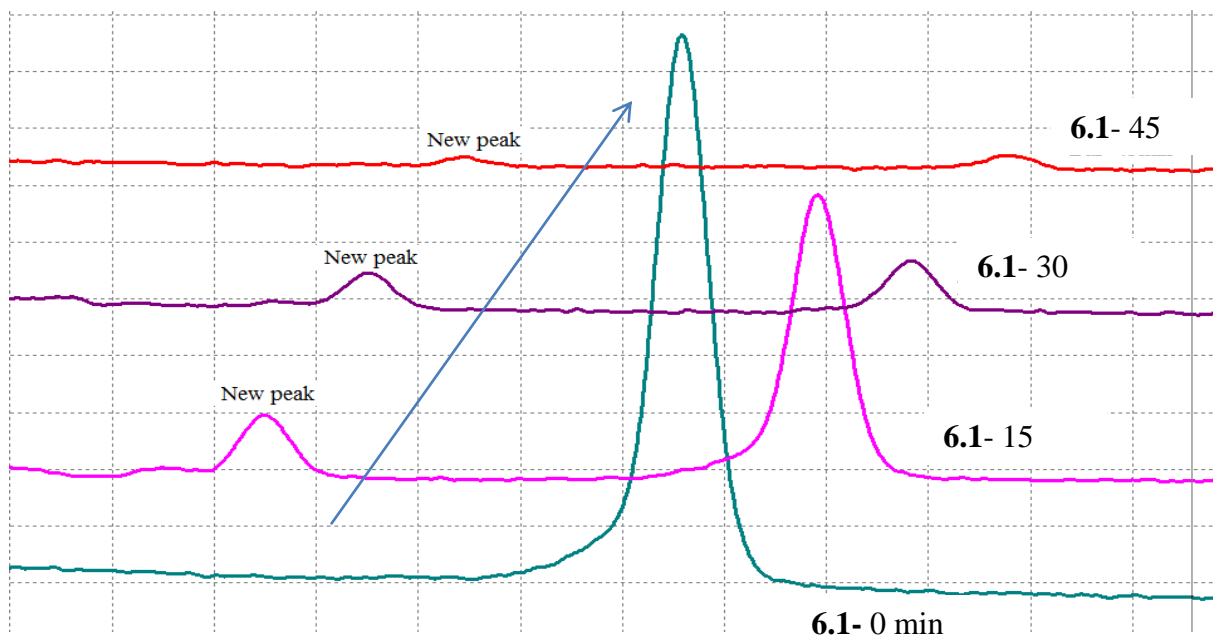


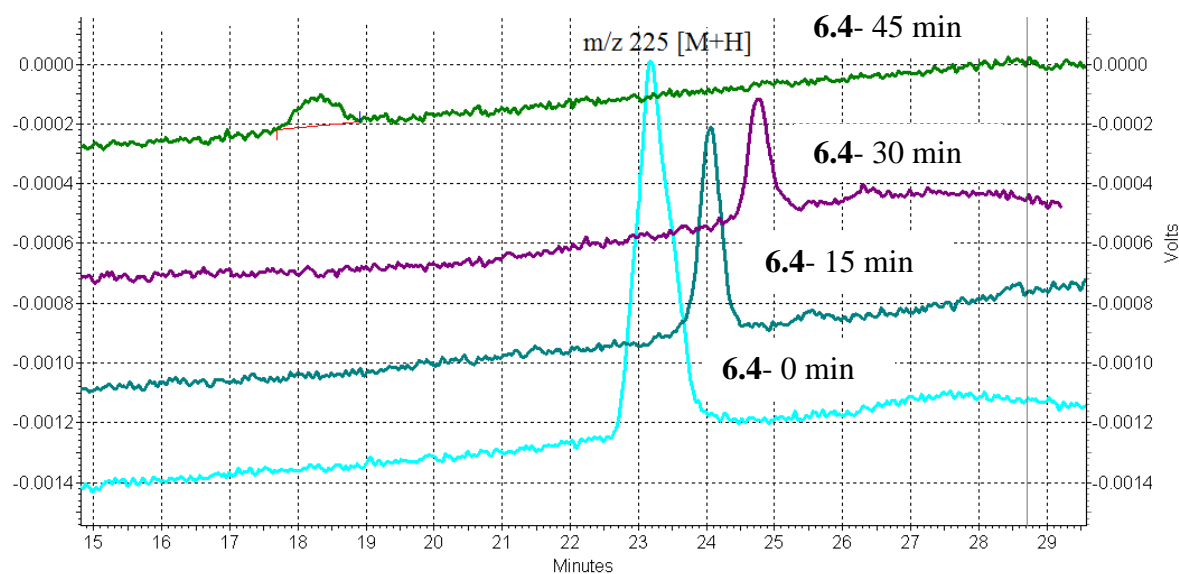
Figure 6.2: Overlay of the HPLC chromatograms of **6.1** (B α P) analysis from metabolism experiments with the human liver S9 fraction from 0-45 min, λ_{\max} 317 nm.

A similar metabolism profile was observed when **6.4** (PhIP) was incubated with human liver S9 (Figure 6.3). The area of the **6.4** (PhIP) peak (t_R 21.4 min) was reduced considerably after 30 min of incubation. Although nearly 100% of **6.4** (PhIP) was metabolized, these metabolites (presumably **6.5** and 4'-OH of **6.4**) could not be detected at λ_{\max} 317 nm. It is also plausible that the metabolites were conjugated by glucuronidases, that are present in the human liver S9 fraction, to more polar products and were eluted with three more polar components (NADPH, glucose 6-phosphate, glucose 6-phosphate dehydrogenase).^{252,273} Therefore, may exist below the limit of detection of the HPLC used.

The metabolism rate of **6.1** (B α P) and **6.4** (PhIP) reduced significantly with time, being greatest for each compound in the first 15 min (Table 6.4), and still occurring at a significant rate in the following 30 min (see Figure 6.2). These data suggest that the most appropriate incubation time for the experiments would be between 15 and 30 min. Therefore, to maximise metabolism and reduce experimental variability, the inhibition of metabolism experiments were performed over 20 min, which is also consistent with other similar studies.^{30,254,265}

Table 6.1: Time-course of the in vitro degradation of **6.1** and **6.4** by human liver S9 (n = 3).

Time (min)	Rate of 6.1 metabolism (pmol/mg protein/min)	Rate of 6.4 metabolism (pmol/mg protein/min)
0-15	475 ± 16	309 ± 19
15-30	172 ± 15	153 ± 13
30-45	24 ± 11	67 ± 18

**Figure 6.3:** Overlay of the HPLC chromatograms of **6.4** (PhIP) analyses from metabolism experiments with the human liver S9 fraction at 0-45 min.

The next parameter to be optimized was the concentration of **6.1** (B α P) and **6.4** (PhIP) to be used in the inhibition experiments. Under the optimised incubation conditions, the S9 system degraded **6.1** (B α P) and **6.4** (PhIP) (Figure 6.4). The rates of **6.1** (B α P) and **6.4** (PhIP) metabolism were no longer linear at concentrations of the substrates above 1 μ M. The degradation rates of these compounds followed simple Michaelis-Menten kinetics. The degradation of **6.1** (B α P) was about 2.5 times faster than that of **6.4** (PhIP), which was reflected in the concentrations at which the degradation rate was at half-maximum (Table 6.2). These data indicated that the human liver S9 fraction was more efficient in degrading **6.1** (B α P) and **6.4** (PhIP).

Based on the data presented in Figure 6.4, the lowest concentration of mutagens yielding the highest rate of metabolism was determined to be approximately 1.5 μ M. This concentration was therefore used during subsequent inhibition experiments.

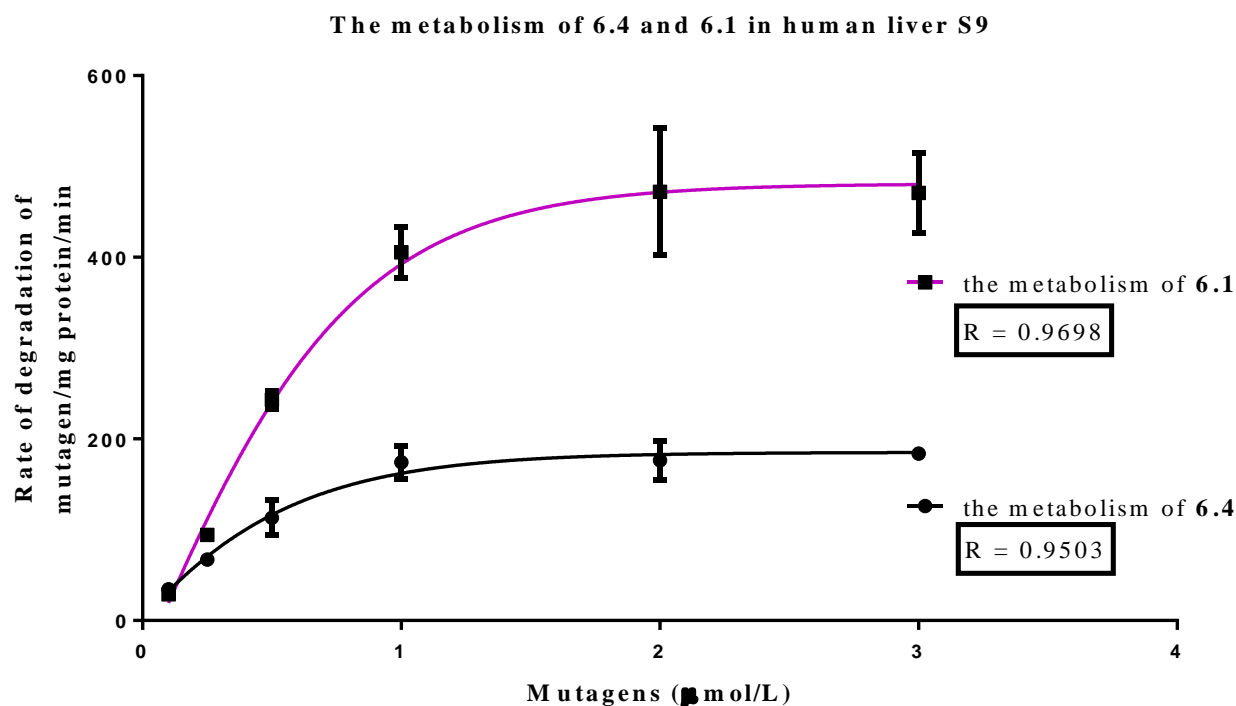


Figure 6.4: Kinetics of **6.1** (B α P) and **6.4** (PhIP) degradation by the human liver S9 fraction after 20 min of incubation (n = 3 per concentration).

Table 6.2: Michaelis-Menten kinetics of **6.1** (B α P) and **6.4** (PhIP) degradation by the human liver S9 fraction in the period of 20 min, EC₅₀ is the concentration of mutagens at which the degradation rate achieves 50%.

Compound	Degradation rate ($\mu\text{mol}/\text{mg protein}/\text{min}$)	Concentration at degradation rate half-maximum (EC ₅₀)(μM)
6.1	481	0.81
6.4	185	0.30

Detection methods: Several methods exist to measure the metabolism rate of **6.1** (B α P) and **6.4** (PhIP) and other compounds in the enzyme reactions. For example, Bulmer et al.¹⁸ used HPLC and UV spectroscopy to detect the concentration of mutagens in the experiments. Abu-Bakar et al.³⁰ determined the metabolism rate of coumarin by using spectrofluorometric methods. Mölzer et al.^{19,20} determined the concentration of tertiary-butyl hydroperoxide by HPLC methods. In our studies, we decided to use RPHPLC fitted with a UV detector set to detect at 317 nm for **6.4** (PhIP) and at 385 nm for **6.1** (B α P) because of the overlay in the absorbance between the two classes of compounds (mutagens and BPs) (Figure 6.5). Measurement of mutagen concentrations using standard UV spectroscopic methods alone would provide unreliable results due to BPs absorbing in the same region of the spectra as the mutagens and thus any absorbance measurement would have

some contribution from the BPs. Furthermore, the addition of the S9 mix to reactions created turbidity which would interfere absorbance measurement using single UV/Vis spectroscopy.

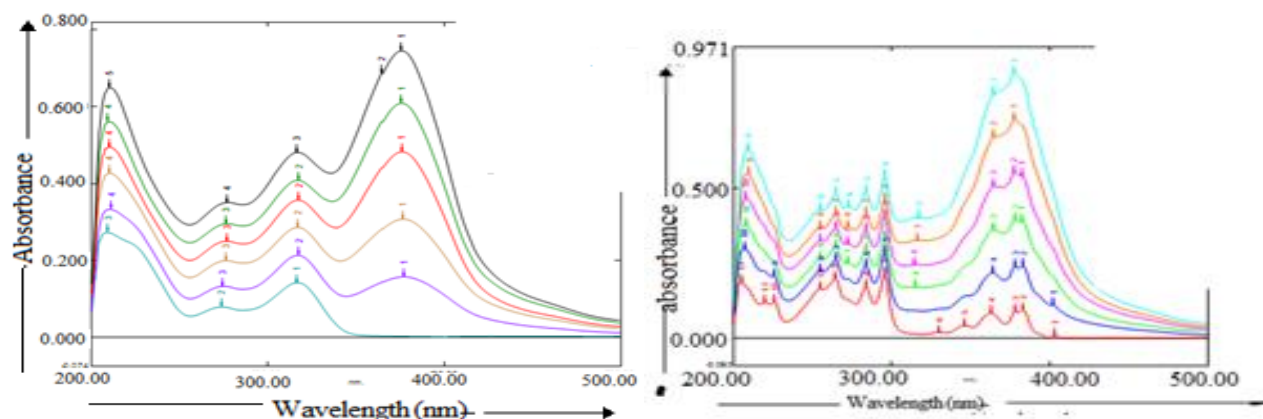


Figure 6.5: Representative overlay of UV spectra of **6.4** (left-blue) and **6.1** (right-red) and its mixtures with various concentrations of **6.8**.

6.2.2 Inhibitory effects of bile pigments on **6.1** and **6.4** metabolism in the human liver S9

To determine whether various BPs (**6.6-6.8**) could inhibit the degradation of **6.1** (B α P) and **6.4** (PhIP), the human liver S9 fraction was incubated with either **6.1** (B α P) and **6.4** (PhIP) (1.5 μ M final concentration) in the presence of BPs at various concentrations ranging from 1.25 μ M to 20 μ M. The concentration range of BPs chosen reflected physiological concentrations of **6.7** in blood.⁵³⁻⁵⁵

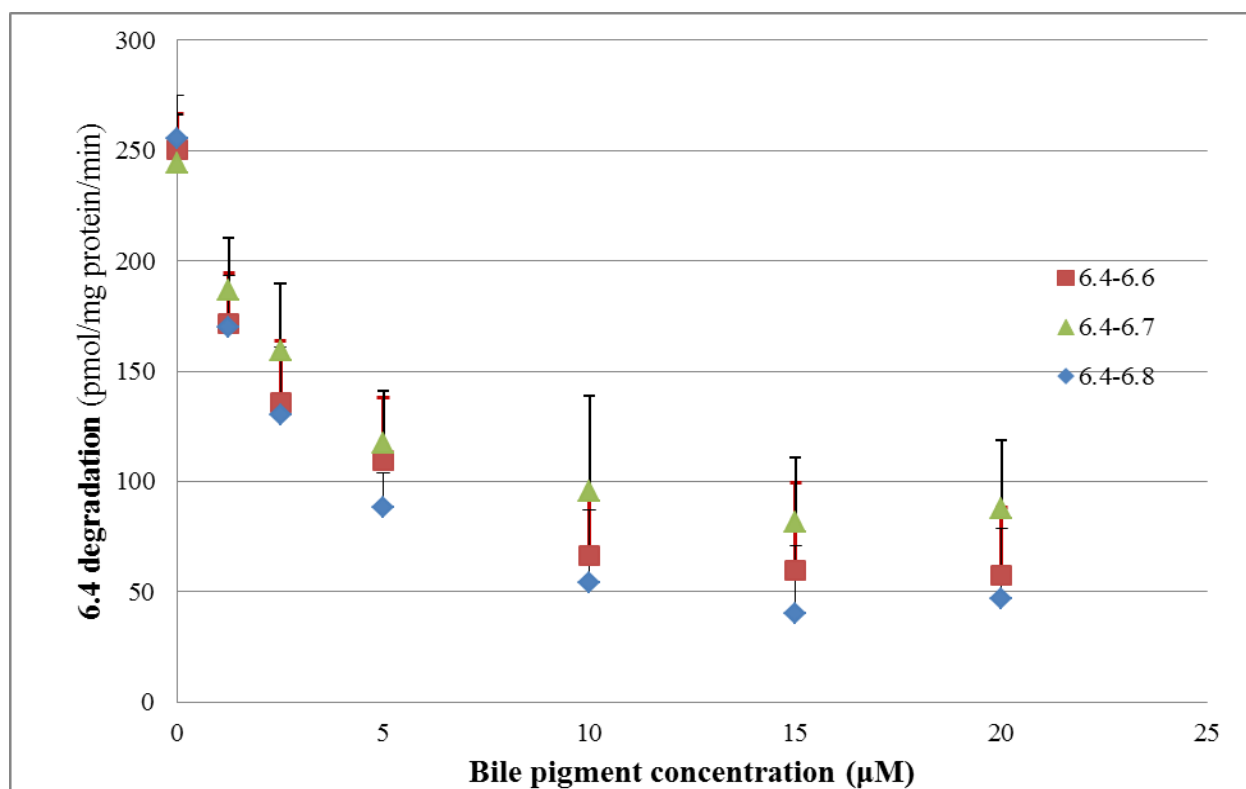
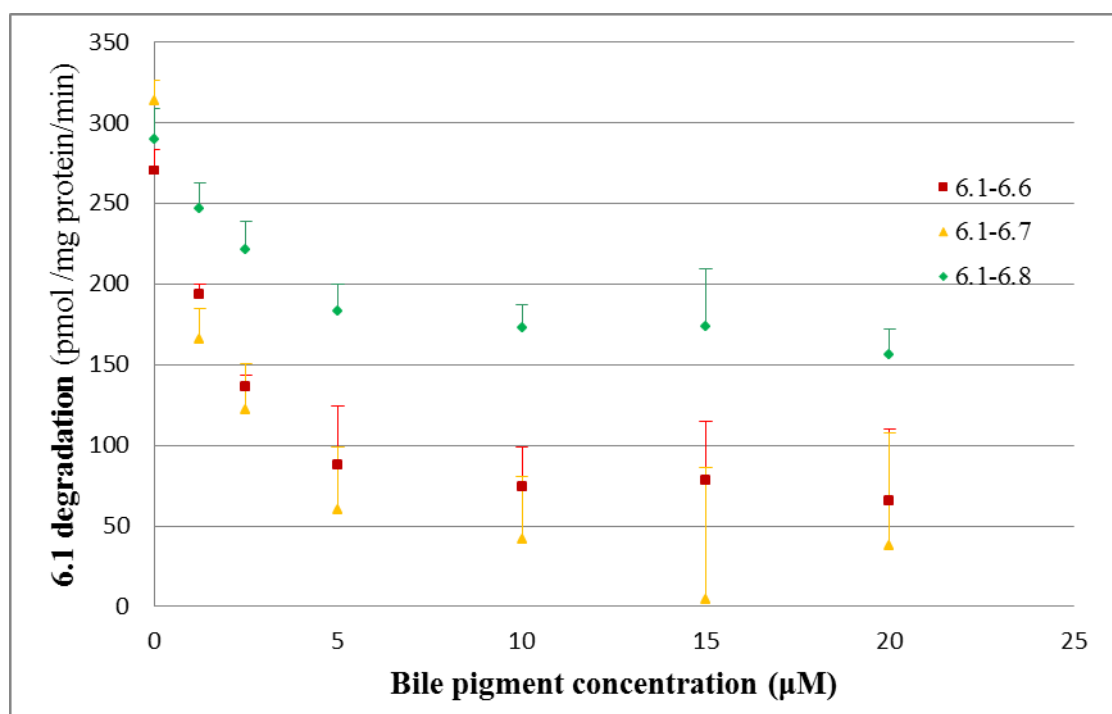


Figure 6.6: Effects of BPs on the degradation of **6.4** in human liver S9 fraction ($n = 3$).

In human liver S9 experiments, all three BPs, **6.6** (PRO), **6.7** (UCB) and **6.8** (BV) inhibited the degradation of **6.4** (PhIP) in a concentration dependent manner up to a BP concentration of approximately 10 μM (Figure 6.6). None of the BPs tested could completely inhibit the reaction. The order of effectiveness for inhibition of **6.4** (PhIP) degradation was **6.7** (UCB, 83%) > **6.6** (PRO, 76%) > **6.8** (BV, 67%) at 10 μM , which was commensurate with the IC_{50} values of 1.0, 1.33, 1.36 μM , for the BPs respectively (at these concentrations, 50% of **6.4** (PhIP) degradation was inhibited by BPs) (Table 6.3 and Table 7.18 in Appendix-E).

**Figure 6.7:** Effects of BPs on degradation of **6.1** (B α P) in human liver S9 fraction ($n = 3$).

By contrast, BPs inhibited the degradation of **6.1** (B α P) in a concentration dependent manner up to 5 μM (Figure 6.7). At 5 μM , **6.7** (UCB) inhibited the degradation of **6.1** (B α P) by almost 85%, whilst at the same concentration **6.8** (BV) and **6.6** (PRO) inhibited the consumption of **6.1** (B α P) by 48% and 71%, respectively (Figure 6.7). Thus, the order of BPs' effectiveness at inhibiting the degradation of **6.1** (B α P) in human S9 was **6.7** (UCB) > **6.6** (PRO) > **6.8** (BV), which was also reflected in the IC_{50} values of 1.00, 1.00, and 1.43 μM , respectively (Table 6.3).

Table 6.3: Potency of BPs inhibitory effects on **6.1** (B α P) and **6.4** (PhIP) degradation in the human liver S9 fraction, IC₅₀ values were derived from the GraphPad Prism using non-linear regression analysis (see Table 7.18 and Table 7.19 in Appendix-E)

Bile Pigments	IC ₅₀ (μ M)	
	50% inhibition of 6.1 degradation	50% inhibition of 6.4 degradation
6.6 (PRO)	1.00	1.33
6.7 (UCB)	1.00	1.00
6.8 (BV)	1.43	1.43

Based on the IC₅₀ values (**Table 6.3**), the potency of **6.7** and **6.8** to inhibit **6.1** (B α P) and **6.4** (PhIP) were similar though **6.6** more potently inhibited the degradation of **6.1** than that of **6.4**.

Overall, these results indicated that the human liver S9 fraction effectively degraded **6.1** (B α P) and **6.4**(PhIP). The degradation rates followed simple Michaelis-Menten kinetics, which indicated that the degradation of these compounds was enzyme mediated. Importantly, BPs, especially **6.7**, efficiently inhibited the degradation of **6.1** (B α P) and **6.4**(PhIP). These inhibition profiles also followed Michaelis-Menten kinetics. However, from these experiments it was not possible to discern the degree of BPs inhibitory effects on CYP-specific **6.4** and **6.1** metabolism. The human liver S9 fraction contains a mixture of CYP isoforms (Table 7.17 in appendix-E) and glucuronidases that are also involved in the metabolism of **6.1** (B α P) and **6.4**(PhIP) and therefore, inhibitory effects of BPs may have been non-specific. As these CYPs are known to metabolise **6.1** (B α P) and **6.4**(PhIP) to mutagenic intermediates, it is plausible that the observed inhibition of degradation was partly a consequence of inhibition of these CYPs. This however, requires confirmation within selective inhibition studies using recombinant CYP1A, 1B1, and perhaps CYP2A as well as CYP3A4.

The inhibitory capacity of BPs on the metabolism of **6.1** (B α P) has also been reported by Bulmer et al.¹⁴ and Arimoto et al.³⁵ who performed their experiments on rat liver S9 and bacteria (*Salmonella typhinurium* TA98 and TA100). While Bulmer et al.¹⁴ reported that the order of effectiveness suggested **6.8** (BV) was more effective than **6.7** (UCB), Arimoto's results indicated **6.7** (UCB) was more effective compared to **6.8** (BV).^{34,35} Therefore, it is also important to determine the BPs' ability to inhibit mutagens in rat liver S9.

Although using a different method to determine the effectiveness of BPs to the degradation of **6.1** (B α P) and **6.4** (PhIP), the results are an important evidence for further research on rat liver S9.

Indeed, the results showed that the degradation rate of **6.1** and **6.4** in rat liver S9 is higher than that of in human liver S9. However, it also indicated the order of inhibitory effectiveness of BPs on **6.1** and **6.4** was **6.7** (UCB) > **6.6** (PRO) > **6.8** (BV), the order observed with human liver S9. The comparison of tested results may provide preliminary evidence to evaluate the action of CYP enzymes on the metabolism of **6.1**, **6.4** and the inhibitory ability of BPs.

Table 6.4: Effects of BPs (10 μ M) on degradation rate of **6.1** (B α P, 1.5 μ M) and **6.4** (PhIP, 1.5 μ M) in rat liver S9 fraction (n = 3).

Samples	The degradation rate of 6.4 (pmol /mg protein/min)	% inhibition	The degradation rate of 6.1 (pmol /mg protein/min)	% inhibition
S9+ mutagen	309 \pm 19	--	476 \pm 16	--
S9+ mutagen + 6.6	151 \pm 22	51	306 \pm 23	36
S9+ mutagen + 6.7	128 \pm 32	59	240 \pm 19	50
S9+ mutagen + 6.8	205 \pm 26	34	417 \pm 18	12

Table 6.5: Effects of BPs (10 μ M) on degradation rate of **6.1** (B α P, 1.5 μ M) and **6.4** (PhIP, 1.5 μ M) in human liver S9 fraction (n = 3).

Samples	The degradation rate of 6.4 (pmol /mg protein/min)	% inhibition	The degradation rate of 6.1 (pmol /mg protein/min)	% inhibition
S9+ mutagen	244 \pm 22	--	314 \pm 12	--
S9+ mutagen + 6.6	66 \pm 22	72	74 \pm 24	76
S9+ mutagen + 6.7	54 \pm 32	77	41 \pm 39	87
S9+ mutagen + 6.8	95 \pm 43	60	173 \pm 14	45

Multiple hypotheses exist to explain the inhibitory effects and order of effectiveness of BPs towards **6.1** (B α P) and **6.4** (PhIP) mutagenesis (**6.7** > **6.6** > **6.8**). Compound **6.7** (UCB) may possess the most potent inhibitory effect on the metabolism of **6.1** (B α P) and **6.4** (PhIP) due to unique physico-chemical properties, which results in the formation of a 'ridge-tile' structure. Furthermore, four different isomers of **6.7** (UCB) exist in an equilibrium mixture, the formation of which is induced by photo-isomerization, (4*E*, 15*E*)-, (4*Z*, 15*E*)-, (4*E*, 15*Z*)- and (4*Z*-15*Z*)-bilirubin IX α (Figure 6.8).⁵⁸⁻⁶⁰ The most stable isomer is bilirubin IX α (4*Z*, 15*Z*), in which six intramolecular hydrogen bonds are formed between carboxylic acid and amide pyrrole N-H groups. The intramolecularly

hydrogen-bonded conformers create a ridge-tile shape in the central molecule and form enantiomeric conformations (*M* and *P*) (Figure 6.9).^{58-60,65} All of **6.7**'s photoisomers exist in reversible states that will generate greater efficiency and opportunities for **6.7** (UCB) binding to enzyme active sites. In addition, the saturated C10-bridge in the structure of **6.7** (UCB) can rotate freely and flex to produce more conformational states which may serve to inhibit (either competitively or non-competitively) mutagen metabolism.

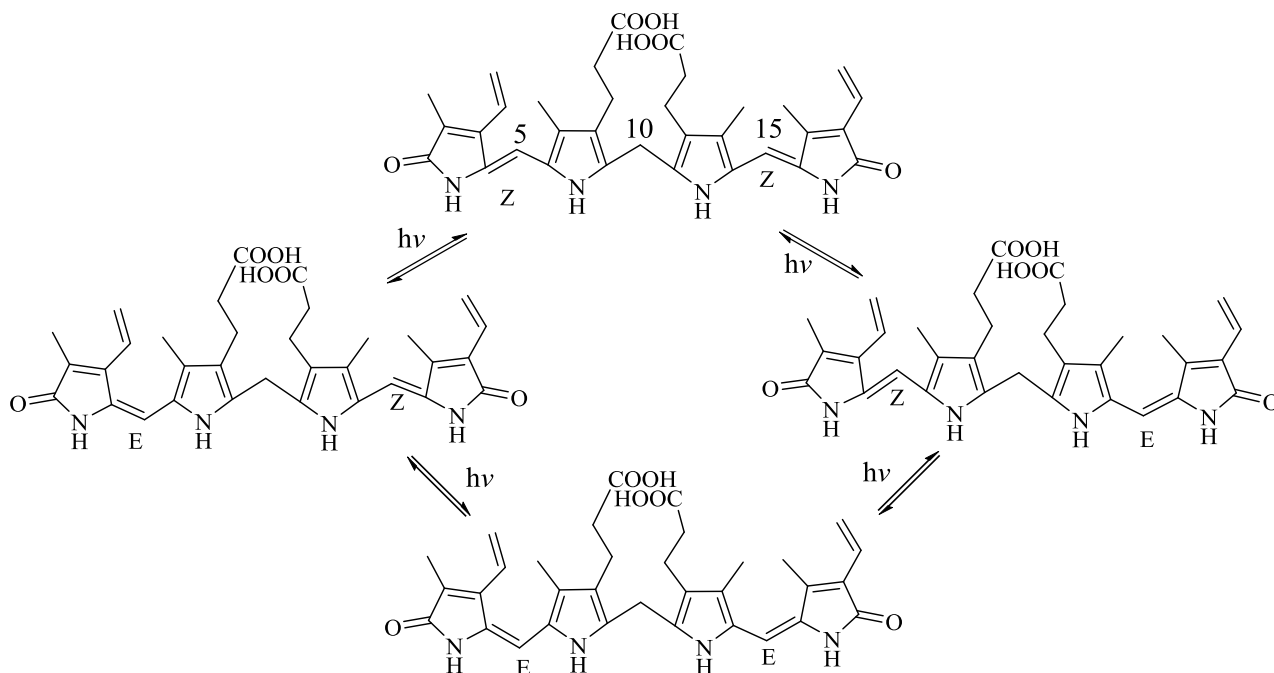


Figure 6.8: Configurational photo-isomerisation of **6.7** (UCB), leading to the formation of four isomers (4Z,15Z)-, (4E,15Z)-, (4Z,15E)-, (4E,15E).

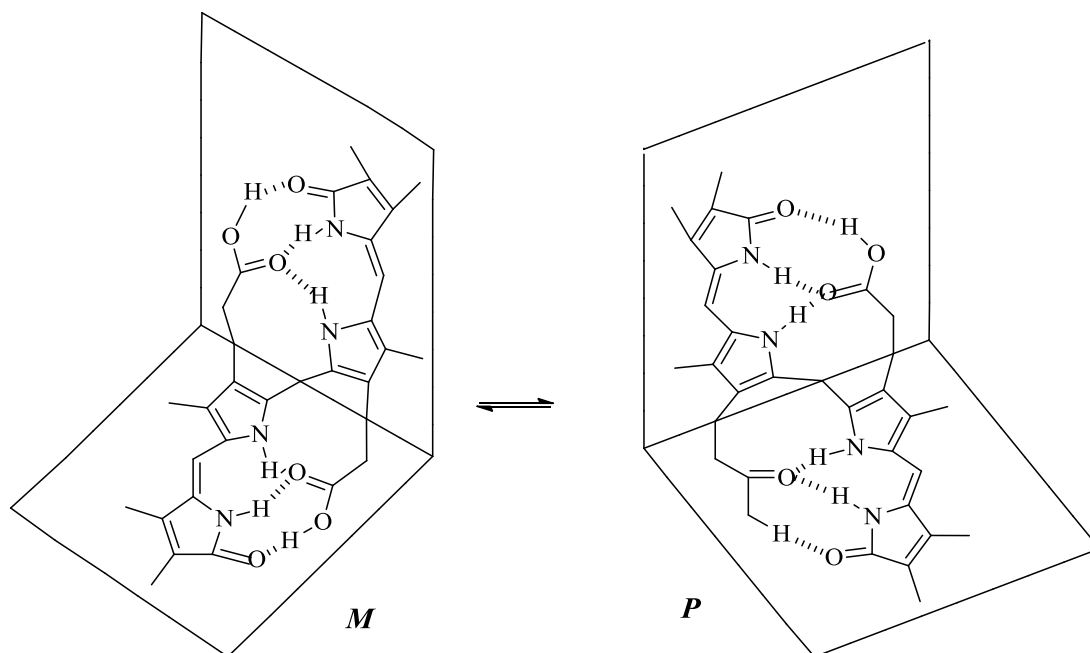


Figure 6.9: The enantiomers of (4Z, 15Z)-bilirubin (P =plus, M =minus) demonstrate the presence of ‘ridge-tile’ conformers via the formation of intramolecular hydrogen bonds.^{58,59}

In contrast, the unsaturated C10-bridge in **6.8** (BV) holds the molecule in an almost planar (4Z, 10Z, 15Z)-configuration, which is quite stable in the presence of light.⁶⁶ As a result, **6.8**'s structure does not allow for intramolecular hydrogen bonding. Biliverdin's rigid structure may reduce its ability to inhibit **6.1** (B α P) and **6.4** (PhIP) metabolism and may not possess the strong binding affinity of **6.7** (UCB) with enzyme active sites. The hypothesis was supported by Abu-Bakar et al.³⁰ who found that **6.7** (UCB) was substrate of CYP2A6 and one of its metabolism products was **6.8** (BV).

Although **6.6** (PRO) did not form photo-isomers, it was a more potent inhibitor of **6.1** (B α P) and **6.4** (PhIP) metabolism than **6.8** (BV). The Different structural shape of Compound **6.6** may be easy to be metabolised by enzymes or interact efficiently with enzymes. In addition, the four nitrogens in **6.6** (PRO) are sufficient for forming stable complexes with metal ions.^{274,275} The special structure of **6.6** (PRO) therefore, may result in unique interactions with enzymes active sites that are stronger than **6.6** (PRO), but weaker than **6.7** (UCB).

6.2.3 Docking simulation of **6.1**, **6.4** and BPs on CYP1A1, 1A2 and 1B1 active sites

Many studies indicated that CYP1A1, 1A2, 3A4 and 1B1 are responsible for the metabolism of **6.1** (B α P) and **6.4** (PhIP).^{127,221,252} CYP1A2 and 3A4 are known to be present in the human liver S9 fraction and CPY1A1 and 1B1 are hypothesized to be present in the extract (Table 7.18 and Table 7.19 in appendix-E). Therefore, the molecular docking of BPs, **6.1** (B α P) and **6.4** (PhIP) with CYP1A1(4I8V)²⁵⁸, 1A2(2HI4)²⁷⁶, 3A4(4NY4)²⁷⁷ and 1B1(3PM0)²⁷⁸ was under taken crystal

structures of the protein data bank (PDB) to attempt to explain the inhibitory ability of BPs towards **6.1** (B α P) and **6.4** (PhIP) metabolism (Figure 6.10 and Figure 6.11).

Table 6.6: Active site amino acid residues of human CYP 1A2²⁵⁸, 1A1²⁵⁸, 3A4²⁷⁷ and 1B1^{27,58}, Amino acid residues that are conserved in all four P450s are shown. Residues that interact with **6.1** are highlighted using a grey background.

P450 1B1 ^{258,278}	P450 1A1 ²⁵⁸	P450 1A2 ²⁵⁸	P450 3A4 ²⁷⁷
Ile ¹¹⁷	Ile ¹¹⁵	Val ¹²⁶	Phe ²¹⁵
Thr ¹¹⁸	Ser ¹¹⁶	Ser ¹²⁷	Phe ¹⁰⁸
Ser ¹²²	Ser ¹²⁰	Val ³⁹⁵	Arg ¹⁰⁶
Thr ¹²⁴	Ser ¹²²	Ala ¹³³	Arg ¹⁰⁵
Phe ¹²⁵	Phe ¹²³	Phe ¹³⁴	Ser ¹¹⁹
Asn ²²³	Asn ²⁵⁵	Asn ²²⁸	Ile ¹²⁰
Phe ²²⁶	Phe ²²⁴	Phe ²³¹	Ala ³⁷⁰
Asn ²⁵⁷	Leu ⁴⁹⁶	Asp ³³³	Ile ³⁰¹
Phe ²⁶⁰	Gly ³¹⁶	Thr ³³⁴	Ala ³⁰⁵
Asp ³²⁰	Phe ²⁵⁸	Asn ²⁶⁵	Thr ³⁰⁴
Thr ³²¹	Leu ³¹²	Phe ²⁶⁸	Thr ³⁰⁹
Leu ³⁸²	Asp ³¹³	Leu ⁵⁰⁹	Arg ²¹²
Leu ⁴⁹⁷	Asn ²²²		Ile ³⁶⁹
	Phe ³¹⁹		Phe ²¹³
	Asp ³²⁰		Phe ²⁴¹
	Thr ³²¹		

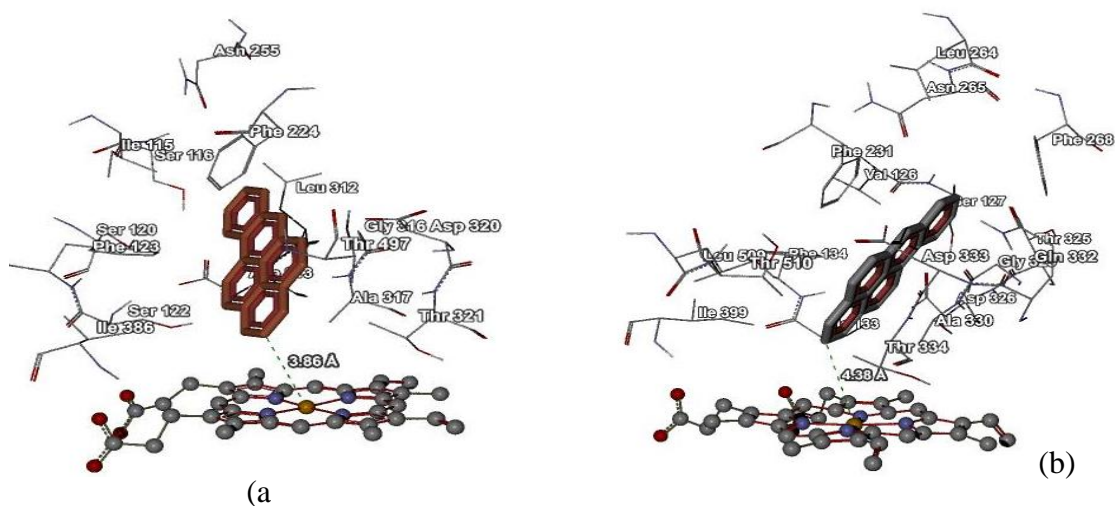
Table 6.6 shows the amino acid sequence of the binding site of **6.1** (B α P) and BPs in CYP1A1, 1A2, 3A4 and 1B1 predicted in the docking studies. Most of the amino acids within the active site were the same as those reported by Walsh and Tian^{222,258} and Bronden²⁷⁷ who reported a crystal structure of a complex of CYP3A4 with an aromatic molecule bound in the active site.²⁷⁷ A small number of amino acids were not detected in our simulations (Figure 6.9 and Figure 6.10) because the residue distance in our docking simulations was set to only 4 Å from the ligand.

Table 6.7: A comparison of the active site residues of CYP1A2 found within a range of 4 Å distance from ligands docked into the active site (Figure 6.10, Figure 6.14). The grey background shows the same amino acids residues of the active site were found in the docking of CYP 1A2 with α -naphthoflavone.²⁷⁶

6.1, 6.4 and BPs (within a range of 4Å from ligands to amino acid residues of 1A2)				
CYP1A2 (6.1)	CYP1A2 (6.4)	CYP1A2 (6.7)	CYP1A2 (6.8)	CYP1A2 (6.4)
Phe-260	Phe-260	Phe-260	Phe-260	Phe-260
Phe-226	Phe-226	Phe-226	Phe-226	Phe-226
Val-227	Val-227	Val-227	Val-227	Val-227
Leu-497	Leu-497	Lue 497	Leu-497	Lue 497
Gly-316	Gly-316	--	Gly-316	Gly-316
Asp-320	Asp-320	Asp-320	Asp-320	Asp-320
Thr-498	Thr-498	Thr-498	Thr-498	Thr-498
Thr-321	Thr-321	Thr-321	Thr-321	Thr-321
Leu-382	Leu-382	Leu-382	Leu-382	Leu-382
Ile-386	Ile-386	Ile-386	Ile-386	--
Thr-124	Thr-124	Thr-124	Thr-124	Thr-124
Phe-125	Phe-125	Phe-125	Phe-125	Phe-125
Asn-312	Asn-312	Asn-312	Asn-312	Asn-312
Ser-122	Ser-122	Ser-122	Ser-122	Ser-122
Thr-118	Thr-118	Thr-118	Thr-118	Thr-118
Ala-317	Ala-317	--	Ala-317	Ala-317
--	--	Thr-223	Thr-223	Thr-223
--	--	Val-220	Val-220	--
--	--	--	Lys-500	Lys-500
--	--	Phe-256	Phe-256	Phe-256
--	--	Leu-219	Leu-219	Leu-219
--	--	--	Met-216	--
--	--	Phe-319	--	--
--	--	Asp-313	Asp-313	Asp-313
--	Ile-117	Ile-117	--	--
--	--	--	Asn-257	Asn-257
--	--	--	--	Arg-108
--	--	--	--	Leu-123

--	--	--	--	Arg-456
--	--	--	--	Phe-381
--	--	--	Asn-222	--
--	--	--	Phe-315	--
--	--	Gly-318	--	--
--	--	--	Leu-264	--

Table 6.7 and the Figure 6.10-Figure 7.27 indicated that the active site residues of CYP1A2, 1A1, 1B1 and 3A4 that interact with **6.1** (B α P) and **6.4** (PhIP) are the same amino acid residues that interact with BPs. The interactions between BPs and amino acids in the active site are stronger than those of **6.1** (B α P) and **6.4** (PhIP) due to more hydrogen bonds forming between carboxylic and amides groups. For example, **6.7** (UCB) exhibited hydrogen bonds with Ser-122, Thr-498, Asp-313, Asp-320; **6.6** (PRO) had hydrogen bonds with Thr-321, Arg-108, Leu-123; **6.8** (BV) had hydrogen bonds with Thr-118, Gly-316 and Asp-320. These stronger interactions may facilitate BPs dominating the active site residues of enzymes in competitive reactions with **6.1** (B α P) and **6.4** (PhIP). Similarly, the hydrogen bonds were found in other docking simulations between CYP1A1, 3A4, 1B1 and BPs (Figure 6.12-Figure 6.14).



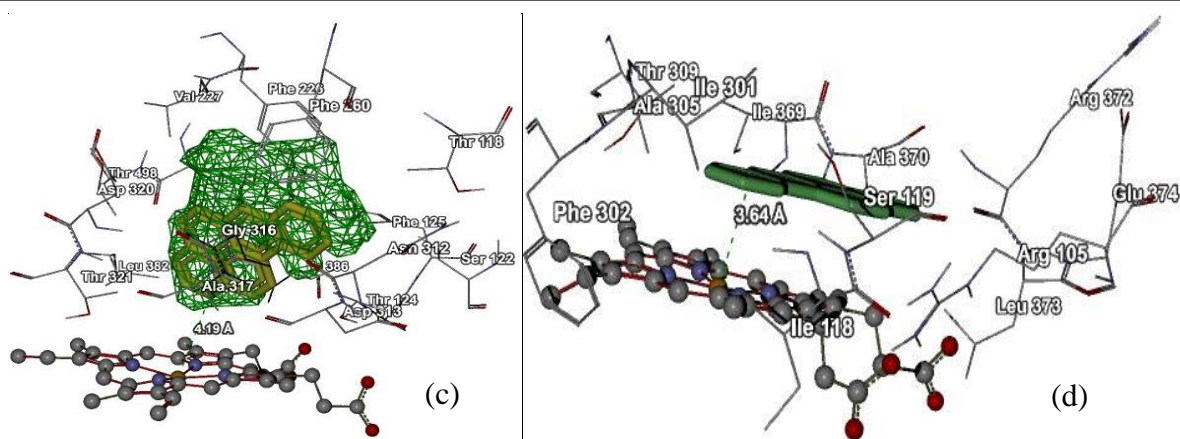


Figure 6.10: The docking of **6.1** (B α P) into the active site of CYP1A1 (a), CYP1B1 (b), CYP1A2 (c) and CYP3A4 (d). Simulations were performed using Molegro Virtual Docker.

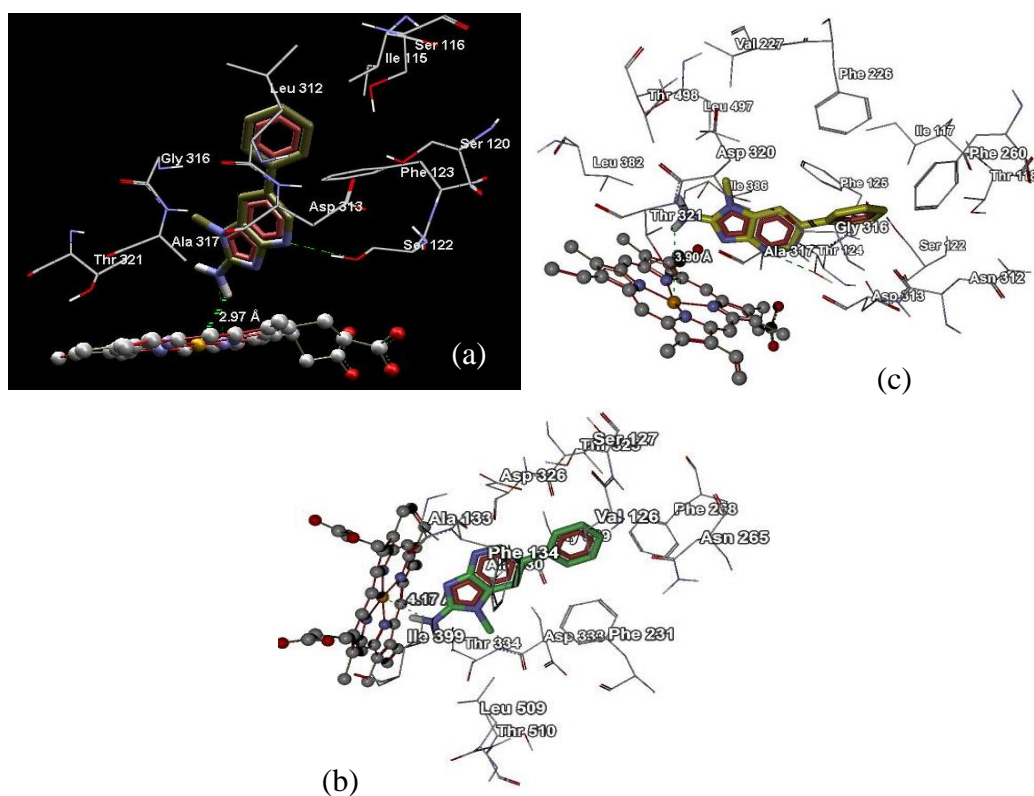


Figure 6.11: The docking of **6.4** into the active site of CYP1A1(a), CYP1B1(b) and CYP1A2(c). Simulations were performed using Molegro Virtual Docker.

Although **6.1** (B α P) does not have any polar groups, the docking simulation results show that **6.1** (B α P) bound effectively to the active site of CYP enzymes. There are more than 13 amino acids in the active site of CYP1A1 within a distance of 4 Å from **6.1** (B α P, Figure 6.10). Similarly, more than 18 amino acids in the active site of CYP1A2 and 14 amino acids in CYP1B1's active site enclosed **6.1**'s surface. Benzo[α]pyrene is directed toward iron in the haem complex at a distance of less than 4.38 Å for CYP1A and 1B1 enzymes. The short distance between enzyme active site

residues and the surface of **6.1** (B α P) indicates that **6.1** (B α P) has very strong interactions with the enzyme active site to facilitate the oxidation of **6.1** (B α P) to benzo[a]pyrene -7,8-epoxide and **6.3**.

The interactions of **6.4** (PhIP) with the active site residues of CYP enzymes appear stronger than those of **6.1** (B α P) due to hydrogen bonds between the nitrogen within the pyridine ring of **6.4** (PhIP) with Ser-122 in the active site of CYP1A1, Thr-124 of CYP1B1 and Ala-305 of CYP3A4. The distance between the haem iron of CYP1A1 and **6.4** (PhIP) was 2.97 Å, 3.90 Å for CYP1B1 and 4.17 Å for CYP1A2 (Figure 6.11). Interestingly, the NH₂ group in **6.4** (PhIP) was the closest group to the iron within the haem complex. This amine group is oxidised to the carcinogenic N-hydroxylated metabolite **6.5** (Figure 6.1).^{127,251-253}

Molegro Virtual Docker revealed the interactions between amino acids in the active site of CYP1A1, 1A2, 3A4 and 1B1 to **6.7** (UCB) showed that **6.7** (UCB) used both its carboxylic acid groups and pyrrole nitrogens to form hydrogen bonds and electrostatic interactions with amino acids at the active site of the enzymes (Figure 6.12). The docking of **6.6** (PRO) and **6.8** (BV) in the active site of CYP1A1, 1A2, 3A4 and 1B1 suggested interactions were mainly by hydrogen bonds between carboxylic groups and amino acids (Figure 6.13 and Figure 6.14). Our simulations suggested that although BPs possess a larger molecular structure than **6.1** (B α P) and **6.4** (PhIP), they still could bind with the small active site cavities of CYP1A1, 1A2, 1B1 and 2A6. These observations provided evidence to explain the inhibitory action of BPs against **6.1** (B α P) versus **6.4** (BV) metabolisms.

The cavities of the active sites of CYP1A1 (volume 98.82 Å³, surface 291.84 Å²)²⁵⁸, 1A2 (volume 74.24 Å³, surface 241.92 Å²)²⁷⁶ and 1B1 (volume 75.26 Å³, surface 249.60 Å²)²⁷⁸ are quite small and narrow, and therefore, are difficult for bulky molecules to enter and effectively interact. Due to **6.7**'s more flexible structure, which accommodates multiple three dimensional conformations,^{58,59} this could facilitate **6.7** (UCB) entering the active site and interacting with amino acids. This interaction could result in enzyme inhibition. Protoporphyrin possesses a fused macrocycle with a narrow surface-unique structure (less steric effect) which could facilitate its movement to the enzyme active site. In contrast, **6.8** (BV) has an unsaturated C10-bridge holding its non-planar two dipyrrolic halves which creates more steric effect potentially hindering the molecule's entry into the cavity of the enzyme active site. On this basis, it is not surprising that **6.8** (BV) represents the weakest inhibitor. Strong hydrogen bonds and electrostatic interactions forming between carboxylic groups of BPs and amino acid residues in the active site also suggest BPs could act as non-competitive inhibitors. This class of inhibitors does not compete with the substrate for binding to

the active site, but rather forms a bond outside of the active site and, in doing so, changes the enzymes conformation, thus reducing or increasing the size of the active site. In turn, it may influence the affinity of a substrate to the active site. The inhibitor could also dock in the active site and reduce the interactions of the active site with substrate.

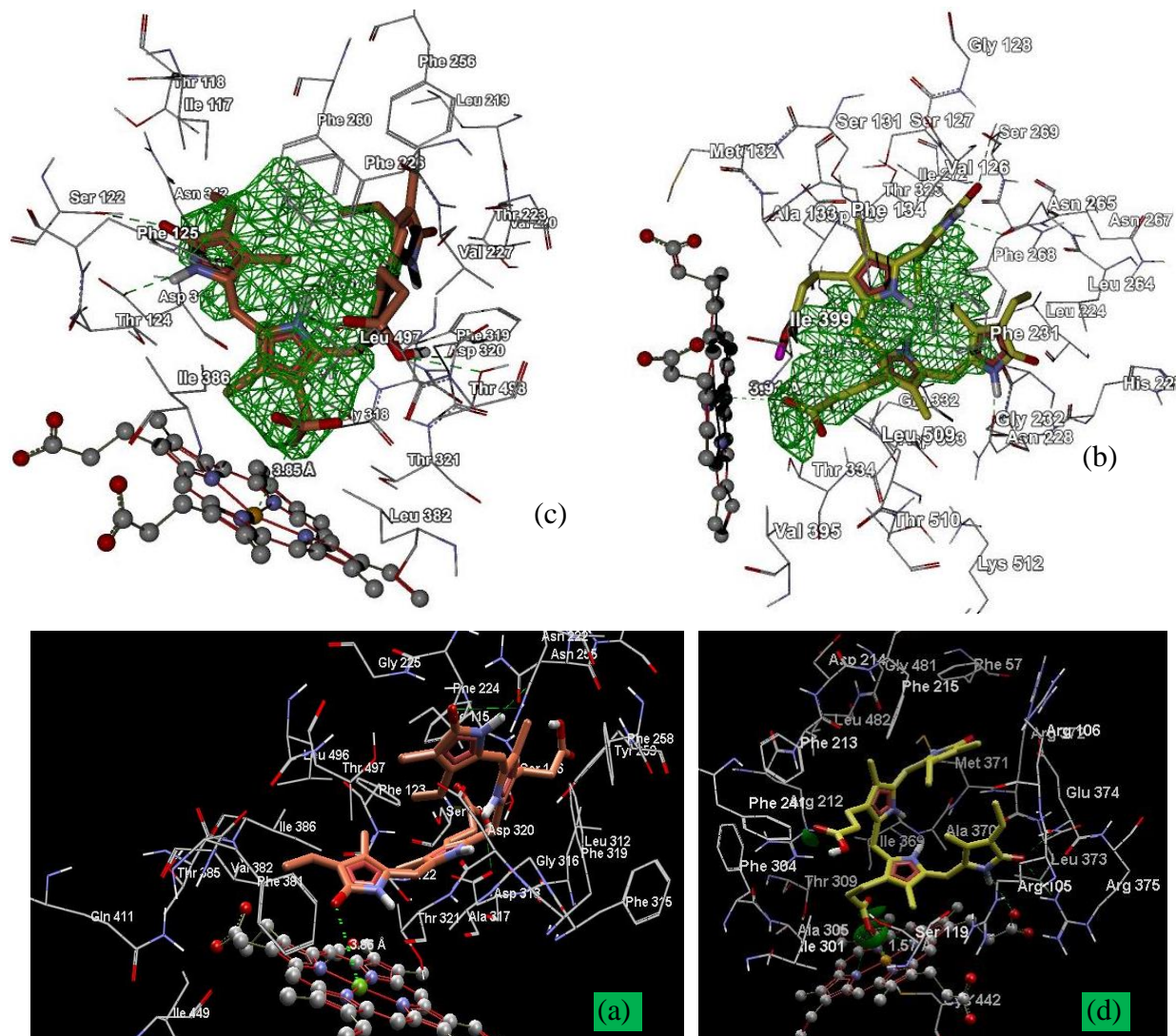


Figure 6.12: The interactions of 6.7 (UCB) with amino acids on the active site of CYP1A1(a), CYP1A2(c), CYP1B1(b) and CYP3A4(d).

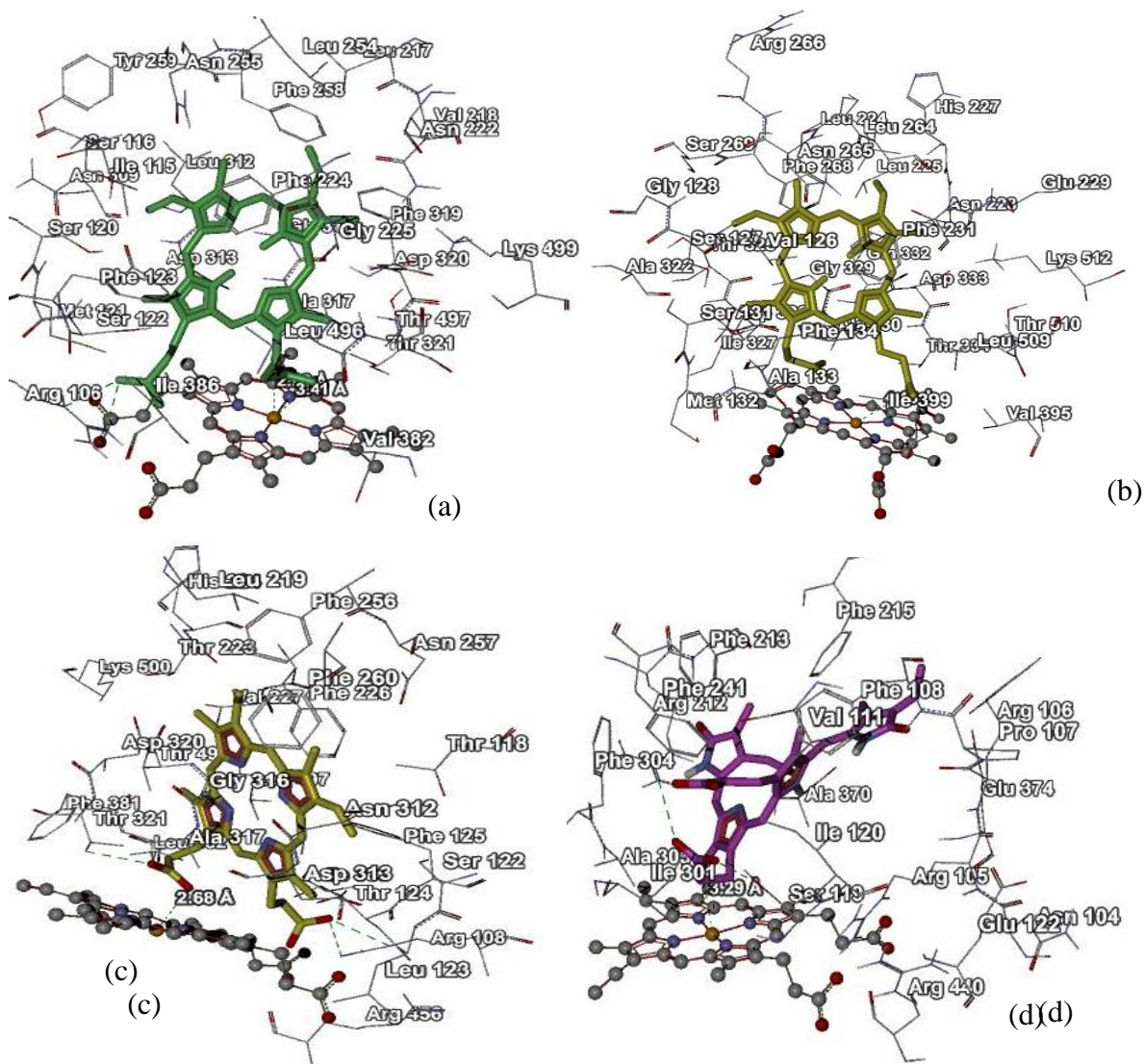


Figure 6.13: The interactions of 6.6 (PRO) with amino acids in the active site of CYP1A1(a), CYP1A2(c), CYP1B1(b) and CYP3A4(d).

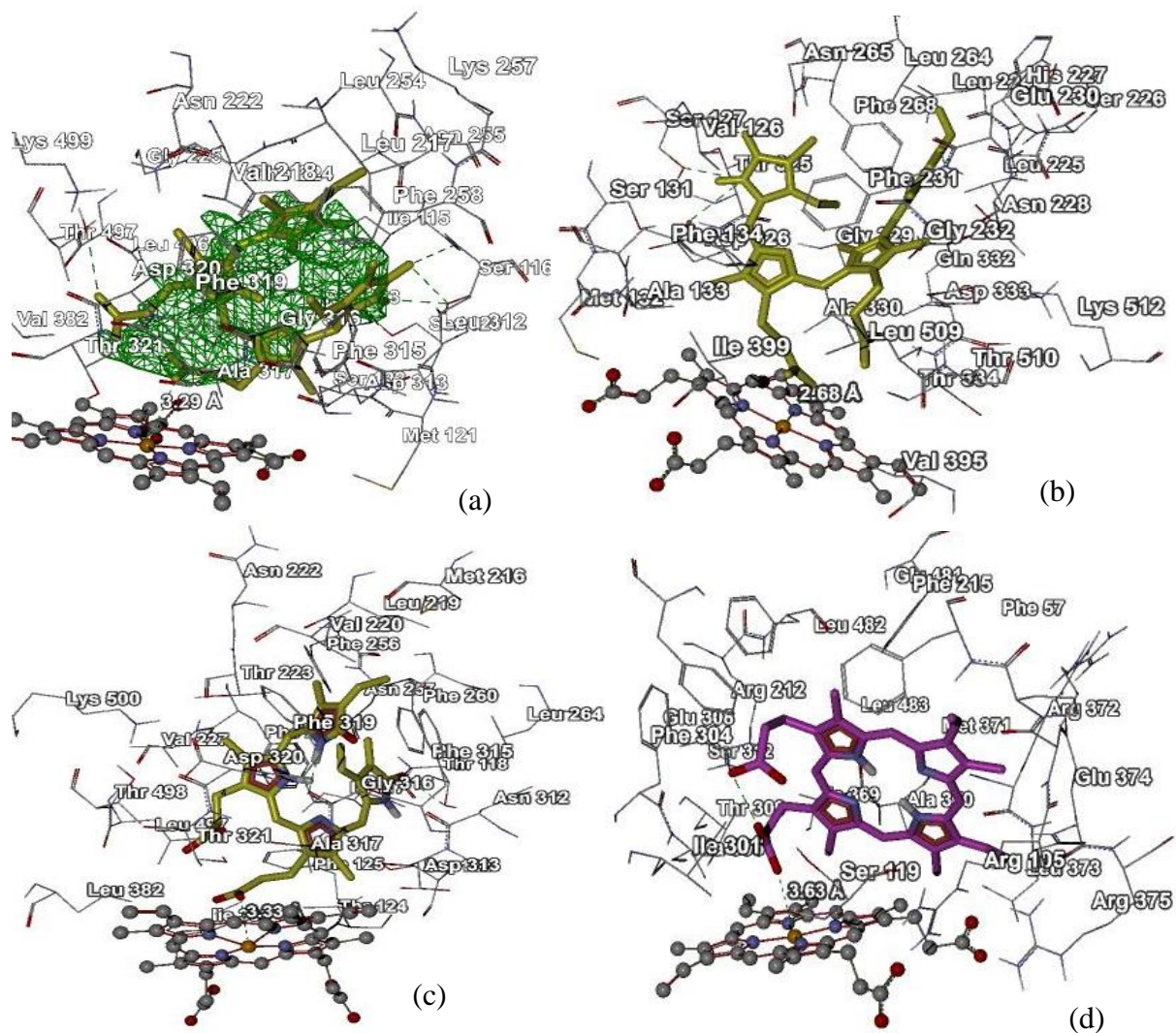


Figure 6.14: The interactions of **6.8** (BV) with amino acids in the active site of CYP1A1(a), CYP1A2(c), CYP1B1(b) and CYP3A4 (d).

6.3 Conclusions

The ability of BPs to inhibit mutagens (**6.1** (B α P) and **6.4** (PhIP)) degradation has successfully been explored in vitro whilst human and rat liver S9 fractions were employed. Preliminary data indicated the concentrations of **6.1** (B α P) and **6.4** (PhIP) that resulted in the saturation of **6.1** (B α P) and **6.4** (PhIP) degradative enzymes in the S9 mixtures. The results of the inhibition studies indicate that **6.7** (UCB) had the greatest inhibitory effect on the metabolism of both **6.1** (B α P) and **6.4** (PhIP), followed by **6.6** (PRO) and then **6.8** (BV).

Simulated docking studies using published crystal structures of the CYP enzymes known to metabolise **6.1** (B α P) and **6.4** (PhIP) indicated multiple interactions between the mutagens and the BPs (inhibitors) with active site amino acids of the CYPs. This provided new data to suggest that BPs could competitively inhibit mutagens binding and thus metabolism. These data largely agreed with the in vitro data presented in this chapter, indicating that **6.7** (UCB) was the most potent inhibitor of mutagen metabolism.

6.4 Experimental

Material and methods

The S9 fraction from pooled human and rat liver (Sigma Aldrich, Sydney, Australia; Cat No S2442 and S2067, Lot number 031M1399 and SLBG4796V, respectively) were used as a source of CYP enzymes. Potential inhibition of BPs (Frontier Scientific, USA) to **6.4** (Wako pure chemical industries, Japan) and **6.1** (Sigma Aldrich, Sydney, Australia) metabolism was assessed by measuring the degradation rate of **6.1** (B α P) and **6.4** (PhIP) in the absence and presence of BPs *in vitro*. Phosphate-buffered saline (PBS) 100 mL, 1M, pH 7.4 (stock solution) was created from 8 g NaCl (1.37 M), 0.2 g KCl (27 mM), 1.44 g Na₂HPO₄ (100 mM), 0.24 g KH₂PO₄ (18 mM). pH of PBS was adjusted to 7.4 with HCl and then sterilized by autoclaving for 20 min with steam water at 120 °C. The stock NADPH generating system, which increased CYP enzyme activity was prepared including fresh NADPH (26 mM), 66 mM glucose 6-phosphate, MgCl₂ (5 mM) and eight units/ml of glucose 6-phosphate dehydrogenase which was stored at 4 °C before performing the experiments with S9.^{259,279} The human liver S9 fraction was stored at -80 °C and then warmed to room temperature and kept on ice before use for S9 experiments at 37 °C.

The concentrations of BPs and mutagens were calculated using the absorption of UV light (λ_{\max} **6.7** = 450 nm, **6.8** = 375 nm, **6.6** = 409 nm). Analytical reverse phase high performance liquid chromatography (RPHPLC) was performed using a Shimadzu CLASS VP LCsolution system and software and a Waters 3.5 μ m C18 column (150 x 4.6 mm). Compound retention times (t_R) were obtained using gradient mixtures of MQ-water (solvent A) and MeOH (solvent B-Sigma Aldrich, Sydney, Australia) at 1 mL/min. An elution gradient for **6.4** (PhIP) was performed from 30% B to 70% B over 20 min returning to 30% B for 5 min and held for 5 min. After 5 injections, the HPLC analytical column was eluted with 100% B for 1 hour to remove any adsorbed BPs. An isocratic mobile phase of 90% B was used to elute **6.1** (B α P). Salts, BPs and remaining compounds adsorbed to the column were removed by pumping 30% B through the column for 10 min, followed by increased concentration of solvent B to 100% in 20 min, followed by washing in solvent B for another 1 hour. The eluent was monitored using a wavelength UV detector set at 317 nm for **6.4** (PhIP) and 385 nm for **6.1** (B α P). Low resolution mass spectra were acquired on a Bruker Esquire HCT spectrometer (positive and negative ion ESI mode). Kinetics and statistical analysis were performed using the Michaelis-Menten Equation and dose-response-inhibition on Graphpad Prism 6 software (La Jolla, CA, USA). The statistics was performed by the distribution of experimental data in around 95% confidence of the curve.

Molegro Virtual Docker 4.00 simulated an integrated environment for the prediction and examination of the interaction between ligands and crystal structures of the enzymes obtained from the protein data bank (PDB). Simulation software required 3D-structures of protein and ligands that were downloaded from the protein data bank. Structures of **6.1** (B α P), **6.4** (PhIP) and BPs were created from X-ray structures or ChemBio3D Ultra 13.0 with MM2 energy minimisation.

6.4.1 Metabolism of **6.1** and **6.4** in vitro

Determination of 6.1 and 6.4 concentrations in metabolism experiments

Experiments were conducted separately using the S9 testing method in which 20 μ g of S9 fraction (10 μ L) was mixed with 190 μ L of 100 mM potassium phosphate, pH 7.4, 3.3 mM of MgCl₂ 1.3 mM of NADPH 3.3 mM of glucose 6-phosphate and 0.4 U/mL of glucose 6-phosphate dehydrogenase. A wide range of **6.1** (B α P) and **6.4** (PhIP) concentrations were tested by adding stock solution (in DMSO) to the tubes in order to obtain final concentrations of 0.1 μ M, 0.25 μ M, 0.5 μ M, 1 μ M, 2 μ M, 3 μ M of **6.1** (B α P) and **6.4** (PhIP) for each experiment (DMSO concentration < 0.2%). The reaction mixtures were incubated at 37 °C for 20 min. Control reactions were performed using the same method; however 10 μ L of distilled water replaced the volume of the S9 fraction. All experiments were performed in triplicate. The reaction was stopped by adding 200 μ L of methanol to the reaction mixtures before storage at -20 °C. The S9 samples were centrifuged at 860 g (2800 rpm/min) for 5 min to isolate the cell suspension and the aqueous supernatant was used for HPLC analysis.

Determination of the optimal time to assess metabolism of 6.1 and 6.4

Experiments were performed using the method described above in the presence of 1.5 μ M of **6.1** (B α P) and **6.4** (PhIP). Assay tubes were incubated in 37 °C and a 200 μ L of sample from reaction mixtures were taken every 15 min for 45 min. To inhibit the metabolic action of enzymes, 200 μ L of methanol was added to the samples, which were vortexed and then stored in -20 °C prior to centrifugation and HPLC analysis. All experiments were conducted in triplicate.

6.4.2 The inhibitory effects of BPs on **6.1** and **6.4** degradation in vitro

In these experiments, each BP (**6.7**, **6.7** and **6.6**) was added to 200 μ L of S9 test mixtures in 7 tubes to obtain final BP concentrations of 0, 1.25, 2.5, 5, 10, 15 and 20 μ M. All tubes were incubated at 37 °C for 20 min, the experiments were stopped by adding 200 μ L of MeOH. The supernatant was isolated by centrifugation at 860 g for 5 min and stored at -20 °C prior to HPLC analysis.

Chapter 7: Conclusion and future direction

The studies of physical and chemical interactions between bile pigments (BPs) and polycyclic aromatic mutagens, described in the preceding chapters, were successful in determining the contributions of physical and chemical interactions on the inhibitory action of BPs on environmental mutagens. Each chapter describes in detail the significant findings of this PhD project. Chapter I demonstrates background knowledge of special chemical and physiological properties of BPs and mutagens. This chapter summarises and evaluates a vast range of studies on anti-mutagenic function of BPs. It also explains why our studies are key to understanding biological mechanisms occurring in vivo and facilitating future cancer research and drug developments.

The results presented in Chapter II support our hypothesis that the aggregates forming via π -stacking interactions leading to the modification of their UV and ^1H NMR spectra of polyaromatic mutagens and BPs were unlikely to occur in biological systems. All the slight modifications of ^1H NMR spectra of BPs and mutagens were determined by the changes in the protonation state of the compounds. It is unlikely that physical interactions are a major contributing mechanism to the anti-mutagenic effects of the BPs.

However, due to the low water solubility of the compounds, these studies were performed in the presence of organic solvents (DMSO, D_2O and MeOH) and there remains some uncertainty about what might occur in a biological system. Therefore, the study was performed further using a caco-2-cell monolayer in Chapter III.

The study was successful in using caco-2 cell monolayer to determine physical interactions between 2-Amino-1-methyl-6-phenylimidazo(4,5-b)pyridine (PhIP) and BPs (bilirubin, biliverdin, protoporphyrin) or bilirubin dimethyl ester or biliverdin dimethyl ester. The study explored novel physical interactions occurring between two aromatic ring systems of PhIP and BPs or BPs dimethyl esters. The interactions resulted in a slight change of apparent permeability of PhIP through the caco-2 cell monolayer. The higher absorption rate of PhIP in the presence of bilirubin suggested that carboxylic groups play an important role in the interactions with the polar surface of the caco-2 cell monolayer surface. Therefore, this study leads to the general conclusion that the physical interactions between aromatic rings of bilirubin, biliverdin, its dimethyl esters and PhIP supported the transport rate of PhIP crossing the cell monolayer. The interactions are a result of the formation of aggregations between aromatic rings of BPs with polycyclic aromatic rings of PhIP to maximise the exposure of hydrophilic property of the aggregates. The increase of the polarity facilitates the excretion of foreign agents from the body. The study also found the presence of

protoporphyrin did not affect the apparent permeability of PhIP or the physical interactions between the two compounds did not occur or were not strong enough for changing the apparent permeability.

Chapter IV outlines the previous methods used for synthesis of substituted pyrrole, dipyrroles and BPs dimethyl ester. Modification of the synthesis methods in order to obtain high yield of the desired products was successful. A number of compounds critical for current studies into the chemical reactivity of BPs were synthesised and characterised by ^1H NMR, ^{13}C NMR, ^1H - ^1H COSY, HSQC, HMBC, mp, ESIMS, TLC, GC-MS and UV spectroscopy. The full assignment of the ^1H and ^{13}C NMR characteristics of pyrrole, dipyrroles and BPs dimethyl ester will provide valuable guidance in NMR studies of BPs and their derivatives.

A previous finding (described in Chapter III) indicated the minor contribution of anti-mutagenic environments belonging to physical interactions between PhIP and BPs or its dimethyl esters. Therefore, the investigation of possible chemical reactions between activated mutagens and BPs is a focus of our study to elucidate the mechanism of this inhibition (Chapter V). Reactions between these two classes of compounds performed in biological systems both in vitro and in vivo produce very tiny amounts of products that can only be analysed by MS.^{121,122,222,272} Having a larger amount of products for structure analyses has been a challenge for biological studies. Therefore, developing and using a mimic of the biological conditions, as well as using more readily available compounds as mimics for the biologically generated compounds is a vital strategy in our study into the chemical interactions of BPs and mutagens. This study was successful in developing a set of conditions to mimic the biological conditions in which we explored some important novel aspects.

Firstly, indole and imidazole possess higher reactivity to the activated epoxide than guanine. The chemical interactions of BPs with styrene epoxide, the epoxide chosen to mimic the reactive epoxide metabolites of benzo[a]pyrene (B α P) and Aflatoxin B, were investigated. Secondly, our studies showed that the carboxylic groups on the BPs were the main sites of reaction with styrene epoxide. In addition, the aromatic ring system of BPs may also have made a minor contribution to the reaction of styrene epoxide with BPs, which may have contributed to their inhibition of the reaction of styrene epoxide with guanine. Our results clearly demonstrated that, under our in vitro reaction conditions, indole, imidazole, and all of BPs studied totally inhibited the reaction of styrene epoxide with guanine.

The reactions of styrene epoxide with BPs and model of PBs gave rise to 14 new compounds and five known compounds which were isolated and characterised by TLC, mp, HPLC, UV, GC/MS,

ESIMS, ^1H NMR and ^{13}C NMR. In addition, 11 components were detected from the products of guanine, BPs, BP dimethyl esters and substituted dipyrroles with styrene epoxide by ESIMS.

The major finding in our study of the reaction of BPs and styrene epoxide was that the site of reaction of BPs with the epoxide is the carboxylic acid groups and that other groups in the aromatic system of BPs may play a minor role. However, despite being poorly reactive toward the model epoxide, the dimethyl esters of the BPs completely protected guanine from reactions with the activated epoxide in competition reactions. This is in agreement with recent studies that have clearly shown that the bile pigment dimethyl esters are as effective inhibitors of mutagens in some biological systems as the parent BPs.^{19,186} Free carboxylic acid groups are ubiquitous in biological systems, thus it seems unlikely that this reaction is a major contributor to the unique inhibition activity exhibited by BPs towards the mutagenic effects of activated epoxides, while the major inhibitory action of BPs toward mutagenic environment remain a mystery.

Therefore, we decided to focus on the inhibition metabolism of mutagens of BPs in vitro by using the human liver S9 fraction in which the ability of BPs to inhibit mutagens (PhIP and B α P) degradation has successfully been explored. Preliminary data indicated the concentrations of PhIP and B α P that resulted in the saturation of PhIP and B α P degradative enzymes in the S9 mixtures. The results of the inhibition studies indicate that bilirubin had the greatest inhibitory effect on the metabolism of both PhIP and B α P, followed by protoporphyrin and then biliverdin.

Docking studies using published crystal structures of the CYP enzymes known to metabolise PhIP and B α P indicated multiple interactions between the mutagens and the BPs (inhibitors) with active site amino acids of the CYP1A1, 1A2, 2A6, 3A4. This provided new data to suggest that BPs could competitively inhibit mutagen binding to the active site of these enzymes. These data largely agreed with the in vitro data presented in this chapter VI, indicating that bilirubin was the most potent inhibitor of mutagen metabolism.

At the very least, our research goes some way to explaining why, though which mutagenic chemicals are commonly presented in our environment, the human cancer rate is relatively low. Our own physiology contains methods that protect us from these potentially damaging compounds.

Future work

The study introduced a new key method to explore the physical interactions occurring in biological system that can be used for testing all mutagenic environments (2-aminofluorene, aflatoxin B1, 2,4,7-TNFone and other mutagens) with the inhibitors in the future.

While the protective effects of BPs and their derivatives are now established, the nature of these compounds makes it unlikely that they could be developed as viable supplements or pharmaceuticals. Thus, the investigation of the anti-carcinogenic effects of substructures such as dipyrroles also requires an efficient and robust synthesis of the compounds. The long term aim of this area of study is to develop small molecules that can act to protect patients from the effects of environmental mutagens.

Human liver S9 contains a variety of different enzymes, which makes it difficult to identify which enzymes contribute to the metabolism of PhIP and B α P. Therefore, determining the contribution of each CYP enzyme to mutagen metabolism is vital for future studies in this area. The contribution of the various CYP enzymes in human liver S9 to PhIP and B α P metabolism could be determined by studying the inhibitory effects of known inhibitors of the various CYP enzymes hypothesised to be involved in the metabolism of the two mutagens (below). Known specific inhibitors include:

- a) α -naphthoflavone for CYP1A1 and CYP1A2;^{258,276}
- b) 2,3',4,5'-tetramethoxystilbene (TMS) for CYP1B;
- c) coumarin and methoxypsoralen for CYP2A; and
- d) midazolam and ketoconazole for CYP3A.

Once the contribution of specific CYP forms to PhIP and B α P metabolism has been determined, the inhibitory effects of BPs can be compared to these known inhibitors for a better understanding of which enzymes the BPs are targeting.

Another essential progression of this work is the expression and isolation of recombinant CYPs, or the use of human microsomes containing high activity of specific relevant CYPs. Inhibition studies using isolated enzymes would allow for accurate K_i values to be determined and thus a profile of the specificity of BPs as inhibitors of CYP enzymes could be generated. CYP enzymes are involved in many vital processes within the human body and thus, specificity of inhibition is a key to any potential these compounds may have as protective agents against environmental carcinogens. The use of recombinant proteins also opens the possibility of crystallisation of the proteins with BPs bound to the enzyme, which would allow evaluation of the accuracy of the simulated docking studies discussed above.

References

- (1) Wang, D. Q. H.; Carey, M. C.: Therapeutic uses of animal biles in traditional Chinese medicine: An ethnopharmacological, biophysical chemical and medicinal review. *World J. Gastroenterol.* **2014**, *20*, 9952-9975.
- (2) Bulmer, A.: Efficacy of bile pigment supplementation: In vitro and in vivo considerations. The University of Queensland, School of Human Movement Studies, 2008.
- (3) Shapiro, S. M.: Bilirubin toxicity in the developing nervous system. *Pediatr. Neurol.* **2003**, *29*, 410-421.
- (4) Wang, X.; Chowdhury, J. R.; Chowdhury, N. R.: Bilirubin metabolism: Applied physiology. *Curr. Paediatr.* **2005**, *16*, 70-74.
- (5) Seyfried, H.; Klicpera, M.; Leithner, C.; Penner, E.: Bilirubin metabolism (author's transl). *Wien. Klin. Wochenschr.* **1976**, *88*, 477.
- (6) Robinson, S. H.: The Origins of Bilirubin. *N. Engl. J. Med.* **1968**, *279*, 143-149.
- (7) Maddrey, W. C.; Schiff, E. R.; Sorrell, M. F.: *Schiff's diseases of the liver*; Lippincott Williams & Wilkins: Philadelphia, 2007.
- (8) Adachi, Y.; Inufusa, H.; Yamashita, M.; Kambe, A.; Yamazaki, K.; Sawada, Y.; Yamamoto, T.: Clinical application of serum bilirubin fractionation by simplified liquid chromatography. *Clin. Chem.* **1988**, *34*, 385-388.
- (9) McDonagh, A. F.: Turning green to gold. *Nat. Struct. Biol.* **2001**, *8*, 198-200.
- (10) McDonagh, A. F.; Palma, L. A.: Preparation and properties of crystalline biliverdin IX alpha. Simple methods for preparing isomerically homogeneous biliverdin and [¹⁴C]biliverdin by using 2,3-dichloro-5,6-dicyanobenzoquinone. *Biochem. J* **1980**, *189*, 193-208.
- (11) Matcham, G. W. J.; Battersby, A. R.; McDonald, E.; Fookes, C. J. R.: Biosynthesis of the pigments of life: formation of the macrocycle. *Nature* **1980**, *285*, 17-21.
- (12) Leeper, F. J.: The biosynthesis of porphyrins, chlorophylls, and vitamin B12. *Nat. Prod. Rep.* **1989**, *6*, 171-203.
- (13) Layer, G.; Reichelt, J.; Jahn, D.; Heinz, D. W.: Structure and function of enzymes in haem biosynthesis. *Protein Sci.* **2010**, *19*, 1137-1161.
- (14) Bulmer, A. C.; Ried, K.; Coombes, J. S.; Blanchfield, J. T.; Toth, I.; Wagner, K. H.: The anti-mutagenic and antioxidant effects of bile pigments in the Ames Salmonella test. *Mutat. Res. Genet. Toxicol. Environ. Mutagen* **2007**, *629*, 122-132.
- (15) Bulmer, A. C.; Ried, K.; Blanchfield, J. T.; Wagner, K. H.: The anti-mutagenic properties of bile pigments. *Mutat. Res.* **2008**, *658*, 28-41.

References

- (16) Lightner, D. A.; Cu, A.: On the autoxidation of bilirubin. *Biochem. Biophys. Res. Commun.* **1976**, *69*, 648.
- (17) Rao, P.; Suzuki, R.; Mizobuchi, S.; Yamaguchi, T.; Sasaguri, S.: Bilirubin exhibits a novel anti-cancer effect on human adenocarcinoma. *Biochem. Biophys. Res. Commun.* **2006**, *342*, 1279-1283.
- (18) Bulmer, A. C.; Ried, K.; Coombes, J. S.; Blanchfield, J. T.; Toth, I.; Wagner, K. H.: The anti-mutagenic and antioxidant effects of bile pigments in the Ames Salmonella test. *Mutat. Res. Genet. Toxicol. Environ. Mutagen* **2007**, *629*, 122-132.
- (19) Mölzer, C.; Huber, H.; Steyrer, A.; Ziesel, G. V.; Wallner, M.; Hong, H. T.; Blanchfield, J. T.; Bulmer, A. C.; Wagner, K. H.: Bilirubin and related tetrapyrroles inhibit food-borne mutagenesis: A mechanism for antigenotoxic action against a model epoxide. *J. Nat. Prod.* **2013**, *76*, 1958-1965.
- (20) Mölzer, C.; Huber, H.; Steyrer, A.; Ziesel, G.; Ertl, A.; Plavotic, A.; Wallner, M.; Bulmer, A. C.; Wagner, K.-H.: In vitro antioxidant capacity and antigenotoxic properties of protoporphyrin and structurally related tetrapyrroles. *Free Radical Res.* **2012**, *46*, 1369-1377.
- (21) Mölzer, C.; Huber, H.; Steyrer, A.; Ziesel, G. V.; Wallner, M.; Goncharova, I.; Orlov, S.; Urbanová, M.; Ahlfors, C. E.; Vitek, L.; Bulmer, A. C.; Wagner, K.-H.: Interaction between TNF α and tetrapyrroles may account for their anti-genotoxic effects - A novel mechanism for DNA-protection. *J. Porphyrins Phthalocyanines* **2013**, *17*, 1157-1166.
- (22) Stocker, R.: Antioxidant activities of bile pigments. *Antioxid. Redox Signaling* **2004**, *6*, 841-849.
- (23) Laokuldilok, T.; Shoemaker, C. F.; Jongkaewwattana, S.; Tulyathan, V.: Antioxidants and Antioxidant Activity of Several Pigmented Rice Brans. *J. Agric. Food Chem.* **2011**, *59*, 193-199.
- (24) Yamaguchi, T.; Sugimoto, A.: Diversity and anti-oxidative effects of bilirubin. *Seikagaku* **2003**, *75*, 224-233.
- (25) Mireles, L. C.; Lum, M. A.; Dennery, P. A.: Antioxidant and cytotoxic effects of bilirubin on neonatal erythrocytes. *Pediatr. Res.* **1999**, *45*, 355-362.
- (26) Asad, S. F.; Singh, S.; Ahmad, A.; Khan, N. U.; Hadi, S. M.: Prooxidant and antioxidant activities of bilirubin and its metabolic precursor biliverdin: a structure-activity study. *Chem.-Biol. Interact.* **2001**, *137*, 59-74.

References

- (27) Maghzal, G. J.; Leck, M.-C.; Collinson, E.; Li, C.; Stocker, R.: Limited Role for the Bilirubin-Biliverdin Redox Amplification Cycle in the Cellular Antioxidant Protection by Biliverdin Reductase. *J. Biol. Chem.* **2009**, *284*, 29251-29259.
- (28) McCaughan, D.; Au, C.; Benedetto, A.; Milatovic, D.; Aschner, J.; Aschner, M.: Antioxidant properties of bilirubin in the model organism, *Caenorhabditis elegans*. *Int. J. Neuroprot. Neuroregener.* **2008**, *4*, 252-262.
- (29) Phelan, D.; Winter, G. M.; Rogers, W. J.; Lam, J. C.; Denison, M. S.: Activation of the Ah Receptor Signal Transduction Pathway by Bilirubin and Biliverdin. *Arch. Biochem. Biophys.* **1998**, *357*, 155-163.
- (30) Abu-Bakar, A. e.; Arthur, D. M.; Wikman, A. S.; Rahnasto, M.; Juvonen, R. O.; Vepsäläinen, J.; Raunio, H.; Ng, J. C.; Lang, M. A.: Metabolism of bilirubin by human cytochrome P450 2A6. *Toxicol. Appl. Pharmacol.* **2012**, *261*, 50-58.
- (31) Tanii, H.; Shitara, Y.; Torii, M.; Sekine, S.; Iwata, H.; Horie, T.: Induction of Cytochrome P450 2A6 by Bilirubin in Human Hepatocytes. *J. Pharm. Pharmacol.* **2013**, *4*, 182-190.
- (32) MacLean, P. D.; Chapman, E. E.; Dobrowolski, S. L.; Thompson, A.; Barclay, L. R. C.: Pyrroles as antioxidants: solvent effects and the nature of the attacking radical on antioxidant activities and mechanisms of pyrroles, dipyrinones, and bile pigments. *J. Org. Chem.* **2008**, *73*, 6623-6635.
- (33) Stocker, R.; Yamamoto, Y.; McDonagh, A. F.; Glazer, A. N.; Ames, B. N.: Bilirubin is an antioxidant of possible physiological importance. *Science (New York, N.Y.)* **1987**, *235*, 1043-1046.
- (34) Arimoto, S.; Kan-yama, K.; Rai, H.; Hayatsu, H.: Inhibitory effect of hemin, chlorophyllin and related pyrrole pigments on the mutagenicity of benzo[a]pyrene and its metabolites. *Mutat Res-genet Tox* **1995**, *345*, 127-135.
- (35) Arimoto, S.; Negishi, T.; Hayatsu, H.: Inhibitory effect of hemin on the mutagenic activities of carcinogens. *Cancer Lett* **1980**, *11*, 29-33.
- (36) Tang, X.; Edenharder, R.: Inhibition of the mutagenicity of 2-nitrofluorene, 3-nitrofluoranthene and 1-nitropyrene by vitamins, porphyrins and related compounds, and vegetable and fruit juices and solvent extracts. *Food Chem. Toxicol.* **1997**, *35*, 373-378.
- (37) Arimoto, S.; Ohara, Y.; Namba, T.; Negishi, T.; Hayatsu, H.: Inhibition of the mutagenicity of amino acid pyrolysis products by hemin and other biological pyrrole pigments. *Biochem. Biophys. Res. Commun.* **1980**, *92*, 662-668.

References

- (38) Haino, T.; Fujii, T.; Watanabe, A.; Takayanagi, U.: *Supramolecular polymer formed by reversible self-assembly of tetrakisporphyrin*; National Academy of Sciences, 2009; Vol. 106.
- (39) Bock, K. W.: Homeostatic control of xeno- and endobiotics in the drug-metabolizing enzyme system. *Biochem. Pharmacol.* **2014**, *90*, 1-6.
- (40) Chang, J.-L.; Bigler, J.; Schwarz, Y.; Li, S. S.; Li, L.; King, I. B.; Potter, J. D.; Lampe, J. W.: UGT1A1 polymorphism is associated with serum bilirubin concentrations in a randomized, controlled, fruit and vegetable feeding trial. *J. Nutr.* **2007**, *137*, 890-897.
- (41) Shibuya, A.; Itoh, T.; Tukey, R. H.; Fujiwara, R.: Impact of fatty acids on human UDP-glucuronosyltransferase 1A1 activity and its expression in neonatal hyperbilirubinemia. *Sci. Rep.* **2013**, *3*, 2903.
- (42) Rowland, A.; Miners, J. O.; Mackenzie, P. I.: The UDP-glucuronosyltransferases: Their role in drug metabolism and detoxification. *Int. J. Biochem. Cell Biol.* **2013**, *45*, 1121-1132.
- (43) Abu-Bakar, A. e.; Moore, M. R.; Lang, M. A.; Medicinska och farmaceutiska, v.; Uppsala, u.; Institutionen för farmaceutisk, b.; Farmaceutiska, f.: Evidence for induced microsomal bilirubin degradation by cytochrome P450 2A5. *Biochem. Pharmacol.* **2005**, *70*, 1527-1535.
- (44) Pons, N.; Pipino, S.; De Matteis, F.: Interaction of polyhalogenated compounds of appropriate configuration with mammalian or bacterial CYP enzymes: Increased bilirubin and uroporphyrinogen oxidation in vitro. *Biochem. Pharmacol.* **2003**, *66*, 405-414.
- (45) Sinal, C. J.; Bend, J. R.: Aryl Hydrocarbon Receptor-Dependent Induction of Cyp1a1 by Bilirubin in Mouse Hepatoma Hepa 1c1c7 Cells. *Mol. Pharmacol.* **1997**, *52*, 590-599.
- (46) *Developments in Tryptophan and Serotonin Metabolism*; Springer US, 2003.
- (47) Kapitulnik, J.; Gonzalez, F. J.: Marked endogenous activation of the CYP1A1 and CYP1A2 genes in the congenitally jaundiced Gunn rat. *Mol. Pharmacol.* **1993**, *43*, 722-725.
- (48) Rendic, S.: Summary of information on human CYP enzymes: human P450 metabolism data. *Drug Metab Rev* **2002**, *34*, 83-448.
- (49) Abu-Bakar, A. e.; Hakkola, J.; Juvonen, R.; Rahnasto-Rilla, M.; Raunio, H.; Lang, M. A.: Function and Regulation of the Cyp2a5/CYP2A6 Genes in Response to Toxic Insults in the Liver. *Curr. Drug Metab.* **2013**, *14*, 137-150.
- (50) Inui, H.; Itoh, T.; Yamamoto, K.; Ikushiro, S. I.; Sakaki, T.: Mammalian Cytochrome P450-Dependent Metabolism of Polychlorinated Dibenzo-p-dioxins and Coplanar Polychlorinated Biphenyls. *Int. J. Mol. Sci.* **2014**, *15*, 14044-14057.
- (51) Nguyen, L. P.; Bradfield, C. A.: The search for endogenous activators of the aryl hydrocarbon receptor. *Chem. Res. Toxicol.* **2008**, *21*, 102-116.

References

- (52) Shapiro, S. M.: Chronic bilirubin encephalopathy: diagnosis and outcome. *Semin Fetal Neonatal Med* **2010**, *15*, 157-163.
- (53) Chernecky, C. C.; Berger, B. J.: *Laboratory tests and diagnostic procedures*; Elsevier: St. Louis, Mo, 2013.
- (54) Golonka, D.: Digestive Disorders Health Center: Bilirubin. WebMD, 2013; Vol. 2014; pp Bilirubin levels in adults.
- (55) Julian Barth, J. K. R., Denielle Freedman: Harmonisation of reference intervals. *Clinical Biochemistry*, 2011; Vol. 2014; pp Agreed Adult Clinical Biochemistry Reference Intervals.
- (56) Stocker, R.: Antioxidant activities of bile pigments. *Antioxid. Redox Signaling* **2004**, *6*, 841-849.
- (57) Lightner, D. A.: *Bilirubin : Jekyll and Hyde Pigment of Life*; Springer Vienna: Dordrecht, 2013.
- (58) Dey, S. K.; Lightner, D. A.: Toward an amphiphilic bilirubin: the crystal structure of a bilirubin e-isomer. *J. Org. Chem.* **2008**, *73*, 2704-2714.
- (59) McDonagh, A. F.: Bilirubin photo-isomers: regiospecific acyl glucuronidation in vivo. *Monatsh. Chem.* **2014**, *145*, 465-482.
- (60) Brodersen, R.: Bilirubin. Solubility and interaction with albumin and phospholipid. *J. Biol. Chem.* **1979**, *254*, 2364.
- (61) Ostrow, J. D.; Pascolo, L.; Brites, D.; Tiribelli, C.: Molecular basis of bilirubin-induced neurotoxicity. *Trends Mol. Med* **2004**, *10*, 65-70.
- (62) Fog, J.; Jellum, E.: Structure of bilirubin. *Nature* **1963**, *198*, 88-89.
- (63) Holmes, D. L.: On the Acid Dissociation Constants of Bilirubin and Biliverdin. *J. Biol. Chem.* **1996**, *271*, 2397-2405.
- (64) Boiadjev, S. E.; Person, R. V.; Lightner, D. A.: synthesis, intramolecular hydrogen-bonding and conformation of optically-active bilirubin amides-analysis by circular-dichroism and NMR. *Tetrahedron: Asymmetry* **1993**, *4*, 491-510.
- (65) Pescitelli, G.; Di Bari, L.; Berova, N.: Conformational aspects in the studies of organic compounds by electronic circular dichroism. *Chem. Soc. Rev.* **2011**, *40*, 4603-4625.
- (66) Falk o. Univ.-Prof. Dr. phil, H.: *Chemistry of Linear Oligopyrroles and Bile Pigments*; Springer Vienna, 1989.
- (67) Yokoyama, T.; Ogino, T.; Onishi, S.; Isobe, K.; Itoh, S.; Yamakawa, T.: Significance of the endo-vinyl group of bilirubin in photochemical reactions. *Biochem. J* **1984**, *220*, 377-383.

References

- (68) Onishi, S.; Itoh, S.; Kawade, N.; Isobe, K.; Sugiyama, S.: The separation of configurational isomers of bilirubin by high pressure liquid chromatography and the mechanism of jaundice phototherapy. *Biochem. Biophys. Res. Commun.* **1979**, *90*, 890.
- (69) Lightner, D. A.: *Bilirubin: Jekyll and Hyde Pigment of Life : Pursuit of Its Structure Through Two World Wars to the New Millenium*; Springer Vienna: Vienna, 2013; Vol. 98.
- (70) McDonagh, A. F.: Light Effects on Transport and Excretion of Bilirubin in Newborns. *Ann.NY Acad.Sci.* **1985**, *453*, 65-72.
- (71) Knobloch, E.; Hodr, R.; Herzmann, J.; Houdková, V.: Kinetics of the formation of biliverdin during the photochemical oxidation of bilirubin monitored by column liquid chromatography. *J. Chromatogr.* **1986**, *375*, 245.
- (72) McDonagh, A. F.; Assisi, F.: The ready isomerization of bilirubin IX- in aqueous solution. *Biochem. J.* **1972**, *129*, 797-800.
- (73) McDonagh, A. F.: Thermal and photochemical reactions of bilirubin IX α . *Ann. N.Y. Acad. Sci.* **1975**, *244*, 553-569.
- (74) Yamaguchi, T.; Nakajima, H.: Changes in the composition of bilirubin-IX isomers during human prenatal development. *Eur. J. Biochem.* **1995**, *233*, 467-472.
- (75) Yamaguchi, T.; Komoda, Y.; Nakajima, H.: Biliverdin-IX alpha reductase and biliverdin-IX beta reductase from human liver. Purification and characterization. *J. Biol. Chem.* **1994**, *269*, 24343-24348.
- (76) Le Bas, G.; Allegret, A.; Mauguen, Y.; de Rango, C.; Bailly, M.: The structure of triclinic bilirubin chloroform-methanol solvate. *Acta Cryst. B* **1980**, *36*, 3007-3011.
- (77) Ostrow, J. D.; Celic, L.; Mukerjee, P.: Molecular and micellar associations in the pH-dependent stable and metastable dissolution of unconjugated bilirubin by bile salts. *J. Lipid Res.* **1988**, *29*, 335-348.
- (78) Ghosh, B.; Catalano, V. J.; Lightner, D. A.: Crystal Structure and Conformation of a Bilirubin Ester. *Monatsh. Chem.* **2004**, *135*, 1503-1517.
- (79) Ding, Z. K.; Xu, Y. Q.: Purification and Characterization of Biliverdin IX α from Atlantic Salmon (*Salmo salar*) Bile. *Biochemistry (Moscow, Russ. Fed.)* **2002**, *67*, 927-932.
- (80) Bulmer, A. C.; Ried, K.; Coombes, J. S.; Blanchfield, J. T.; Toth, I.; Wagner, K. H.: The anti-mutagenic and antioxidant effects of bile pigments in the Ames Salmonella test. *Mutat. Res., Genet. Toxicol. Environ. Mutagen.* **2007**, *629*, 122-132.
- (81) Bulmer, A. C.: The efficacy of bile pigment supplementation: in vitro and in vivo considerations. The University of Queensland, 2008.

References

- (82) Bach, F. H.; Csizmadia, E.; Erat, A.; Öllinger, R.; Thomas, M.; Yamashita, K.; Bilban, M.; Kogler, P.; Margreiter, R.; Usheva, A.: Bilirubin and Biliverdin Treatment of Atherosclerotic Diseases. *Cell cycle* **2007**, *6*, 39-43.
- (83) Matysik, J.; Hildebrandt, P.; Smit, K.; Mark, F.; Gärtner, W.; Braslavsky, S. E.; Schaffner, K.; Schrader, B.: Raman spectroscopic analysis of isomers of biliverdin dimethyl ester. *J. Pharm. Biomed. Anal.* **1997**, *15*, 1319-1324.
- (84) Holt, R. E.; Farrens, D. L.; Song, P. S.; Cotton, T. M.: Surface-enhanced resonance Raman scattering (SERRS) spectroscopy applied to phytochrome and its model compounds. I. Biliverdin photoisomers. *J. Am. Chem. Soc.* **1989**, *111*, 9156-9162.
- (85) Leeper, F. J.: The biosynthesis of porphyrins, chlorophylls, and vitamin B12. *Nat. Prod. Rep.* **1985**, *2*, 19-47.
- (86) Shemin, D.; Rittenberg, D.: The biological utilization of glycine for the synthesis of the protoporphyrin of hemoglobin. *J. Biol. Chem.* **1946**, *166*, 621.
- (87) Ajioka, R. S.; Phillips, J. D.; Kushner, J. P.: Biosynthesis of haem in mammals. *BBA - Molecular Cell Research* **2006**, *1763*, 723-736.
- (88) Bhosale, S. V.; Bhosale, S. V.; Shitre, G. V.; Bobe, S. R.; Gupta, A.: Supramolecular Chemistry of Protoporphyrin IX and Its Derivatives. *Eur. J. Org. Chem.* **2013**, *2013*, 3939.
- (89) Cox, G. S.; Krieg, M.; Whitten, D. G.: Self-sensitized photooxidation of protoporphyrin IX derivatives in aqueous surfactant solutions: Product and mechanistic studies. *J. Am. Chem. Soc.* **1982**, *104*, 6930-6937.
- (90) Cox, G. S.; Krieg, M.; Whitten, D. G.: Photochemical reactivity in organized assemblies.30. sele-sensitized photo-oxidation of photoporphyrin-IX derivatives in aqueous surfactant solution-product and mechanism studies. *J. Am. Chem. Soc.* **1982**, *104*, 6930-6937.
- (91) Kaiserman, M. J.; Rickert, W. S.: Carcinogens in tobacco smoke: benzo[a]pyrene from Canadian cigarettes and cigarette tobacco. *Am. J. Public Health* **1992**, *82*, 1023-1026.
- (92) Shim, G. A.; Lee, B. M.: Dietary Exposure Estimation of Benzo[a]pyrene and Cancer Risk Assessment. *J. Toxicol. Environ. Health* **2007**, *70*, 1391-1394.
- (93) Aygun, S. F.; Kabad, F.: Determination of benzo[a]pyrene in charcoal grilled meat samples by HPLC with fluorescence detection. *Int J Food Sci Nutr* **2005**, *56*, 581.
- (94) Le Marchand, L.; Hankin, J. H.; Pierce, L. M.; Sinha, R.; Nerurkar, P. V.; Franke, A. A.; Wilkens, L. R.; Kolonel, L. N.; Donlon, T.; Seifried, A.; Custer, L. J.; Lum-Jones, A.; Chang, W.: Well-done red meat, metabolic phenotypes and colorectal cancer in Hawaii. *Mutat Res Fund Mol Mech Mut* **2002**, *506-507*, 205-214.

References

- (95) Gloria Y. Kwei, J. Z., Susan E. Irwin, Ronald G. Thurman, and Frederick C. Kauffman: Conjugation of Benzo(a)pyrene 7,8-dihydrodiol-9,10-epoxide in Infant Swiss-Webster Mice. *Cancer Res* **1992**, *52*, 1639-1642.
- (96) Kennedy, C. J.; Gill, K. A.; Walsh, P. J.: Thermal modulation of benzo[a]pyrene metabolism by the gulf toadfish, *Opsanus beta*. *Aquat. Toxicol.* **1989**, *15*, 331-343.
- (97) Frank, E. G.; Sayer, J. M.; Kroth, H.; Ohashi, E.; Ohmori, H.; Jerina, D. M.; Woodgate, R.: Translesion replication of benzo[a]pyrene and benzo[c]phenanthrene diol epoxide adducts of deoxyadenosine and deoxyguanosine by human DNA polymerase ϵ . *Nucleic Acids Res.* **2002**, *30*, 5284-5292.
- (98) Ennever, J. F.; McDonagh, A. F.; Speck, W. T.: Phototherapy for neonatal jaundice: optimal wavelengths of light. *J. Pediatr.* **1983**, *103*, 295-299.
- (99) Kushman, M. E.; Kabler, S. L.; Fleming, M. H.; Ravoori, S.; Gupta, R. C.; Doehmer, J.; Morrow, C. S.; Townsend, A. J.: Expression of human glutathione S-transferase P1 confers resistance to benzo[a]pyrene or benzo[a]pyrene-7,8-dihydrodiol mutagenesis, macromolecular alkylation and formation of stable N2-Gua-BPDE adducts in stably transfected V79MZ cells co-expressing hCYP1A1. *Carcinogenesis.* **2007**, *28*, 207-214.
- (100) Bauer, J.; Xing, G.; Yagi, H.; Sayer, J. M.; Jerina, D. M.; Ling, H.: A structural gap in Dpo4 supports mutagenic bypass of a major benzo[a]pyrene dG adduct in DNA through template misalignment (vol 104, pg 14905, 2007). *Proc. Natl. Acad. Sci. U. S. A.* **2007**, *104*, 17240-17240.
- (101) Bauer, J.; Xing, G.; Yagi, H.; Sayer, J. M.; Jerina, D. M.; Ling, H.: A structural gap in Dpo4 supports mutagenic bypass of a major benzo[a]pyrene dG adduct in DNA through template misalignment. *Proc Natl Acad Sci U S A* **2007**, *104*, 14905-14910.
- (102) Campbell, S. C.: *Benzo(a)pyrene and benzo(a)pyrene-induced protein adducts in hair as biomarkers of toxic benzo(a)pyrene exposures*, 2011; Vol. 72.
- (103) Monographs, T. I.: Agents Classified by the IARC Monographs. 2014 ed.; Mattock, H., Ed.; <http://monographs.iarc.fr/ENG/Classification/ClassificationsAlphaOrder.pdf>, 2014.
- (104) Rojas, M.; Marie, B.; Vignaud, J. M.; Martinet, N.; Siat, J.; Grosdidier, G.; Cascorbi, I.; Alexandrov, K.: High DNA damage by benzo[a]pyrene 7,8-diol-9,10-epoxide in bronchial epithelial cells from patients with lung cancer: comparison with lung parenchyma. *Cancer letters* **2004**, *207*, 157-163.
- (105) Rechkoblit, O.; Kolbanovskiy, A.; Malinina, L.; Geacintov, N. E.; Broyde, S.; Patel, D. J.: Mechanism of error-free and semitargeted mutagenic bypass of an aromatic amine lesion by Y-family polymerase Dpo4. *Nat Struct Mol Biol* **2010**, *17*, 379-88.

References

- (106) Ross, M. K.; Said, B.; Shank, R. C.: DNA-damaging effects of genotoxins in mixture: modulation of covalent binding to DNA. *Toxicol. Sci.* **2000**, *53*, 224-236.
- (107) Isola, V. J.; Hartman, T. C.; Trumble, S. J.; Ruzek, M. C.; Gentile, J. M.: Metabolism of 2-aminofluorene by human polymorphonuclear leukocytes: more evidence for the association between inflammation and cancer. *Environ. Health Perspect.* **1993**, *101 Suppl 3*, 27-31.
- (108) Williams, G. M.; Duan, J.-D.; Iatropoulos, M. J.; Kobets, T.: A no observed adverse effect level for DNA adduct formation in rat liver with prolonged dosing of the hepatocarcinogen 2-acetylaminofluorene. *Toxicol Res* **2015**, *4*, 233-24.
- (109) Verna, L.; Whysner, J.; Williams, G. M.: 2-Acetylaminofluorene mechanistic data and risk assessment: DNA reactivity, enhanced cell proliferation and tumor initiation. *Pharmacol Ther* **1996**, *71*, 83-105.
- (110) Eckel, L. M.; Krugh, T. R.: 2-aminofluorene modified DNA duplex exists in 2 interchangeable conformations. *Nat. Struct. Biol.* **1994**, *1*, 89-94.
- (111) Boyd, J. A.; Eling, T. E.: Evidence for a one-electron mechanism of 2-aminofluorene oxidation by prostaglandin H synthase and horseradish peroxidase. *J. Biol. Chem.* **1984**, *259*, 13885.
- (112) Böge, N.; Jacobsen, M. I.; Szombati, Z.; Baerns, S.; Di Pasquale, F.; Marx, A.; Meier, C.: Synthesis of DNA strands site-specifically damaged by c8-arylamine purine adducts and effects on various DNA polymerases. *Chem.--Eur. J.* **2008**, *14*, 11194-11208.
- (113) Stillwell, W. G.; Turesky, R. J.; Sinha, R.; Skipper, P. L.; Tannenbaum, S. R.: Biomonitoring of heterocyclic aromatic amine metabolites in human urine. *Cancer Lett* **1999**, *143*, 145-148.
- (114) Tang, D.; Liu, J. J.; Bock, C. H.; Neslund-Dudas, C.; Rundle, A.; Savera, A. T.; Yang, J. J.; Nock, N. L.; Rybicki, B. A.: Racial differences in clinical and pathological associations with PhIP-DNA adducts in prostate. *Int J Cancer* **2007**, *121*, 1319-1324.
- (115) Bennion, B. J.; Cosman, M.; Lightstone, F. C.; Knize, M. G.; Montgomery, J. L.; Bennett, L. M.; Felton, J. S.; Kulp, K. S.: PhIP carcinogenicity in breast cancer: Computational and experimental evidence for competitive interactions with human estrogen receptor. *Chem. Res. Toxicol.* **2005**, *18*, 1528-1536.
- (116) Ishibe, N.; Sinha, R.; Hein, D. W.; Kulldorff, M.; Strickland, P.; Fretland, A. J.; Chow, W. H.; Kadlubar, F. F.; Lang, N. P.; Rothman, N.: Genetic polymorphisms in heterocyclic amine metabolism and risk of colorectal adenomas. *Pharmacogenetics* **2002**, *12*, 145-150.
- (117) Xu, M.; Dashwood, R. H.: Chemoprevention studies of heterocyclic amine-induced colon carcinogenesis. *Cancer Lett* **1999**, *143*, 179-183.

References

- (118) Peluso, M.; Castegnaro, M.; Malaveille, C.; Friesen, M.; Garren, L.; Hautefeuille, A.; Vineis, P.; Kadlubar, F.; Bartsch, H.: 32 postlabelling analysis of urinary mutagens from smokers of black tobacco implicates 2-amino-1-methyl-6-phenylimidazo[4,5-b]pyridine (PhIP) as a major DNA-damaging agent. *Carcinogenesis* **1991**, *12*, 713-717.
- (119) Felton, J. S.; Malfatti, M. A.; Knize, M. G.; Salmon, C. P.; Hopmans, E. C.; Wu, R. W.: Health risks of heterocyclic amines. *Mutat Res Fund Mol Mech Mut* **1997**, *376*, 37-41.
- (120) Kim, D.; Lee, Y.-J.; Ryu, H.-Y.; Lee, J.-H.; Kim, H.-K.; Kim, E.; Moon, J.-D.; Chang, D. D.; Yoon, H.-S.: Genetic polymorphisms in metabolism of 2-amino-1-methyl-6-phenylimidazo[4,5-b] pyridine. *J. Appl. Toxicol.* **2013**, *33*, 1.
- (121) Zhao, K.; Murray, S.; Davies, D. S.; Boobis, A. R.; Gooderham, N. J.: Metabolism of the food derived mutagen and carcinogen 2-amino-1-methyl-6-phenylimidazo(4,5-b)pyridine (PhIP) by human liver microsomes. *Carcinogenesis* **1994**, *15*, 1285-1288.
- (122) Crofts, F. G.; Sutter, T. R.; Strickland, P. T.: Metabolism of 2-amino-1-methyl-6-phenylimidazo[4,5-b]pyridine by human cytochrome P4501A1, P4501A2 and P4501B1. *Carcinogenesis* **1998**, *19*, 1969-1973.
- (123) Felton, J. S.; Knize, M. G.; Wu, R. W.; Colvin, M. E.; Hatch, F. T.; Malfatti, M. A.: Mutagenic potency of food-derived heterocyclic amines. *Mutat. Res.* **2007**, *616*, 90-94.
- (124) Bendaly, J.; Metry, K. J.; Doll, M. A.; Jiang, G.; States, J. C.; Smith, N. B.; Neale, J. R.; Holloman, J. L.; Pierce, W. M., Jr.; Hein, D. W.: Role of human CYP1A1 and NAT2 in 2-amino-1-methyl-6-phenylimidazo[4,5-b]pyridine-induced mutagenicity and DNA adducts. *Xenobiotica* **2009**, *39*, 399-406.
- (125) Gu, D.; Turesky, R. J.; Tao, Y.; Langouët, S. A.; Nauwelaërs, G. C.; Yuan, J.-M.; Yee, D.; Yu, M. C.: DNA adducts of 2-amino-1-methyl-6-phenylimidazo[4,5-b]pyridine and 4-aminobiphenyl are infrequently detected in human mammary tissue by liquid chromatography/tandem mass spectrometry. *Carcinogenesis* **2012**, *33*, 124-130.
- (126) So, M.; Schenkman, J. B.; Rusling, J. F.: Electrochemical biosensor featuring a two-enzyme pathway and DNA for screening toxic reactive metabolites of arylamines. *Chem. Commun.* **2008**, 4354-4356.
- (127) Cheung, C.; Ma, X.; Krausz, K. W.; Kimura, S.; Feigenbaum, L.; Dalton, T. P.; Nebert, D. W.; Idle, J. R.; Gonzalez, F. J.: Differential Metabolism of 2-Amino-1-methyl-6-phenylimidazo[4,5-b]pyridine (PhIP) in Mice Humanized for CYP1A1 and CYP1A2. *Chem. Res. Toxicol.* **2005**, *18*, 1471-1478.
- (128) Fogh, J.: New Human Tumor Cell Lines. Springer US, 1975; pp 115-159.

References

- (129) Pinto, M.; Robine Leon, S.; Appay, M. D.: Enterocyte-like differentiation and polarization of the human colon carcinoma cell line Caco-2 in culture. *Biology of the Cell* **1983**, *47*, 323-330.
- (130) Hidalgo, I. J.; Raub, T. J.; Borchardt, R. T.: Characterization of the human colon carcinoma cell line (Caco-2) as a model system for intestinal epithelial permeability. *Gastroenterology* **1989**, *96*, 736-749.
- (131) Yamashita, S.; Furubayashi, T.; Kataoka, M.; Sakane, T.; Sezaki, H.; Tokuda, H.: Optimized conditions for prediction of intestinal drug permeability using Caco-2 cells. *Eur. J. Pharm. Sci.* **2000**, *10*, 195-204.
- (132) Demirbas Ucpinar, S.: Oligonucleotides and protease inhibitors transport across CaCo-2 cell monolayers-permeability effects of dimethylsulfoxide and citicholine. ProQuest, UMI Dissertations Publishing, 2000.
- (133) Hilgers, A. R.; Conradi, R. A.; Burton, P. S.: Caco-2 cell monolayers as a model for drug transport across the intestinal mucosa. *Pharm. Res.* **1990**, *7*, 902-910.
- (134) Galkin, A.; Fallarero, A.; Vuorela, P. M.: Coumarins permeability in Caco-2 cell model. *J. Pharm. Pharmacol.* **2009**, *61*, 177-184.
- (135) Willenberg, I.; von Elsner, L.; Steinberg, P.; Schebb, N. H.: Development of an online-SPE-LC-MS method for the investigation of the intestinal absorption of 2-amino-1-methyl-6-phenylimidazo[4,5-b]pyridine (PHIP) and its bacterial metabolite PHIP-M1 in a Caco-2 Transwell system. *Food Chem.* **2015**, *166*, 537.
- (136) Kitchens, K. M.; Kolhatkar, R. B.; Swaan, P. W.; Ghandehari, H.: Endocytosis inhibitors prevent poly(amidoamine) dendrimer internalization and permeability across Caco-2 cells. *Mol. Pharm.* **2008**, *5*, 364-369.
- (137) Yee, S.: In Vitro Permeability Across Caco-2 Cells (Colonic) Can Predict In Vivo (Small Intestinal) Absorption in Man—Fact or Myth. *Pharm. Res.* **1997**, *14*, 763-766.
- (138) Gelhaus, S. L.; Harvey, R. G.; Penning, T. M.; Blair, I. A.: Regulation of Benzo[a]pyrene-Mediated DNA- and Glutathione-Adduct Formation by 2,3,7,8-Tetrachlorodibenzo-p-dioxin in Human Lung Cells. *Chem. Res. Toxicol.* **2011**, *24*, 89-98.
- (139) Santella, R. M.; Zhang, Y.-J.: Immunologic detection of benzo(a)pyrene-DNA adducts. *Methods Mol. Biol. (N. Y., NY, U. S.)* **2011**, *682*, 271-278.
- (140) Shapiro, S. M.: Bilirubin toxicity in the developing nervous system. *Pediatr Neurol* **2003**, *29*, 410-421.
- (141) Anslyn, E. V.; Dougherty, D. A.: *Modern physical organic chemistry*; University Science: Sausalito, Calif, 2006.

- (142) McGaughey, G. B.; Gagné, M.; Rappé, A. K.: π -Stacking interactions. Alive and well in proteins. *J. Biol. Chem.* **1998**, *273*, 15458-15463.
- (143) Wang, Y.; Zheng, Q.-C.; Zhang, J.-L.; Cui, Y.-L.; Xue, Q.; Zhang, H.-X.: Highlighting a π - π interaction: a protein modeling and molecular dynamics simulation study on *Anopheles gambiae* glutathione S-transferase 1-2. *J. Mol. Model.* **2013**, *19*, 5213-5223.
- (144) Meyer, E. A.; Castellano, R. K.; Diederich, F.: Interactions with aromatic rings in chemical and biological recognition. *Angew. Chem. Int. Ed.* **2003**, *42*, 1210-1250.
- (145) Salonen, L. M.; Ellermann, M.; Diederich, F.: Aromatic rings in chemical and biological recognition: Energetics and structures. *Angew. Chem. Int. Ed.* **2011**, *50*, 4808-4842.
- (146) Mecozzi, S.; West Jr, A. P.; Dougherty, D. A.: Cation- π interactions in aromatics of biological and medicinal interest: Electrostatic potential surfaces as a useful qualitative guide. *Proc Natl Acad Sci U S A* **1996**, *93*, 10566-10571.
- (147) Tsuzuki, S.; Uchamaru, T.: Magnitude and Physical Origin of Intermolecular Interactions of Aromatic Molecules: Recent Progress of Computational Studies. *Curr. Org. Chem.* **2006**, *10*, 745-762.
- (148) Kim, D.; Lee, E. C.; Kim, K. S.; Tarakeshwar, P.: Cation- π -Anion Interaction: A Theoretical Investigation of the Role of Induction Energies. *J. Phys. Chem. A* **2007**, *111*, 7980-7986.
- (149) Braunschweig, H.; Damme, A.; Jimenez-Halla, J. O. C.; Hörl, C.; Krummenacher, I.; Kupfer, T.; Mailänder, L.; Radacki, K.: 1-Heteroaromatic-Substituted Tetraphenylboroles: π - π Interactions Between Aromatic and Antiaromatic Rings Through a B-C Bond. *J. Am. Chem. Soc.* **2012**, *134*, 20169-20177.
- (150) Cubberley, M. S.; Iverson, B. L.: ¹H NMR Investigation of Solvent Effects in Aromatic Stacking Interactions. *J. Am. Chem. Soc.* **2001**, *123*, 7560-7563.
- (151) Jennings, W. B.; McCarthy, N. J. P.; Kelly, P.; Malone, J. F.: Topically resolved intramolecular CH- π interactions in phenylalanine derivatives. *Org. Biomol. Chem.* **2009**, *7*, 5156.
- (152) Martinez, C. R.; Iverson, B. L.: Rethinking the term "pi-stacking". *Chem. Sci.* **2012**, *3*, 2191-2201.
- (153) Sun, H.; Ye, K.; Wang, C.; Qi, H.; Li, F.; Wang, Y.: The π - π stacked geometries and association thermodynamics of quinacridone derivatives studied by ¹H NMR. *J. Phys. Chem. A* **2006**, *110*, 10750.
- (154) Bosch, E.; Barnes, C. L.; Brennan, N. L.: Cation-Induced π -Stacking. *J. Org. Chem.* **2008**, *73*, 3931.

References

- (155) Lembo, A.; Tagliatesta, P.; Cicero, D.; Leoni, A.; Salvatori, A.: A glyceryl-substituted porphyrin as a starting compound for the synthesis of a pi-pi-stacked porphyrin-fullerene dyad with a frozen geometry. *Org. Biomol. Chem.* **2009**, *7*, 1093.
- (156) Zhang, H.; Bork, M. A.; Riedy, K. J.; McMillin, D. R.; Choi, J. H.: Understanding photophysical interactions of semiconducting carbon nanotubes with porphyrin chromophores. *J. Phys. Chem. C* **2014**, *118*, 11612-11619.
- (157) Ye, T.-x.; Ye, S.-l.; Chen, D.-m.; Chen, Q.-a.; Qiu, B.; Chen, X.: Spectroscopic characterization of tetracationic porphyrins and their noncovalent functionalization with graphene. *Spectrochim. Acta Mol. Biomol. Spectrosc.* **2012**, *86*, 467-471.
- (158) Bomfim, J. A. S.; Wardell, J. L.; Low, J. N.; Skakle, J. M. S.; Glidewell, C.: pi-Stacked hydrogen-bonded sheets in N,N'-bis(4-nitrobenzylidene)ethane-1,2-diamine and pi-stacked hydrogen-bonded chains in N,N'-bis(4-nitrobenzylidene)propane-1,3-diamine. *Acta Crystallogr. Sect. C* **2005**, *61*, o53.
- (159) Cho, Y.-S.; Kim, B.-Y.; Lee, S.-T.; Surh, Y.-J.; Chung, A.-S.: Chemopreventive effect of chlorophyllin on mutagenicity and cytotoxicity of 6-sulfooxymethylbenzo[a]pyrene. *Cancer Lett* **1996**, *107*, 223-228.
- (160) Romert, L.; Jansson, T.; Curvall, M.; Jenssen, D.: Screening for agents inhibiting the mutagenicity of extracts and constituents of tobacco products. *Mutat. Res.* **1994**, *322*, 97.
- (161) Camoirano, A.; Balansky, R. M.; Bennicelli, C.; Izzotti, A.; D'Agostini, F.; De Flora, S.: Experimental databases on inhibition of the bacterial mutagenicity of 4-nitroquinoline 1-oxide and cigarette smoke. *Mutat Res-Rev Mutat* **1994**, *317*, 89-109.
- (162) Li, H.; Lu, Y.; Liu, Y.; Zhu, X.; Liu, H.; Zhu, W.: Interplay between halogen bonds and π - π stacking interactions: CSD search and theoretical study Electronic supplementary information (ESI) available: The search criteria and the results of the survey of the CSD and Table S1 listing the energetic data without BSSE corrections. **2012**, *14*, 9948-9955.
- (163) Varma, A. K.; Patil, R.; Das, S.; Stanley, A.; Yadav, L.; Sudhakar, A.: Optimized hydrophobic interactions and hydrogen bonding at the target-ligand interface leads the pathways of Drug-Designing. *PLoS ONE* **2010**, *5*, e12029.
- (164) Choudhury, R. R.; Chitra, R.: Stacking interaction between homostacks of simple aromatics and the factors influencing these interactions. *CrystEngComm* **2010**, *12*, 2113-2121.
- (165) Wheeler, S. E.; Bloom, J. W. G.: Toward a more complete understanding of noncovalent interactions involving aromatic rings. *J. Phys. Chem.* **2014**, *118*, 6133.

References

- (166) Lau, Y. Y.; Chen, Y.-H.; Liu, T.-t.; Li, C.; Cui, X.; White, R. E.; Cheng, K. C.: Evaluation of a novel in vitro caco-2 hepatocyte hybrid system for predicting in vivo oral bioavailability. *Drug Metab. Dispos.* **2004**, *32*, 937-942.
- (167) Li, C.; Liu, T.; Cui, X.; Uss, A. S.; Cheng, K. C.: Development of In Vitro Pharmacokinetic Screens Using Caco-2, Human Hepatocyte, and Caco-2/Human Hepatocyte Hybrid Systems for the Prediction of Oral Bioavailability in Humans. *J. Biomol. Screen.* **2007**, *12*, 1084-1091.
- (168) Grès, M.-C.; Julian, B.; Bourrié, M.; Meunier, V.; Roques, C.; Berger, M.; Boulenc, X.; Berger, Y.; Fabre, G.: Correlation Between Oral Drug Absorption in Humans, and Apparent Drug Permeability in TC-7 Cells, A Human Epithelial Intestinal Cell Line: Comparison with the Parental Caco-2 Cell Line. *Pharm. Res.* **1998**, *15*, 726-733.
- (169) Palumbo, P.; Picchini, U.; Beck, B.; van Gelder, J.; Delbar, N.; DeGaetano, A.: A general approach to the apparent permeability index. *J Pharmacokinet Pharmacodyn* **2008**, *35*, 235-248.
- (170) Qin, X.; Yuan, F.; Zhou, D.; Huang, Y.: Oral characteristics of bergenin and the effect of absorption enhancers in situ, in vitro and in vivo. *Arzneim.-Forsch.* **2010**, *60*, 198-204.
- (171) Foster, D. R.; Zheng, X.: Cephalexin inhibits N-formylated peptide transport and intestinal hyperpermeability in Caco2 cells. *J. Pharm. Pharmacol.* **2007**, *10*, 299-310.
- (172) Watanabe, K.; Jinriki, T.; Sato, J.: Effects of progesterone and norethisterone on cephalixin transport and peptide transporter PEPT1 expression in human intestinal cell line Caco-2. *Biol. Pharm. Bull.* **2006**, *29*, 90-95.
- (173) Wallace, C. J.; Medina, S. H.; ElSayed, M. E. H.: Effect of rhamnolipids on permeability across Caco-2 cell monolayers. *Pharm. Res.* **2014**, *31*, 887-894.
- (174) Liu, J.-M.; Lin, L.-P.; Wang, X.-X.; Lin, X.; Zhou, P.; Lin, S.-Q.; Zheng, Z.-Y.: Highly sensitive detection of residual chlorpromazine hydrochloride with solid substrate room temperature phosphorimetry. *J Fluoresc* **2012**, *22*, 1087-1094.
- (175) Broeders, J. J. W.; Blaauboer, B. J.; Eijkeren, J. C. H.; Hermens, J. L. M.: Transport of chlorpromazine in the Caco-2 cell permeability assay: a kinetic study. *Chem. Res. Toxicol.* **2012**, *25*, 1442-1451.
- (176) Berlin, K.; Desiderio, M.; Ebert, C.; Gamble, D.; Gowen, T. M.; Hall, J.; Howes, M.; Lesmes, S.; Raines, F. D.; Sahadi, R. J.: Measurement and verification for emissions reductions. Google Patents, 2003.

References

- (177) Chen, X.; Lenhart, S.; Hirtz, M.; Lu, N.; Fuchs, H.; Chi, L.: Langmuir–Blodgett Patterning: A Bottom–Up Way To Build Mesostuctures over Large Areas. *Acc. Chem. Res.* **2007**, *40*, 393-401.
- (178) Reisfeld, R.: Fluorescent Dyes in Sol-Gel Glasses. *J Fluoresc* **2002**, *12*, 317-325.
- (179) Choi, S. H.; Pang, K.; Kim, K.; Churchill, D. G.: Cu²⁺ Colorimetric Sensing and Fluorescence Enhancement and Hg²⁺ Fluorescence Diminution in “Scorpionate”-like Tetrathienyl-Substituted Boron–Dipyrins. *Inorg. Chem.* **2007**, *46*, 10564-10577.
- (180) Krishnan, K. S.; Bengtsson, C.; Good, J. A. D.; Mirkhanov, S.; Chorell, E.; Johansson, L. B. Å.; Almqvist, F.: Synthesis of Fluorescent Ring-Fused 2-Pyridone Peptidomimetics. *J. Org. Chem* **2013**, *78*, 12207-12213.
- (181) Loudet, A.; Burgess, K.: BODIPY Dyes and Their Derivatives: Syntheses and Spectroscopic Properties. *Chem. Rev.* **2007**, *107*, 4891-4932.
- (182) Wood, T. E.; Thompson, A.: Advances in the Chemistry of Dipyrins and Their Complexes. *Chem. Rev.* **2007**, *107*, 1831-1861.
- (183) Chepelev, L. L.; Beshara, C. S.; MacLean, P. D.; Hatfield, G. L.; Rand, A. A.; Thompson, A.; Wright, J. S.; Barclay, L. R. C.: Polypyrroles as Antioxidants: Kinetic Studies on Reactions of Bilirubin and Biliverdin Dimethyl Esters and Synthetic Model Compounds with Peroxyl Radicals in Solution. Chemical Calculations on Selected Typical Structures. *J. Org. Chem* **2006**, *71*, 22-30.
- (184) García-Moreno, I.; Costela, A.; Campo, L.; Sastre, R.; Amat-Guerri, F.; Liras, M.; López Arbeloa, F.; Bañuelos Prieto, J.; López Arbeloa, I.: 8-Phenyl-Substituted Dipyrromethene·BF₂ Complexes as Highly Efficient and Photostable Laser Dyes. *J. Phys. Chem. A* **2004**, *108*, 3315-3323.
- (185) Liras, M.; Bañuelos Prieto, J.; Pintado-Sierra, M.; García-Moreno, I.; Costela, Á.; Infantes, L.; Sastre, R.; Amat-Guerri, F.: Synthesis, Photophysical Properties, and Laser Behavior of 3-Amino and 3-Acetamido BODIPY Dyes. *Org. Lett.* **2007**, *9*, 4183-4186.
- (186) Mölzer, C.; Huber, H.; Diem, K.; Wallner, M.; Bulmer, A. C.; Wagner, K. H.: Extracellular and intracellular anti-mutagenic effects of bile pigments in the *Salmonella typhimurium* reverse mutation assay. *Toxicol. In Vitro* **2013**, *27*, 433-437.
- (187) Johnson, A. W.; Price, R.: 2,3,4,5-Tetramethylpyrrole. *Org. Synth.* **1962**, *42*, 92-4.
- (188) Amarnath, V.; Anthony, D. C.; Amarnath, K.; Valentine, W. M.; Wetterau, L. A.; Graham, D. G.: Intermediates in the Paal-Knorr synthesis of pyrroles. *J. Org. Chem.* **1991**, *56*, 6924-31.

References

- (189) Paal, C.: Ueber die Derivate des Acetophenonacetessigesters und des Acetylacetessigesters. *Berichte der deutschen chemischen Gesellschaft* **1884**, *17*, 2756-2767.
- (190) Knorr, L.: Synthese von Furfurderivaten aus dem Diacetbernsteinsäureester. *Berichte der deutschen chemischen Gesellschaft* **1884**, *17*, 2863-2870.
- (191) Stedman, R. J.; MacDonald, S. F.: The synthesis of uroporphyrin I. *Can. J. Chem.* **1954**, *32*, 896-900.
- (192) Kleinspehn, G. G.; Corwin, A. H.: Cyclizations leading to 2-acylpyrroles and 2-pyrrolicarboxylic esters. *J. Org. Chem.* **1960**, *25*, 1048-1050.
- (193) Wood, T. E.; Berno, B.; Beshara, C. S.; Thompson, A.: ¹⁵N NMR chemical shifts for the identification of dipyrrolic structures. *J. Org. Chem.* **2006**, *71*, 2964-2971.
- (194) Tu, B.; Wang, C.; Ma, J.: Improved synthesis of symmetrical dipyrromethenes. *Org. Prep. Proced. Int.* **1999**, *31*, 349-352.
- (195) Yutanova, S. L.; Berezin, M. B.; Semeikin, A. S.; Antina, E. V.; Guseva, G. B.; V'Yugin, A. I.: Thermal oxidative degradation of the functionally substituted 2,2'-dipyrrolylmethenes hydrobromides and difluoroborates. *Russ. J. Gen. Chem.* **2013**, *83*, 545-551.
- (196) Hambrecht, J.: Simple synthesis of substituted furans and pyrroles. *Synthesis* **1977**, 280-2.
- (197) Li, J. J.: Paal-Knorr pyrrole synthesis. Springer Berlin Heidelberg: Berlin, Heidelberg, 2009; pp 411-412.
- (198) Qin, Y.; Zhu, C.; Cao, Q.: Preparation of cyanopyrrolidine and cyanothiazolidine derivatives as insulin sensitizers and dipeptidyl peptidase-IV inhibitors. *Peop. Rep. China* . 2008; pp 47pp.
- (199) Leis, J. R.; Peña, M. E.; Williams, D. L. H.: Involvement of the enol tautomers in the nitrosation of ketones. *J. Chem. Soc., Chem. Commun.* **1987**, 45-47.
- (200) Cai, X.-h.; Yang, H.-j.; Zhang, G.-l.: Synthesis of 2,4,5-trisubstituted oxazoles. *Synthesis* **2005**, 1569-1571.
- (201) Mohammed, A. H. A.; Nagendrappa, G.: A Remarkably Simple α -Oximation of Ketones to 1,2-Dione Monooximes Using the Chlorotrimethylsilane—Isoamyl Nitrite Combination. *ChemInform* **2003**, *34*.
- (202) Tan, Z.: Preparation of tetramethylpyrazine ferulate as platelet aggregation inhibitor and antithrombotic. *Inst. of Medicament, Guangdong Medicine College, Peop. Rep. China* . 2000; pp 7.

References

- (203) Selim, O.; Stoddard, R. L.; Cameron, T. S.; Thompson, A.; Crawford, S. M.; Ali, A. A.-S.; Cipot-Wechsler, J.: The first series of alkali dipyrinato complexes. *Can. J. Chem.* **2010**, *88*, 725-735.
- (204) Semeik, A. S.; Berez, M. B.; Chernova, O. M.; Antina, E. V.; Syrбу, S. A.; Lyubimova, T. V.; Kutepov, A. M.: Alkyl-substituted dipyrrolymethenes and their oxa- and thia-analogs: “structure—solvation properties” correlations. *Russ. Chem. Bull.* **2003**, *52*, 1807-1813.
- (205) Lash, T. D.; Chen, S.: Syntheses of per-15N labeled etioporphyrins I–IV and a related tetrahydrobenzoporphyrin for applications in organic geochemistry and vibrational spectroscopy. *Tetrahedron* **2005**, *61*, 11577-11600.
- (206) Crawford, S. M.; Thompson, A.: Conversion of 4,4-Difluoro-4-bora-3a,4a-diaza-s-indacenes (F-BODIPYs) to Dipyrins with a Microwave-Promoted Deprotection Strategy. *Org. Lett.* **2010**, *12*, 1424-1427.
- (207) Smithen, D. A.; Baker, A. E. G.; Offman, M.; Crawford, S. M.; Cameron, T. S.; Thompson, A.: Use of F-BODIPYs as a Protection Strategy for Dipyrins: Optimization of BF₂ Removal. *J. Org. Chem.* **2012**, *77*, 3439-3453.
- (208) Rumyantsev, E. V.; Marfin, Y. S.; Antina, E. V.: Donor-acceptor complexes of dipyrrolymethenes with boron trifluoride as intermediates in the synthesis of Bodipy. *Russ. Chem. Bull.* **2010**, *59*, 1890-1895.
- (209) Kuenzle, C. C.; Weibel, M. H.; Pelloni, R. R.: The reaction of bilirubin with diazomethane. *Biochem. J* **1973**, *133*, 357-364.
- (210) Nichol, A. W.; Morell, D. B.: Tautomerism and hydrogen bonding in bilirubin and biliverdin. *Biochimica et Biophysica Acta (BBA) - General Subjects* **1969**, *177*, 599-609.
- (211) Hutchinson, D. W.; Johnson, B.; Knell, A. J.: The synthesis of esters of bilirubin. *Biochem. J* **1973**, *133*, 493-498.
- (212) Lightner, D. A.; Trull, F. R.; Zhang, M.-H.: Novel synthesis of bilirubin mono-esters. *Tetrahedron Lett.* **1987**, *28*, 1047-1050.
- (213) Wooldridge, T. A.; Lightner, D. A.: Separation of the III- α , IX- α , and XIII- α Isomers of Bilirubin and Bilirubin Dimethyl Ester by High Performance Liquid Chromatography. *J. Liq. Chromatogr.* **1978**, *1*, 653-658.
- (214) Price, A. W. J. a. R.: 2,3,4,5-TETRAMETHYLPYRROLE. *Organic Syntheses* **1973**, *5*, 1022.
- (215) Boulet, C. A.; Hansen, A. S.: Synthesis and structure of some phosphorylated oximes related to organophosphate nerve agents. *Phosphorus, Sulfur, and Silicon and the Related Elements* **1991**, *57*, 147-161.

References

- (216) Rodionov, V. M.; Machinskaya, I. V.; Belikov, V. M.: Preparation of esters of α -nitro carboxylic acids. I. Ethyl nitroacetate. *Zh. Obshch. Khim.* **1948**, *18*, 917-20.
- (217) Cho, D. H.; Lee, J. H.; Kim, B. H.: An Improved Synthesis of 1,4-Bis(3,4-dimethyl-5-formyl-2-pyrryl)butadiyne and 1,2-Bis(3,4-dimethyl-5-formyl-2-pyrryl)ethyne. *J. Org. Chem.* **1999**, *64*, 8048-8050.
- (218) Paine, J. B., III; Dolphin, D.: Pyrrole chemistry. An improved synthesis of ethyl pyrrole-2-carboxylate esters from diethyl aminomalonate. *J. Org. Chem.* **1985**, *50*, 5598-604.
- (219) Mary E.Kushman, S. L. K., Melissa H.Fleming, Srivani Ravoori, Ramesh C.Gupta, Johannes Doehmer, Charles S.Morrow and Alan J.Townsend: Expression of human glutathione S-transferase P1 confers resistance to benzo[a]pyrene or benzo[a]pyrene-7,8-dihydrodiol mutagenesis, macromolecular alkylation and formation of stable N2-Gua-BPDE adducts in stably transfected V79MZ cells co-expressing hCYP1A1. *Carcinogenesis* **2006**, *28*, 207-214.
- (220) Mass, M. J.; Rodgers, N. T.; Kaufman, D. G.: Benzo[A]pyrene metabolism in organ cultures of human endometrium. *Chem. Biol. Interact.* **1981**, *33*, 195-205.
- (221) Badal, S.; Delgoda, R.: Role of the modulation of CYP1A1 expression and activity in chemoprevention. *J. Appl. Toxicol.* **2014**, *34*, 743-753.
- (222) Tian, S.; Pan, L.; Zhang, H.: Identification of a CYP3A-like gene and CYPs mRNA expression modulation following exposure to benzo[a]pyrene in the bivalve mollusk *Chlamys farreri*. *Mar. Environ. Res.* **2014**, *94*, 7-15.
- (223) Luch, A.: Nature and nurture - lessons from chemical carcinogenesis. *Nat Rev Cancer* **2005**, *5*, 113-125.
- (224) Wang, J. S.; Shen, X.; He, X.; Zhu, Y. R.; Zhang, B. C.; Wang, J. B.; Qian, G. S.; Kuang, S. Y.; Zarba, A.; Egner, P. A.; Jacobson, L. P.; Muñoz, A.; Helzlsouer, K. J.; Groopman, J. D.; Kensler, T. W.: Protective alterations in phase 1 and 2 metabolism of aflatoxin B1 by oltipraz in residents of Qidong, People's Republic of China. *J. Natl. Cancer Inst.* **1999**, *91*, 347-354.
- (225) Groopman, J. D.; Kensler, T. W.; Chen, J.-G.; Qian, G.-S.: Translational strategies for cancer prevention in liver. *Nat Rev Cancer* **2003**, *3*, 321-329.
- (226) Farombi, E. O.; Owoeye, O.: Antioxidative and chemopreventive properties of *Vernonia amygdalina* and *Garcinia biflavonoid*. *Int. J. Environ. Res. Publ. Health.* **2011**, *8*, 2533-2555.
- (227) Khan, N. M.; Poduval, T. B.: Immunomodulatory and immunotoxic effects of bilirubin: molecular mechanisms. *J. Leukoc. Biol.* **2011**, *90*, 997-1015.

References

- (228) Vodicka, P.; Koskinen, M.; Vodicková, L.; Štetina, R.; Šmerák, P.; Bárta, I.; Hemminki, K.: DNA adducts, strand breaks and micronuclei in mice exposed to styrene by inhalation. *Chem. Biol. Interact.* **2001**, *137*, 213-227.
- (229) Phillips, D. H.; Farmer, P. B.: Evidence for DNA and protein binding by styrene and styrene oxide. *Crit. Rev. Toxicol.* **1994**, *24 Suppl*, S35-S46.
- (230) McKillop, I. H.; Moran, D. M.; Jin, X.; Koniaris, L. G.: Molecular Pathogenesis of Hepatocellular Carcinoma. *J Surg Res* **2006**, *136*, 125-135.
- (231) Bedard, L. L.; Massey, T. E.: Aflatoxin B1-induced DNA damage and its repair. *Cancer Lett* **2006**, *241*, 174-183.
- (232) Kotsuki, H.; Hayashida, K.; Shimanouchi, T.; Nishizawa, H.: High-pressure organic chemistry .19. High-pressure-promoted, silica gel-catalyzed reaction of epoxides with nitrogen heterocycles. *J. Org. Chem.* **1996**, *61*, 984-990.
- (233) Motokura, K.; Itagaki, S.; Iwasawa, Y.; Miyaji, A.; Baba, T.: Silica-supported aminopyridinium halides for catalytic transformations of epoxides to cyclic carbonates under atmospheric pressure of carbon dioxide. *Green Chem.* **2009**, *11*, 1876-1880.
- (234) Kotsuki, H.; Hayashida, K.; Shimanouchi, T.; Nishizawa, H.: High-Pressure Organic Chemistry. 19. High-Pressure-Promoted, Silica Gel-Catalyzed Reaction of Epoxides with Nitrogen Heterocycles1. *J. Org. Chem.* **1996**, *61*, 984-990.
- (235) Banfi, A.; Benedini, F.; Sala, A.: Synthesis of new imidazole derivatives as potential inhibitors of thromboxane synthetase. II. *J. Heterocycl. Chem.* **1991**, *28*, 401-404.
- (236) Yang, J.; Wang, B.; Rusling, J. F.: Genotoxicity sensor response correlated with DNA nucleobase damage rates measured by LC-MS. *Mol. Biosyst.* **2005**, *1*, 251-259.
- (237) Schrader, W.; Linscheid, M.: Styrene oxide DNA adducts: in vitro reaction and sensitive detection of modified oligonucleotides using capillary zone electrophoresis interfaced to electrospray mass spectrometry. *Arch. Toxicol.* **1997**, *71*, 588-595.
- (238) Vodicka, P.; Stetina, R.; Kumar, R.; Plna, K.; Hemminki, K.: 7-Alkylguanine adducts of styrene oxide determined by P-32-postlabelling in DNA and human embryonal lung fibroblasts (HEL). *Carcinogenesis* **1996**, *17*, 801-808.
- (239) Hemminki, K.; Vodicka, P.: Styrene: from characterisation of DNA adducts to application in styrene-exposed lamination workers. *Toxicol. Lett.* **1995**, *77*, 153-161.
- (240) Hemminki, K.; Hesso, A.: Reaction products of styrene oxide with guanosine in aqueous media. *Carcinogenesis* **1984**, *5*, 601-607.
- (241) Hemminki, K.; Paasivirta, J.; Kurkirinne, T.; Virkki, L.: Alkylation products of DNA bases by simple epoxides. *Chem. Biol. Interact.* **1980**, *30*, 259-270.

References

- (242) Novák, J.: Syntheses of 7-(2-Hydroxy-1-phenylethyl)- and 7-(2-Hydroxy-2-phenylethyl)guanine, DNA Adducts Derived from Styrene 7,8-Oxide. *Eur. J. Org. Chem.* **2004**, 2004, 2738-2746.
- (243) Wasalathanthri, D. P.; Li, D.; Song, D.; Zheng, Z.; Choudhary, D.; Jansson, I.; Lu, X.; Schenkman, J. B.; Rusling, J. F.: Elucidating organ-specific metabolic toxicity chemistry from electrochemiluminescent enzyme/DNA arrays and bioreactor bead-LC-MS/MS. *Chem.Sci* **2015**.
- (244) Chiappe, C.; Leandri, E.; Hammock, B. D.; Morisseau, C.: Effect of ionic liquids on epoxide hydrolase-catalyzed synthesis of chiral 1,2-diols. *Green Chem.* **2007**, 9, 162-168.
- (245) Chen, W.; Lou, W.; Wang, X.; Zong, M.: Asymmetric hydrolysis of styrene oxide catalyzed by Mung bean epoxide hydrolase in organic solvent/buffer biphasic system. *Chinese J Catal* **2011**, 32, 1557-1563.
- (246) Schwab, M.: Benzo(a)pyrene. Springer: Berlin, Germany, 2008; Vol. 1; pp 331-332.
- (247) Last, J. M.: benzo-a-pyrene. Oxford University Press, 2007.
- (248) Lee, B. M.; Shim, G. A.: Dietary exposure estimation of benzo[a]pyrene and cancer risk assessment. *J. Toxicol. Environ. Health* **2007**, 70, 1391-1394.
- (249) Gunning, W. T.; Kramer, P. M.; Lubet, R. A.; Steele, V. E.; End, D. W.; Wouters, W.; Pereira, M. A.: Chemoprevention of benzo(a)pyrene-induced lung tumors in mice by the farnesyltransferase inhibitor R115777. *Clin. Cancer Res.* **2003**, 9, 1927-1930.
- (250) Alexandrov, K.; Cascorbi, I.; Rojas, M.; Bouvier, G.; Kriek, E.; Bartsch, H.: CYP1A1 and GSTM1 genotypes affect benzo[a]pyrene DNA adducts in smokers' lung: comparison with aromatic/hydrophobic adduct formation. *Carcinogenesis* **2002**, 23, 1969-1977.
- (251) Cross, A. J.; Sinha, R.: Meat-related mutagens/carcinogens in the etiology of colorectal cancer. *Environ. Mol. Mutagen.* **2004**, 44, 44-55.
- (252) Walters, D. G.; Young, P. J.; Agus, C.; Knize, M. G.; Boobis, A. R.; Gooderham, N. J.; Lake, B. G.: Cruciferous vegetable consumption alters the metabolism of the dietary carcinogen 2-amino-1-methyl-6-phenylimidazo[4,5-b]pyridine (PhIP) in humans. *Carcinogenesis* **2004**, 25, 1659-1669.
- (253) Ito, N.; Hasegawa, R.; Sano, M.; Tamano, S.; Esumi, H.; Takayama, S.; Sugimura, T.: A new colon and mammary carcinogen in cooked food, 2-amino-1-methyl-6-phenylimidazo[4,5-b]pyridine (PhIP). *Carcinogenesis* **1991**, 12, 1503-1506.
- (254) Abu-Bakar, A. e.; Arthur, D. M.; Aganovic, S.; Ng, J. C.; Lang, M. A.: Inducible bilirubin oxidase: a novel function for the mouse cytochrome P450 2A5. *Toxicol. Appl. Pharmacol.* **2011**, 257, 14-22.

References

- (255) Jalas, J. R.; Seetharaman, M.; Hecht, S. S.; Murphy, S. E.: Molecular modelling of CYP2A enzymes: application to metabolism of the tobacco-specific nitrosamine 4-(methylnitrosamino)-1-(3-pyridyl)-1-butanone (NNK). *Xenobiotica* **2004**, *34*, 515-533.
- (256) Felicia, N. D.; Rekha, G. K.; Murphy, S. E.: Characterization of Cytochrome P450 2A4 and 2A5-Catalyzed 4-(Methylnitrosamino)-1-(3-pyridyl)-1-butanone (NNK) Metabolism. *Arch. Biochem. Biophys.* **2000**, *384*, 418-424.
- (257) Pelkonen, P.; Kirby, G. M.; Wild, C. P.; Bartsch, H.; Lang, M. A.: Metabolism of nitrosamines and aflatoxin B1 by hamster liver CYP2A enzymes. *Chem. Biol. Interact.* **1994**, *93*, 41-50.
- (258) Walsh, A. A.; Szklarz, G. D.; Scott, E. E.: Human cytochrome P450 1A1 structure and utility in understanding drug and xenobiotic metabolism. *J. Biol. Chem.* **2013**, *288*, 12932-12943.
- (259) Forti, G. C.; Paolini, M.; Hrelia, P.; Corsi, C.; Biagi, G. L.; Bronzetti, G.: NADPH-generating system: influence on microsomal mono-oxygenase stability during incubation for the liver-microsomal assay with rat and mouse S9 fractions. *Mutat. Res.* **1984**, *129*, 281-297.
- (260) Wanwimolruk, P.; Wanwimolruk, S.: Characterization of CYP1A enzyme in Adélie penguin liver. *Comp. Biochem. Physiol. C: Pharmacol. Toxicol.* **2006**, *144*, 148-154.
- (261) Skaanild, M. T.; Friis, C.: Porcine CYP2A Polymorphisms and Activity. *Basic Clin Pharmacol Toxicol* **2005**, *97*, 115-121.
- (262) Di Carlo, D.; Aghdam, N.; Lee, L. P.: Single-cell enzyme concentrations, kinetics, and inhibition analysis using high-density hydrodynamic cell isolation arrays. *Anal. Chem.* **2006**, *78*, 4925-4930.
- (263) Frackenpohl, J.; Arvidsson, P. I.; Schreiber, J. V.; Seebach, D.: The outstanding biological stability of beta- and gamma-peptides toward proteolytic enzymes: an in vitro investigation with fifteen peptidases. *Chembiochem* **2001**, *2*, 445.
- (264) Zhao, Y.: The evaluation of inhibitive effectiveness of the tumour necrosis factor- α converting enzyme selective inhibitors by HPLC. *J Enzyme Inhib Med Chem* **2011**, *26*, 181-187.
- (265) Fogarty, W. M.: *Microbial enzymes and biotechnology*; Applied Science Publishers: London, 1983.
- (266) Reddy, K. G.; Madhavi, G.; Swamy, B. E. K.; Reddy, S.; Reddy, A. V. B.; Madhavi, V.: Electrochemical investigations of lipase enzyme activity inhibition by methyl parathion pesticide: Voltammetric studies. *J. Mol. Liq.* **2013**, *180*, 26-30.

References

- (267) Vaštag, Ž.; Popović, S.; Popović, L.; Krimer, V.; Peričin, D.: Production of enzymatic hydrolysates with antioxidant and angiotensin-I converting enzyme inhibitory activity from pumpkin oil cake protein isolate. *Food Chem.* **2011**, *124*, 1316-1321.
- (268) Prajapati, V.; Patel, H.; Trivedi, U.; Patel, K.: Kinetic and thermodynamic characterization of lipase produced by *Cellulomonas flavigena* UNP3. *J. Basic Microbiol.* **2014**, *54*, 976-983.
- (269) Levova, K.; Moserova, M.; Nebert, D. W.; Phillips, D. H.; Frei, E.; Schmeiser, H. H.; Arlt, V. M.; Stiborova, M.: NAD(P)H:quinone oxidoreductase expression in Cyp1a-knockout and CYP1A-humanized mouse lines and its effect on bioactivation of the carcinogen aristolochic acid I. *Toxicol. Appl. Pharmacol.* **2012**, *265*, 360-367.
- (270) Varghese, A.; Pandita, N.; Gaud, R. S.: In vitro and in vivo Evaluation of CYP1A Interaction Potential of Terminalia Arjuna Bark. *Indian J. Pharm. Sci.* **2014**, *76*, 138-147.
- (271) Trushin, N.; Alam, S.; El-Bayoumy, K.; Krzeminski, J.; Amin, S. G.; Gullett, J.; Meyers, C.; Prokopczyk, B.: Comparative metabolism of benzo[a]pyrene by human keratinocytes infected with high-risk human papillomavirus types 16 and 18 as episomal or integrated genomes. *J. Carcinog.* **2012**, *11*, 1.
- (272) Kim, J. H.; Stansbury, K. H.; Walker, N. J.; Trush, M. A.; Strickland, P. T.; Sutter, T. R.: Metabolism of benzo[a]pyrene and benzo[a]pyrene-7,8-diol by human cytochrome P450 1B1. *Carcinogenesis* **1999**, *20*, 515-515.
- (273) Dellinger, R. W.; Chen, G.; Blevins-Primeau, A. S.; Krzeminski, J.; Amin, S.; Lazarus, P.: Glucuronidation of PhIP and N-OH-PhIP by UDP-glucuronosyltransferase 1A10. *Carcinogenesis* **2007**, *28*, 2412-2418.
- (274) Deeb, R. S.; Peyton, D. H.: Proton NMR study of the interaction of tin(IV) protoporphyrin IX monomers and dimers with apomyoglobin. *Biochemistry* **1992**, *31*, 468-474.
- (275) Lukas, B.: Mossbauer studies on iron protoporphyrin IX complexes. ProQuest, UMI Dissertations Publishing, 1985.
- (276) Sansen, S.; Yano, J. K.; Reynald, R. L.; Schoch, G. A.; Griffin, K. J.; Stout, C. D.; Johnson, E. F.: Adaptations for the Oxidation of Polycyclic Aromatic Hydrocarbons Exhibited by the Structure of Human P450 1A2. *J. Biol. Chem.* **2007**, *282*, 14348-14355.
- (277) Brändén, G.; Sjögren, T.; Schnecke, V.; Xue, Y.; Faculty of, S.; Naturvetenskapliga, f.; University of, G.; Department of, C.; Molecular, B.; Institutionen för kemi och, m.; Göteborgs, u.: Structure-based ligand design to overcome CYP inhibition in drug discovery projects. *Drug Discovery Today* **2014**, *19*, 905.

References

- (278) Wang, A.; Savas, U.; Stout, C. D.; Johnson, E. F.: Structural characterization of the complex between alpha-naphthoflavone and human cytochrome P450 1B1. *J. Biol. Chem.* **2011**, *286*, 5736.
- (279) Mazur, C. S.; Kenneke, J. F.; Goldsmith, M.-R.; Brown, C.: Contrasting Influence of NADPH and a NADPH-Regenerating System on the Metabolism of Carbonyl-Containing Compounds in Hepatic Microsomes. *Drug Metab. Dispos.* **2009**, *37*, 1801-1805.
- (280) Bullock, E.; Johnson, A. W.; Markham, E.; Shaw, K. B.: 287. A synthesis of coproporphyrin III. *J Chem Soc.* **1958**, 1430-1440.

Appendix-A

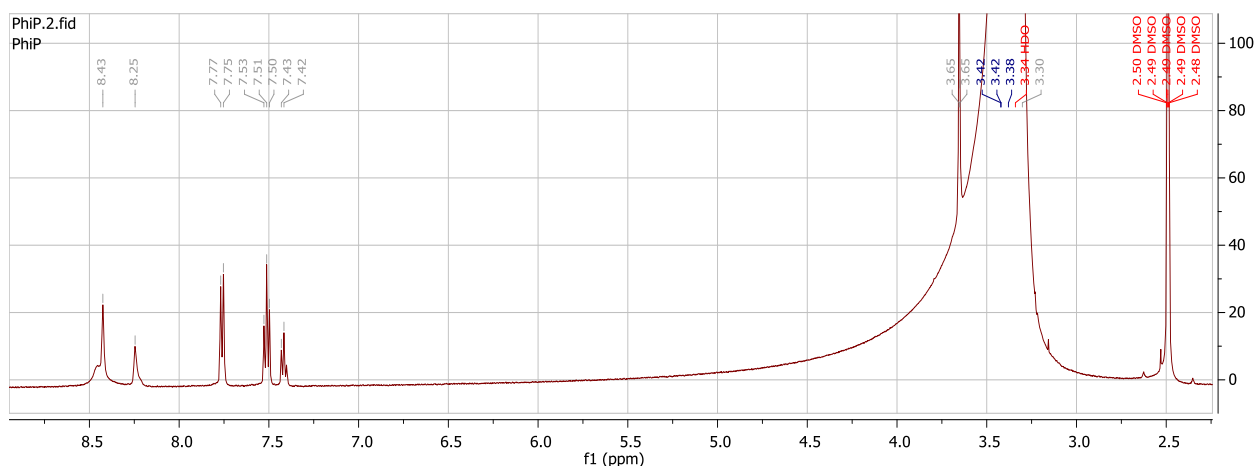


Figure 7.1: ^1H NMR spectrum of **2.9** performed at 500 MHz in sol B.

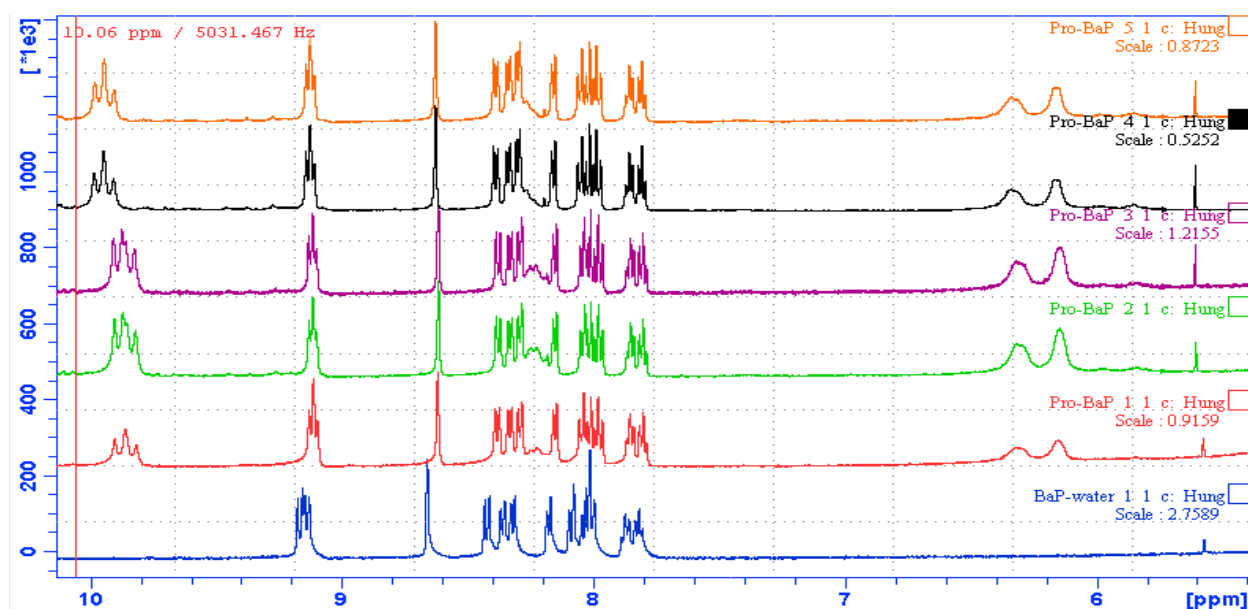


Figure 7.2: Overlay of the ^1H NMR spectra of mixtures of **2.8** (blue) and its mixtures with varying concentrations of **2.1** performed at 500 MHz in Sol B, the mole ratio between **2.1** and **2.8** are 2:1 (red), 1:1 (green), 1:2 (puple), 1:2 (black-yellow in the presence of 1 drop of D_2O).

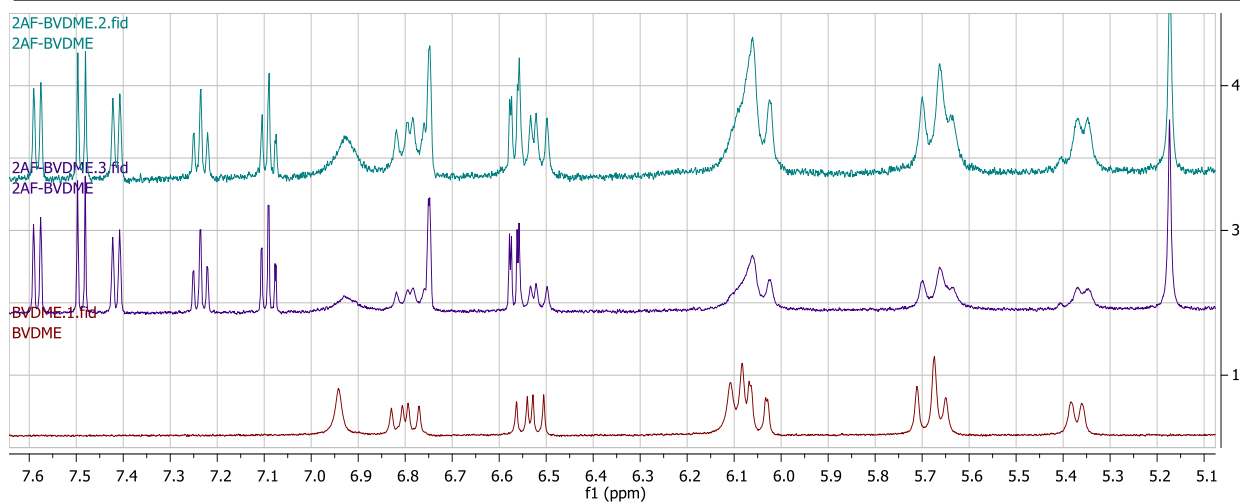


Figure 7.3: Overlay of the ¹H NMR spectra of **2.6** (brown) and its mixtures with **2.9** performed at 500 MHz in Sol A, the mole ratio between **2.6** and **2.9** are 2:1 (red), 1:1 (puple), 2:1 (blue).

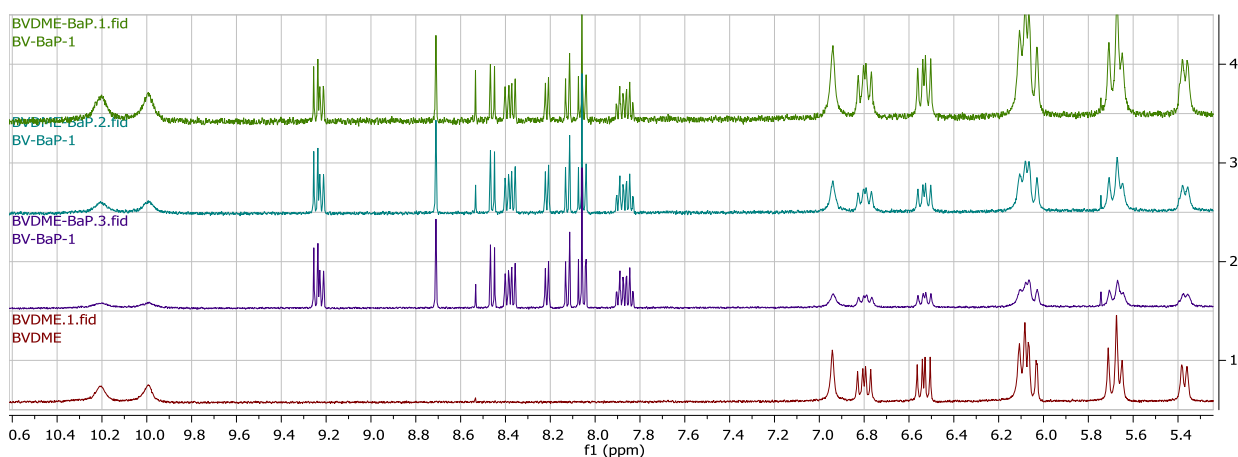


Figure 7.4: Overlay of the ¹H NMR spectra of **2.6** (brown) and its mixtures with varying concentration of **2.8** performed at 500 MHz in Sol A, the mole ratio between **2.6** and **2.8** are 1:2 (puple), 1:1 (blue), 2:1 (green).

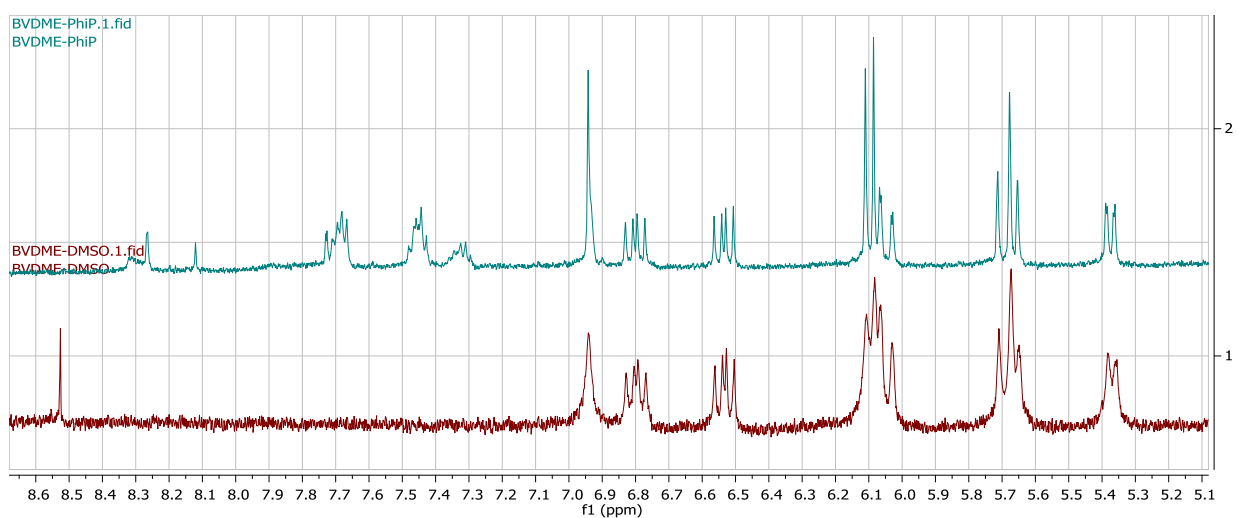


Figure 7.5: Overlay of the ¹H NMR spectra of **2.6** (brown) and its mixtures with **2.7** performed at 500 MHz in Sol A, the mole ratio between **2.6** and **2.7** are 1:1 (blue).

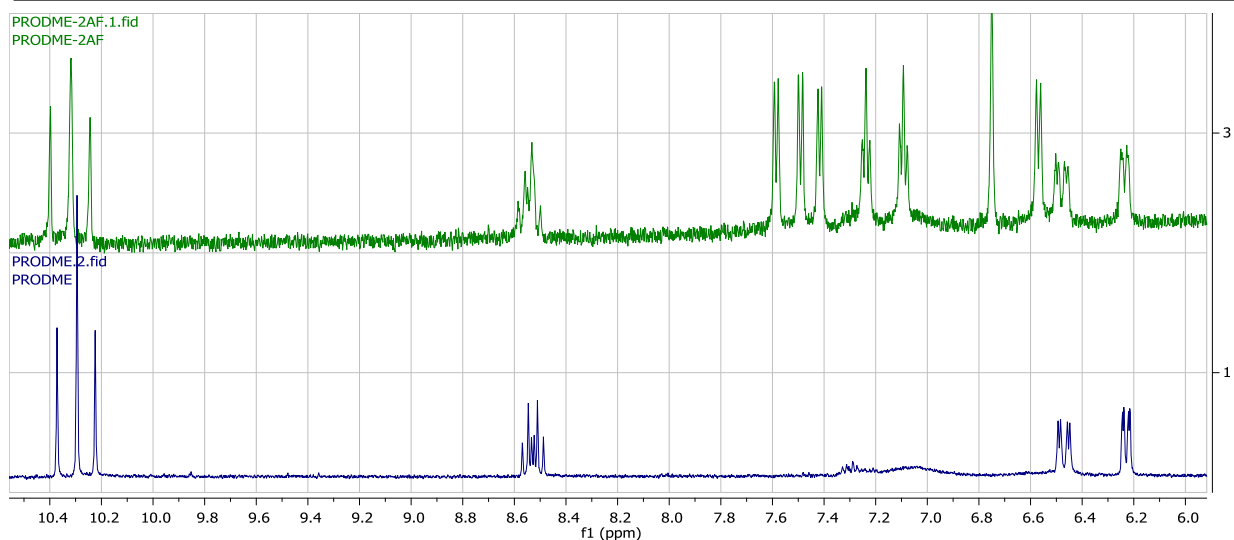


Figure 7.6: Overlay of the ¹H NMR spectra of **2.4** (puple) and its mixtures with **2.9** performed at 500 MHz in Sol A, the mole ratio between **2.4** and **2.9** are 1:1 (green).

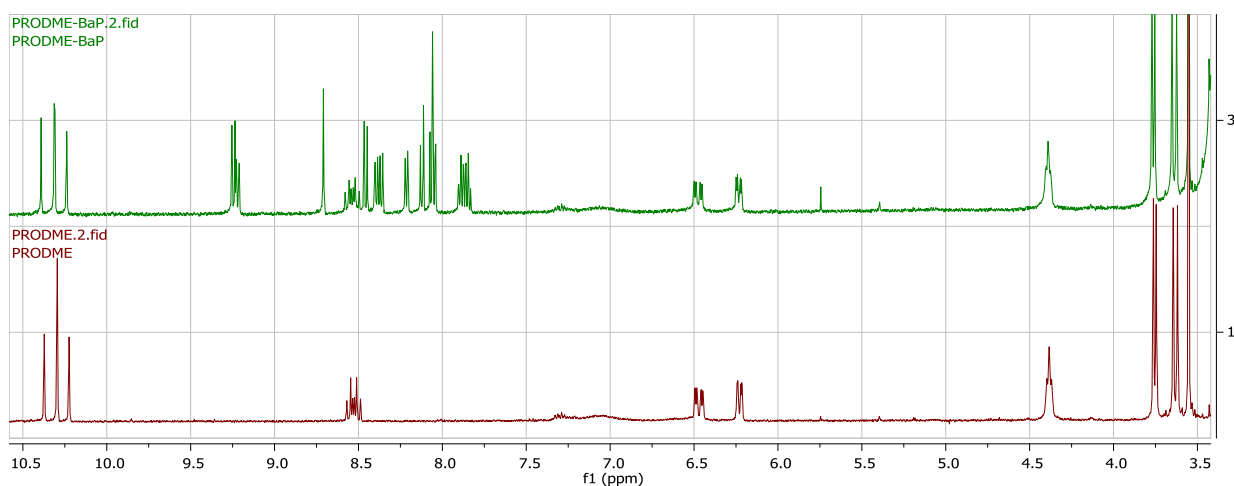


Figure 7.7: Overlay of the ¹H NMR spectra of **2.4** (puple) and its mixtures with **2.8** performed at 500 MHz in Sol A, the mole ratio between **2.4** and **2.8** are 1:1 (green).

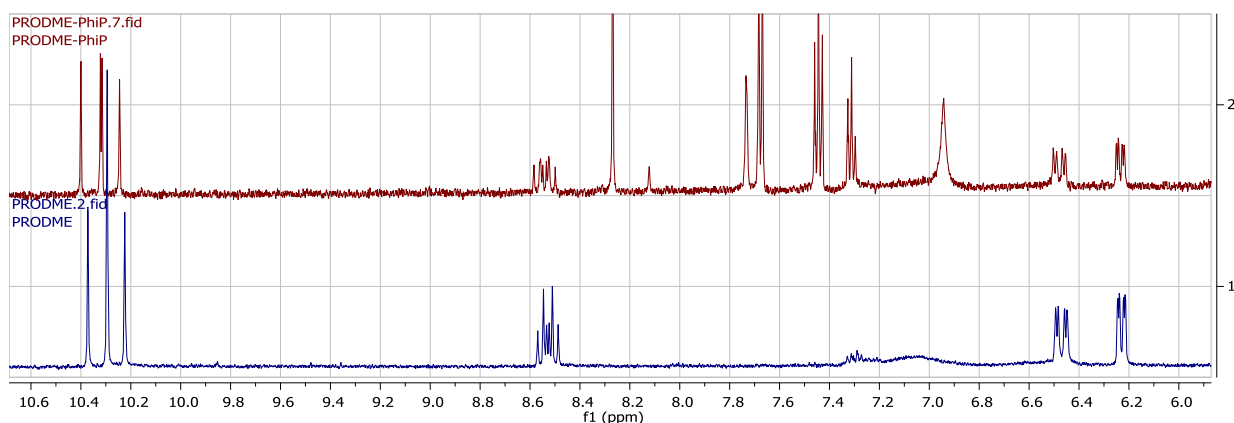


Figure 7.8: Overlay of the ¹H NMR spectra of **2.4** (puple) and its mixtures with **2.7** performed at 500 MHz in Sol A, the mole ratio between **2.4** and **2.7** are 1:1 (brown).

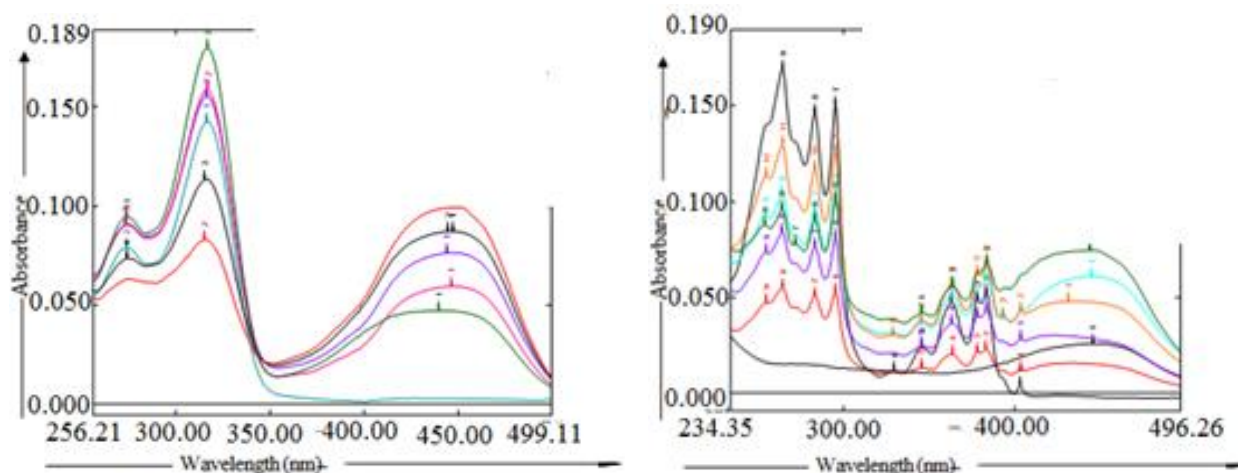


Figure 7.9: Overlay of the UV spectra of the mixture between **2.7** (0.5 μM in methanol (left)), **2.8** (0.5 μM in methanol (right) and varying concentrations of **2.2** (from 0.25 μM to 1.0 μM in methanol). The blue line (left) and red line (right) that were in close proximity to baseline (λ_{max} 317 nm 295 nm, respectively) were the UV spectra of **2.7** and **2.8**. The introduction of **2.2** (from 0.25 μM to 1.0 μM) in the mixture was detected by the increasing UV absorbance at 450 nm in other overlaid spectra.

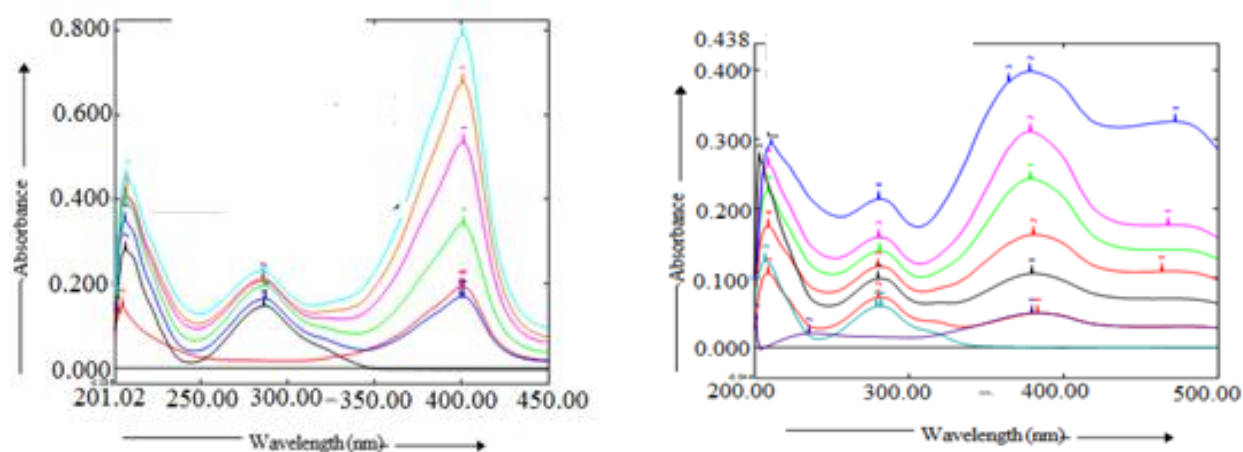


Figure 7.10: Overlay of the UV spectra of the mixture between **2.9** (1.0 μM in methanol (left) and 0.25 μM in buffer (right)) and varying concentrations of **2.1** (from 0.5 μM to 2.0 μM in methanol and from 0.25 μM to 1.5 μM). The black line (left) and blue line (right) that were in close proximity to baseline (λ_{max} 288 nm) were the UV spectra of **2.9**. The introduction of **2.1** (from 0.5 μM to 2.0 μM) in the mixture was detected by the increasing UV absorbance at 401 nm and 385 nm in buffer nm in other overlaid spectra.

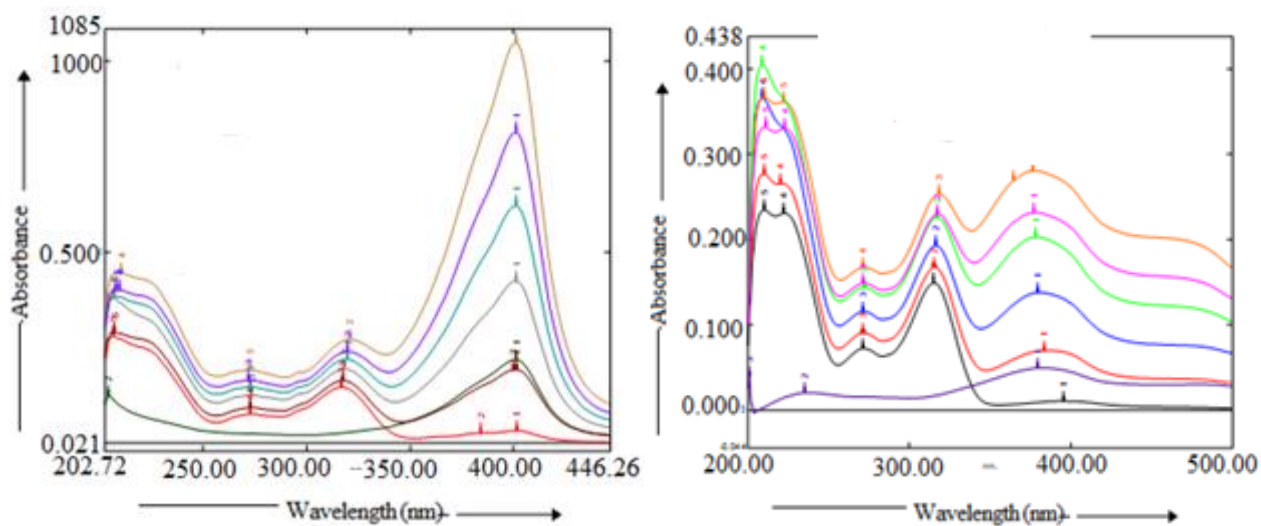


Figure 7.11: Overlay of the UV spectra of the mixture between **2.7** (1.0 μM in methanol (left) and 1.0 μM in buffer (right)) and varying concentrations of **2.1** (from 0.5 μM to 2.5 μM in methanol and from 0.25 μM to 1.0 μM). The black line (right) and red line (right) that were in close proximity to baseline (λ_{max} 317 nm) were the UV spectra of **2.7**. The introduction of **2.1** (from 0.5 μM to 2.0 μM) in the mixture was detected by the increasing UV absorbance at 401 nm in methanol and 385 nm in buffer nm in other overlaid spectra.

Appendix-B

Concentration of 3.6 in the presence of 3.2 (5 μM)						
	Basolateral chamber			Apical chamber		
t (min)	Well-1	Well-2	Well-3	Well-1	Well-2	Well-3
0	0.000	0.000	0.000	9.999	9.999	9.999
30	0.330	0.419	0.404	--	--	--
60	0.438	0.449	0.487	--	--	--
90	0.510	0.537	0.544	--	--	--
120	0.460	0.489	0.497	--	--	--
150	0.422	0.404	0.427	--	--	--
180	0.398	0.416	0.428	1.818	1.822	1.836

Table 7.1: The concentration of **3.6** collected from the AP and BL chamber of wells during the assays.

Linear Regression / Apparent Permeability of 3.6 in the presence of 3.2 (5 μM)						
Wells	Calculated	Intercept	Slope	r ²	N	P _{app} [cm/s]
1	3	1.25 x10 ⁻²	5.99 x10 ⁻⁴	0.957	7	1.806 x10 ⁻⁵
2	3	1.64 x10 ⁻²	6.13 x10 ⁻⁴	0.940	7	1.847 x10 ⁻⁵
3	3	1.61 x10 ⁻²	6.35 x10 ⁻⁴	0.945	7	1.913 x10 ⁻⁵
Mean	2.97	1.50 x10 ⁻²	6.16 x10 ⁻⁴			1.86 x10 ⁻⁵
s.d.	0.30	2.17 x10 ⁻³	1.79 x10 ⁻⁵			5.41 x10 ⁻⁷
rel s.d.	10%	14%	3%			3%

Appendices

Table 7.2: The linear regression and P_{app} of **3.6** in the presence of **3.2** (5 μ M).

Concentration of 3.6 in the presence of 3.2 (10 μ M)						
Basolateral chamber				Apical chamber		
t (min)	Well-1	Well-2	Well-3	Well-1	Well-2	Well-3
0	0.000	0.000	0.000	9.999	9.999	9.999
30	0.331	0.345	0.270	--	--	--
60	0.487	0.500	0.476	--	--	--
90	0.534	0.561	0.544	--	--	--
120	0.518	0.499	0.518	--	--	--
150	0.444	0.447	0.460	--	--	--
180	0.404	0.400	0.403	1.612	1.760	1.691

Table 7.3: The concentration of **3.6** collected from the AP and BL chambers from 0 to 180 min.

Linear Regression / Apparent Permeability of 3.6 in the presence of 3.2 (10 μ M)						
Wells	Calculated	Intercept	Slope	r ²	N	P_{app} [cm/s]
1	3	1.31×10^{-2}	6.39×10^{-4}	0.953	7	1.93×10^{-5}
2	3	1.43×10^{-2}	6.40×10^{-4}	0.945	7	1.93×10^{-5}
3	3	1.02×10^{-2}	6.48×10^{-4}	0.959	7	1.95×10^{-5}
Mean	2.96	1.26×10^{-2}	6.42×10^{-4}			1.94×10^{-5}
s.d.	0.08	2.12×10^{-3}	4.90×10^{-6}			1.48×10^{-7}
rel s.d.	3%	17%	1%			1%

Table 7.4: The linear regression and P_{app} of **3.6** in the presence of **3.2** (10 μ M).

Concentration of 3.6 in the presence of 3.2 (20 μ M)						
Basolateral chamber				Apical chamber		
t (min)	Well-1	Well-2	Well-3	Well-1	Well-2	Well-3
0	0.000	0.000	0.000	9.999	9.999	9.999
30	0.282	0.317	0.306	--	--	--
60	0.451	0.488	0.503	--	--	--
90	0.569	0.590	0.567	--	--	--
120	0.474	0.548	0.522	--	--	--
150	0.450	0.483	0.466	--	--	--
180	0.345	0.391	0.392	1.642	1.657	1.701

Appendices

Table 7.5: The concentration of **3.6** collected from the AP and BL chambers from 0 to 180 min.

Linear Regression / Apparent Permeability of 3.6 in the presence of 3.2 (20 μ M)						
Wells	Calculated	Intercept	Slope	r ²	N	P _{app} [cm/s]
1	3	1.17 x10 ⁻²	6.12 x10 ⁻⁴	0.941	7	1.846 x10 ⁻⁵
2	3	1.25 x10 ⁻²	6.72 x10 ⁻⁴	0.949	7	2.026 x10 ⁻⁵
3	3	1.26 x10 ⁻²	6.55 x10 ⁻⁴	0.949	7	1.974 x10 ⁻⁵
Mean	3.06	1.23 x10 ⁻²	6.47 x10 ⁻⁴			1.95 x10 ⁻⁵
s.d.	0.36	4.89 x10 ⁻⁴	3.08 x10 ⁻⁵			9.29 x10 ⁻⁷
rel s.d.	12%	4%	5%			5%

Table 7.6: The linear regression and P_{app} of **3.6** in the presence of **3.2** (20 μ M).

Concentration of 3.6 in the presence of 3.4 (10 μ M)						
t (min)	Basolateral chamber			Apical chamber		
	Well-1	Well-2	Well-3	Well-1	Well-2	Well-3
0	0.000	0.000	0.000	9.999	9.999	9.999
30	0.352	0.382	0.451	--	--	--
60	0.555	0.577	0.616	--	--	--
90	0.586	0.627	0.644	--	--	--
120	0.607	0.578	0.571	--	--	--
150	0.562	0.545	0.529	--	--	--
180	0.459	0.481	0.487	1.642	1.657	1.701

Table 7.7: The concentration of **3.6** collected from the AP and BL chambers from 0 to 180 min.

Linear Regression / Apparent Permeability of 3.6 in the presence of 3.4 (10 μ M)						
Wells	Calculated	Intercept	Slope	r ²	N	P _{app} [cm/s]
1	3	1.29 x10 ⁻²	7.50 x10 ⁻⁴	0.962	7	2.259 x10 ⁻⁵
2	3	1.50 x10 ⁻²	7.53 x10 ⁻⁴	0.957	7	2.269 x10 ⁻⁵
3	3	1.90 x10 ⁻²	7.53 x10 ⁻⁴	0.942	7	2.27 x10 ⁻⁵
Mean	1.69	1.56 x10 ⁻²	7.52 x10 ⁻⁴			2.27 x10 ⁻⁵
s.d.	0.23	3.06 x10 ⁻³	2.04 x10 ⁻⁶			6.16 x10 ⁻⁸
rel s.d.	14%	20%	0%			0%

Table 7.8: The linear regression and P_{app} of **3.6** in the presence of **3.4** (10 μ M).

Appendices

Concentration of 3.6 in the presence of 3.5 (10 μ M)						
Basolateral chamber				Apical chamber		
t (min)	Well-1	Well-2	Well-3	Well-1	Well-2	Well-3
0	0.000	0.000	0.000	9.999	9.999	9.999
30	0.279	0.370	0.366	--	--	--
60	0.467	0.585	0.498	--	--	--
90	0.547	0.606	0.582	--	--	--
120	0.608	0.598	0.578	--	--	--
150	0.509	0.538	0.547	--	--	--
180	0.467	0.486	0.483	2.023	2.318	2.002

Table 7.9: The concentration of **3.6** collected from the AP and BL chambers from 0 to 180 min.

Linear Regression / Apparent Permeability of 3.6 in the presence of 3.5 (10 μ M)						
Wells	Calculated	Intercept	Slope	r ²	N	P _{app} [cm/s]
1	3	8.19 x10 ⁻³	7.16 x10 ⁻⁴	0.974	7	2.159 x10 ⁻⁵
2	3	1.44 x10 ⁻²	7.55 x10 ⁻⁴	0.958	7	2.275 x10 ⁻⁵
3	3	1.21 x10 ⁻²	7.35 x10 ⁻⁴	0.971	7	2.215 x10 ⁻⁵
Mean	2.01	1.16 x10 ⁻²	7.36 x10 ⁻⁴			2.22 x10 ⁻⁵
s.d.	0.35	3.15 x10 ⁻³	1.93 x10 ⁻⁵			5.82 x10 ⁻⁷
rel s.d.	17%	27%	3%			3%

Table 7.10: The linear regression and P_{app} of **3.6** in the presence of **3.5** (10 μ M).

Concentration of 3.6 in the presence of 3.3 (10 μ M)						
Basolateral chamber				Apical chamber		
t (min)	Well-1	Well-2	Well-3	Well-1	Well-2	Well-3
0	0.000	0.000	0.000	9.999	9.999	9.999
30	0.337	0.371	0.384	--	--	--
60	0.459	0.456	0.537	--	--	--
90	0.534	0.607	0.646	--	--	--
120	0.533	0.579	0.596	--	--	--
150	0.525	0.564	0.576	--	--	--
180	0.492	0.511	0.533	1.698	1.712	1.766

Table 7.11: The concentration of **3.6** collected from the AP and BL chambers from 0 to 180 min.

Appendices

Linear Regression / Apparent Permeability of 3.6 in the presence of 3.3 (10 μ M)						
Wells	Calculated	Intercept	Slope	r ²	N	P _{app} [cm/s]
1	3	1.01 x10 ⁻²	7.01 x10 ⁻⁴	0.980	7	2.111 x10 ⁻⁵
2	3	1.08 x10 ⁻²	7.52 x10 ⁻⁴	0.977	7	2.266 x10 ⁻⁵
3	3	1.29 x10 ⁻²	7.88 x10 ⁻⁴	0.971	7	2.374 x10 ⁻⁵
Mean	1.79	1.13 x10 ⁻²	7.47 x10 ⁻⁴			2.25 x10 ⁻⁵
s.d.	0.48	1.45 x10 ⁻³	4.39 x10 ⁻⁵			1.32 x10 ⁻⁶
rel s.d.	27%	13%	6%			6%

Table 7.12: The linear regression and P_{app} of **3.6** in the presence of **3.3** (10 μ M).

Concentration of 3.6 in control experiments						
t (min)	Basolateral chamber			Apical chamber		
	Well-1	Well-2	Well-3	Well-1	Well-2	Well-3
0	0.000	0.000	0.000	9.999	9.999	9.999
30	0.275	0.264	0.315	--	--	--
60	0.446	0.407	0.458	--	--	--
90	0.513	0.471	0.538	--	--	--
120	0.482	0.499	0.507	--	--	--
150	0.474	0.459	0.490	--	--	--
180	0.436	0.424	0.404	2.320	2.756	2.197

Table 7.13: The concentration of **3.6** collected from the AP and BL chambers from 0 to 180 min.

Linear Regression / Apparent Permeability of 3.6 in control experiments						
Wells	Calculated	Intercept	Slope	r ²	N	P _{app} [cm/s]
1	3	1.66 x10 ⁻²	5.83 x10 ⁻⁴	0.9781	7	1.757 x10 ⁻⁵
2	3	1.42 x10 ⁻²	5.73 x10 ⁻⁴	0.9830	7	1.727 x10 ⁻⁵
3	3	2.11 x10 ⁻²	5.75 x10 ⁻⁴	0.9686	7	1.733 x10 ⁻⁵
Mean		1.73 x10 ⁻²	5.77 x10 ⁻⁴			1.74 x10 ⁻⁵
s.d.		3.49 x10 ⁻³	5.27 x10 ⁻⁶			1.59 x10 ⁻⁷
rel s.d.		20%	1%			1%

Table 7.14: The linear regression and P_{app} of **3.6** in control experiments.

Concentration of 3.6 in the presence of 3.1 (10 μ M)						
Basolateral chamber				Apical chamber		
t (min)	Well-1	Well-2	Well-3	Well-1	Well-2	Well-3
0	0.292	0.284	0.319	9.999	9.999	9.999
30	0.493	0.465	0.489	--	--	--
60	0.518	0.538	0.565	--	--	--
90	0.484	0.472	0.5177	--	--	--
120	0.492	0.466	0.462	--	--	--
150	0.431	0.439	0.429	--	--	--
180	0.292	0.284	0.320	2.248	2.770	2.629

Table 7.15: The concentration of **3.6** collected from the AP and BL chambers from 0 to 180 min.

Linear Regression / Apparent Permeability of 3.6 in the presence of 3.1 (10 μ M)						
Wells	Calculated	Intercept	Slope	r^2	N	P_{app} [cm/s]
1	3	1.05×10^{-2}	6.54×10^{-4}	0.9675	7	1.97×10^{-5}
2	3	9.98×10^{-2}	6.45×10^{-4}	0.9684	7	1.944×10^{-5}
3	3	1.22×10^{-2}	6.62×10^{-4}	0.9582	7	1.996×10^{-5}
Mean	2.83	1.09×10^{-2}	6.54×10^{-4}			1.97×10^{-5}
s.d.	0.10	1.16×10^{-3}	8.60×10^{-6}			2.59×10^{-7}
rel s.d.	4%	11%	1%			1%

Table 7.16: The linear regression and P_{app} of **3.6** in the presence of **3.1** (10 μ M).

Appendix-C

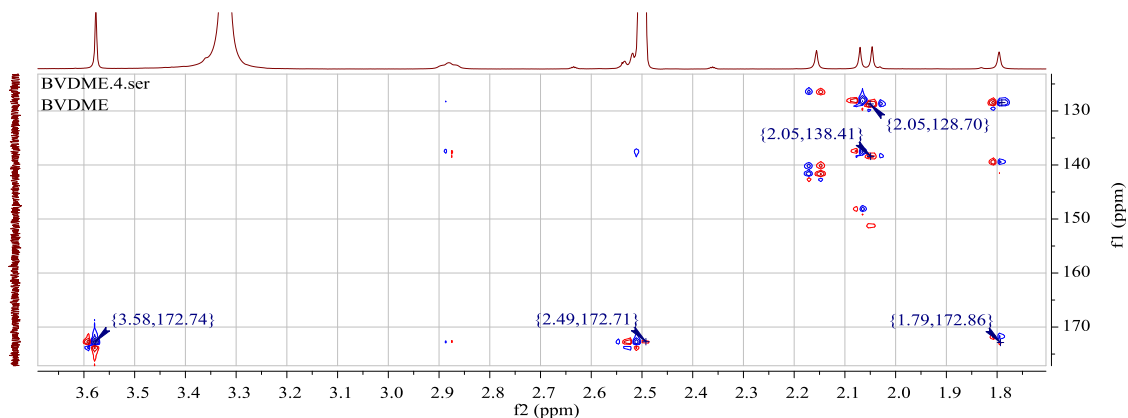


Figure 7.12: The HMBC correlations from protons to carbons of **4.12** performed on a 500 MHz instrument in DMSO-*d*₆.

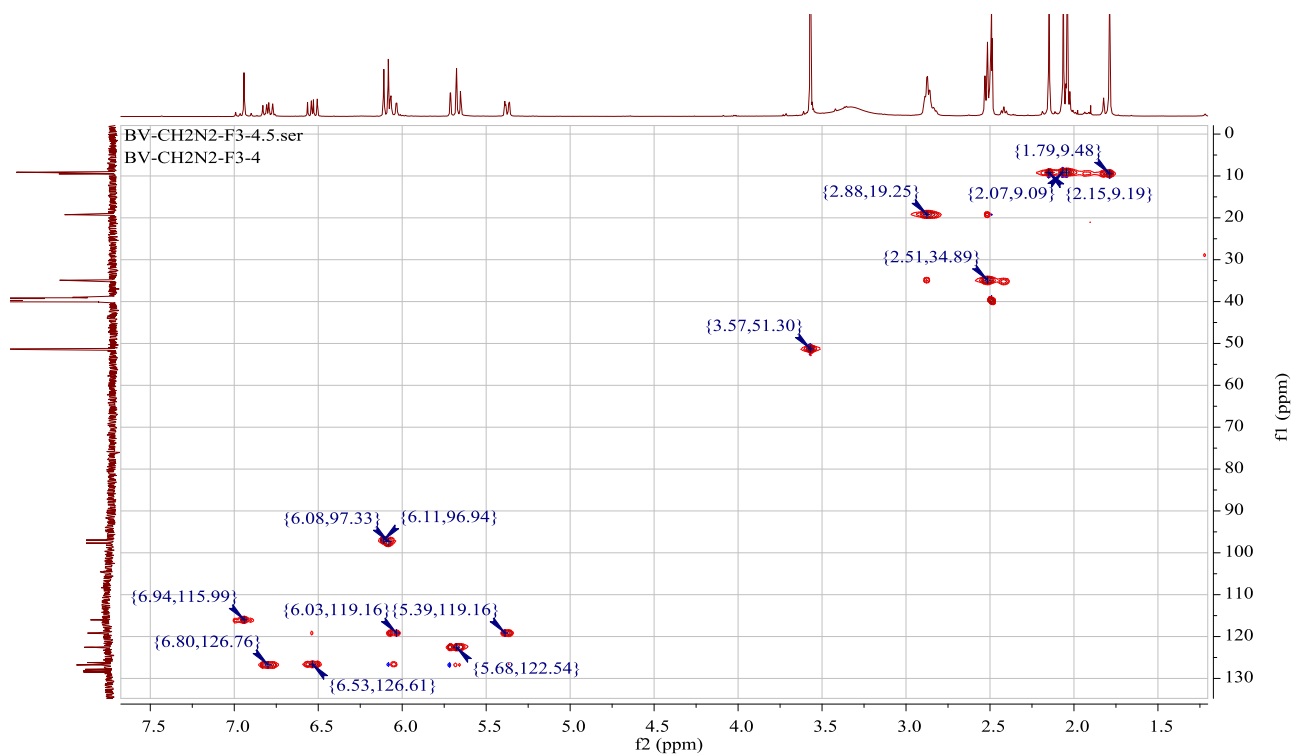


Figure 7.13: The HMBC correlations from protons to carbons of **4.12** performed on a 500 MHz instrument in DMSO-*d*₆.

Appendices

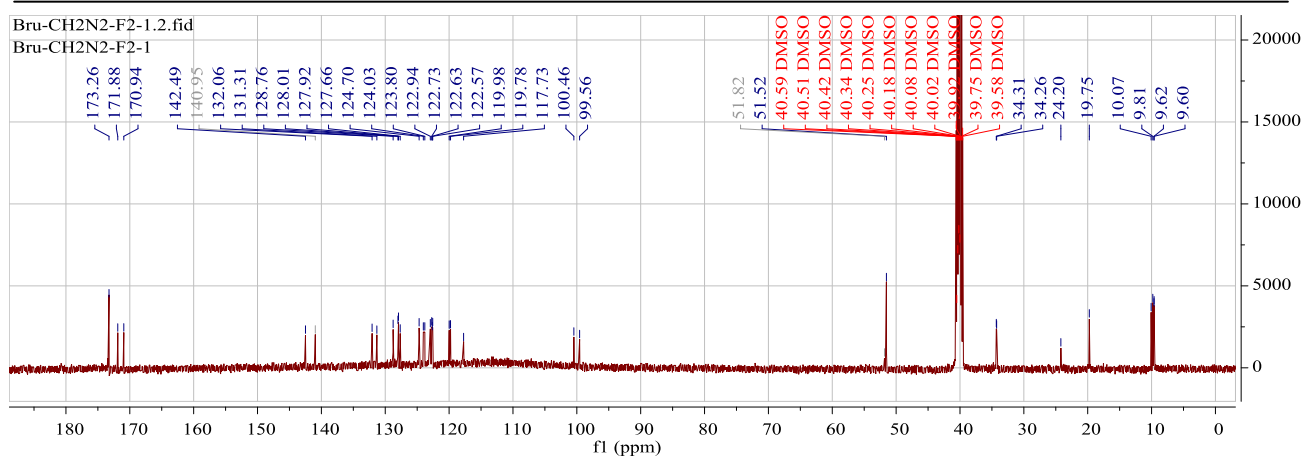


Figure 7.14: The ^{13}C NMR spectroscopy of **4.12** performed on a 500 MHz instrument in $\text{DMSO-}d_6$.

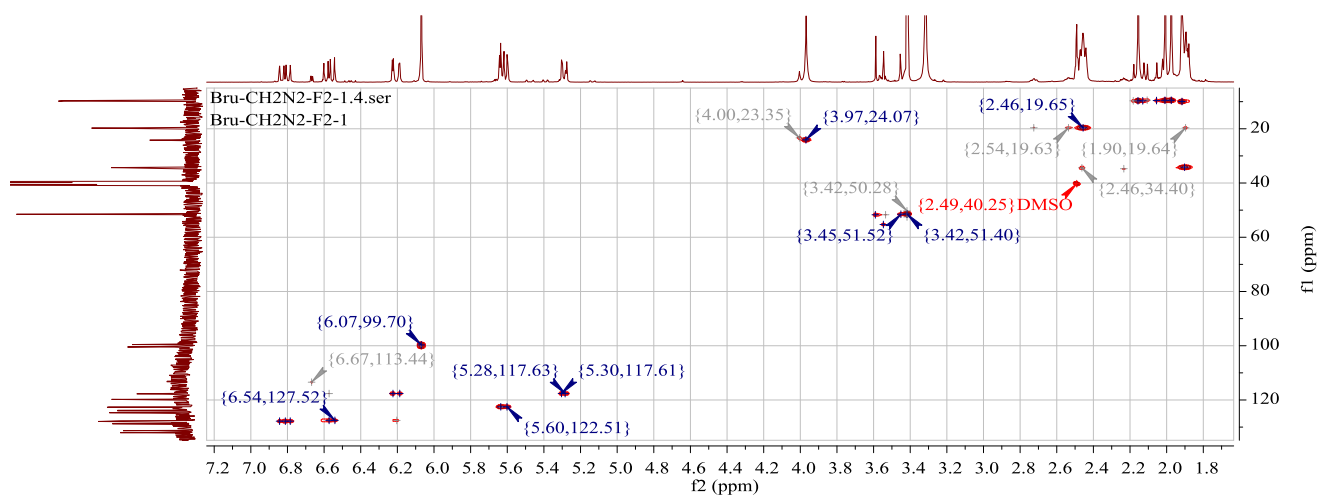


Figure 7.15: The HMBC correlations from protons to carbons of **4.11** performed on a 500 MHz instrument in $\text{DMSO-}d_6$.

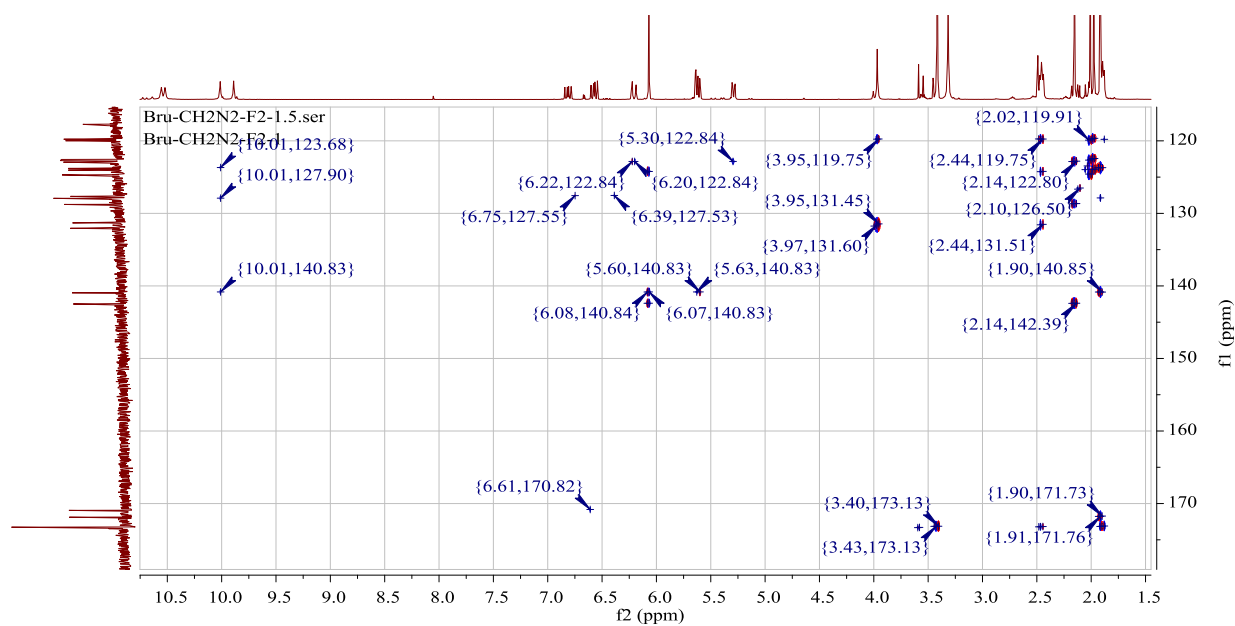


Figure 7.16: The HMBC correlations from protons to carbons of **4.12** performed on a 500 MHz instrument in DMSO- d_6 .

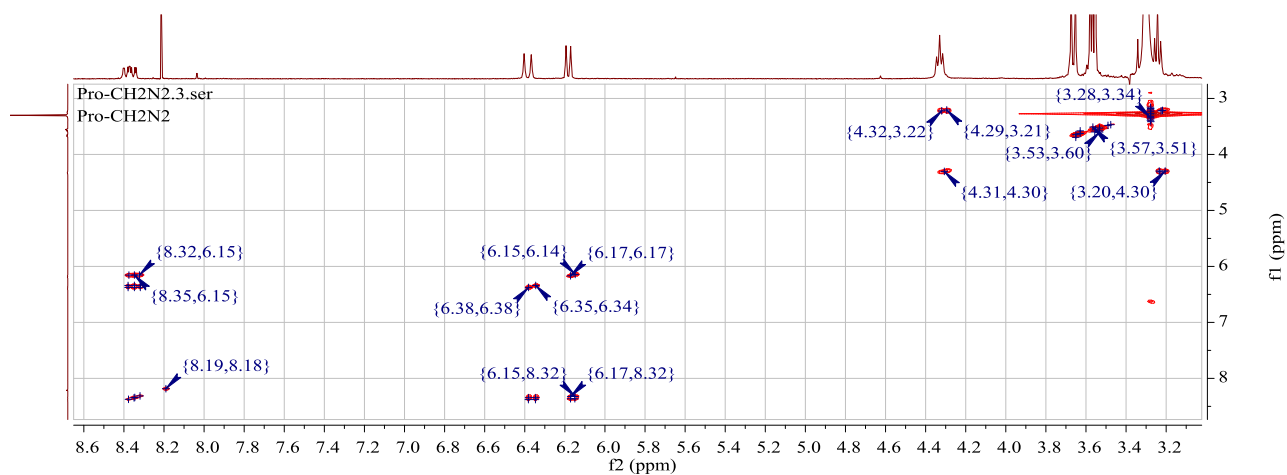


Figure 7.17: The HMBC correlations from protons to carbons of **4.13** performed on a 500 MHz instrument in DMSO- d_6 .

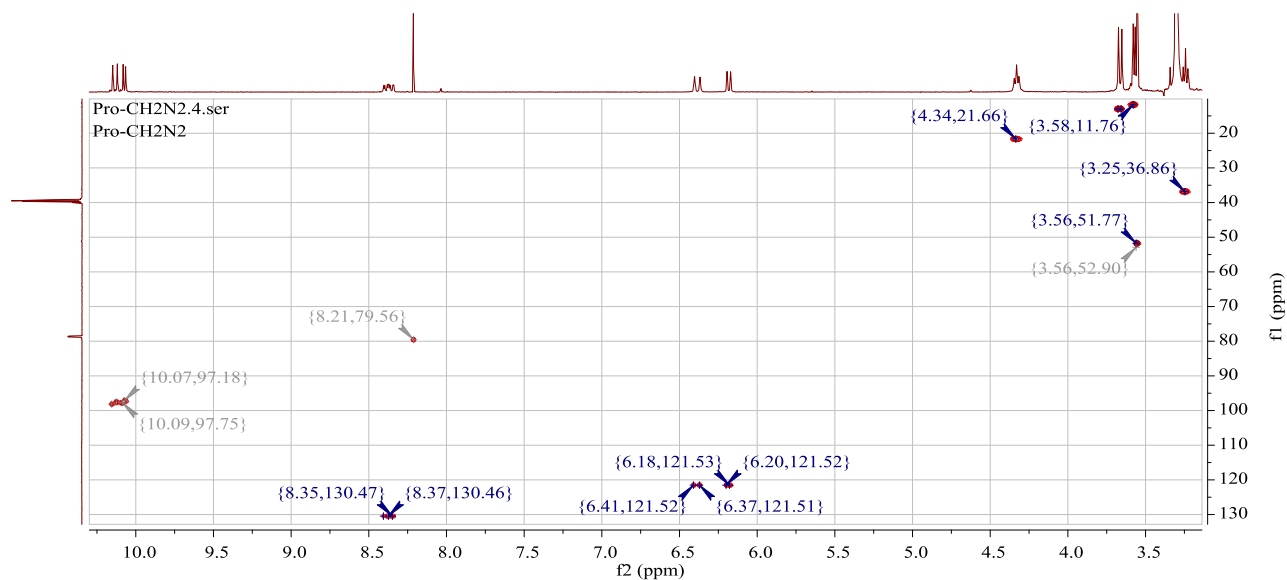


Figure 7.18: The HMBC correlations from protons to carbons of **4.13** performed on a 500 MHz instrument in DMSO- d_6 .

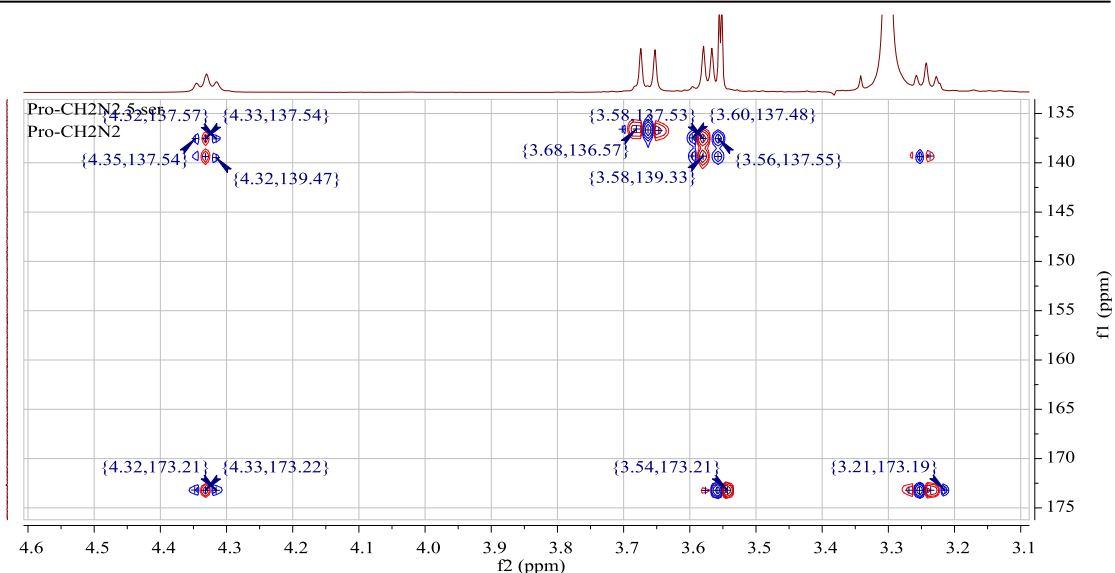


Figure 7.19: The HMBC correlations from protons to carbons of **4.13** performed on a 500 MHz instrument in DMSO- d_6 .

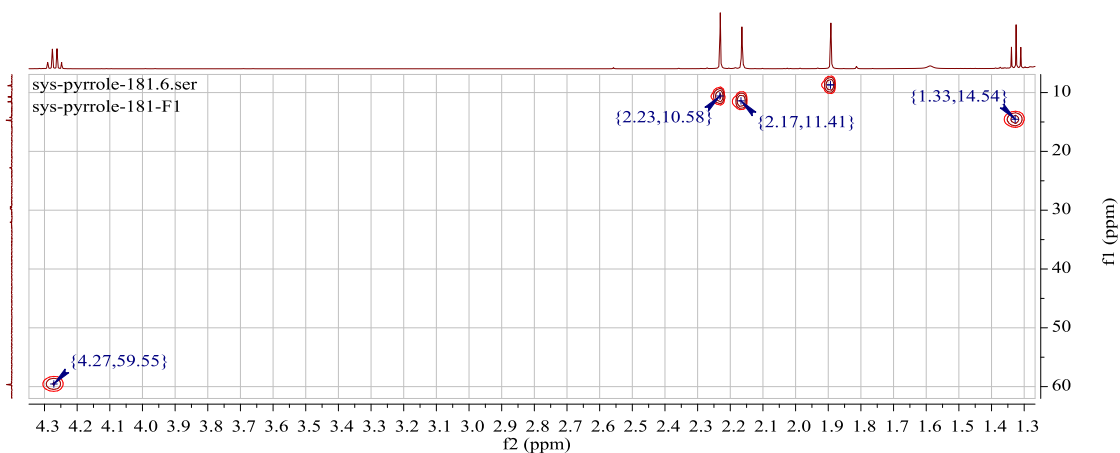


Figure 7.20: The HMBC correlation from protons of three methyl groups to tertiary carbon in pyrrole ring of **8b** performed on a 500 MHz instrument in $CDCl_3$

Appendix-D

Publication 1 arising from this Thesis

<http://pubs.acs.org/doi/abs/10.1021/np4005807>

Figure 7.21: ESI-MS spectrometry of unexpected products in positive ion obtaining from first fraction of the reaction between **5.10** and **5.7**.

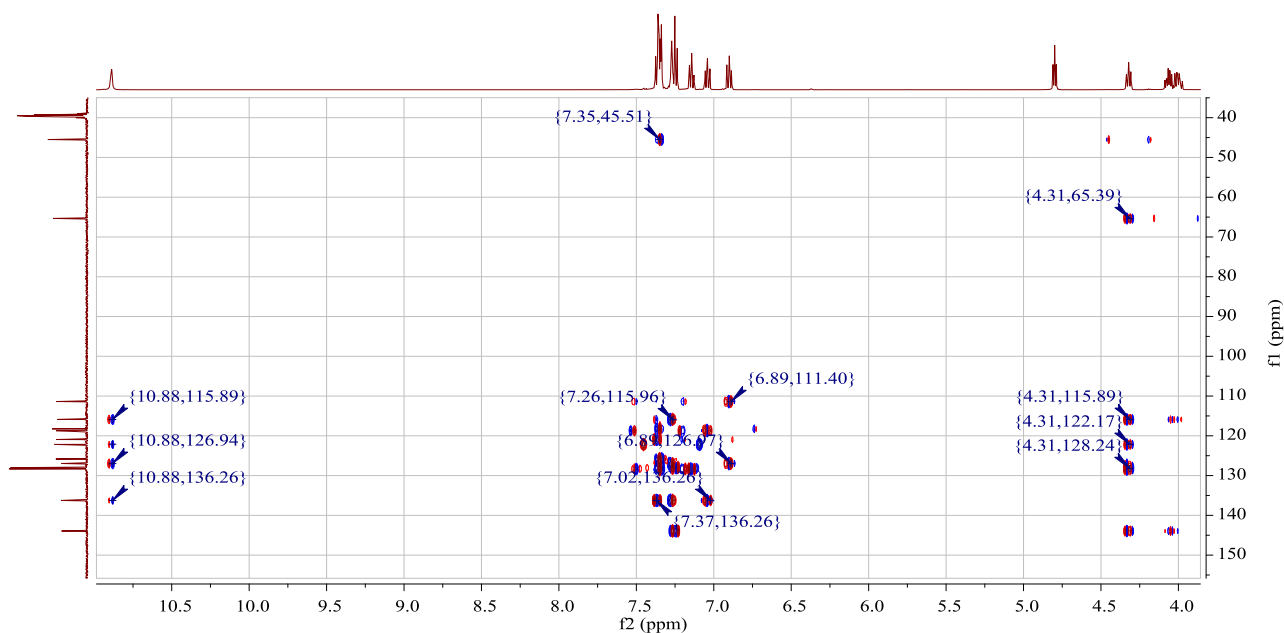


Figure 7.22: An expanded region of the HMBC spectrum of **5.13** showing the key correlations used to identify the structure. All experiments were performed at 500 MHz in DMSO- d_6 .

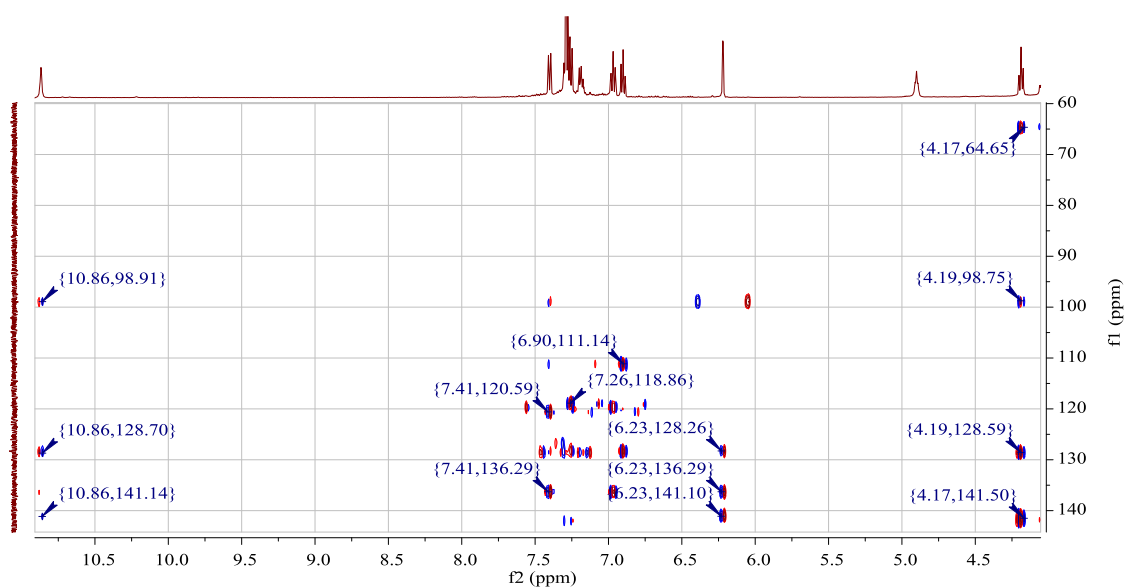


Figure 7.23: An expanded region of the HMBC spectrum of **5.15** showing the key correlations used to identify the structure. All experiments were performed at 500 MHz in DMSO- d_6 .

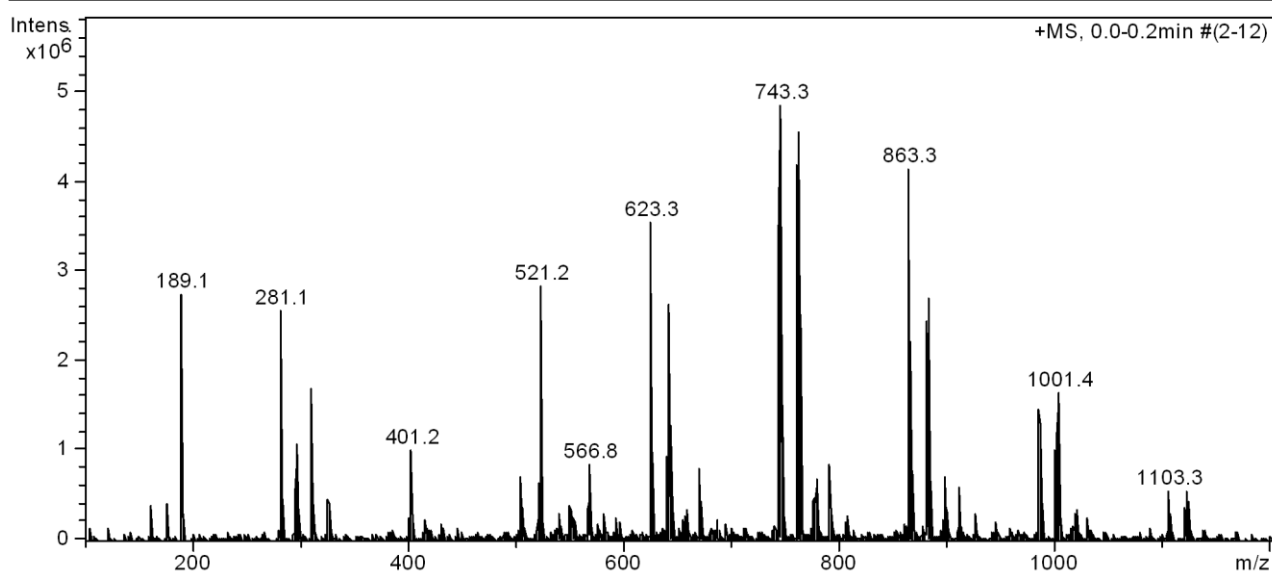


Figure 7.24: ESI-MS spectrometry of polymers in positive ion obtaining from first fraction of the reaction between **5.10** and **5.7**.

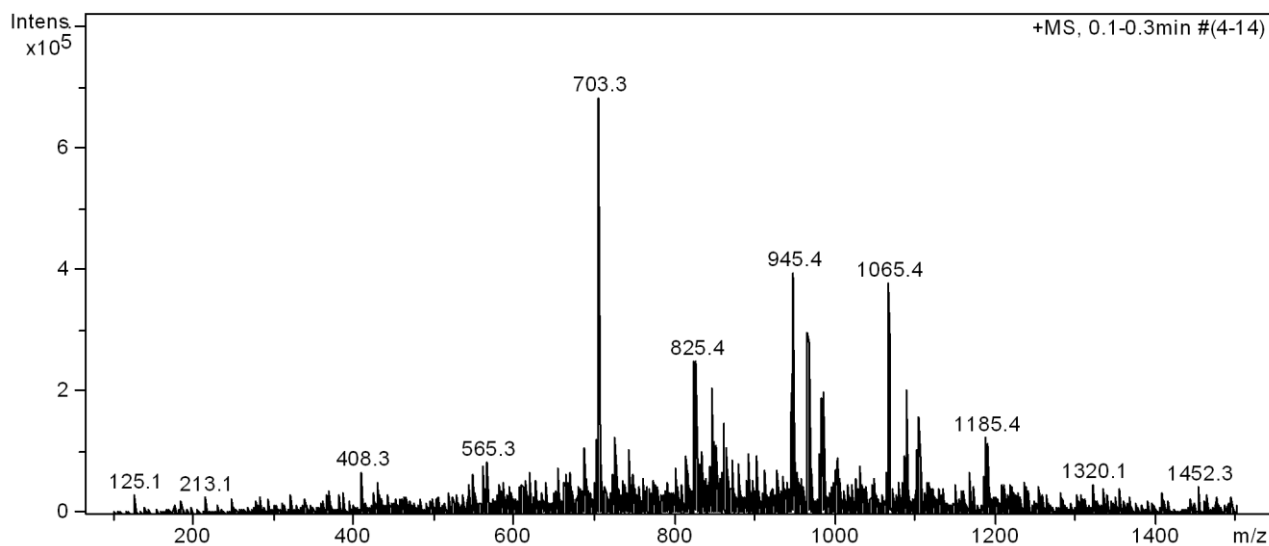


Figure 7.25: ESI-MS spectrometry of a fraction obtaining from the reaction between **5.9** and **5.7**.

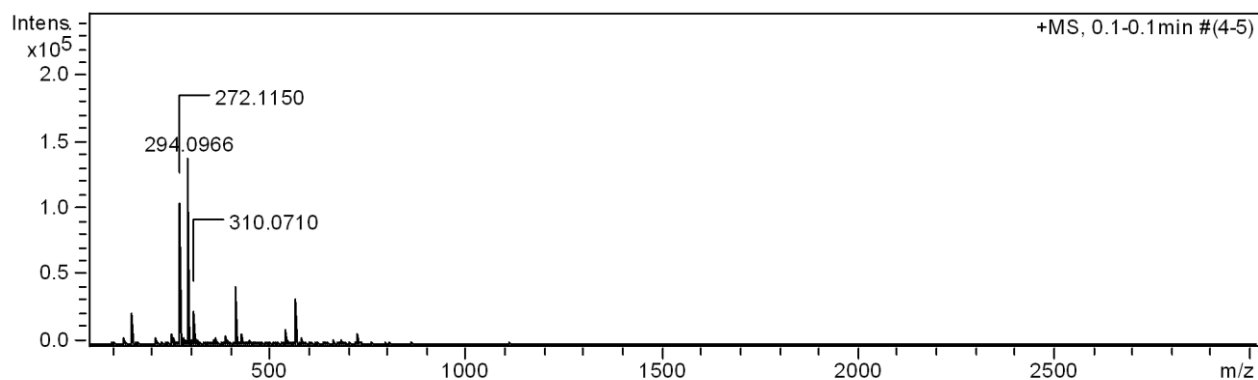


Figure 7.26: HRESI-MS spectra of compound **5.24**, an example of a 1:1 adduct of **5.23** and **5.7**.

Appendix-E

	Enzyme	Enzyme activity (pmol/min/mg protein)	Substrates' products	Result (pmol/min/mg protein)
1	CYP2C8	≥ 500	Paclitaxel 6 α -hydroxylase	800
2	CYP2C9	≥ 1	Diclofenac 4'-hydroxylase	18
3	CYP2C19	≥ 10	(S)-mephenytoin 4'-hydroxylase	15
4	CYP2A6	≥ 1	Coumarin 7-hydroxylase	10
5	CYP1A2	≥ 200	Phenacetin O-deethylase	290
6	CYP2D6	≥ 500	Bufuralo 1'-hydroxylase	580
7	CYP2B6	≥ 15	(S)-mephenytoin N-demethylase	16
8	CYP3A4	≥ 1000	Testosterone 6 β -hydroxylase	1000
9	Other	--	--	--

Table 7.17: A list of hepatic enzymes and the results of enzyme activity tests performed by Sigma-Aldrich upon analysis of S9 human liver.

	6.1 -6.7	6.1 -6.6	6.1 -6.8
log(inhibitor) vs. response (three parameters)	Ambiguous	Ambiguous	
Best-fit values			
Bottom	6.466	55.14	153.0
Top	~ 289989	~ 206735	634.8
LogIC50	~ -3.035	~ -3.016	-0.4433
IC50	~ 0.0009218	~ 0.0009631	0.3603
Span	~ 289982	~ 206680	481.8
Std. Error			
Bottom	26.02	14.99	10.91
Top	~ 1.932e+008	~ 1.020e+008	646.1
LogIC50	~ 289.7	~ 214.5	0.7915
Span	~ 1.932e+008	~ 1.020e+008	638.2
95% Confidence Intervals			
Bottom	-48.21 to 61.14	23.65 to 86.64	130.1 to 175.9
Top	(Very wide)	(Very wide)	-722.7 to 1992

Appendices

LogIC50	(Very wide)	(Very wide)	-2.106 to 1.220
IC50	(Very wide)	(Very wide)	0.007830 to 16.58
Span	(Very wide)	(Very wide)	-859.1 to 1823
Goodness of Fit			
Degrees of Freedom	18	18	18
R square	0.7621	0.8426	0.8388
Absolute Sum of Squares	58700	19474	8118
Sy.x	57.11	32.89	21.24
Number of points			
Analyzed	21	21	21

Table 7.18: Prism statistic applied for the data collected from the inhibition experiments of BPs to **6.1** using dose-response curves-inhibition for nonlinear regression.

	6.4 -6.7	6.4 -6.6	6.4 -6.6
log(inhibitor) vs. response (three parameters)	Ambiguous		
Best-fit values			
Bottom	36.41	64.90	75.65
Top	~ 156002	814.2	743.7
LogIC50	~ -2.886	-0.5487	-0.5143
IC50	~ 0.001301	0.2827	0.3060
Span	~ 155966	749.3	668.0
Std. Error			
Bottom	11.05	10.96	11.97
Top	~ 4.122e+007	1015	957.5
LogIC50	~ 114.9	0.7547	0.8129
Span	~ 4.122e+007	1007	948.9
95% Confidence Intervals			
Bottom	13.18 to 59.63	41.88 to 87.92	50.50 to 100.8
Top	(Very wide)	-1318 to 2947	-1268 to 2755
LogIC50	(Very wide)	-2.134 to 1.037	-2.222 to 1.194
IC50	(Very wide)	0.007340 to 10.89	0.005997 to 15.62
Span	(Very wide)	-1367 to 2865	-1326 to 2662

Appendices

Goodness of Fit			
Degrees of Freedom	18	18	18
R square	0.9109	0.8921	0.8631
Absolute Sum of Squares	10587	8595	10113
Sy.x	24.25	21.85	23.70
Number of points			
Analyzed	21	21	21

Table 7.19: Prism statistic applied for the data collected from the inhibition experiments of BPs to **6.4** using dose-response curves-inhibition for nonlinear regression.

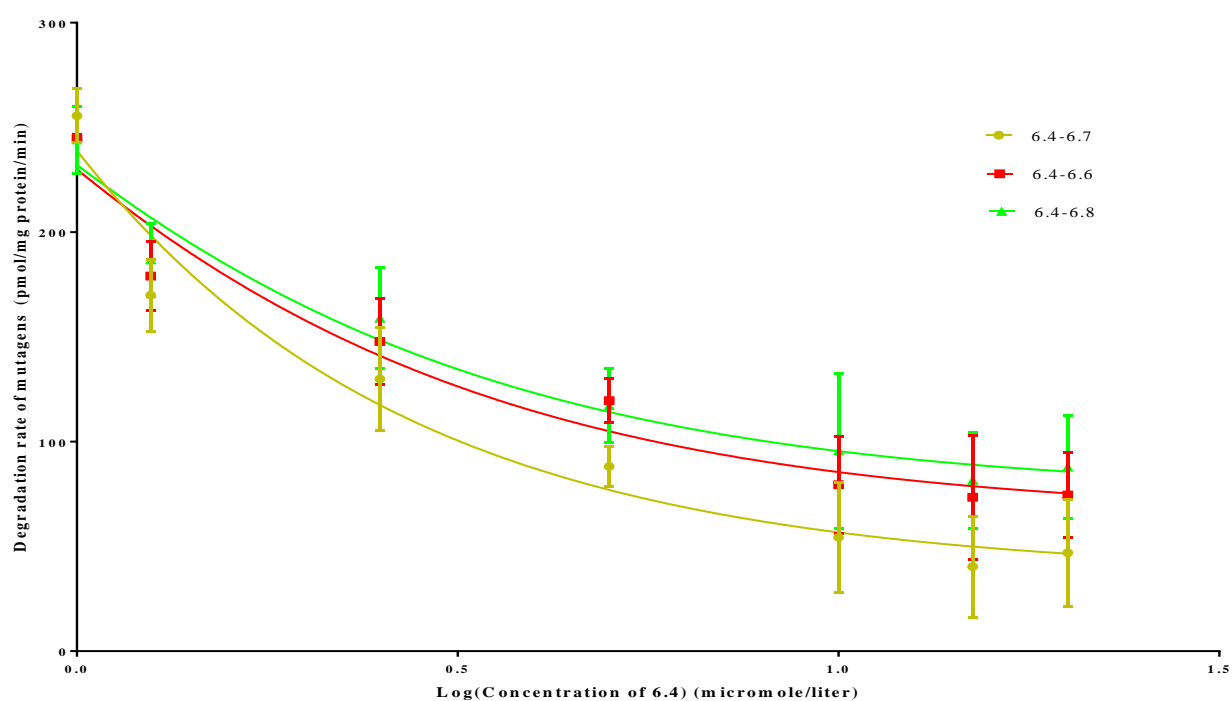


Figure 7.27: Prism statistic applied for the data collected from the inhibition experiments of BPs to **6.4** using dose-response curves-inhibition for nonlinear regression.

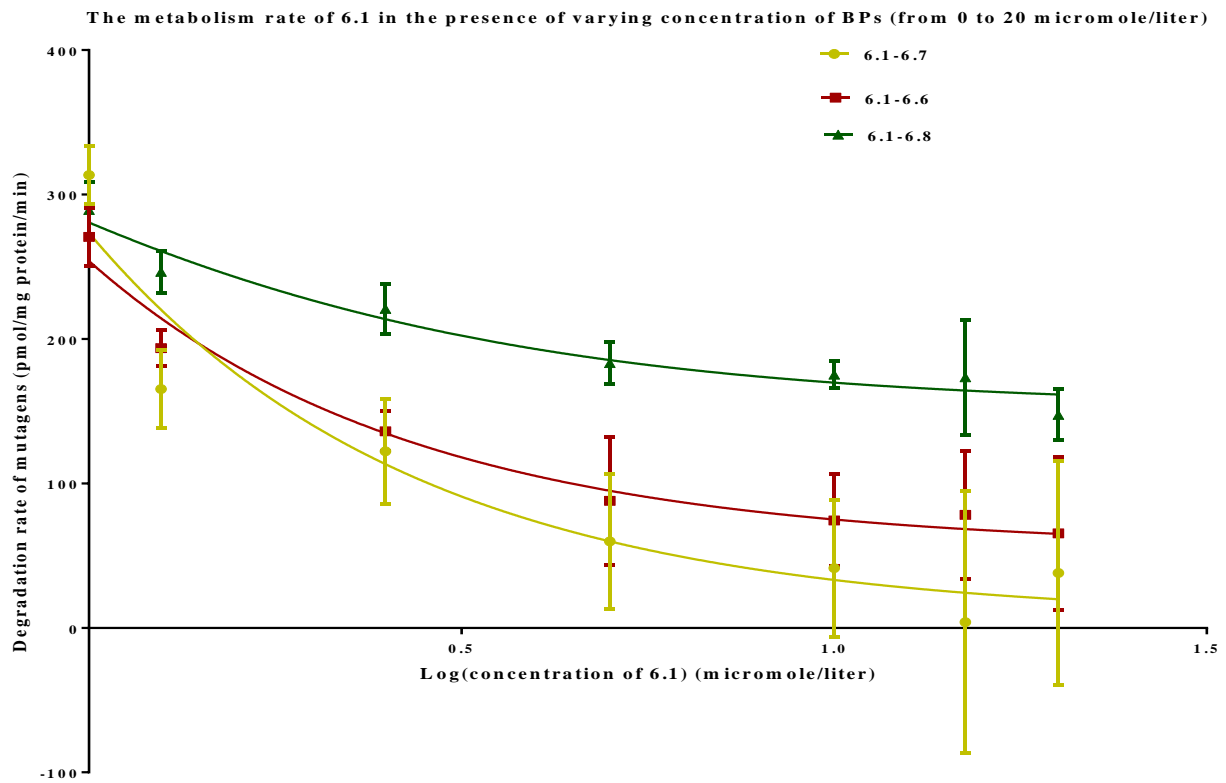


Figure 7.28: Prism statistic applied for the data collected from the inhibition experiments of BPs to 6.1 using dose-response curves-inhibition for nonlinear regression.